# Investigation of 1-Trichloromethyl-1,2,3,4-tetrahydro-β-carboline (TaClo)-Induced Neurotoxicity in the Zebrafish Models (*Danio rerio*)

by

Ji-Hang Yin

A dissertation submitted to the Graduate Faculty of
Auburn University
in partial fulfillment of the
requirements for the Degree of
Doctor of Philosophy

Auburn, Alabama
August 9, 2025

Keywords: 1-methyl-4-phenyl-1,2,3,6-tetrahydropyridine (MPTP), 1-Trichloromethyl-1,2,3,4-tetrahydro-β-carboline (TaClo), transcriptomic RNA-seq, trichloroethylene (TCE), neurotoxicity, zebrafish (*Danio rerio*)



Approved by

Katharine Horzmann, Chair, Associate Professor, Pathobiology
Chad Foradori, Professor, Anatomy, Physiology & Pharmacology
Jennifer Panizzi, Associate Professor, Anatomy, Physiology & Pharmacology
Vinicia Biancardi, Associate Professor, Anatomy, Physiology & Pharmacology

## Abstract

Environmental pollutants have been linked to neurotoxicity and are proposed to contribute to neurodegenerative disorders. Trichloroethylene (TCE) has been identified as an environmental contaminant and a potential risk factor for neurologic diseases. In recent studies, 1-Trichloromethyl-1,2,3,4-tetrahydro-β-carboline (TaClo), one of the metabolic compounds of TCE, has been implicated as a potent neurotoxicant in TCE-induced neurotoxicity. In addition, TaClo has been associated with Parkinson's disease (PD) due to its neurotoxic effects and structural resemblance to 1-methyl-4-phenyl-1,2,3,6-tetrahydropyridine (MPTP). The zebrafish model offers a high-throughput and cost-effective platform for chemical screening and toxicity assessment and is widely used in the study of neurodegenerative diseases. While previous studies have shown that environmentally relevant concentrations of TCE induce neurotoxic effects in developing zebrafish, the specific role of TaClo in zebrafish neurotoxicity remains largely unexplored. Therefore, this dissertation aims to investigate TaClo-induced neurotoxicity and to compare its effects with those of MPTP in zebrafish models. In addition, we sought to elucidate the underlying mechanisms of TaClo toxicity, evaluate its long-term effects following early-life exposure, and explore its potential role in contributing to broader diseases. Using zebrafish models, we demonstrated that early-life exposure to TaClo induces neurotoxicity closely resembling that of MPTP at the larval stage. Moreover, our study demonstrated that early-life exposure to TaClo and MPTP results in long-term neurotoxicity that persists into adulthood. Finally, transcriptomic analysis revealed that TaClo and MPTP utilize distinct molecular pathways to mediate neurotoxicity and contribute to various systemic diseases. These findings underscore the value of zebrafish as a model for studying environmental neurotoxicants, support

the potential role of TaClo in neurodegenerative diseases, and emphasize the need to address TCE contamination to mitigate long-term public health risks. Overall, this dissertation advances our understanding of the neurotoxic effects of TaClo, a metabolite of the widespread environmental contaminant TCE, and its similarities and differences with the established neurotoxin MPTP.

## Acknowledgment

I've written and deleted this section more times than I can count. I had started thinking about what I would write—and who I would thank—long before I even finished my oral preliminary exam.

Now, the day after my final defense, I've finally sat down to write. And once again, I find myself overwhelmed. Every version I've written has been emotional, each one struggling to express all that I want to say—to the people who helped me, supported me, and believed in me. There are so many faces in my mind and so many words I wish I could put down. But in the end, I've decided to keep many of those feelings in my heart—as cherished memories that will stay with me forever.

This journey has been a mix of bitter, sweet, sour, and even spicier than I ever expected—a full range of experiences that have helped me grow. I may not know what the future holds, but I am deeply grateful to everyone who extended a hand when I needed it most at Auburn University and the Auburn community.

This may not be the usual way graduate students write their acknowledgments, but I wanted to dedicate part of this section to my parents—and also, to myself.

Thank you, Mom and Dad.

You won't read this, since the version of my dissertation I shared with you was an early draft—from a typical, shy Asian kid.

As your only child, I've witnessed the countless sacrifices you made to ensure I had the best education and the highest quality of life. I would like to thank my mother, who gave up her career to become a full-time homemaker, so she could care for her family and raise her daughter. I also want to thank my father, who set aside his dream job as a sea captain traveling the world to take on a more stable job—for the sake of his family. You are always the first people I want to share everything with—from the smallest milestones to the biggest achievements. You are my first priority and the reason I've been able to reach this point. Though you don't always agree on many things, one thing both of you've always told me is this: "Don't worry about us and just follow your dream." Today, I hope I've made you proud.

Finally, to myself.

I know this is unusual—as I've rarely seen graduate students write to themselves in this section.

Snoop Dogg thanked himself after receiving the Hollywood star, and I didn't understand until I reached this point in my own journey. A RE-START was terrifying, as many people said it was risky and unwise. But as a student who does not always follow the rules, I've found this is probably the best decision I've ever made and the beginning of self-identification in my life. I also wanted to say thank you to my past self for not quitting. I may never open this dissertation again in the years to come, but the journey behind it has taught me invaluable lessons: it is easy to fail, but when I do, please keep the faith, stand up, chin up, keep moving, stay humble, stay true, be genuine, be kind, be positive, be resilient, be agile, take good care of myself, care for others when I can, reach out a hand to those in need, and share what I've learned—with those around, and with the next generation. And finally, I know I will never be perfect—but I wish to become a better version of myself, every single day.

Table of Contents

List of Tables

List of Figures

## Dissertation overview

This dissertation investigated 1-Trichloromethyl-1,2,3,4-tetrahydro-β-carboline (TaClo)-induced neurotoxicity using zebrafish models (*Danio rerio*). Specifically, we examined the neurotoxic effects of TaClo and explored its underlying mechanisms following early-life exposure through to adulthood. Additionally, we compared TaClo-induced neurotoxicity with that observed in the established MPTP-induced Parkinson's disease-like zebrafish model to evaluate the potential association between TaClo exposure and Parkinson's disease.

The literature review is presented in **Chapter 1** and **Chapter 2. Chapter 1** provides an overview of the chemical compound TaClo, focusing on its formation and its potential role in neurotoxicity. **Chapter 2** summarizes previously published peer-reviewed studies that demonstrate the embryonic zebrafish serve as a powerful platform for evaluating neurotoxicity induced by environmentally relevant concentrations of pollutants. Additionally, **Chapter 2** introduces the concept of Developmental Origins of Health and Disease (DoHaD). The subsequent chapters that present the original research are **Chapters 3, 4, and 5**.

**Chapter 1** reviews the chemical compound TaClo**.**

**Chapter 2** describes the use of embryonic zebrafish as a platform for evaluating neurotoxicity, entitled "*Embryonic zebrafish as a model for investigating the interaction between environmental pollutants and neurodegenerative disorders"* and reviews the Developmental Origins of Health and Disease concept.

**Publication**: Yin JH, Horzmann KA. *Embryonic zebrafish as a model for investigating the interaction between environmental pollutants and neurodegenerative disorders.* Biomedicines. 2024 Jul 13;12(7):1559. doi: 10.3390/biomedicines12071559.

**Chapter 3** describes early life exposure to TaClo-induced neurotoxicity in the larval stage. Chapter 3, entitled "*Developmental exposure of zebrafish to 1-Trichloromethyl-1,2,3,4-tetrahydro-beta-carboline (TaClo) elicits MPTP-like neurotoxicity*" was submitted to *NeuroToxicology* and is currently under review.

**Chapter 4** describes that early-life exposure to TaClo and MPTP induced a long-term neurotoxicity in adult zebrafish. Chapter 4, entitled "*Early-life 1-Trichloromethyl-1,2,3,4-tetrahydro-beta-carboline (TaClo) and 1-Methyl-4-phenyl-1,2,3,6-tetrahydropyridine (MPTP) exposure induces long-term neurotoxicity*" is a follow-up study to the work introduced in Chapter 3, which is currently in preparation for submission to *Scientific Reports* (Nature Porfolio).

**Chapter 5** describes the use of transcriptomic RNA-seq analysis to investigate the underlying mechanisms of neurotoxicity induced by both TaClo and MPTP. Chapter 5, entitled "*Comprehensive transcriptomic RNA seq profiling uncovers new insights into early life exposure to TaClo and MPTP in zebrafish (Danio rerio)*" is a follow-up study to the work introduced in Chapter 3 and Chapter 4, which is currently in preparation for submission to *Toxicological Sciences* (Oxford Academic, Society of Toxicology).

**Chapter 6** presents the overall conclusions of this dissertation.

# Chapter 1

## Brief overview

## Trichloromethyl-1,2,3,4-tetrahydro-β-carboline (TaClo)

1-Trichloromethyl-1,2,3,4-tetrahydro-β-carboline (TaClo) is a metabolic byproduct of trichloroethylene (TCE) or perchloroethylene (PERC), with TCE the more frequently studied (Gash et al., 2008; Keane, 2013). TCE is a volatile organic compound (VOC) widely used as a solvent in many industrial processes (Dorsey et al., 2023). US Environmental Protection Agency (EPA) classifies TCE as an environmental hazardous waste due to its environmental persistence and toxicity (EPA, 2025; *Public Health Statement for Trichloroethylene (TCE)*). TCE has been frequently detected in the air, aquatic systems, and solid waste through industrial discharges (Wu et al., 2022). Although TCE can gradually degrade in the environment, it has been found that the half-life for TCE to break down in nature ranges from weeks to years ("Agency for Toxic Substances and Disease Registry (ATSDR) Toxicological Profiles," 2019; Dorsey et al., 2023). These features have made TCE one of the commonly found contaminants at Superfund sites across the United States (Doty et al., 2017; *Vapor Intrusion at Superfund Sites*). EPA issued a final rule on December 17, 2024, prohibiting all uses of TCE (EPA, 2025). In addition, EPA established a maximum contaminant level (MCL) for TCE in drinking water at 5 parts per billion (ppb) (EPA, 2025; "Update on the Status of TSCA Risk Management Rule for TCE,"). However, TCE has been detected at approximately 350 Superfund sites in the United States, with an exceeding 1000 ppb found in some Superfund sites and the nearby groundwater (ATSDR, 2019; *Public Health Statement for Trichloroethylene (TCE)*; *Vapor Intrusion at Superfund Sites*). Occupational exposure to TCE has been linked to several health effects, such as neurotoxicity, carcinogenicity, respiratory, reproductive, and developmental toxicity (Brown et al., 1990). Among all, the neurologic effect has been largely discussed and TCE is suggested as an environmental risk factor linked to late-onset Parkinson's disease (PD) (De Miranda & Greenamyre, 2020; Goldman et al., 2012; Maiti et al., 2017; Prajjwal et al., 2023). Several metabolites and mechanisms have been investigated to explain the neurotoxic effects of TCE. For example, TCE is metabolized through two primary pathways: oxidative metabolism and glutathione (GSH) conjugation, each generating distinct sets of metabolites (Lash et al., 2000). The oxidative pathway

produces several stable metabolites, including chloral, chloral hydrate, trichloroethanol (TCOH), and trichloroacetic acid (TCA). However, these metabolites are predominantly associated with hepatic and renal toxicity, rather than central nervous system effects. In contrast, the GSH conjugation pathway, primarily active in the liver and kidney, produces more reactive and cytotoxic intermediates. Metabolites such as S-(1,2-dichlorovinyl) glutathione (DCVG) and S-(1,2-dichlorovinyl)-L-cysteine (DCVC) have been implicated in the generation of oxidative stress, apoptosis, and renal tubular damage (Lash et al., 2000; Luo et al., 2018). Lastly, among all metaoblies, TaClo has been largely considered a potent neurotoxicant responsible for the neurotoxicity (Keane et al., 2019). The formation of TaClo has been studied primarily in rodent models as a metabolite of TCE exposure (Luo et al., 2018). Upon exposure, TCE is primarily metabolized in the liver by cytochrome P450 enzymes, particularly CYP2E1, into chloral hydrate (Luo et al., 2018; Ramdhan et al., 2008). Chloral hydrate then undergoes a Pictet–Spengler condensation reaction with tryptamine, resulting in the formation of TaClo **(Figure 1)** (Bringmann et al., 1999; Grote et al., 1995).

Current studies on TaClo have primarily focused on its neurotoxic effects, with researchers predominantly using cell lines and rodent models to investigate the underlying mechanisms (Sharma et al., 2017). For instance, in vitro studies have demonstrated that TaClo exposure induces apoptosis in human neuroblastoma cell lines (Sharma et al., 2017). Additionally, TaClo has been shown to cause significant cell death in primary dopaminergic neuron cultures. TaClo is structurally and chemically similar to 1-methyl-4-phenyl-1,2,3,6-tetrahydropyridine (MPTP), a well-known neurotoxicant that induces Parkinson's disease (PD)-like symptoms and is widely used in experimental PD models (Omar et al., 2023a; Sarath Babu et al., 2016; Yao et al., 2017). Both TaClo and MPTP have been reported to cross the blood–brain barrier and selectively target dopaminergic neurons in the substantia nigra and lead to neurodegeneration (Akundi et al., 2004; Bringmann, God, Feineis, Janetzky, et al., 1995). In vivo studies have shown that TaClo causes a loss of tyrosine hydroxylase-positive neurons in the substantia nigra pars compacta, reduces dopamine levels in the striatum, and impairs locomotor activity in rodent models (Sontag et al., 1995). Investigations into the mechanisms underlying TaClo-induced neurotoxicity suggest that it promotes apoptosis of dopaminergic neurons primarily through oxidative stress and neuroinflammatory processes (Yang et al., 2019).

Specifically, TaClo increases reactive oxygen species (ROS) production and disrupts mitochondrial membrane potential, leading to oxidative damage within the nigrostriatal system (Bringmann, God, Feineis, Janetzky, et al., 1995; Yang et al., 2019). Additionally, TaClo induces neuroinflammation and activates microglia in the striatum of rodents (Yang et al., 2019). Furthermore, caspase-3 activation has been shown to mediate TaClo-induced apoptotic cell death in the rat striatum (Yang et al., 2019). Finally, TaClo exposure has been shown to impair glial function by reducing astrocyte populations in mesencephalic cultures (Rausch et al., 1995).

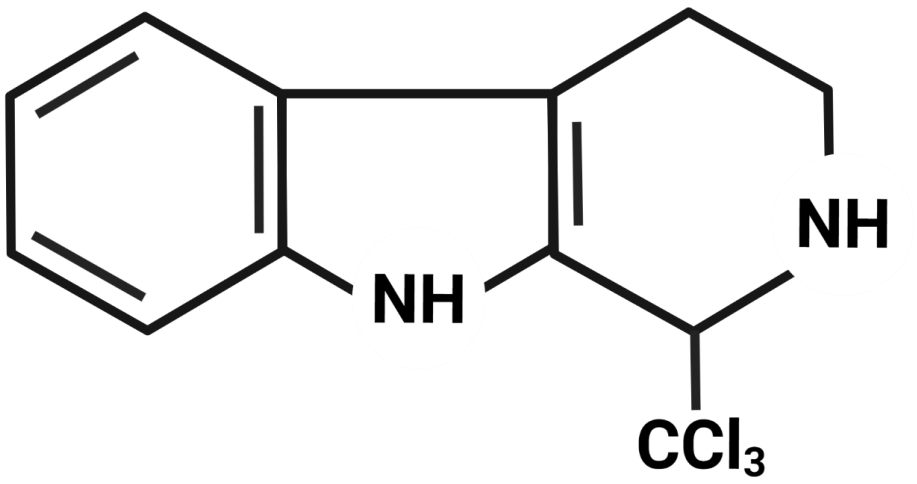


1-Trichloromethyl-1,2,3,4-tetrahydro-beta-carboline
(TaClo)

**Figure 1. Chemical structure of 1-Trichloromethyl-1,2,3,4-tetrahydro-β-carboline (TaClo)**

**Reference**


Agency for Toxic Substances and Disease Registry (ATSDR) Toxicological Profiles. (2019). In *Toxicological Profile for Trichloroethylene*. Agency for Toxic Substances and Disease Registry (US).

Akundi, R. S., Macho, A., Muñoz, E., Lieb, K., Bringmann, G., Clement, H. W., Hüll, M., & Fiebich, B. L. (2004). 1-trichloromethyl-1,2,3,4-tetrahydro-beta-carboline-induced apoptosis in the human neuroblastoma cell line SK-N-SH. *J Neurochem*, *91*(2), 263-273. https://doi.org/10.1111/j.1471-4159.2004.02710.x

ATSDR. (2019). Public Health Statement for Trichloroethylene (TCE). https://wwwn.cdc.gov/TSP/PHS/PHS.aspx?phsid=171&toxid=30

Bringmann, G., God, R., Fähr, S., Feineis, D., Fornadi, K., & Fornadi, F. (1999). Identification of the dopaminergic neurotoxin 1-trichloromethyl-1,2, 3,4-tetrahydro-beta-carboline in human blood after intake of the hypnotic chloral hydrate. *Anal Biochem*, *270*(1), 167-175. https://doi.org/10.1006/abio.1999.4088

Bringmann, G., God, R., Feineis, D., Janetzky, B., & Reichmann, H. (1995). TaClo as a neurotoxic lead: improved synthesis, stereochemical analysis, and inhibition of the mitochondrial respiratory chain. *J Neural Transm Suppl*, *46*, 245-254.

Brown, L. P., Farrar, D. G., & de Rooij, C. G. (1990). Health risk assessment of environmental exposure to trichloroethylene. *Regul Toxicol Pharmacol*, *11*(1), 24-41. https://doi.org/10.1016/0273-2300(90)90005-v

De Miranda, B. R., & Greenamyre, J. T. (2020). Trichloroethylene, a ubiquitous environmental contaminant in the risk for Parkinson's disease. *Environ Sci Process Impacts*, *22*(3), 543-554. https://doi.org/10.1039/c9em00578a

Dorsey, E. R., Zafar, M., Lettenberger, S. E., Pawlik, M. E., Kinel, D., Frissen, M., Schneider, R. B., Kieburtz, K., Tanner, C. M., De Miranda, B. R., Goldman, S. M., & Bloem, B. R. (2023). Trichloroethylene: An Invisible Cause of Parkinson's Disease? *J Parkinsons Dis*, *13*(2), 203-218. https://doi.org/10.3233/jpd-225047

Doty, S. L., Freeman, J. L., Cohu, C. M., Burken, J. G., Firrincieli, A., Simon, A., Khan, Z., Isebrands, J. G., Lukas, J., & Blaylock, M. J. (2017). Enhanced Degradation of TCE on a Superfund Site Using Endophyte-Assisted Poplar Tree Phytoremediation. *Environ Sci Technol*, *51*(17), 10050-10058. https://doi.org/10.1021/acs.est.7b01504

EPA. (2025, March 24). Update on the Status of TSCA Risk Management Rule for TCE. *Update on the Status of TSCA Risk Management Rule for TCE*. https://www.epa.gov/chemicals-under-tsca/update-status-tsca-risk-management-rule-tce

Gash, D. M., Rutland, K., Hudson, N. L., Sullivan, P. G., Bing, G., Cass, W. A., Pandya, J. D., Liu, M., Choi, D. Y., Hunter, R. L., Gerhardt, G. A., Smith, C. D., Slevin, J. T., & Prince, T. S. (2008). Trichloroethylene: Parkinsonism and complex 1 mitochondrial neurotoxicity. *Ann Neurol*, *63*(2), 184-192. https://doi.org/10.1002/ana.21288

Goldman, S. M., Quinlan, P. J., Ross, G. W., Marras, C., Meng, C., Bhudhikanok, G. S., Comyns, K., Korell, M., Chade, A. R., Kasten, M., Priestley, B., Chou, K. L., Fernandez, H. H., Cambi, F., Langston, J. W., & Tanner, C. M. (2012). Solvent exposures and Parkinson disease risk in twins. *Ann Neurol*, *71*(6), 776-784. https://doi.org/10.1002/ana.22629

Grote, C., Clement, H. W., Wesemann, W., Bringmann, G., Feineis, D., Riederer, P., & Sontag, K. H. (1995). Biochemical lesions of the nigrostriatal system by TaClo (1-trichloromethyl-1,2,3,4-tetrahydro-beta-carboline) and derivatives. *J Neural Transm Suppl*, *46*, 275-281.

Keane, P. (2013). *The Mechanism of Trichloroethylene Neurotoxicity and its Relation to Parkinsonism* Newcastle University].

Keane, P. C., Hanson, P. S., Patterson, L., Blain, P. G., Hepplewhite, P., Khundakar, A. A., Judge, S. J., Kahle, P. J., LeBeau, F. E. N., & Morris, C. M. (2019). Trichloroethylene and its metabolite TaClo lead to degeneration of substantia nigra dopaminergic neurones: Effects in wild type and human A30P mutant α-synuclein mice. *Neurosci Lett*, *711*, 134437. https://doi.org/10.1016/j.neulet.2019.134437

Luo, Y. S., Furuya, S., Soldatov, V. Y., Kosyk, O., Yoo, H. S., Fukushima, H., Lewis, L., Iwata, Y., & Rusyn, I. (2018). Metabolism and Toxicity of Trichloroethylene and Tetrachloroethylene in Cytochrome P450 2E1 Knockout and Humanized Transgenic Mice. *Toxicol Sci*, *164*(2), 489-500. https://doi.org/10.1093/toxsci/kfy099

Maiti, P., Manna, J., & Dunbar, G. L. (2017). Current understanding of the molecular mechanisms in Parkinson's disease: Targets for potential treatments. *Transl Neurodegener*, *6*, 28. https://doi.org/10.1186/s40035-017-0099-z

Omar, N. A., Kumar, J., & Teoh, S. L. (2023). Neuroprotective effects of Neurotrophin-3 in MPTP-induced zebrafish Parkinson's disease model. *Front Pharmacol*, *14*, 1307447. https://doi.org/10.3389/fphar.2023.1307447

Prajjwal, P., Flores Sanga, H. S., Acharya, K., Tango, T., John, J., Rodriguez, R. S. C., Dheyaa Marsool Marsool, M., Sulaimanov, M., Ahmed, A., & Hussin, O. A. (2023). Parkinson's disease updates: Addressing the pathophysiology, risk factors, genetics, diagnosis, along with the medical and surgical treatment. *Ann Med Surg (Lond)*, *85*(10), 4887-4902. https://doi.org/10.1097/ms9.0000000000001142

*Public Health Statement for Trichloroethylene (TCE)*. https://wwwn.cdc.gov/TSP/PHS/PHS.aspx?phsid=171&toxid=30

Ramdhan, D. H., Kamijima, M., Yamada, N., Ito, Y., Yanagiba, Y., Nakamura, D., Okamura, A., Ichihara, G., Aoyama, T., Gonzalez, F. J., & Nakajima, T. (2008). Molecular mechanism of trichloroethylene-induced hepatotoxicity mediated by CYP2E1. *Toxicol Appl Pharmacol*, *231*(3), 300-307. https://doi.org/10.1016/j.taap.2008.04.020

Rausch, W. D., Abdel-mohsen, M., Koutsilieri, E., Chan, W. W., & Bringmann, G. (1995). Studies of the potentially endogenous toxin TaClo (1-trichloromethyl-1,2,3,4-tetrahydro-beta-carboline) in neuronal and glial cell cultures. *J Neural Transm Suppl*, *46*, 255-263.

Sarath Babu, N., Murthy Ch, L., Kakara, S., Sharma, R., Brahmendra Swamy, C. V., & Idris, M. M. (2016). 1-Methyl-4-phenyl-1,2,3,6-tetrahydropyridine induced Parkinson's disease in zebrafish. *Proteomics*, *16*(9), 1407-1420. https://doi.org/10.1002/pmic.201500291

Sharma, R. K., Candelario-Jalil, E., Feineis, D., Bringmann, G., Fiebich, B. L., & Akundi, R. S. (2017). 1-Trichloromethyl-1,2,3,4-tetrahydro-beta-carboline (TaClo) Alters Cell Cycle Progression in Human Neuroblastoma Cell Lines. *Neurotox Res*, *32*(4), 649-660. https://doi.org/10.1007/s12640-017-9782-1

Sontag, K. H., Heim, C., Sontag, T. A., God, R., Reichmann, H., Wesemann, W., Rausch, W. D., Riederer, P., & Bringmann, G. (1995). Long-term behavioural effects of TaClo (1-trichloromethyl-1,2,3,4-tetrahydro-beta-carboline) after subchronic treatment in rats. *J Neural Transm Suppl*, *46*, 283-289.

Update on the Status of TSCA Risk Management Rule for TCE. (March 24). https://www.epa.gov/chemicals-under-tsca/update-status-tsca-risk-management-rule-tce

*Vapor Intrusion at Superfund Sites*. https://www.epa.gov/vaporintrusion/vapor-intrusion-superfund-sites

Wu, Z., Man, Q., Niu, H., Lyu, H., Song, H., Li, R., Ren, G., Zhu, F., Peng, C., Li, B., & Ma, X. (2022). Recent advances and trends of trichloroethylene biodegradation: A critical review. *Front Microbiol*, *13*, 1053169. https://doi.org/10.3389/fmicb.2022.1053169

Yang, Y., Pang, B., Liu, Z., Li, J., Zhang, Z., Zhang, R., Hou, X., Guo, H., Chi, L., Pang, Q., & Xin, T. (2019). 1-Trichloromethyl-1,2,3,4-tetrahydro-beta-carboline (TaClo) Induces the Apoptosis of Dopaminergic Neurons via Oxidative Stress and Neuroinflammation. *Oxid Med Cell Longev*, *2019*, 1292891. https://doi.org/10.1155/2019/1292891

Yao, L., Peng, S. X., Xu, Y. D., Lin, S. L., Li, Y. H., Liu, C. J., Zhao, H. D., Wang, L. F., & Shen, Y. Q. (2017). Unexpected Neuroprotective Effects of Loganin on 1-Methyl-4-Phenyl-1,2,3,6-Tetrahydropyridine-Induced Neurotoxicity and Cell Death in Zebrafish. *J Cell Biochem*, *118*(3), 615-628. https://doi.org/10.1002/jcb.25749

## Chapter 2

## Embryonic zebrafish as a model for investigating the interaction between environmental pollutants and neurodegenerative disorders


### Abstract

Environmental pollutants have been linked to neurotoxicity and are proposed to contribute to neurodegenerative disorders. The zebrafish model provides a high-throughput platform for large-scale chemical screening and toxicity assessment and is widely accepted as an important animal model for the investigation of neurodegenerative disorders. Although recent studies explore the roles of environmental pollutants in neurodegenerative disorders in zebrafish models, current knowledge of the mechanisms of environmentally induced neurodegenerative disorders is relatively complex and overlapping. This review primarily discusses utilizing embryonic zebrafish as the model to investigate environmental pollutants-related neurodegenerative disease. We also review current applicable approaches and important biomarkers to unravel the underlying mechanism of environmentally related neurodegenerative disorders. We found embryonic zebrafish a powerful tool that provides a platform for evaluating neurotoxicity triggered by environmentally relevant concentrations of neurotoxic compounds. Additionally, using variable approaches to assess neurotoxicity in the embryonic zebrafish allows the researchers to have insights into the complex interaction between environmental pollutants and neurodegenerative disorders and, ultimately, the understanding of the underlying mechanisms related to environmental toxicants

## 1. Introduction

Neurodegenerative disorders are a major public health concern, with an estimate of over 50 million of people affected worldwide (Deuschl et al., 2020; Mathur et al., 2023; Tiwari et al., 2019). Aging has been considered the primary contributory risk factor to neurodegenerative disorders such as Alzheimer's disease (AD), Parkinson's disease (PD), and anxiety-like disorders, (Labadorf et al., 2017; Xie et al., 2014); however, recent studies suggest other potential causes or contributors, such as gender, genetic mutations, stress, and environmental pollutants, could increase the incidence of the disease (MacMahon Copas et al., 2021; Tolosa et al., 2021). Among potential causes, environmental pollutants are largely incriminated with a correlation to neurodegenerative disorders development (Dauer & Przedborski, 2003). The progressive production of synthetic chemical products for industrial applications and the rapid population growth have resulted in innumerable environmental chemical wastes (Johnston & Cushing, 2020). To date, the Toxic Substances Control Act (TSCA) chemical substances inventory lists 70,000 existing chemicals in commerce (*Summary of the Toxic Substances Control Act*, 2023). Up to 30% of used chemicals may be potentially neurotoxic and play a role in neurodevelopmental diseases and disabilities (Fitzgerald et al., 2021). The recognition of environmental toxicant-related neurologic disorders generates a high demand for establishing new approaches to assess the neurotoxic effects of environmental chemicals (Fitzgerald et al., 2021).

Since the 1950s, mammalian laboratory animals, such as rodents and rabbits, have served as the standard experimental animals for assessing toxicity in the USA (2018; Wolfle, 2003). The Organization for Economic Cooperation and Development (OECD) primarily uses rodents to evaluate the toxic characteristics of test chemicals in a variety of toxicity studies (OECD, 2008, 2018). However, traditional methods using rodents, rabbits, and non-human primates remain costly and time-consuming (Smith & Lilley, 2019). Driven by the concepts of 3Rs (reduction, replacement, and refinement), European legislation regulates the use of laboratory animals for experimental and scientific purposes in European Council Directive 86/609/EEC and 2010/63/EU ("Council Directive 86/609/EEC of 24 November 1986 on the approximation of laws, regulations and administrative provisions of the Member States regarding the protection of animals used for experimental and other scientific purposes," 1986; Parliament & Council, 2010).

Registration, Evaluation, Authorisation, and Restriction of Chemicals (REACH) under the European Union requires that tests on vertebral animals be minimized (*ECHA and alternatives to animal testing*). Moreover, thousands of new chemicals are introduced to the market yearly and may potentially disperse into the environment, highlighting the importance of employing a high-throughput-based system for neurotoxicity assessment (Kang et al., 2021). Although in vitro-cell-based assays generally follow the concept of high-throughput screening, they provide limited information on the principles of absorption, distribution, metabolism, excretion, and toxicity (ADME-Tox) (Shou, 2020). In vivo models, on the other hand, largely mimic human physiology systems and provide relevant results; however, they are often not suitable for high-throughput platforms (Yoon et al., 2015). Due to the current regulations and animal welfare considerations, fish appear to be a good alternative candidate for large-scale screening in neurotoxicity studies (Wlodkowic & Campana, 2021). To date, test guidelines concerning the use of fish in toxicity testing has been released by OECD including: the fish acute toxicity test (OECD test guideline 203), the fish short-term toxicity on embryos and sac-fry stages (OECD 212), the early life stage toxicity test (OECD 210), the juvenile fish growth test (OECD 215), and the bioaccumulation in fish (OECD 305) (OECD, 1998, 2012, 2013a, 2019).

Several fish species are recommended for assessing toxicity study under OECD guidelines due to their availability, easy maintenance, and historical use (OECD, 2019). Zebrafish are recognized as a well-established biomedical model bridging the gap between in vitro cell-based and in vivo mammalian platforms (Strähle et al., 2012). The US Environmental Protection Agency (US EPA) indicates zebrafish are valuable animals for studying developmental neurotoxicity (de Abreu et al., 2020; Jarema et al., 2022). The zebrafish is a powerful neurotoxicologic fish model in pharmaceutical and chemical compound screening (d'Amora & Giordani, 2018). Studies have demonstrated that zebrafish-based neurotoxic responses can predict chemical hazards in human health and ecological hazard assessments (Ali et al., 2011; d'Amora & Giordani, 2018). Using zebrafish embryos as alternatives in toxicity tests has been advocated in many studies, which proved that zebrafish embryos provided equivalent sensitivity to juveniles in the acute fish toxicity test (AFT) (OECD, 2013b; Vaughan & van Egmond, 2010). The concept of adopting zebrafish embryos in toxicity test studies is widely accepted. Following the German Federal Environment Agency's submission and two validation

studies, OECD in 2013 approved the test guideline "Fish embryo acute toxicity test" (OECD 236), particularly on zebrafish embryos, to determine the acute or lethal toxicity of test chemicals (OECD, 2013b). Recently, studies focusing on environmental pollutant-induced neurodegenerative disorders in zebrafish models are increasing (Ahkin Chin Tai et al., 2021). This review article is mainly focused on neurodegeneration in the zebrafish model after an early life stage environmental exposure. In addition, we investigate the pathways associated with neurodegenerative disorders and emphasized the methodologies currently discussed in zebrafish models **(Figure 2)**.

## 2. The zebrafish model as a high-throughput platform in neurologic studies

The zebrafish model is a well-established platform for research studies in neurologic fields, such as neurotoxicology, neurodevelopmental disorders, neurodegenerative diseases, and drug discovery (Bailey et al., 2013; Basnet et al., 2019; Cassar et al., 2020). Zebrafish have a considerable anatomical and physiological resemblance to mammalian counterparts (Bailone et al., 2020; Goldsmith & Jobin, 2012). The zebrafish genome is fully sequenced and is reported to share 70-80% identity at the nucleotide level with the human genome and 80-90% similarity in amino acid in functional domains (Barbazuk et al., 2000; Howe et al., 2013). The zebrafish brain shows structural and functional similarities in neuroanatomy and neurolocalization to mammals (Kinkhabwala et al., 2011). Although the zebrafish brain lacks the amygdala, hippocampus, and substantia nigra, it has been proposed that other regions of the brain contain cells that serve similar functions (Lal & Kawakami, 2022; Verma et al., 2022).

Zebrafish are small, inexpensive, easily manipulated, and have high fecundity with a short generation time (Horzmann & Freeman, 2016) Fertilization occurs externally and zebrafish embryos are transparent during early development (Sáez-Espinosa et al., 2022). These features make zebrafish a suitable platform for neurodevelopmental and neurotoxicity studies through in vivo, high-throughput screening systems (Bailey et al., 2013; d'Amora & Giordani, 2018). Zebrafish have a distinct, well characterized development of central nervous system with the zebrafish brain developing early at the beginning of gastrulation around 6 hours post fertilization (hpf) (Schmidt et al., 2013; Woo & Fraser, 1995). The neural signaling system, including

catecholaminergic, gamma-aminobutyric acid (GABA)-ergic, and glutamatergic systems, develops between 18-32 hpf (Verma et al., 2022). The brain forms distinct regions and is divided into the forebrain (diencephalon, telencephalon), midbrain, hindbrain, and spinal cord by 24 hpf (Gutzman et al., 2008; Kimmel et al., 1995). Primary neurons interconnected by axonal tracts occur at 21-27 hpf, and embryos start to respond to touch stimuli (Carmean & Ribera, 2010). At 48 hpf, the zebrafish brain ventricle forms (Chang et al., 2016). A functional blood-brain barrier presents at 3 days post fertilization (dpf) (Fleming et al., 2013; Quiñonez-Silvero et al., 2020). Glial cells, including oligodendrocytes, Schwann cells, and astrocytes, are found in zebrafish larvae at 4 dpf (Neely & Lyons, 2021). This rapid neurogenesis allows advanced studies to be performed in the early stages of zebrafish development. In contrast to mammals, zebrafish complete embryogenesis at 3 dpf and have most discrete organs developed at 5 dpf (Bauer et al., 2021; Chu & Sadler, 2009). European animal welfare legislation (Directive 2010/63/EU) defines "protected vertebrae" as independently feeding larval stages (Parliament & Council, 2010). Zebrafish embryos predominantly feed on yolk until 5 dpf and, therefore, are not protected by European animal welfare legislation and are not considered as independently feeding animals, which allows researchers to take advantage of this exposure window for neurotoxicity studies, such as neurobehavior (Sales Cadena et al., 2021), neurodevelopment (Sales Cadena et al., 2021), neurological drug screening (Rosa et al., 2022), and receptor function (McLean & Fetcho, 2004).

## 3. The fish embryo acute toxicity test as a method to determine the lethal effect of environmental pollutants

The assessment of acute toxicity provides information on the adverse effects of the test chemicals after immediate or short-term exposure. The measurement of the lethal concentration 50 (LC50) is one of the endpoints used in chemical screening for acute toxicity in the zebrafish model (OECD, 2013b; Wolf & Segner, 2023). The LC50, by definition, is the amount of a test substance estimated to be lethal to 50% of the test animals within a specific duration of exposure (Gad, 2014). The fish embryo toxicity test (FET) has been approved by the working group of national coordinators of the OECD as a tool to determine LC50 on embryonic zebrafish (Braunbeck et al., 2015). Briefly, fertilized zebrafish eggs (before 16 cell-stage) are collected and are immediately exposed to test solution until 96 hpf. Fertilized eggs are screened with

stereomicroscopy and transferred to 24-well plates. The test medium is renewed daily, and the lethal endpoints are recorded from 24-96 hours. The lethal endpoints specified by the OECD include coagulation of the embryo (24 hr-96hr), lack of somite formation (24 hr-96hr), non-detachment of the tail (24 hr-96hr), and lack of heartbeat (48-96 hr). At the end of the exposure, acute toxicity and the LC50 is determined by cumulative mortality.

The FET is a good surrogate for rodent models and the AFT (Belanger et al., 2013; Braunbeck et al., 2015; Lammer et al., 2009). For example, Ali et al. suggested zebrafish embryos are a good predictive model for evaluating toxicity due to a strong correlation between the zebrafish LC50 from the FET and the rodent lethal dose 50 (LD50) over 60 test chemicals (Ali et al., 2011). Lammer et al. found that both the FET and the AFT provided highly similar results in an evaluation of 143 test substances (Lammer et al., 2009). The FET appears to be a valuable assay in determining LC50 from test chemicals; however, the characteristics of the test chemical and limited bioavailability capacity in embryonic zebrafish may affect the applicability of the FET (Sobanska et al., 2018). For example, the chorion is fenestrated with 0.5 μM diameter pores that allow passage of small molecules, including water, ions, and chemicals; however, it may act as a barrier for chemicals with a high molecular weight (≥ 3 kDa) or molecules with solvents, side chains, and electric charges (OECD, 2013b). Although many studies support embryonic zebrafish as a more sensitive model than adult fish, zebrafish at the early stage may have limited bioavailability or biotransformation capacity for specific chemical compounds (Klüver et al., 2015). For example, Kluver et al. indicated that some neurotoxic compounds were more toxic in adult zebrafish than embryonic zebrafish (Klüver et al., 2015). Glaberman et al. found that the embryo-based test had a lower sensitivity for neurotoxic pesticides than the juvenile fish toxicity test (Glaberman et al., 2017). Additionally, it has been argued whether using chorionated or dechorionated zebrafish embryos benefits the FET (Henn & Braunbeck, 2011). Dechorionation has been suggested to improve the results of the FET but dechorionation is often associated with lower survival rates (Henn & Braunbeck, 2011). Olivares et al. indicated the removal of the chorion in arsenic-exposure zebrafish embryos increased mortality and developmental abnormalities at 120 hpf (Olivares et al., 2016). However, Coral et al. evaluated the arsenic bimodal concentration responses in embryonic zebrafish and found both

dechorionated and chorionated zebrafish embryos had similar findings at 96 hpf (Coral et al., 2021).

## 4. Investigating the exposure to environmental pollutants as a risk factor for neurodegenerative disorders in the zebrafish model

Neurodegenerative disorders encompass a broad range of conditions characterized by progressive loss of selectively vulnerable cells in the nervous system that are essential for movement, coordination, and cognition (Ball et al., 2019). Current studies have linked environmental pollutant exposure to neurodegenerative disorders, with the majority focusing on unraveling the underlying mechanisms (Huat et al., 2019). Studies have shown that neurodegenerative disorders are multifactorial and involve a relatively complex and overlapping network (MacMahon Copas et al., 2021). Most studies suggest that environmentally induced oxidative stress, apoptosis, altered neurotransmission, and epigenetic modification contribute to neurodegenerative disorders (Franco et al., 2009; Rana, 2008). Among these, oxidative stress is proposed to be the central regulator in response to environmental stressors and leads to neurologic deficits (Dionísio et al., 2021; Sayre et al., 2008).

AD is the most prevalent neurodegenerative disorder that primarily affects the elder population (Chen & Zhong, 2014). Clinical manifestations of AD patients include dementia, impaired learning, and progressive cognitive dysfunction (Goel et al., 2022; Zhao & Zhao, 2013). The hallmark of the neuropathologic finding is the intraneuronal and extracellular amyloid β (Aβ) aggregates accompanied by intracellular neurofibrillary tangles (NFTs) composed of hyperphosphorylated tau protein, distributed throughout hippocampus, temporal lobe, frontal lobes, and frontal cortex of the brain (Glenner & Wong, 1984). The pathogenesis of AD is still unclear; however, oxidative stress has been considered as the primary contributor in AD patients (Chen & Zhong, 2014). Oxidative stress induces mitochondrial dysfunction, triggers the caspase pathway, and leads to cellular apoptosis (Betteridge, 2000). Oxidative stress also promotes the production of hyperphosphorylation Tau protein by down-regulating protein phosphatase 2A (PP2A), a major tau phosphatase in the human brain (Tönnies & Trushina, 2017). Moreover, oxidative stress impairs the proteasome, results in protein misfolding and leads to Aβ plaque

accumulation (Zhao & Zhao, 2013). Furthermore, studies have shown that oxidative stress mediates increased levels of neuroinflammation with microglial cell activation (Bisht et al., 2018; Wilkinson & Landreth, 2006). Collectively, oxidative stress facilitates cellular apoptosis, formation of Aβ plaques, hyperphosphorylation of Tau protein, and neuroinflammation that prompts AD development (Chen & Zhong, 2014).

Metal exposure has been proposed to have a role in AD patients (Huat et al., 2019). Increased amounts of copper, zinc, iron, aluminum, and mercury had been detected in the serum and brain of AD patient (Huat et al., 2019). Aluminum has the potential for neurotoxicity and strongly correlates to neurodegeneration (Exley, 2014). Studies reported a higher incidence rate of AD patients in the areas where the drinking water detected more elevated levels of aluminum (Flaten, 2001; Martyn et al., 1989). The Tau mouse model with 2 mM orally administrated aluminum progressively showed tau accumulation, apoptosis, and neurologic dysfunction (Oshima et al., 2013). It is suggested that an excess glutamate level induces neuronal cell damage by generating free reactive radicals and inhibiting antioxidant enzymatic activity. Kaur et al. investigated aluminum-induced neurotoxicity in the zebrafish model and found zebrafish with 200 mg/kg daily exposure of AlCl3 had increased oxidative stress, reduced antioxidant levels, altered neurotransmitters, and exhibited learning and memory deficits (Kaur et al., 2022). Lee et al. suggested other metals, such as lead, trigger AD by identifying sortilin-related receptor, L (DLR class) A repeats-containing (SORL1), an AD genetic risk factor, in the lead-exposed embryonic zebrafish (Lee et al., 2017).

PD is the second most common neurodegenerative disorder that begins in mid to late life (Tanner & Goldman, 1996). PD patients show typical symptoms such as bradykinesia, slow movement, and difficulties in fine motor control (Hayes, 2019). Degeneration and loss of dopaminergic neurons in the substantia nigra and the deposition of Lewy bodies containing α-synuclein in the less affected dopaminergic neurons are the main pathologic findings reported in PD patient (Borghammer, 2021). Diagnostic biomarkers for PD have been proposed, such as DNA oxidative products, reduced proteasome 20s activity, increased caspase-3, 8, and 9 expression, reduced dopamine levels, decreased expression of dopamine type 3 receptor (D3R),

and the presence of α-synuclein (Dauer & Przedborski, 2003; Emamzadeh & Surguchov, 2018; Hartmann et al., 2000; Hartmann et al., 2001; Miller & O'Callaghan, 2015).

While the underlying mechanism remains obscure, it is proposed that similar to that of AD, oxidative stress, dysfunctional mitochondria, apoptosis, neuroinflammation, altered neurotransmission, and antioxidant deficiency in response to environmental pollutants play a role in the dopaminergic neuronal cell death in the substantia nigra of PD patients (Dionísio et al., 2021; Yuan et al., 2007). For example, rotenone is a historically used pesticide (Yuan et al., 2007). Rats exposed to rotenone develop an impaired mitochondria complex I, in which the dysfunctional mitochondria then reduces ATP production, triggering the formation of reactive oxygen species, and resulting in cellular apoptosis and a dysfunctional proteasome, leading to cytoplasmic accumulation of α-synuclein (Heinz et al., 2017). These findings largely resemble that of the mechanism found in human PD patients. Similar findings were also observed in Fischer 344 rats orally administrated 500 and 1000 mg/kg Trichloroethylene (TCE), an industrial degreasing agent, for six weeks (Liu et al., 2010). Rats had significantly reduced mitochondrial activity with increased oxidative stress and intracellular α-synuclein accumulation. Wang et al. found 10 and 100 μM paraquat, a dipyridyl herbicide, impaired mitochondrial function, upregulated oxidative stress-related genes, altered dopamine signaling genes, and increased locomotor activity in the zebrafish larvae at 7 dpf after the exposure for 96 hrs (Wang et al., 2018). Additionally, propamocarb, a systemic fungicide, is linked to neurodegenerative disorders in the larval zebrafish through abnormal swimming behavior in response to light-dark changes after the exposure at the concentration of 100, and 1000 μg/l for 96 hrs (Liu et al., 2020). In this study, the authors also found that propamocarb exposure affected antioxidant and dopaminergic enzymatic activity and neurotoxicity-related genes. Besides pesticides, Kayln et al. reported that embryonic zebrafish exposed to anthropogenic fluorosurfactant, perfluorooctanesulfonic acid (PFOS) (0.1 mg/l), 6:2 chlorinated polyfluorinated ether sulfonate (F-53B) (1 mg/l) and sodium p-perfluorous nonenoxybenzene sulfate (OBS) (1 mg/l), from 72 to 120 hpf showed hypo-locomotion, reduced subpallial dopaminergic neurons, and reduced dopamine transporter expression (Kalyn et al., 2023).

Diagnosing neurodegenerative disorders remains challenging. Patients with neurodegenerative disorders at an early stage frequently show subtle and unclear symptoms that may overlap with other neurodegenerative conditions (Alfalahi et al., 2023). Validating diagnostic biomarkers is, therefore, essential for early diagnosis. Several biomarkers related to oxidative stress, such as elevated levels of oxidative products, increased reactive oxygen species, and altered levels of antioxidants and neurotransmitters have been widely used for detecting AD and PD.

*4.1 Oxidative stress*

Oxidative stress reflects an imbalance between the production of reactive oxygen species (ROS) and antioxidant defenses in the body (Betteridge, 2000). Excessive ROS can potentially cause severe damage to cells (Betteridge, 2000). ROS can be produced endogenously in cells as a natural by-product of normal cellular metabolism, including superoxide anion ($O^{-2}$), hydrogen peroxide ($H_2O_2$), and hydroxyl radical (HO•) (Birben et al., 2012; Murphy et al., 2022). Recent studies indicated that environmental pollution such as cigarette smoke, ozone exposure, ionizing radiation, stress, and heavy metal ions generate exogenous free radicals (Valko et al., 2005). Vertebrates are equipped with antioxidant systems, such as superoxide dismutases (SOD), catalase (CAT), glutathione peroxidase (GPx), glutathione reductase (GR), and glutathione (GSH) to counteract the adverse oxidant effects(Betteridge, 2000). However, when oxidative status is disrupted ROS attack nucleic acid, lipids, and proteins, resulting in DNA base oxidation, lipid peroxidation, and protein carbonylation, respectively. The brain is highly vulnerable to oxidative stress, having a high rate of oxygen utilization, relatively low concentrations of antioxidants and associated enzymes and, in addition, it contains a high content of polyunsaturated lipids and the biomacromolecules that are most susceptible to oxidation (Cobley et al., 2018; Sayre et al., 2008). Moreover, substantial nigral neurons appear more vulnerable to oxidative stress than other brain regions due to much lower antioxidant activity and higher metabolic rate (Ni & Ernst, 2022; Percário et al., 2020).

*4.1.1 Zebrafish as a model in oxidative stress studies*

Zebrafish at different life stages, from embryos to juvenile to adult, have been used to evaluate oxidative stress in vivo (Abbate et al., 2021). Zebrafish contain similar ROS-based signaling and defense mechanisms against environmental chemicals, including oxidants and electrophiles, to that of mammals. Many studies have adopted the zebrafish model in investigating environmental pollutant-induced oxidative stress.

The evaluation of oxidative stress is important for studying environmentally induced neurotoxicity. Many approaches have been designed to directly or indirectly measure oxidative damage (Murphy et al., 2022; Somogyi et al., 2007). An increase in ROS reflects an uncontrolled oxidative status; however, it has long been a challenge to directly analyze ROS in cells because ROS are short-lived (milliseconds or less), rapidly altered, and have low steady-state levels (picomolar to low micromolar) (Murphy et al., 2022). Conventional studies utilize dichlorodihydrofluorescein diacetate ($H_2$DCFDA) as a chemically reduced indicator to detect cellular production of ROS (Kim & Xue, 2020). In brief, this assay requires a membrane-permeable fluorogenic probe $H_2$DCFDA to diffuse into targeted cells and transform to an oxidant-sensitive compound, 2',7'-dichlorodihydrofluorescein ($H_2$DCF) through deacetylation in reaction to cellular esterase (Katerji et al., 2019). Cellular ROS rapidly oxidize $H_2$DCF to a highly fluorescent compound, 2',7'-dichlorofluorescein (DCF), for detection. $H_2$DCFDA has been reported to detect hydrogen peroxide, hydroxyl radicals, and peroxyl radicals by measuring the fluorescence intensity as analyzed by flow cytometry or by fluorescence plate reader (Bode et al., 2020; Ng & Ooi, 2021). Yang et al. found that after exposure to isoprocarb at the concentration of 1, 1.75, and 2.5 mg/L, a carbamate insecticide, the embryonic zebrafish had elevated ROS levels by increasing $H_2$DCFDA fluorescence signals after 72 hr exposure (Yang et al., 2011). Researchers are also inclined to search for more stable and enduring biomarkers for oxidative damage assessment. Although these alternative methods may not fully represent the cellular ROS status, they are promising to evaluate oxidative damage by indirectly measuring oxidative products from DNA/RNA, lipids, and protein in cells. These biomarkers include DNA/RNA oxidation, lipid peroxidation, and protein carbonylation (Murphy et al., 2022).

Oxidative nucleic acid modifications are frequently used as markers to evaluate oxidative damage. The comet assay and 8-oxo-7, 8-dihydro-2'-deoxyguanosine (8-oxo-dG)/ 8-hydroxy-2' -deoxyguanosine (8-OHdG) are two widely studied methods (Urbaniak et al., 2020; Valavanidis et al., 2009). The comet assay, also called single-cell gel electrophoresis, is a method to measure the general cellular oxidative damage to DNA by detecting DNA strand breaks and alkali-labile sites (McKelvey-Martin et al., 1993). Some research focuses on measuring the level of 8-oxo-dG or 8-OHdG, pivotal oxidative products of DNA, with several techniques such as ultraperformance liquid chromatography-mass spectrometry (UPLC-MS), enzyme-linked immunosorbent assay (ELISA), and high-performance liquid chromatography (HPLC) coupled with an electrochemical detector. Lipid peroxidation has been commonly used to indicate cell membrane damage in response to ROS-mediate injury (Ayala et al., 2014; Yoshida et al., 2013). Malondialdehyde (MDA) is one of the lipid peroxidation end-products that is well-studied, relatively stable, and is often considered a good index to estimate oxidative stress levels by reacting with TBARS (thiobarbituric acid reactive substances) (Aguilar Diaz De Leon & Borges, 2020; Ayala et al., 2014). The TBARS assay is widely applied to measure lipid peroxidation in cells, tissue, and biological fluids. It is designed to detect the reaction of lipid peroxidation products, primarily malondialdehyde (MDA), with thiobarbituric acid (TBA) (Aguilar Diaz De Leon & Borges, 2020; Apak, 2019). This end product, MDA-TBA2 adducts, also called TBARS, can be detected spectrophotometrically by colorimetric or fluorometric plate readers. Measuring the protein carbonyl level is another common approach for oxidative damage evaluation . Carbonyl groups are produced during protein carbonylation by oxidizing the protein backbones and amino acid residues such as proline, arginine, lysine, and threonine. Carbonylated proteins are reported to have relative early formation and stability compared with other oxidative products and are thus frequently used in oxidative stress studies. Detection of protein carbonylation involves the reaction with 2,4-dinitrophenylhydrazine (DNPH) with the formation of stable dinitrophenylhydrazone products, which then can be analyzed by a variety of means such as spectrophotometric assay, ELISA, and one-dimensional or two-dimensional electrophoresis followed by western blot immunoassay. Zhu et al. studied the effects of developmental exposure to the $SiO_2$ in the zebrafish model (B. Zhu et al., 2019). They found that zebrafish larvae exposed to 100 mg/L SiO2 for 5 days had significant changes in ROS levels, increased 8-OHdG content, and decreased GSH. 100 μ/L bisphenol A has been found to trigger

oxidative stress in 120 hpf zebrafish by observing an increase in fluorescence lipid peroxidation after 24 hr exposure (Guru & Arockiaraj, 2023). Butylated hydroxyanisole (BHA), a widely used chemical in cosmetics, pharmaceutical, and food industries, had been reported to trigger ROS-induced apoptosis in zebrafish larvae after 96 hr exposure with positive 8-OHdG immunofluorescence at the treated group with 1, 5, 7.5 and 10 ppm (Baran et al., 2021).

Balanced redox homeostasis requires a large amount of antioxidants to counteract ROS from causing cell damage. A variety of direct or indirect methods of measuring antioxidants are available. For example, many commercial superoxide dismutase activity kits are produced according to Beauchamp and Fridovich's method. Briefly, this method measures SOD enzymatic activity by indirectly monitoring the reduction of nitroblue tetrazolium (NBT) (Spitz & Oberley, 1989). Superoxide ions are generated from the xanthine-xanthine oxidase system and can convert NBT to NBT-formazan. The SOD in the test sample, therefore, can compete with the superoxide ions and lowers the rate of NBT-diformazan conversion. The decreased signal determines the SOD inhibition activity. CAT can be quantified by observing the decrease of hydrogen peroxide through the spectrophotometric method (Beers & Sizer, 1952; Zitka et al., 2012). Glutathione peroxidase converts glutathione (GSH) to glutathione disulfide (GSSH) (Zitka et al., 2012). The GSH/GSSG ratio is commonly accepted as an indicator that reflects cellular redox homeostasis. Sun et al. exposed zebrafish to 0, 25, 50, 75, or 150 μg/L AsIII until 120 hpf and their results indicated that a low concentration of AsIII induced oxidative stress by detecting elevated SOD, altered Cu/ZnSOD and MnSOD mRNA transcriptional levels, and increased malondialdehyde levels (Sun et al., 2019). Adeyemi et al. found increased levels of lipid peroxidation and DNA oxidation. The decreased GSH and catalase activity was observed in 96 hpf zebrafish embryonically co-exposed to atrazine (0.1 mM) and arsenic (0.8 mM) by utilizing TB, and spectrophotometric methods (Adeyemi et al., 2015).

Several transgenic zebrafish models are also employed in the study of oxidative stress (Kusik et al., 2008; Liu et al., 2015). Nuclear factor erythroid 2-related factor (Nrf2) is a key transcription factor regulating the cellular response against oxidative and nitrosative stress and has been used as a marker for monitoring oxidative stress (Ngo & Duennwald, 2022).Liu et al. successfully created a nrf2a-eGPF zebrafish model to evaluate PCB126-induced oxidative stress

mediated apoptosis and developmental toxicity (Liu et al., 2015). Kusik et al. used the EPRE-LUC-GFP zebrafish model to study mercury-induced oxidative stress (Kusik et al., 2008). Finally, Mourabit et al. developed the first stable transgenic zebrafish line Tg(3EpRE:hsp70:mCerry) to investigate the imbalance cellular redox against various environmental conditions (Mourabit et al., 2019).

### *4.2 Apoptosis*

Apoptosis, also known as programed cell death, is a pathway of cell death associated with normal eukaryotic development and maintenance of organismal homeostasis (Fadeel & Orrenius, 2005; Klim et al., 2018). The pathway is controlled by several families of proteins and is classified into two pathways: intrinsic (mitochondrial) and extrinsic (death receptor) (Elmore, 2007). Viable cells are sustained by receiving survival signals, such as growth factors, to induce the production of anti-apoptotic proteins (BCL2, BCL-XL, and MCL1) that prevent cytochrome c leakage from mitochondria. In the intrinsic apoptotic pathway, conditions such as growth factor withdrawal, DNA damage, and protein misfolding induced by endoplasmic reticulum stress activate cellular sensors to antagonize anti-apoptotic proteins and activate pro-apoptotic proteins, BAX and BAK, to form channels on the outer mitochondrial membrane and release cytochrome c, triggering caspase cascades. The extrinsic pathway employs death receptors that deliver an apoptotic signal, leading to autocatalytic caspase activation through initiator caspase 8, 9, and 10 and executioner caspases 3 and 6 (D'Arcy, 2019). Following the apoptotic pathway, the cells become shrunken with chromatin condensation, membrane blebbing, and nuclear fragmentation (Elmore, 2007).

#### *4.2.1 Zebrafish as a model in apoptosis studies*

The zebrafish is a useful experimental animal model to investigate apoptosis in vivo (McGrath & Seng, 2013). A variety of methods have been designed to evaluate apoptosis in zebrafish studies (Sorrells et al., 2013; Tucker & Lardelli, 2007). Several staining methods are used to detect apoptosis in tissue sections (Banfalvi, 2017). Acridine orange (AO), Hoechst staining, Annexin V, DNA ladder, Terminal deoxynucleotidyl transferase dUTP nick end labeling (TUNEL) assay, Caspase-3/7 activity, and ssDNA staining have been described

(Butterick et al., 2014; Crowley et al., 2016; Frankfurt et al., 1996; Kyrylkova et al., 2012; Majtnerová & Roušar, 2018; van Engeland et al., 1998).

AO stain, first described by Strugge and Hilbrich in 1941, is a nucleic acid selective metachromatic fluorescent dye that permeates both live and dead cells and preferentially binds to nucleic acid, but particularly stains apoptotic nuclei (Ribble et al., 2005; S, 1941). AO stain is one of the most commonly used techniques, which can be performed rapidly on embryonic zebrafish in multiwell plates (Pinheiro-da-Silva & Luchiari, 2021). Parlak et al. observed zebrafish larvae at 96 hpf were oxidatively stressed with decreased SOD, CAT, GPx, increased MDA and ROS, and elevated apoptosis signaling, highlighted with AO stains after 96 hr exposure to 50 mg/l deltamethrin (Parlak, 2018). Embryonic zebrafish exposed to 400 nM methylmercury had increased AO-positive apoptotic cells detected in the brain at 96 hpf (J. Zhu et al., 2019). Similarly, 9 μM cadmium-induced apoptosis was detected by AO stain at 24 hpf (Monaco et al., 2017).

TUNEL assay has been considered a sensitive, quantitative, and universally applicable method for identifying apoptotic DNA fragmentation (Kyrylkova et al., 2012; Mirzayans & Murray, 2020). Nuclear fragmentation accompanied by 3' hydroxyl terminus of DNA breaks is a hallmark finding of apoptosis. The TUNEL assay utilizes a unique enzyme, Terminal deoxynucleotidyl Transferase (TdT), to detect and catalyze modified fluorescent conjugated deoxynucleotides (dUTPs) that preferentially bind to DNA breaks. The catalyzed dUTPs emit a fluorescence signal and are detected by fluorescence microscopy or flow cytometry.

Studies have used monoclonal antibodies to directly detect caspase-3 in fixed zebrafish embryos (Sorrells et al., 2013). With the advancement of molecular techniques, more studies have chosen quantitative polymerase chain reaction (qPCR) and whole-mount immunofluorescence to detect apoptotic-related genes (Guo et al., 2021; Sorrells et al., 2013). Moreover, with the advantage of clustered, regularly interspaced, short palindromic repeats (CRISPR-Cas9) genome editing methods, multiple transgenic zebrafish lines have been created (van Ham et al., 2010; Yamashita et al., 2008). For example, Annexin V (A5) is a phospholipid-binding protein with a high affinity for phosphatidylserine and has been used as a maker to detect

apoptotic cells (Farber et al., 2003; Mirsaeidi et al., 2016). van Ham et al. developed a secA5-YFP transgenic line by fusing secreted A5 to yellow fluorescent protein to label apoptotic cells in zebrafish embryos (van Ham et al., 2010). Synthetic zebrafish pro-caspase-3 had been microinjected to one-cell stage zebrafish embryos, and pro-caspase-3 transgenic zebrafish have shown markedly sensitive to UV irradiation which induced extensive apoptosis (Yamashita et al., 2008).

*4.3 Neurotransmission*

Neurotransmitters are chemical messengers carrying information between neurons and are critical for neurodevelopment, learning and memory, and behavior (Carvajal-Oliveros & Campusano, 2020; Hyman, 2005; Teleanu et al., 2022). The neurotransmitter system is conserved throughout vertebrates (Ncube et al., 2022). Major neurotransmitters such as glutamate, GABA, catecholamines, serotonin (hydroxytryptamine or 5-HT), and histamine systems have been well-described (Teleanu et al., 2022). Exposure to environmental stimuli, drugs, chemotherapeutic agents, radiation, or food additives is linked to neurodegenerative diseases and neurologic disorders by affecting synthesis, storage, and the release of neurotransmitters (Fuertes & Barata, 2021; Horzmann & Freeman, 2016; Li et al., 2016).

Glutamate is the primary excitatory neurotransmitter that regulates synaptic transmission and neuronal excitability (Meldrum, 2000; Pal, 2021). Glutamate is important for memory, cognition, and mood regulation and is associated with neurodegenerative diseases (Pal, 2021; Reddy-Thootkur et al., 2022). Conversely, GABA is the major inhibitory neurotransmitter and is widely distributed throughout the brain (Ngo & Vo, 2019; Owens & Kriegstein, 2002). GABA modulates post-synaptic receptor activity, hyperpolarizes the cells, and inhibits the transmission of action potentials (Gerrard et al., 2018; Shrivastava et al., 2011). Impaired GABA signaling is linked to multitudes of neurologic and psychiatric disorders (Chiapponi et al., 2016; Sarawagi et al., 2021; Schür et al., 2016). Catecholamines are monoamine neurotransmitters that consist of a group of chemicals with hydroxyl groups on a benzene ring, in which dopamine, norepinephrine, and epinephrine are the main neurotransmitters, that are associated with movement, memory, and depression (Jung-Klawitter & Kuseyri Hübschmann, 2019). The histaminergic system exerts

effects on memory, cognition, circadian rhythm, and feeding and drinking (Ishizuka et al., 2006; Passani et al., 2000; Provensi et al., 2020; Rozov et al., 2015). Finally, serotonin (5-HT) is a biological amine and is implicated in neurodevelopment, neuroendocrine function, mood, and circadian rhythms (Bao & Swaab, 2019; Chaouloff, 2000; Martinowich & Lu, 2008).

### *4.3.1 Zebrafish as a model for neurotransmission*

The neurotransmitter system is highly conserved between zebrafish and mammals (Horzmann & Freeman, 2016). Zebrafish share the common neurotransmitter pathways with mammals, making the zebrafish model a powerful tool for studying mechanisms of chemical neurotoxicity (Rico et al., 2011; Rosa et al., 2022). Neurotransmitters are mainly measured and quantified by HPLC coupled with fluorescence, optical density, mass spectroscopy, luminescence, or electrochemical methods (Cifuentes Castro et al., 2014). Tufi et al. detected and quantified multiple neurotransmitters by hydrophilic interaction liquid chromatography (HILIC) coupled to tandem mass spectrometry (MS/MS) and further used this analytical method to study neurotransmitters in zebrafish embryos (Tufi et al., 2016). Several molecular techniques have been used to evaluate gene expression associated with neurotransmitters, such as qPCR, microarray, RNA-seq, and next-generation technologies (Horzmann & Freeman, 2016; Weber et al., 2013; Wirbisky et al., 2015).

Tufi et al. first used HILIC to evaluate neurotransmitters in the zebrafish model (Tufi et al., 2016). Eight neurotoxic pesticides were selected and exposed to embryonic zebrafish for 5 days, and a significant change in neurotransmitter levels during early zebrafish development was observed in their study. Wirbisky et al. investigated GABA during the early life stage of zebrafish with lead exposure (Wirbisky et al., 2014). HPLC results showed increased GABA levels at 48 hpf in the 10 and 50 ppb treatments but revealed a significantly decreased GABA level at 72 hpf in all treated groups (10, 50, and 100 ppb). Altered GABAergic pathway gene expression was also detected during the study. Kanungo et al. found that zebrafish embryos exposed to inorganic arsenic had reduced acetylcholinesterase (AChE) activity, altered tyrosine hydroxylase positive (TH) (dopaminergic) neuron development, and increased spinal motor neurons in 72 hpf zebrafish larvae with 200 and 400 mg/L exposures (Kanungo et al., 2023). Finally, Ding et al. found that 10–100 μg/L photoaged microplastics, ubiquitous neurotoxic

environmental contaminants, induced neurotoxicity through oxidative stress and abnormal neurotransmission in the zebrafish at 120 hpf by observing significantly altered antioxidant enzymes, oxidative products, and increased levels of neurotransmitters (Ding et al., 2023).

*4.4 Epigenetic modification*

Epigenetics involves the molecular modification of genes and proteins that occurs without changing DNA's primary structure. DNA methylation, histone modification, and non-coding RNA (ncRNA) are the three most studied epigenetic mechanisms (Nikolac Perkovic et al., 2021). DNA methylation is a heritable epigenetic modification and has been most intensely investigated (Almatarneh et al., 2022). DNA methylation is essential for gene expression, genomic imprinting, embryonic development, and memory formation and storage (Elhamamsy, 2017). The principal role in regulating gene expression of DNA methylation is adding methyl groups to the C5 position of the cytosine ring of DNA, forming 5-methylcytosine (5mC) (Ahkin Chin Tai et al., 2021). In mammals, this process frequently occurs within CpG islands through a group of DNA methyltransferases (Dnmts). Several Dnmts have been discovered, with Dnmt1, Dnmt3A, and Dnmt3B most frequently discussed (Jin & Robertson, 2013). Dnmt1 is a major enzyme mainly responsible for DNA methylation and is involved in inheritance. Dnmt3A and Dnmt3B are predominantly associated with de novo methylation. Hypermethylated genes with the presence of mC typically result in transcriptional silencing by forming compacted and closed chromatin. However, ten-eleven translocation (TET) enzymes can actively demethylate genes by oxidizing 5mC to 5-hydroxymethylcytosine (5hmC), 5-formylcytosine (5fC) and further to 5-carboxycytosine (5caC) and activate gene transcription.

Histone modification is one of the most important reversible epigenetic modifications. Histone modification has been discovered as a regulator in neurogenesis and neurodegenerative and neuropsychiatric disease development (Bannister & Kouzarides, 2011; Millán-Zambrano et al., 2022; Santana et al., 2023). Mechanisms of histone modification include methylation, acetylation, biotinylation, SUMOylation, phosphorylation, and other chemical modifications that alter the structure of the chromatin or histone core. Enzymes such as histone-deacetylases (HDACs), histone-acetyltransferases (HATs), and histone-methyltransferases (HMTs) are

essential in transcriptional regulation (Bannister & Kouzarides, 2011). Four core histone proteins (H2A, H2B, H3, and H4) are wrapped by 147 bp of DNA and stabilized by a linker histone (H1). N terminal histone tails and histone globular domains are locations frequently targeted. Histone methylation with methylated lysines or arginines may be associated with either transcriptional activation or repression. Histone acetylation with lysine residues acetylated by HAT leads to increased transcription. On the other hand, chromatin condensation can occur with histone deacetylation by HDAC.

Non-coding RNAs (ncRNAs) have been implicated as critical epigenetic regulators in posttranscriptional silencing (Morris, 2009). Regulatory ncRNAs include micro-RNA (miRNA), small interfering RNA (siRNA), piwi-interacting RNA (piRNA), and long non-coding RNA (lncRNA) (Kaikkonen et al., 2011). Among tese, miRNA are well-described, play a fundamental role in gene regulation, and are linked to normal developmental pathways and pathologic conditions. miRNAs are single-stranded, relatively short, and approximate 18-22 nucleotides. miRNAs are formed from long double-stranded RNA enzymatically processed into smaller fragments by RNase III enzymes (DICER). Repression on targeted genes occurs when miRNA and RNA-induced silencing complex (RISC) detect an improper base pairing.

### *4.4.1 Zebrafish as a model of epigenetic modification*

Many studies indicate that zebrafish are good models for studying the epigenetics (Cavalieri & Spinelli, 2017). First, with genome editing becoming more mature and prevalent, such as zinc finger activator–like effector nucleases (TALENs) and CRISPR/Cas9, the design and generation of mutants of proteins involved in the epigenetic process have become possible (Y. Li et al., 2018; Nomura, 2018; Waryah et al., 2018). Second, zebrafish contains 8 DNA methyltransferase orthologs to mammalian DNMTs (Balasubramanian et al., 2019). Third, zebrafish do not have genome imprinting; rather, different from mammals and other species of fish, zebrafish have maternal genome reprogramming with passive demethylation during early development, whereas the paternal zebrafish genome is resistant to demethylation (Balasubramanian et al., 2019; Kamstra et al., 2015). Therefore, many genes involved in the epigenetics process in the early embryos are maternally transferred, and prolonged survival is possible in these mutants during the first stage of development.

Numerous methods of evaluating epigenetic modifications have been designed (Li, 2021). For example, conventional techniques such as bisulfite genomic sequencing analysis are used for analyzing DNA methylation (Li & Tollefsbol, 2011; Miyata et al., 2017). In brief, this method utilizes sodium bisulfite to convert cytosine to uracil in single-stranded DNA and recognized as thymine in subsequent PCR amplification and sequencing; however, 5mCs are spared this conversion and remain as cytosine, allowing 5mCs to be detected from unmethylated cytosine (Li & Tollefsbol, 2011; Miyata et al., 2017; Strömqvist et al., 2010). Other emerging tools, such as global analysis and third-generation sequencing-based technologies, are also frequently applied (Macleod et al., 1999; Martin et al., 1999; Searle et al., 2023). Chromatin immunoprecipitation (CHIP) assay is a commonly used method for detecting histone modification (Yan et al., 2016). This specific antibody-directed ChIP assay is a particularly useful technique in studying DNA-protein interactions that allows the chromatin structure surrounding particular DNA sequence to be analyzed (Bogdanović et al., 2013; Terrazas-Salgado et al., 2022). Novel methodologies have been developed to identify chromatin occupancy sites using immunoprecipitation-based approaches followed by next-generation sequencing (NGS) (O'Neill et al., 2006).

It is widely accepted that stimuli such as changes in environment, nutrition, and chemical compound exposure trigger epigenetic modifications (Lakstygal et al., 2018; S. Wang et al., 2022). For example, Li et al. used a 5-methylcytidine-specific antibody to assess global methylation on zebrafish that were exposed to sodium arsenite at the embryonic stage (Baran et al., 2021). They found zebrafish larvae at 24 and 48 hpf had abnormal genomic DNA methylation patterns with decreased methylation in the brain with exposure to 2 mM sodium arsenite. Bian et al. investigated DNA methylation and gene expression in cadmium-exposed embryonic zebrafish (Bian & Gao, 2021). They targeted global methylation and DNMTs levels in 24 hpf zebrafish and observed a significantly up-regulated *dnmt1* expression and down-regulated *dnmt3* and global methylation at 0.89 μM. Wirbisky et al. utilized microarray to analyze zebrafish larvae at 72 hpf and found zebrafish in the 30 ppb treated group had altered miRNA related to neurodevelopment, differentiation, and maturation after atrazine exposure (Wirbisky et al., 2016). Wang et al. used whole genome bisulfite sequencing to assess the

neurologic effects of atrazine exposure on DNA methylation in female zebrafish that were exposed at embryonic stages (S. Wang et al., 2022). Their results demonstrated that atrazine at 30 ppb had the most increased methylation of genes associated with neurological pathways.

## 5. Zebrafish neurobehavior

Neurobehavior evaluation is one of the most sensitive methods of neurotoxicity assessment (Anger, 2003). Zebrafish behavior is becoming increasingly popular as a measurable phenotype reflecting alterations in normal physiology (Kalueff et al., 2013). The deviated behavior may represent possible functional outcomes of chemical toxicity, disruption of neurotransmission, altered intracellular signaling, abnormal musculoskeletal system, and altered growth and development (Bailey et al., 2013; Tufi et al., 2016; Vorhees et al., 2021). In addition, zebrafish models have frequently been used to evaluate neurotoxic compound-associated neurobehavioral changes, such as locomotor activity, anxiety, agitation, sedative effects, and learning and memory behaviors (A. Stewart et al., 2012).

### *5.1 Zebrafish embryonic and larval locomotor activity*

Zebrafish embryos begin spontaneous muscle contractions at 18 hpf (Menelaou et al., 2008). Embryos start to twitch in response to mechanical stimulation at 24 hpf (Saint-Amant & Drapeau, 1998). By 2 dpf, embryos present tail-flip and fast escape response to touch stimuli (McClenahan et al., 2012; McKeown et al., 2009). Zebrafish develop mature swimming at 4-5 dpf, following the inflation of the swim bladder (Winata et al., 2009). Zebrafish at early life stages exhibit a broad range of behavioral phenotypes, such as optomotor response, optokinetic response, photomotor response (PMR), spontaneous activity, prey capture, startle response, thigmotaxis, habituation, and visual motor response (VMR) (Apak, 2019; Basnet et al., 2019; Carbaugh et al., 2020; Fleisch & Neuhauss, 2006; Schnörr et al., 2012). Among these, PMR and VWR are frequently used neurobehavioral endpoints in the zebrafish model (Horzmann & Freeman, 2018; Ortmann et al., 2022; Reif et al., 2016).

The PMR is a nonvisual, robust, reproducible behavioral response to intense photic stimuli by activating light-sensitive neurons in the hindbrain of the developing zebrafish embryos (Kokel et al., 2013). Briefly, at 24-30 hpf, zebrafish embryos during the PMR test are kept in the dark with two light pulses. Following the light stimulus, zebrafish embryos go through three phases: latency phase, excitation phase (PMR phase), and refractory phase (Carbaugh et al., 2020; Kokel & Peterson, 2011). The changes in movement in response to light stimuli have been reported to be related to increased relative risk for developmental malformations at 120 hpf (Ortmann et al., 2022; Reif et al., 2016).

The VMR, compared to the PMR, is a visual motor response provoked by changes in ambient illumination (Burton et al., 2017). Zebrafish larvae make frequent and low-amplitude propulsive and turning movements at stable lighting conditions but present a high-angle turn, followed by a propulsive movement at an abrupt transition from light to dark (Burton et al., 2017; Horzmann & Freeman, 2018). The altered locomotor activity may reflect impaired brain function, neurodevelopment, neurotransmission, or visual pathways (Burton et al., 2017).

Many studies utilized the PMR and VMR in investigating environmental-induced neurotoxicity (Horzmann et al., 2020; Huang et al., 2023). For example, Horzmann et al. found that zebrafish embryos exposed to TCE showed altered behavioral responses during PMR and VMR assays after exposure to 5, 50, and 500 ppb for PMR, and 500 ppb for VMR assays for 72 hr (Horzmann et al., 2020). Olivares et al. detected hypoactive locomotor PMR in the zebrafish larvae exposed to 900-1000 mM arsenic (Olivares et al., 2016). Perfluoroheptanoic acid (PFHpA) is an organic molecule with fluorinated carbons used in many consumer products (Petrovic et al., 2013). Huang et al. found that zebrafish embryos exposed to 0.1 μM PFHpA for 7 days showed developmental and mitochondrial toxicity and reduced locomotor activity on the VMR (Huang et al., 2023). Gyimah et al. found that Bisphenol AF (BPAF), a chemical widely used in manufacturing, induced oxidative stress and apoptosis in the zebrafish model (Gyimah et al., 2022). They further assessed locomotor activity on larvae at 120 hpf by VMR in 0.1, 0.3, and 1.0 μM treatment groups, and their findings indicated that BPAF induced a dramatic reduction of locomotor activity. Lockwood et al. demonstrated a hypoactive locomotor response with sedative effects at 4% ethanol after exposure to ethanol in larval zebrafish (Lockwood et al., 2004).

Zebrafish larvae are sensitive to neuroactive agents, and it is suggested that they have locomotor activity responses similar to those of mammals (F. Li et al., 2018). Some neurotoxic substances were found to be less acutely toxic to the zebrafish embryos than to the adult fish; however, Kluver et al. found zebrafish larvae exhibited altered locomotor activity in response to the concentrations of neuroactive compounds that caused lethality in adult zebrafish (Klüver et al., 2015). Therefore, their studies suggested the alteration of locomotor in zebrafish larvae could improve the prediction of acute toxicity for neurotoxic compounds in adult zebrafish.

Although in our review article we mainly focus on investigating the early life zebrafish exposed to environmental pollutants; several studies emphasize the effect of early life exposure-induced long-term neurotoxicity in adult zebrafish.

*5.2 Adult zebrafish behavior*

Adult zebrafish have a higher complexity of behavioral responses than those in the early stage of zebrafish (Kalueff et al., 2013; Norton & Bally-Cuif, 2010). For example, associative learning is described in adult zebrafish but has yet to be established in zebrafish larvae (Kenney, 2020; Tan et al., 2022). Adult zebrafish behavioral assays have frequently been used for evaluating locomotor activity, sedation, agitation, anxiety, learning and memory, social reaction, and changes after xenobiotic exposure (Norton & Bally-Cuif, 2010). Neurobehavioral tests usually require video tracking software to analyze parameters such as velocity, movement, mobility, total distance moved, and latency to first zone entry (Cachat et al., 2011; Wang et al., 2020).

Several behavioral assessment tests in the adult zebrafish model have been adapted from rodent models and are used in neurotoxicity studies, such as novel tank test, open-field test, inhibitory avoidance test, novel object recognition test, maze test, shoaling test, and light and dark test (Bailey et al., 2013). For example, novel tank and open field tests in the zebrafish model are neurobehavioral tests similar to rodent open field tests for assessing anxiety-related behavior (Ahmad & Richardson, 2013; A. M. Stewart et al., 2012). Researchers use maze tests to

evaluate rodent cognition deficits in the zebrafish model as well (Benvenutti et al., 2021). (Mathur & Guo, 2011)

Few studies have investigated the long-term neurotoxicity in adult zebrafish exposed to neurotoxic compounds during the early life stage. In one example, Wang et al. investigated the continuance of the toxic effects of lead on zebrafish neurobehavior from larval to adult age (Wang et al., 2015). They found that the gene expression linked to neurodevelopment and neurotransmitter systems altered in a similar pattern in both larvae and adult zebrafish. In addition, zebrafish behaviors were evaluated through VMR, open field test, novel tank test, social interaction test, and T maze test. The result revealed consistency in locomotion parameters in both larvae and adult zebrafish, including increased distance traveling, cumulative mobility, and velocity. They, therefore, speculated that the disruption of early neurodevelopment, as well as prolonged modulation of neurotransmitter systems, contributed to the lead-induced neurobehavioral disorders observed in juveniles and adults. Moreover, embryonic exposure to methylmercury had been found to alter locomotor activity and anxiety-related responses, in addition to dopamine level changes in both larval and adult zebrafish (Glazer & Brennan, 2021). Although several zebrafish neurobehavior assays have been proven to provide a phenotypic outcome of neurotoxicity and are useful to assess xenobiotic exposure, the limitation of lack of standardization in methods has long been a concern.

## 6. Developmental origins of health and disease (DOHaD) concept

The Developmental Origins of Health and Disease (DOHaD) concept proposes that environmental factors acting during critical periods of development, such as the preconceptional, prenatal, and early postnatal stages, can have lasting effects on health and disease risk later in life (Hanson, 2015; Heindel et al., 2015; Lacagnina, 2020). First introduced by David Barker and colleagues, the concept emerged from the observation that low birth weight was associated with an increased risk of heart disease, diabetes, and hypertension in adulthood (Barker et al., 1993). Barker et al. proposed that poor nutrition or stress during fetal development and gestation could lead to permanent alterations in organ structure and function, a process now known as developmental programming (Barker et al., 1993). While these early-life adaptations may confer

short-term survival advantages, they can increase susceptibility to non-communicable diseases later in life (Hanson, 2015; Lamberto et al., 2021).

Several studies have demonstrated that developmental exposure to environmental chemicals can cause long-term changes in mammalian models (Bihaqi & Zawia, 2013). For instance, early-life exposure to lead (Pb) is strongly linked to persistent neurological impairments. Studies in rodents and non-human primates have shown that Pb exposure during infancy disrupts the expression of the tau gene later in life, potentially increasing susceptibility to tauopathies (Bihaqi & Zawia, 2013). Additionally, infantile Pb exposure has been associated with altered regulation of amyloid precursor protein (APP) and its beta-amyloid (Aβ) products in old age (Wu et al., 2008).

Unlike mammals, zebrafish develop externally, allowing direct exposure to environmental stressors from the earliest embryonic stages without maternal influence (Bambino & Chu, 2017; Zhao et al., 2024). Their transparent embryos enable real-time observation of developmental abnormalities, making zebrafish uniquely suited for studying teratogenic and toxicological effects (Aluru, 2017). Additionally, their high fecundity promotes experimental reproducibility (Tan et al., 2022). In addition, a wide range of validated larval and adult behavioral assays further allows assessment of long-term effects of developmental toxicant exposure, establishing zebrafish as a powerful model for investigating the DoHaD principles (Horzmann & Freeman, 2016; Horzmann & Freeman, 2018).

Several studies have investigated environmental stressors in zebrafish models within the framework of the DOHaD concept. For example, Horzmann et al. used transcriptomic approaches to investigate the effects of atrazine exposure during embryogenesis and observed significant changes in the female zebrafish brain. Transcriptomic profiling at 9 mpf female revealed altered gene expression pathways associated with organismal injury and cancer, with beta-estradiol and the estrogen receptor identified as key upstream regulators. Additionally, global brain DNA methylation analysis at 12 mpf showed increased levels of 5-methylcytosine (5 mC) in females exposed to 0.3 ppb atrazine during embryogenesis. These findings demonstrate that early atrazine exposure induces delayed neurotoxicity consistent with the

DOHaD framework (Horzmann et al., 2022). Lee et al. found that embryonic exposure of zebrafish to 100 μg/L Pb results in sex-specific changes in gene expression within the adult brain, particularly affecting genes related to the neurological system in females and genes associated with cancer in males. These results suggest that early-life lead exposure has long-term, sex-dependent effects on brain development and function and align with the DOHaD framework (Lee et al., 2018).

## 7. Limitations in using embryonic zebrafish as models in assessing neurotoxicity associated with environmental pollutants

Although embryonic zebrafish as a model provides a powerful platform for neurotoxicity biomedical research, interspecies differences should be considered when translating the findings in zebrafish to humans. For example, despite genetic similarities to humans, zebrafish genes are duplicated, which increases the genetic variability and the challenge of investigating genomic function (Howe et al., 2013). Such variability and species differences may influence the neurotoxic effects. The nervous system in early-stage zebrafish may not fully represent the neuroanatomy and neural functions of adult zebrafish or humans (Bloch et al., 2019). For example, embryonic zebrafish have an incomplete blood-brain barrier, which may result in neurotoxic compound penetration differences (Fleming et al., 2013). In addition, while the transparency of zebrafish at the early developmental stages enhances neuroanatomic studies and gains valuable insights into fields of neurodevelopment, neurologic functions, and neurodegenerative diseases, the embryonic zebrafish brain is less complex and lacks specific neural structures compared to humans, and therefore, it is crucial to consider the variation while interpreting the zebrafish findings and translating to humans (Bloch et al., 2019). Neurobehavioral assessment in embryonic zebrafish are limited by a small range of measurable behaviors compared to adult zebrafish; in addition, more complex neurobehavior, such as cognitive function, may be less sophisticated compared to adult stage or mammalian models (Bailey et al., 2013). Zebrafish possess metabolism and pharmacokinetics similar to humans in drug absorption, distribution, metabolism, and excretion; however, while using zebrafish as the model for evaluating neurotoxic compounds, the difference in metabolite processing and enzymatic activity between zebrafish embryos, later developmental stages, and humans will need

to be taken into consideration during interpretation. For example, the metabolic pathway of methylmercury in humans mainly involves cysteine and glutathione, particularly in the process of detoxification (Bridges et al., 2012), whereas glutathione S transferase and metallothioneins have been considered the important detoxify enzymes in the metabolic processing pathway of methylmercury in zebrafish, which may lead to variations of toxic efficacy between species (Henriques et al., 2023).

## 8. Future direction

Public awareness of environmental concerns including widespread chemical contamination has increased over the past few years and studying the potential neurotoxicity associated with environmentally relevant concentrations of pollutants is critical to understanding potential human health effects. While most studies emphasize evaluating the effects of early life exposure to neurotoxic compounds in the zebrafish model, fewer studies have investigated the neurotoxicity from environmentally relevant concentrations of neurotoxic compounds **(Table 2)**. For example, Sun et al. explored an environmentally relevant concentration of organic benzophenone-3 (BP3) and inorganic UV filters containing titanium dioxide nanoparticles co-exposure induced neurodevelopment toxicity in zebrafish (Sun et al., 2023). The US EPA regulated maximum contaminant level (MCL) of atrazine in drinking water is 3 ppb; however, Tai et al. observed that zebrafish had hyperactive locomotion on VMR when exposed to 0.3 ppb (Ahkin Chin Tai et al., 2021). TCE is regulated in drinking water by the US EPA with MCL of 5 ppb. Horzmann et al. exposed embryonic zebrafish to 0, 5, 50, and 500 ppb and observed a decreased percent hatch, shorter and narrow head, and increased duration of inactivity of PMR beginning at 5 ppb (Horzmann et al., 2020).

## 9. Conclusion

The zebrafish model is widely accepted in neurotoxicity assessment studies. Zebrafish embryos are suitable for high-throughput systems for chemical screening under current animal welfare legislations and appear more sensitive in response to environmental chemicals than in

adult zebrafish. Advances in FET tests enable fast preliminary acute toxicity results of test chemicals. Currently existing and newly introduced chemical wastes are environmental concerns. Environmental pollutants have been strongly linked to neurodegenerative disorders in humans. Although the underlying mechanisms are relatively complex, the zebrafish model provides a platform for evaluating neurotoxicity induced by environmentally relevant concentrations of toxicants. Mechanisms that can be evaluated include oxidative stress, apoptosis, neurotransmitter systems, neurobehavior, and epigenetic modifications. Although more research is needed to better expand the zebrafish platform, the embryonic model has shown great potential for environmentally induced neurotoxicity research.

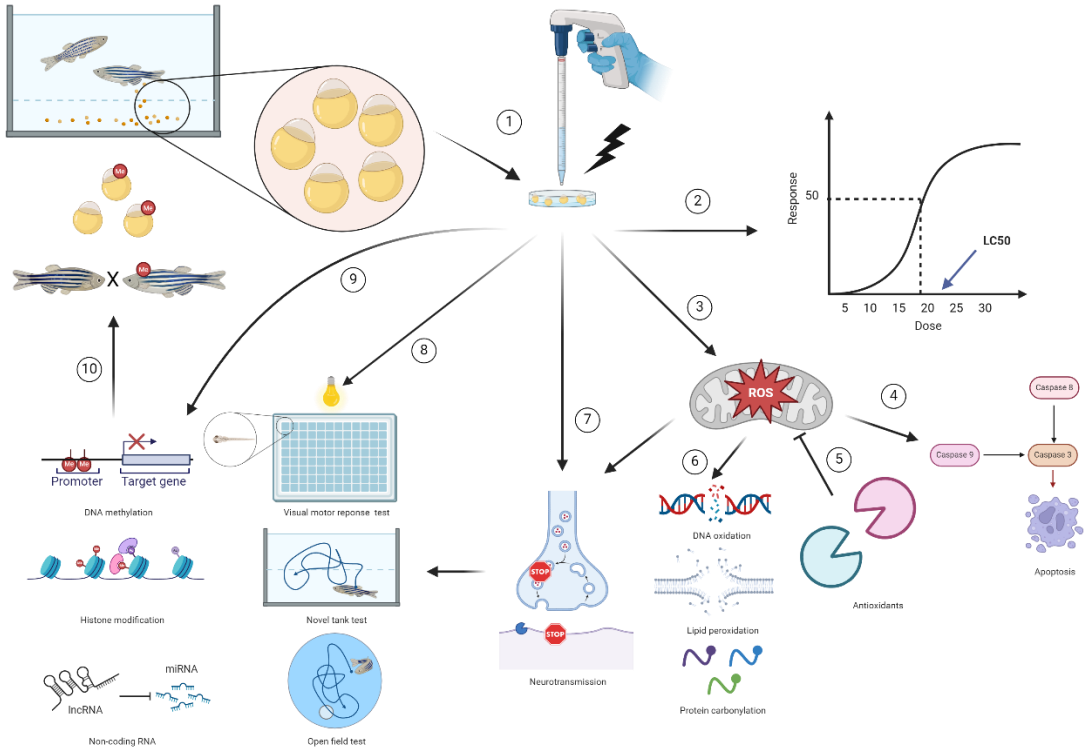


**Figure 2. Approaches to assess neurotoxicity induced by environmentally relevant concentrations of pollutants in the zebrafish model**

① Fertilized embryonic zebrafish are collected for neurotoxicity assessment and the embryos are dosed with environmentally relevant concentrations of chemicalsfor assessing neurotoxicity. ② The LC50 reflects the acute toxicity of thechemicals. ③ The exposure of embryonic zebrafish to the test chemicalsinduces mitochondrial dysfunction and oxidative stress, which directly (chemicals) or indirectly (ROS) triggers ④ apoptosis cascades and ⑦ improper neurotransmitter release. Detection of ⑤ antioxidants and ⑥ the levels of DNA oxidation, lipid peroxidation, protein carbonylation, and are common methodologies to evaluate ROS. ④ Caspases 3, 8, and 9 are frequently used biomarkers for detecting apoptosis. ⑧ Neurobehavioral tests are sensitive assays to evaluate neurotoxicity in the zebrafish model. The visual motor response test, novel tank test, and open field test are neurobehavioral assays commonly applied to neurotoxicity studies. ⑨DNA methylation, histone modification, and non-coding RNA are parameters used to investigate epigenetics mechanism triggered by test chemicals, ⑩ which can pass to the embryos through transgenerational epigenetic inheritance.

**Table 2. Experimental examples of developmental zebrafish exposed to environmental pollutants induced acute neurotoxicity, altered locomotor activity, neurotransmission, apoptosis, neural related genes**

Abbreviations: ↑: increase; ↓:decrease; CAT: catalase; GABA: γ-aminobutyric; GSH: glutathione; MDA: malonaldehyde; SOD: superoxide dismutase.

| Environmental pollutants | | Concentrations | Exposure duration | Results | Reference |
|---|---|---|---|---|---|
| Insecticide | Fenpropathrin | 0.016 mg/L, 0.032 mg/L, 0.064 mg/L | 96 hpf | • Motor ability↓<br>• Oxidative stress ↑, reactive oxygen species generation↑, CAT, SOD↓<br>• Apoptosis-associated genes in brain and heart↑<br>• Nrf2 signaling pathway↓ | (T. Yu et al., 2022) |
| | Isofenphos-methyl | 2, 4, and 8 mg/L | 6-96 hpf | • Survival rate, hatchability, heart rate, and body length ↓<br>• Developmental malformations (uninflated swim bladder)↑<br>• Locomotive behavior↓<br>• Acetylcholinesterase↓<br>• Reactive oxygen species↑, MDA↑, SOD↑, CAT↑GSH↑<br>• Altered apoptosis-related genes (bcl2, p53, bax, and puma) | (Wu et al., 2023) |
| | Bifenthrin | 103.9 and 362.1 | <3-120 hpf | • Tail coiling frequency↑, altered locomotor activity (distance | (Eghan et |

| | | | | | |
|---|---|---|---|---|---|
| | | μg/L | | moved↑, turn angel↓)<br>• Acetylcholinesterase and dopamine levels↓<br>• Neurogenesis defects (shortened brain and axon widths, and demyelination of oligodendrocytes and Schwann cells)<br>neurodevelopment related genes (gap43, manf, gfap, nestin, sox2) ↑<br>• Neurotransmitters related genes (nlgn1, drd1, slc6a4a, ache) ↓ | al., 2023) |
| Fungicide | Difenoconazole | 0.25, 0.5, and 1 mg/L | 120 hpf | • Malformation rate, spontaneous movement↑<br>• Locomotor activity↓<br>• Dopamine and acetylcholine↓, acetylcholinesterase ↑<br>• Altered neurodevelopmental related genes | (Q. Yang et al., 2023) |
| | Fluxapyroxad | 0.5, 0.75, and 1 mg/L | 96 hpf | • Malformations↑ (shorter body length, smaller head and eyes, yolk sac edema)<br>• Motor aberrations<br>• Dopamine level↓<br>• Altered acetylcholinesterase and acetylcholine | (H. Yu et al., 2022) |
| | Trichlorfon | 0, 0.1, 2 and 5 mg/L | 144 hpf | • Survival rate, hatching rate↓, heart beat↓<br>• Malformation rate↑ (body length↓) | (Shi, Yang, Chen, et al., |

| | | | | | |
|---|---|---|---|---|---|
| | | | | • Locomotor activity↓<br>• Acetylcholinesterase, acetylcholine dopamine and serotonin ↓<br>• Central nervous system related gene (a1-tubulin, mbp, syn2a, shha and gap-43) ↓ | 2023) |
| Pesticide | Chlorphoxim | 2.5, 5, 7.5, 10, and 12.5 mg/L | 96 hpf | • Mortality↑, hatchability rate and heart rate↓<br>• Pericardial edema rate↑<br>• Swimming behavior↓<br>• Acetylcholinesterase↓<br>• Altered neural-related genes (syn2a,gfap,elavl3,neurog,gap43, andsox19b)<br>• Oxidative stress ↑, CAT and SOD ↓<br>• Apoptosis ↑ Bax, Bcl2, p53↑ | (Xiong et al., 2023) |
| | Fenvalerate | 0, 3.5, 7 and 14 μg/L | 4-96 hpf | • Survival rate, heart rate↓ | (Zhu et al., |

| | | | | |
|---|---|---|---|---|
| | | | • Malformation rate↑ (body length↓)<br>• Neurobehavioral alterations (spontaneous movement↓ swimming distance and velocity, movement time and clockwise rotation times↓)<br>• Cholinesterase activity↓<br>• Neurodevelopment related genes (elavl3, gfap, gap43 and mbp)<br>• Oxidative stress↑(reactive oxygen species↑, antioxidant enzyme↓)<br>• Apoptosis↑ (p53, bcl-2, bax and caspase 3) | 2023) |
| Emamectin benzoate (EMB) | 0.1, 0.25, 0.5, 1, 2, 4 and 8 μg/mL | 4-144 hpf | • Hatching rate↑<br>• Malformation rate↑<br>• Locomotor behavior↓<br>• Oxidative damage↑, reactive oxygen species↑, altered oxidative stress-related genes (cat, sod and Cu/Zn-sod)<br>• Altered GABA neural pathway-related genes (gat1, gabra1, gad1b, abat and glsa)<br>• Altered neurodevelopmental-related genes (syn2a, gfap, elavl3, shha, gap43 and Nrd) | (Gu et al., 2023) |
| Lead | 0.1, 1, and 10 μM | 120 hpf | • Locomotor activity↓ | (Liu et al., 2022) |

| | | | | | |
|---|---|---|---|---|---|
| Metal and mineral | | | | • Apoptosis↑<br>• Ambra1a and ambra1b (activating molecule in Beclin1-regulated autophagy)↓ | |
| | Nickel | 0, 10, 50, 100, 500, and 1000 μM | 144 hpf | • Hatching rate, heart rate, body length ↓<br>• Tail coiling frequency↓, swimming behavior (swimming distance, velocity, cumulative mobility) ↓<br>• Microglial activation ↑<br>• Neuronal and vascular development ↓ | (Wang et al., 2023) |
| | Selenium | 0.125, 0.25, 0.5, and 1 μM | 96 hpf | • Locomotor activity ↓<br>• Cell apoptosis↑<br>• Neuroinflammation↑<br>• Dopaminergic neuron, motor neuron, GABAergic neuron and neurotransmitter transport marker genes↓ | (Zhao et al., 2022) |
| | Halobenzoquinones | 0-8 μmol/L | 120 hpf | • Locomotor activity ↓<br>• Dopamine, GABA↓acetylcholinesterase ↓<br>• Neuronal morphogenesis related genes (gfap, α1-tubulin, mbp, and syn-2α) ↓ | (Yang et al., 2022) |

| | | | | | |
|---|---|---|---|---|---|
| Disinfectant | Perfluorononanoic Acid | 0.01, 0.1, 1, 10,and 100 μg/L | 120 hpf | • Swimming behavior↓<br>• Acetylcholine, glutamate, 5-hydroxytryptamine, GABA, dopamine, and noradrenaline↓ | (Liu et al., 2023) |
| | | 0, 100, 500, and 1000 μg/L | 4-120 hpf | • Mortality↑ Hatching↓<br>• Developmental malforamtions (body length↓, bent spine↑, pericardial, and yolk sac edema↑)<br>• Spontaneous movement frequency↓, altered touch-evoked response, and locomotor behavior<br>• Microglial activation↑<br>• Acetylcholinesterase↓, dopaminergic hyperactivity | (Mahapatra et al., 2023) |
| | 2, 5-dichloro-1, 4-benuinone (2, 5-DCBQ) | 0.2, 0.4, and 0.6 mg/L | 4-120 hpf | • Developmental defects (body length↓)<br>• Heart rate ↓<br>• Abnormal motor axon structure<br>• Locomotor activity↓<br>• Neuronal development associated genes (gfap, mbp, syn2a, elavl3, ache, and a1-tubulin) ↓<br>• Dsrupted neuroactive ligand-receptor interaction and apoptotic pathway | (Chen et al., 2022) |

| | | | | | |
|---|---|---|---|---|---|
| Nanoparticles | polystyrene nanoparticles | 0.2, 1, and 5 mg/L | 120 hpf | • Eye and head size ↓, pericardial area ↑<br>• Activity and anxiety↑ (lower dose), lethargy↑ (higher dose)<br>• Burst quality↓tail activity ↑<br>• Acetylcholinesterase↓<br>• Altered endocrine-related gene expression | (Torres-Ruiz et al., 2023) |
| | Microplastics | 0.1 to 100 μg/L | 120 hpf | • Swimming speed ↓<br>• Dopamine, 5-hydroxytryptamine (5-HT), GABA, acetylcholine, and related genes ↑ | (Xiang et al., 2023) |
| Flame retardant | Resorcinol bis(diphenyl phosphate) | 0, 0.3, 3, 90, 300 and 900 nM | 2-144 hpf | • Heart rates↓<br>• Malformation rates (body length↓)<br>• Locomotor behavior↓<br>• Acetylcholinesterase↓<br>• Alterd neurotransmitters (GABA↑, glutamate↓, acetylcholine↑, choline and epinephrine↓) | (Shi, Yang, Zheng, et al., 2023) |
| | Decabromodiphenyl ethane | 50-400 μg/L | 120 hpf | • Swimming speed↑<br>• Developmental defects (pericardial edema, yolk sac edema, spine bending, and tail bending) | (L. Yang et al., 2023) |

| | | | | | |
|---|---|---|---|---|---|
| | | | | • Mitochondrial dysfunction ↑<br>• GABA, 5-hydroxyindole-aceticacid↓<br>• Glutamicacid,norepinephrine,epinephrine, and acetylcholine↑ | |
| Drug | Mirtazapine | 3.9 and 43.5 ng/L | 2.5-96 hpf | • Heart rate↓, hatching↑<br>• Spontaneous contraction ↓, swimming frequency and swimming speed↓<br>• Altered epinephrine and neuregulin signaling | (Zhou et al., 2023) |
| | Flubendazole | 0.05, 0.1, 0.2, 0.4, and 0.8 mg/ml | 96 hpf | • Survival rate, hatching rate, and heart rate↓<br>• Developmental abnormalities (body length, head and eye size) ↓<br>• Apoptosis↑, apoptosis-related genes (p53, casp3, and casp8) ↑<br>• Neural differentiation-related genes (shha, nrd, ngn1, and elavl3)↓ | (Kim et al., 2023) |
| Others | Bisphenol AF | 0.03, 0.1, 0.3, and 1.0 μM | 144 hpf | • Locomotor activity↓<br>• Apoptosis↑<br>• Reactive oxygen species↑SOD↓CAT↓<br>• Altered normal dopaminergic signaling and genes | (Gyimah et al., 2022) |
| | Lanthanide phosphate (TbPO4) | 10, 20, and 50 mg/L | 144 hpf | • Mortality ↓ | (Chen et al., 2023) |

| | | | | |
|---|---|---|---|---|
| | | | • Spontaneous tail movement (24 hpf) ↓<br>• Dopaminergic and serotoninergic signaling↓ | |
| Octocrylene (OC) | 5, 50 and 500 µg/L | 3-96 hpf | • Hatching rate and heartbeat rate↓<br>• Developmental abnormalities<br>• Oxidative damage↑, antioxidant enzyme (SOD, CAT and GST)↑<br>• Acetylcholinesterase (AChE)↓<br>• Apoptosis↑ | (Gayathri et al., 2023) |

**Reference**


Abbate, F., Maugeri, A., Laurà, R., Levanti, M., Navarra, M., Cirmi, S., & Germanà, A. (2021). Zebrafish as a Useful Model to Study Oxidative Stress-Linked Disorders: Focus on Flavonoids. *Antioxidants (Basel)*, *10*(5). https://doi.org/10.3390/antiox10050668

Adeyemi, J. A., da Cunha Martins-Junior, A., & Barbosa, F., Jr. (2015). Teratogenicity, genotoxicity and oxidative stress in zebrafish embryos (Danio rerio) co-exposed to arsenic and atrazine. *Comp Biochem Physiol C Toxicol Pharmacol*, *172-173*, 7-12. https://doi.org/10.1016/j.cbpc.2015.04.001

Aguilar Diaz De Leon, J., & Borges, C. R. (2020). Evaluation of Oxidative Stress in Biological Samples Using the Thiobarbituric Acid Reactive Substances Assay. *J Vis Exp*(159). https://doi.org/10.3791/61122

Ahkin Chin Tai, J. K., Horzmann, K. A., Franco, J., Jannasch, A. S., Cooper, B. R., & Freeman, J. L. (2021). Developmental atrazine exposure in zebrafish produces the same major metabolites as mammals along with altered behavioral outcomes. *Neurotoxicol Teratol*, *85*, 106971. https://doi.org/10.1016/j.ntt.2021.106971

Ahmad, F., & Richardson, M. K. (2013). Exploratory behaviour in the open field test adapted for larval zebrafish: impact of environmental complexity. *Behav Processes*, *92*, 88-98. https://doi.org/10.1016/j.beproc.2012.10.014

Alfalahi, H., Dias, S. B., Khandoker, A. H., Chaudhuri, K. R., & Hadjileontiadis, L. J. (2023). A scoping review of neurodegenerative manifestations in explainable digital phenotyping. *NPJ Parkinsons Dis*, *9*(1), 49. https://doi.org/10.1038/s41531-023-00494-0

Ali, S., van Mil, H. G., & Richardson, M. K. (2011). Large-scale assessment of the zebrafish embryo as a possible predictive model in toxicity testing. *PLoS One*, *6*(6), e21076. https://doi.org/10.1371/journal.pone.0021076

Almatarneh, M. H., Kayed, G. G., Abbad, S. S. A., Alsunaidi, Z. H. A., Al-Sheraideh, M. S., & Zhao, Y. (2022). Mechanistic study on DNA mutation of the cytosine methylation reaction at C5 position. *Arabian Journal of Chemistry*, *15*(8), 103956. https://doi.org/https://doi.org/10.1016/j.arabjc.2022.103956

Aluru, N. (2017). Epigenetic effects of environmental chemicals: insights from zebrafish. *Curr Opin Toxicol*, *6*, 26-33. https://doi.org/10.1016/j.cotox.2017.07.004

Anger, W. K. (2003). Neurobehavioural tests and systems to assess neurotoxic exposures in the workplace and community. *Occup Environ Med*, *60*(7), 531-538, 474. https://doi.org/10.1136/oem.60.7.531

Apak, R. (2019). Current Issues in Antioxidant Measurement. *J Agric Food Chem*, *67*(33), 9187-9202. https://doi.org/10.1021/acs.jafc.9b03657

Ayala, A., Muñoz, M. F., & Argüelles, S. (2014). Lipid peroxidation: production, metabolism, and signaling mechanisms of malondialdehyde and 4-hydroxy-2-nonenal. *Oxid Med Cell Longev*, *2014*, 360438. https://doi.org/10.1155/2014/360438

Bailey, J., Oliveri, A., & Levin, E. D. (2013). Zebrafish model systems for developmental neurobehavioral toxicology. *Birth Defects Res C Embryo Today*, *99*(1), 14-23. https://doi.org/10.1002/bdrc.21027

Bailone, R. L., Fukushima, H. C. S., Ventura Fernandes, B. H., De Aguiar, L. K., Corrêa, T., Janke, H., Grejo Setti, P., Roça, R. O., & Borra, R. C. (2020). Zebrafish as an alternative animal model in human and animal vaccination research. *Lab Anim Res*, *36*, 13. https://doi.org/10.1186/s42826-020-00042-4

Balasubramanian, S., Raghunath, A., & Perumal, E. (2019). Role of epigenetics in zebrafish development. *Gene*, *718*, 144049. https://doi.org/10.1016/j.gene.2019.144049

Ball, N., Teo, W. P., Chandra, S., & Chapman, J. (2019). Parkinson's Disease and the Environment. *Front Neurol*, *10*, 218. https://doi.org/10.3389/fneur.2019.00218

Bambino, K., & Chu, J. (2017). Zebrafish in Toxicology and Environmental Health. *Curr Top Dev Biol*, *124*, 331-367. https://doi.org/10.1016/bs.ctdb.2016.10.007

Banfalvi, G. (2017). Methods to detect apoptotic cell death. *Apoptosis*, *22*(2), 306-323. https://doi.org/10.1007/s10495-016-1333-3

Bannister, A. J., & Kouzarides, T. (2011). Regulation of chromatin by histone modifications. *Cell Research*, *21*(3), 381-395. https://doi.org/10.1038/cr.2011.22

Bao, A. M., & Swaab, D. F. (2019). The human hypothalamus in mood disorders: The HPA axis in the center. *IBRO Rep*, *6*, 45-53. https://doi.org/10.1016/j.ibror.2018.11.008

Baran, A., Yildirim, S., Ghosigharehaghaji, A., Bolat, İ., Sulukan, E., & Ceyhun, S. B. (2021). An approach to evaluating the potential teratogenic and neurotoxic mechanism of BHA based on apoptosis induced by oxidative stress in zebrafish embryo (Danio rerio). *Hum Exp Toxicol*, *40*(3), 425-438. https://doi.org/10.1177/0960327120952140

Barbazuk, W. B., Korf, I., Kadavi, C., Heyen, J., Tate, S., Wun, E., Bedell, J. A., McPherson, J. D., & Johnson, S. L. (2000). The syntenic relationship of the zebrafish and human genomes. *Genome Res*, *10*(9), 1351-1358. https://doi.org/10.1101/gr.144700

Barker, D. J., Gluckman, P. D., Godfrey, K. M., Harding, J. E., Owens, J. A., & Robinson, J. S. (1993). Fetal nutrition and cardiovascular disease in adult life. *Lancet*, *341*(8850), 938-941. https://doi.org/10.1016/0140-6736(93)91224-a

Basnet, R. M., Zizioli, D., Taweedet, S., Finazzi, D., & Memo, M. (2019). Zebrafish Larvae as a Behavioral Model in Neuropharmacology. *Biomedicines*, *7*(1). https://doi.org/10.3390/biomedicines7010023

Bauer, B., Mally, A., & Liedtke, D. (2021). Zebrafish Embryos and Larvae as Alternative Animal Models for Toxicity Testing. *Int J Mol Sci*, *22*(24). https://doi.org/10.3390/ijms222413417

Beers, R. F., Jr., & Sizer, I. W. (1952). A spectrophotometric method for measuring the breakdown of hydrogen peroxide by catalase. *J Biol Chem*, *195*(1), 133-140.

Belanger, S. E., Rawlings, J. M., & Carr, G. J. (2013). Use of fish embryo toxicity tests for the prediction of acute fish toxicity to chemicals. *Environ Toxicol Chem*, *32*(8), 1768-1783. https://doi.org/10.1002/etc.2244

Benvenutti, R., Marcon, M., Gallas-Lopes, M., de Mello, A. J., Herrmann, A. P., & Piato, A. (2021). Swimming in the maze: An overview of maze apparatuses and protocols to assess zebrafish behavior. *Neurosci Biobehav Rev*, *127*, 761-778. https://doi.org/10.1016/j.neubiorev.2021.05.027

Betteridge, D. J. (2000). What is oxidative stress? *Metabolism*, *49*(2 Suppl 1), 3-8. https://doi.org/10.1016/s0026-0495(00)80077-3

Bian, X., & Gao, Y. (2021). DNA methylation and gene expression alterations in zebrafish embryos exposed to cadmium. *Environ Sci Pollut Res Int*, *28*(23), 30101-30110. https://doi.org/10.1007/s11356-021-12691-6

Bihaqi, S. W., & Zawia, N. H. (2013). Enhanced taupathy and AD-like pathology in aged primate brains decades after infantile exposure to lead (Pb). *Neurotoxicology*, *39*, 95-101. https://doi.org/10.1016/j.neuro.2013.07.010

Birben, E., Sahiner, U. M., Sackesen, C., Erzurum, S., & Kalayci, O. (2012). Oxidative stress and antioxidant defense. *World Allergy Organ J*, *5*(1), 9-19. https://doi.org/10.1097/WOX.0b013e3182439613

Bisht, K., Sharma, K., & Tremblay, M.-È. (2018). Chronic stress as a risk factor for Alzheimer's disease: Roles of microglia-mediated synaptic remodeling, inflammation, and oxidative stress. *Neurobiology of Stress*, *9*, 9-21. https://doi.org/https://doi.org/10.1016/j.ynstr.2018.05.003

Bloch, S., Thomas, M., Colin, I., Galant, S., Machado, E., Affaticati, P., Jenett, A., & Yamamoto, K. (2019). Mesencephalic origin of the inferior lobe in zebrafish. *BMC Biol*, *17*(1), 22. https://doi.org/10.1186/s12915-019-0631-y

Bode, K., Link, C., Krammer, P. H., & Weyd, H. (2020). Flow-cytometric Detection of Low-level Reactive Oxygen Species in Cell Lines and Primary Immune Cells. *Bio Protoc*, *10*(17), e3737. https://doi.org/10.21769/BioProtoc.3737

Bogdanović, O., Fernández-Miñán, A., Tena, J. J., de la Calle-Mustienes, E., & Gómez-Skarmeta, J. L. (2013). The developmental epigenomics toolbox: ChIP-seq and MethylCap-seq profiling of early zebrafish embryos. *Methods*, *62*(3), 207-215. https://doi.org/10.1016/j.ymeth.2013.04.011

Borghammer, P. (2021). The α-Synuclein Origin and Connectome Model (SOC Model) of Parkinson's Disease: Explaining Motor Asymmetry, Non-Motor Phenotypes, and Cognitive Decline. *J Parkinsons Dis*, *11*(2), 455-474. https://doi.org/10.3233/jpd-202481

Braunbeck, T., Kais, B., Lammer, E., Otte, J., Schneider, K., Stengel, D., & Strecker, R. (2015). The fish embryo test (FET): origin, applications, and future. *Environ Sci Pollut Res Int*, *22*(21), 16247-16261. https://doi.org/10.1007/s11356-014-3814-7

Bridges, C. C., Krasnikov, B. F., Joshee, L., Pinto, J. T., Hallen, A., Li, J., Zalups, R. K., & Cooper, A. J. (2012). New insights into the metabolism of organomercury compounds: mercury-containing cysteine S-conjugates are substrates of human glutamine transaminase K and potent inactivators of cystathionine γ-lyase. *Arch Biochem Biophys*, *517*(1), 20-29. https://doi.org/10.1016/j.abb.2011.11.002

Burton, C. E., Zhou, Y., Bai, Q., & Burton, E. A. (2017). Spectral properties of the zebrafish visual motor response. *Neurosci Lett*, *646*, 62-67. https://doi.org/10.1016/j.neulet.2017.03.002

Butterick, T. A., Duffy, C. M., Lee, R. E., Billington, C. J., Kotz, C. M., & Nixon, J. P. (2014). Use of a caspase multiplexing assay to determine apoptosis in a hypothalamic cell model. *J Vis Exp*(86). https://doi.org/10.3791/51305

Cachat, J. M., Canavello, P. R., Elkhayat, S. I., Bartels, B. K., Hart, P. C., Elegante, M. F., Beeson, E. C., Laffoon, A. L., Haymore, W. A. M., Tien, D. H., Tien, A. K., Mohnot, S., & Kalueff, A. V. (2011). Video-Aided Analysis of Zebrafish Locomotion and Anxiety-Related Behavioral Responses. In A. V. Kalueff & J. M. Cachat (Eds.), *Zebrafish Neurobehavioral Protocols* (pp. 1-14). Humana Press. https://doi.org/10.1007/978-1-60761-953-6_1

Carbaugh, C. M., Widder, M. W., Phillips, C. S., Jackson, D. A., DiVito, V. T., van der Schalie, W. H., & Glover, K. P. (2020). Assessment of zebrafish embryo photomotor response sensitivity and phase-specific patterns following acute- and long-duration exposure to neurotoxic chemicals and chemical weapon precursors. *J Appl Toxicol*, *40*(9), 1272-1283. https://doi.org/10.1002/jat.3984

Carmean, V., & Ribera, A. B. (2010). Genetic Analysis of the Touch Response in Zebrafish (Danio rerio). *Int J Comp Psychol*, *23*(1), 91.

Carvajal-Oliveros, A., & Campusano, J. M. (2020). Studying the Contribution of Serotonin to Neurodevelopmental Disorders. Can This Fly? *Front Behav Neurosci*, *14*, 601449. https://doi.org/10.3389/fnbeh.2020.601449

Cassar, S., Adatto, I., Freeman, J. L., Gamse, J. T., Iturria, I., Lawrence, C., Muriana, A., Peterson, R. T., Van Cruchten, S., & Zon, L. I. (2020). Use of Zebrafish in Drug Discovery Toxicology. *Chem Res Toxicol*, *33*(1), 95-118. https://doi.org/10.1021/acs.chemrestox.9b00335

Cavalieri, V., & Spinelli, G. (2017). Environmental epigenetics in zebrafish. *Epigenetics Chromatin*, *10*(1), 46. https://doi.org/10.1186/s13072-017-0154-0

Chang, J. T., Lehtinen, M. K., & Sive, H. (2016). Zebrafish cerebrospinal fluid mediates cell survival through a retinoid signaling pathway. *Dev Neurobiol*, *76*(1), 75-92. https://doi.org/10.1002/dneu.22300

Chaouloff, F. (2000). Serotonin, stress and corticoids. *J Psychopharmacol*, *14*(2), 139-151. https://doi.org/10.1177/026988110001400203

Chen, S., Wang, X., Ye, X., Qin, Y., Wang, H., Liang, Z., Zhu, L., Zhou, L., Martyniuk, C. J., & Yan, B. (2023). Dopaminergic and serotoninergic neurotoxicity of lanthanide phosphate (TbPO(4)) in developing zebrafish. *Chemosphere*, *340*, 139861. https://doi.org/10.1016/j.chemosphere.2023.139861

Chen, Y., Xiao, L., Gao, G., He, L., Zhao, K., Shang, X., & Liu, C. (2022). 2, 5-dichloro-1, 4-benuinone exposure to zebrafish embryos/larvae causes neurodevelopmental toxicity. *Ecotoxicol Environ Saf*, *243*, 114007. https://doi.org/10.1016/j.ecoenv.2022.114007

Chen, Z., & Zhong, C. (2014). Oxidative stress in Alzheimer's disease. *Neurosci Bull*, *30*(2), 271-281. https://doi.org/10.1007/s12264-013-1423-y

Chiapponi, C., Piras, F., Caltagirone, C., & Spalletta, G. (2016). GABA System in Schizophrenia and Mood Disorders: A Mini Review on Third-Generation Imaging Studies. *Front Psychiatry*, *7*, 61. https://doi.org/10.3389/fpsyt.2016.00061

Chu, J., & Sadler, K. C. (2009). New school in liver development: lessons from zebrafish. *Hepatology*, *50*(5), 1656-1663. https://doi.org/10.1002/hep.23157

Cifuentes Castro, V. H., López Valenzuela, C. L., Salazar Sánchez, J. C., Peña, K. P., López Pérez, S. J., Ibarra, J. O., & Villagrán, A. M. (2014). An update of the classical and novel methods used for measuring fast neurotransmitters during normal and brain altered function. *Curr Neuropharmacol*, *12*(6), 490-508. https://doi.org/10.2174/1570159x13666141223223657

Cobley, J. N., Fiorello, M. L., & Bailey, D. M. (2018). 13 reasons why the brain is susceptible to oxidative stress. *Redox Biol*, *15*, 490-503. https://doi.org/10.1016/j.redox.2018.01.008

Coral, J. A., Heaps, S., Glaholt, S. P., Karty, J. A., Jacobson, S. C., Shaw, J. R., & Bondesson, M. (2021). Arsenic exposure induces a bimodal toxicity response in zebrafish. *Environ Pollut*, *287*, 117637. https://doi.org/10.1016/j.envpol.2021.117637

Council Directive 86/609/EEC of 24 November 1986 on the approximation of laws, regulations and administrative provisions of the Member States regarding the protection of animals used for experimental and other scientific purposes, 1-28 358 (1986). http://data.europa.eu/eli/dir/1986/609/oj

Crowley, L. C., Marfell, B. J., & Waterhouse, N. J. (2016). Analyzing Cell Death by Nuclear Staining with Hoechst 33342. *Cold Spring Harb Protoc*, *2016*(9). https://doi.org/10.1101/pdb.prot087205

d'Amora, M., & Giordani, S. (2018). The Utility of Zebrafish as a Model for Screening Developmental Neurotoxicity. *Front Neurosci*, *12*, 976. https://doi.org/10.3389/fnins.2018.00976

D'Arcy, M. S. (2019). Cell death: a review of the major forms of apoptosis, necrosis and autophagy. *Cell Biol Int*, *43*(6), 582-592. https://doi.org/10.1002/cbin.11137

Dauer, W., & Przedborski, S. (2003). Parkinson's disease: mechanisms and models. *Neuron*, *39*(6), 889-909. https://doi.org/10.1016/s0896-6273(03)00568-3

de Abreu, M. S., Genario, R., Giacomini, A., Demin, K. A., Lakstygal, A. M., Amstislavskaya, T. G., Fontana, B. D., Parker, M. O., & Kalueff, A. V. (2020). Zebrafish as a Model of Neurodevelopmental Disorders. *Neuroscience*, *445*, 3-11. https://doi.org/10.1016/j.neuroscience.2019.08.034

Deuschl, G., Beghi, E., Fazekas, F., Varga, T., Christoforidi, K. A., Sipido, E., Bassetti, C. L., Vos, T., & Feigin, V. L. (2020). The burden of neurological diseases in Europe: an analysis for the Global Burden of Disease Study 2017. *Lancet Public Health*, *5*(10), e551-e567. https://doi.org/10.1016/s2468-2667(20)30190-0

Ding, P., Xiang, C., Li, X., Chen, H., Shi, X., Huang, C., Yu, Y., Qi, J., Li, A. J., Zhang, L., & Hu, G. (2023). Photoaged microplastics induce neurotoxicity via oxidative stress and abnormal neurotransmission in zebrafish larvae (Danio rerio). *Sci Total Environ*, *881*, 163480. https://doi.org/10.1016/j.scitotenv.2023.163480

Dionísio, P. A., Amaral, J. D., & Rodrigues, C. M. P. (2021). Oxidative stress and regulated cell death in Parkinson's disease. *Ageing Res Rev*, *67*, 101263. https://doi.org/10.1016/j.arr.2021.101263

*ECHA and alternatives to animal testing*. https://echa.europa.eu/animal-testing-under-reach/infographic

Eghan, K., Lee, S., Yoo, D., Kim, C. H., & Kim, W. K. (2023). Adverse effects of bifenthrin exposure on neurobehavior and neurodevelopment in a zebrafish embryo/larvae model. *Chemosphere*, *341*, 140099. https://doi.org/10.1016/j.chemosphere.2023.140099

Elhamamsy, A. R. (2017). Role of DNA methylation in imprinting disorders: an updated review. *J Assist Reprod Genet*, *34*(5), 549-562. https://doi.org/10.1007/s10815-017-0895-5

Elmore, S. (2007). Apoptosis: a review of programmed cell death. *Toxicol Pathol*, *35*(4), 495-516. https://doi.org/10.1080/01926230701320337

Emamzadeh, F. N., & Surguchov, A. (2018). Parkinson's Disease: Biomarkers, Treatment, and Risk Factors. *Front Neurosci*, *12*, 612. https://doi.org/10.3389/fnins.2018.00612

Exley, C. (2014). What is the risk of aluminium as a neurotoxin? *Expert Rev Neurother*, *14*(6), 589-591. https://doi.org/10.1586/14737175.2014.915745

Fadeel, B., & Orrenius, S. (2005). Apoptosis: a basic biological phenomenon with wide-ranging implications in human disease. *J Intern Med*, *258*(6), 479-517. https://doi.org/10.1111/j.1365-2796.2005.01570.x

Farber, S. A., De Rose, R. A., Olson, E. S., & Halpern, M. E. (2003). The zebrafish annexin gene family. *Genome Res*, *13*(6a), 1082-1096. https://doi.org/10.1101/gr.479603

Fitzgerald, J. A., Könemann, S., Krümpelmann, L., Županič, A., & Vom Berg, C. (2021). Approaches to Test the Neurotoxicity of Environmental Contaminants in the Zebrafish Model: From Behavior to Molecular Mechanisms. *Environ Toxicol Chem*, *40*(4), 989-1006. https://doi.org/10.1002/etc.4951

Flaten, T. P. (2001). Aluminium as a risk factor in Alzheimer's disease, with emphasis on drinking water. *Brain Res Bull*, *55*(2), 187-196. https://doi.org/10.1016/s0361-9230(01)00459-2

Fleisch, V. C., & Neuhauss, S. C. (2006). Visual behavior in zebrafish. *Zebrafish*, *3*(2), 191-201. https://doi.org/10.1089/zeb.2006.3.191

Fleming, A., Diekmann, H., & Goldsmith, P. (2013). Functional characterisation of the maturation of the blood-brain barrier in larval zebrafish. *PLoS One*, *8*(10), e77548. https://doi.org/10.1371/journal.pone.0077548

Franco, R., Sánchez-Olea, R., Reyes-Reyes, E. M., & Panayiotidis, M. I. (2009). Environmental toxicity, oxidative stress and apoptosis: ménage à trois. *Mutat Res*, *674*(1-2), 3-22. https://doi.org/10.1016/j.mrgentox.2008.11.012

Frankfurt, O. S., Robb, J. A., Sugarbaker, E. V., & Villa, L. (1996). Monoclonal antibody to single-stranded DNA is a specific and sensitive cellular marker of apoptosis. *Exp Cell Res*, *226*(2), 387-397. https://doi.org/10.1006/excr.1996.0240

Fuertes, I., & Barata, C. (2021). Characterization of neurotransmitters and related metabolites in Daphnia magna juveniles deficient in serotonin and exposed to neuroactive chemicals that affect its behavior: A targeted LC-MS/MS method. *Chemosphere*, *263*, 127814. https://doi.org/10.1016/j.chemosphere.2020.127814

Gad, S. C. (2014). LD50/LC50 (Lethal Dosage 50/Lethal Concentration 50). In P. Wexler (Ed.), *Encyclopedia of Toxicology (Third Edition)* (pp. 58-60). Academic Press. https://doi.org/https://doi.org/10.1016/B978-0-12-386454-3.00867-8

Gayathri, M., Sutha, J., Mohanthi, S., Ramesh, M., & Poopal, R. K. (2023). Ecotoxicological evaluation of the UV-filter octocrylene (OC) in embryonic zebrafish (Danio rerio): Developmental, biochemical and cellular biomarkers. *Comp Biochem Physiol C Toxicol Pharmacol*, *271*, 109688. https://doi.org/10.1016/j.cbpc.2023.109688

Gerrard, L. B., Tantirigama, M. L. S., & Bekkers, J. M. (2018). Pre- and Postsynaptic Activation of GABA(B) Receptors Modulates Principal Cell Excitation in the Piriform Cortex. *Front Cell Neurosci*, *12*, 28. https://doi.org/10.3389/fncel.2018.00028

Glaberman, S., Padilla, S., & Barron, M. G. (2017). Evaluating the zebrafish embryo toxicity test for pesticide hazard screening. *Environ Toxicol Chem*, *36*(5), 1221-1226. https://doi.org/10.1002/etc.3641

Glazer, L., & Brennan, C. H. (2021). Developmental Exposure to Low Concentrations of Methylmercury Causes Increase in Anxiety-Related Behaviour and Locomotor Impairments in Zebrafish. *Int J Mol Sci*, *22*(20). https://doi.org/10.3390/ijms222010961

Glenner, G. G., & Wong, C. W. (1984). Alzheimer's disease: initial report of the purification and characterization of a novel cerebrovascular amyloid protein. *Biochem Biophys Res Commun*, *120*(3), 885-890. https://doi.org/10.1016/s0006-291x(84)80190-4

Goel, P., Chakrabarti, S., Goel, K., Bhutani, K., Chopra, T., & Bali, S. (2022). Neuronal cell death mechanisms in Alzheimer's disease: An insight. *Front Mol Neurosci*, *15*, 937133. https://doi.org/10.3389/fnmol.2022.937133

Goldsmith, J. R., & Jobin, C. (2012). Think small: zebrafish as a model system of human pathology. *J Biomed Biotechnol*, *2012*, 817341. https://doi.org/10.1155/2012/817341

Gu, J., Guo, L., Zhu, Y., Qian, L., Shi, L., Zhang, H., & Ji, G. (2023). Neurodevelopmental Toxicity of Emamectin Benzoate to the Early Life Stage of Zebrafish Larvae (Danio rerio). *Int J Mol Sci*, *24*(4). https://doi.org/10.3390/ijms24043757

Guo, M., Lu, B., Gan, J., Wang, S., Jiang, X., & Li, H. (2021). Apoptosis detection: a purpose-dependent approach selection. *Cell Cycle*, *20*(11), 1033-1040. https://doi.org/10.1080/15384101.2021.1919830

Guru, A., & Arockiaraj, J. (2023). Exposure to environmental pollutant bisphenol A causes oxidative damage and lipid accumulation in Zebrafish larvae: Protective role of WL15 peptide derived from cysteine and glycine-rich protein 2. *J Biochem Mol Toxicol*, *37*(1), e23223. https://doi.org/10.1002/jbt.23223

Gutzman, J. H., Graeden, E. G., Lowery, L. A., Holley, H. S., & Sive, H. (2008). Formation of the zebrafish midbrain-hindbrain boundary constriction requires laminin-dependent basal constriction. *Mech Dev*, *125*(11-12), 974-983. https://doi.org/10.1016/j.mod.2008.07.004

Gyimah, E., Zhu, X., Zhang, Z., Guo, M., Xu, H., Mensah, J. K., Dong, X., & Gyimah, G. N. W. (2022). Oxidative Stress and Apoptosis in Bisphenol AF-Induced Neurotoxicity in Zebrafish Embryos. *Environ Toxicol Chem*, *41*(9), 2273-2284. https://doi.org/10.1002/etc.5412

Hanson, M. (2015). The birth and future health of DOHaD. *J Dev Orig Health Dis*, *6*(5), 434-437. https://doi.org/10.1017/s2040174415001129

Hartmann, A., Hunot, S., Michel, P. P., Muriel, M. P., Vyas, S., Faucheux, B. A., Mouatt-Prigent, A., Turmel, H., Srinivasan, A., Ruberg, M., Evan, G. I., Agid, Y., & Hirsch, E. C. (2000). Caspase-3: A vulnerability factor and final effector in apoptotic death of dopaminergic neurons in Parkinson's disease. *Proc Natl Acad Sci U S A*, *97*(6), 2875-2880. https://doi.org/10.1073/pnas.040556597

Hartmann, A., Troadec, J. D., Hunot, S., Kikly, K., Faucheux, B. A., Mouatt-Prigent, A., Ruberg, M., Agid, Y., & Hirsch, E. C. (2001). Caspase-8 is an effector in apoptotic death of dopaminergic neurons in Parkinson's disease, but pathway inhibition results in neuronal necrosis. *J Neurosci*, *21*(7), 2247-2255. https://doi.org/10.1523/jneurosci.21-07-02247.2001

Hayes, M. T. (2019). Parkinson's Disease and Parkinsonism. *Am J Med*, *132*(7), 802-807. https://doi.org/10.1016/j.amjmed.2019.03.001

Heindel, J. J., Balbus, J., Birnbaum, L., Brune-Drisse, M. N., Grandjean, P., Gray, K., Landrigan, P. J., Sly, P. D., Suk, W., Cory Slechta, D., Thompson, C., & Hanson, M. (2015). Developmental Origins of Health and Disease: Integrating Environmental Influences. *Endocrinology*, *156*(10), 3416-3421. https://doi.org/10.1210/en.2015-1394

Heinz, S., Freyberger, A., Lawrenz, B., Schladt, L., Schmuck, G., & Ellinger-Ziegelbauer, H. (2017). Mechanistic Investigations of the Mitochondrial Complex I Inhibitor Rotenone in

the Context of Pharmacological and Safety Evaluation. *Sci Rep*, *7*, 45465. https://doi.org/10.1038/srep45465

Henn, K., & Braunbeck, T. (2011). Dechorionation as a tool to improve the fish embryo toxicity test (FET) with the zebrafish (Danio rerio). *Comp Biochem Physiol C Toxicol Pharmacol*, *153*(1), 91-98. https://doi.org/10.1016/j.cbpc.2010.09.003

Henriques, M. C., Carvalho, I., Santos, C., Herdeiro, M. T., Fardilha, M., Pavlaki, M. D., & Loureiro, S. (2023). Unveiling the molecular mechanisms and developmental consequences of mercury (Hg) toxicity in zebrafish embryo-larvae: A comprehensive approach. *Neurotoxicol Teratol*, *100*, 107302. https://doi.org/10.1016/j.ntt.2023.107302

Horzmann, K. A., & Freeman, J. L. (2016). Zebrafish Get Connected: Investigating Neurotransmission Targets and Alterations in Chemical Toxicity. *Toxics*, *4*(3). https://doi.org/10.3390/toxics4030019

Horzmann, K. A., & Freeman, J. L. (2018). Making Waves: New Developments in Toxicology With the Zebrafish. *Toxicological Sciences*, *163*(1), 5-12. https://doi.org/10.1093/toxsci/kfy044

Horzmann, K. A., Lin, L. F., Taslakjian, B., Yuan, C., & Freeman, J. L. (2022). Anxiety-related behavior and associated brain transcriptome and epigenome alterations in adult female zebrafish exposed to atrazine during embryogenesis. *Chemosphere*, *308*(Pt 3), 136431. https://doi.org/10.1016/j.chemosphere.2022.136431

Horzmann, K. A., Portales, A. M., Batcho, K. G., & Freeman, J. L. (2020). Developmental toxicity of trichloroethylene in zebrafish (Danio rerio). *Environ Sci Process Impacts*, *22*(3), 728-739. https://doi.org/10.1039/c9em00565j

Howe, K., Clark, M. D., Torroja, C. F., Torrance, J., Berthelot, C., Muffato, M., Collins, J. E., Humphray, S., McLaren, K., Matthews, L., McLaren, S., Sealy, I., Caccamo, M., Churcher, C., Scott, C., Barrett, J. C., Koch, R., Rauch, G. J., White, S.,…Stemple, D. L. (2013). The zebrafish reference genome sequence and its relationship to the human genome. *Nature*, *496*(7446), 498-503. https://doi.org/10.1038/nature12111

Huang, M., Ivantsova, E., Konig, I., Patel, N., English, C., Souders, C. L., 2nd, & Martyniuk, C. J. (2023). Developmental and mitochondrial toxicity assessment of perfluoroheptanoic acid (PFHpA) in zebrafish (Danio rerio). *Environ Toxicol Pharmacol*, *97*, 104037. https://doi.org/10.1016/j.etap.2022.104037

Huat, T. J., Camats-Perna, J., Newcombe, E. A., Valmas, N., Kitazawa, M., & Medeiros, R. (2019). Metal Toxicity Links to Alzheimer's Disease and Neuroinflammation. *J Mol Biol*, *431*(9), 1843-1868. https://doi.org/10.1016/j.jmb.2019.01.018

Hyman, S. E. (2005). Neurotransmitters. *Curr Biol*, *15*(5), R154-158. https://doi.org/10.1016/j.cub.2005.02.037

Ishizuka, T., Nomura, S., Hosoda, H., Kangawa, K., Watanabe, T., & Yamatodani, A. (2006). A role of the histaminergic system for the control of feeding by orexigenic peptides. *Physiol Behav*, *89*(3), 295-300. https://doi.org/10.1016/j.physbeh.2006.05.049

Jarema, K. A., Hunter, D. L., Hill, B. N., Olin, J. K., Britton, K. N., Waalkes, M. R., & Padilla, S. (2022). Developmental Neurotoxicity and Behavioral Screening in Larval Zebrafish with a Comparison to Other Published Results. *Toxics*, *10*(5). https://doi.org/10.3390/toxics10050256

Jin, B., & Robertson, K. D. (2013). DNA methyltransferases, DNA damage repair, and cancer. *Adv Exp Med Biol*, *754*, 3-29. https://doi.org/10.1007/978-1-4419-9967-2_1

Johnston, J., & Cushing, L. (2020). Chemical Exposures, Health, and Environmental Justice in Communities Living on the Fenceline of Industry. *Curr Environ Health Rep*, *7*(1), 48-57. https://doi.org/10.1007/s40572-020-00263-8

Jung-Klawitter, S., & Kuseyri Hübschmann, O. (2019). Analysis of Catecholamines and Pterins in Inborn Errors of Monoamine Neurotransmitter Metabolism-From Past to Future. *Cells*, *8*(8). https://doi.org/10.3390/cells8080867

Kaikkonen, M. U., Lam, M. T., & Glass, C. K. (2011). Non-coding RNAs as regulators of gene expression and epigenetics. *Cardiovasc Res*, *90*(3), 430-440. https://doi.org/10.1093/cvr/cvr097

Kalueff, A. V., Gebhardt, M., Stewart, A. M., Cachat, J. M., Brimmer, M., Chawla, J. S., Craddock, C., Kyzar, E. J., Roth, A., Landsman, S., Gaikwad, S., Robinson, K., Baatrup, E., Tierney, K., Shamchuk, A., Norton, W., Miller, N., Nicolson, T., Braubach, O.,…Schneider, H. (2013). Towards a comprehensive catalog of zebrafish behavior 1.0 and beyond. *Zebrafish*, *10*(1), 70-86. https://doi.org/10.1089/zeb.2012.0861

Kalyn, M., Lee, H., Curry, J., Tu, W., Ekker, M., & Mennigen, J. A. (2023). Effects of PFOS, F-53B and OBS on locomotor behaviour, the dopaminergic system and mitochondrial

function in developing zebrafish (Danio rerio). *Environ Pollut*, *326*, 121479. https://doi.org/10.1016/j.envpol.2023.121479

Kamstra, J. H., Aleström, P., Kooter, J. M., & Legler, J. (2015). Zebrafish as a model to study the role of DNA methylation in environmental toxicology. *Environ Sci Pollut Res Int*, *22*(21), 16262-16276. https://doi.org/10.1007/s11356-014-3466-7

Kang, S. Y., Joshi, P., & Lee, M. Y. (2021). High-Throughput Screening of Compound Neurotoxicity Using 3D-Cultured Neural Stem Cells on a 384-Pillar Plate. *Curr Protoc*, *1*(4), e107. https://doi.org/10.1002/cpz1.107

Kanungo, J., Twaddle, N. C., Silva, C., Robinson, B., Wolle, M., Conklin, S., MacMahon, S., Gu, Q., Edhlund, I., Benjamin, L., Beland, F. A., & Fitzpatrick, S. C. (2023). Inorganic arsenic alters the development of dopaminergic neurons but not serotonergic neurons and induces motor neuron development via Sonic hedgehog pathway in zebrafish. *Neurosci Lett*, *795*, 137042. https://doi.org/10.1016/j.neulet.2022.137042

Katerji, M., Filippova, M., & Duerksen-Hughes, P. (2019). Approaches and Methods to Measure Oxidative Stress in Clinical Samples: Research Applications in the Cancer Field. *Oxid Med Cell Longev*, *2019*, 1279250. https://doi.org/10.1155/2019/1279250

Kaur, K., Narang, R. K., & Singh, S. (2022). AlCl(3) induced learning and memory deficit in zebrafish. *Neurotoxicology*, *92*, 67-76. https://doi.org/10.1016/j.neuro.2022.07.004

Kenney, J. W. (2020). Chapter 12 - Associative and nonassociative learning in adult zebrafish. In R. T. Gerlai (Ed.), *Behavioral and Neural Genetics of Zebrafish* (pp. 187-204). Academic Press. https://doi.org/https://doi.org/10.1016/B978-0-12-817528-6.00012-7

Kim, H., & Xue, X. (2020). Detection of Total Reactive Oxygen Species in Adherent Cells by 2',7'-Dichlorodihydrofluorescein Diacetate Staining. *J Vis Exp*(160). https://doi.org/10.3791/60682

Kim, J., Bang, J., Ryu, B., Kim, C. Y., & Park, J. H. (2023). Flubendazole exposure disrupts neural development and function of zebrafish embryos (Danio rerio). *Sci Total Environ*, *898*, 165376. https://doi.org/10.1016/j.scitotenv.2023.165376

Kimmel, C. B., Ballard, W. W., Kimmel, S. R., Ullmann, B., & Schilling, T. F. (1995). Stages of embryonic development of the zebrafish. *Dev Dyn*, *203*(3), 253-310. https://doi.org/10.1002/aja.1002030302

Kinkhabwala, A., Riley, M., Koyama, M., Monen, J., Satou, C., Kimura, Y., Higashijima, S., & Fetcho, J. (2011). A structural and functional ground plan for neurons in the hindbrain of zebrafish. *Proc Natl Acad Sci U S A*, *108*(3), 1164-1169. https://doi.org/10.1073/pnas.1012185108

Klim, J., Gładki, A., Kucharczyk, R., Zielenkiewicz, U., & Kaczanowski, S. (2018). Ancestral State Reconstruction of the Apoptosis Machinery in the Common Ancestor of Eukaryotes. *G3 (Bethesda)*, *8*(6), 2121-2134. https://doi.org/10.1534/g3.118.200295

Klüver, N., König, M., Ortmann, J., Massei, R., Paschke, A., Kühne, R., & Scholz, S. (2015). Fish embryo toxicity test: identification of compounds with weak toxicity and analysis of behavioral effects to improve prediction of acute toxicity for neurotoxic compounds. *Environ Sci Technol*, *49*(11), 7002-7011. https://doi.org/10.1021/acs.est.5b01910

Kokel, D., Dunn, T. W., Ahrens, M. B., Alshut, R., Cheung, C. Y., Saint-Amant, L., Bruni, G., Mateus, R., van Ham, T. J., Shiraki, T., Fukada, Y., Kojima, D., Yeh, J. R., Mikut, R., von Lintig, J., Engert, F., & Peterson, R. T. (2013). Identification of nonvisual photomotor response cells in the vertebrate hindbrain. *J Neurosci*, *33*(9), 3834-3843. https://doi.org/10.1523/jneurosci.3689-12.2013

Kokel, D., & Peterson, R. T. (2011). Using the zebrafish photomotor response for psychotropic drug screening. *Methods Cell Biol*, *105*, 517-524. https://doi.org/10.1016/b978-0-12-381320-6.00022-9

Kusik, B. W., Carvan, M. J., 3rd, & Udvadia, A. J. (2008). Detection of mercury in aquatic environments using EPRE reporter zebrafish. *Mar Biotechnol (NY)*, *10*(6), 750-757. https://doi.org/10.1007/s10126-008-9113-x

Kyrylkova, K., Kyryachenko, S., Leid, M., & Kioussi, C. (2012). Detection of apoptosis by TUNEL assay. *Methods Mol Biol*, *887*, 41-47. https://doi.org/10.1007/978-1-61779-860-3_5

Labadorf, A., Choi, S. H., & Myers, R. H. (2017). Evidence for a Pan-Neurodegenerative Disease Response in Huntington's and Parkinson's Disease Expression Profiles. *Front Mol Neurosci*, *10*, 430. https://doi.org/10.3389/fnmol.2017.00430

Lacagnina, S. (2020). The Developmental Origins of Health and Disease (DOHaD). *Am J Lifestyle Med*, *14*(1), 47-50. https://doi.org/10.1177/1559827619879694

Lakstygal, A. M., de Abreu, M. S., & Kalueff, A. V. (2018). Zebrafish models of epigenetic regulation of CNS functions. *Brain Res Bull*, *142*, 344-351. https://doi.org/10.1016/j.brainresbull.2018.08.022

Lal, P., & Kawakami, K. (2022). Integrated Behavioral, Genetic and Brain Circuit Visualization Methods to Unravel Functional Anatomy of Zebrafish Amygdala. *Front Neuroanat*, *16*, 837527. https://doi.org/10.3389/fnana.2022.837527

Lamberto, F., Peral-Sanchez, I., Muenthaisong, S., Zana, M., Willaime-Morawek, S., & Dinnyés, A. (2021). Environmental Alterations during Embryonic Development: Studying the Impact of Stressors on Pluripotent Stem Cell-Derived Cardiomyocytes. *Genes (Basel)*, *12*(10). https://doi.org/10.3390/genes12101564

Lammer, E., Carr, G. J., Wendler, K., Rawlings, J. M., Belanger, S. E., & Braunbeck, T. (2009). Is the fish embryo toxicity test (FET) with the zebrafish (Danio rerio) a potential alternative for the fish acute toxicity test? *Comp Biochem Physiol C Toxicol Pharmacol*, *149*(2), 196-209. https://doi.org/10.1016/j.cbpc.2008.11.006

Lee, J., Horzmann, K. A., & Freeman, J. L. (2018). An embryonic 100µg/L lead exposure results in sex-specific expression changes in genes associated with the neurological system in female or cancer in male adult zebrafish brains. *Neurotoxicol Teratol*, *65*, 60-69. https://doi.org/10.1016/j.ntt.2017.10.006

Lee, J., Peterson, S. M., & Freeman, J. L. (2017). Sex-specific characterization and evaluation of the Alzheimer's disease genetic risk factor sorl1 in zebrafish during aging and in the adult brain following a 100 ppb embryonic lead exposure. *J Appl Toxicol*, *37*(4), 400-407. https://doi.org/10.1002/jat.3372

Li, F., Lin, J., Liu, X., Li, W., Ding, Y., Zhang, Y., Zhou, S., Guo, N., & Li, Q. (2018). Characterization of the locomotor activities of zebrafish larvae under the influence of various neuroactive drugs. *Annals of Translational Medicine*, *6*(10), 173. https://atm.amegroups.org/article/view/19504

https://www.ncbi.nlm.nih.gov/pmc/articles/PMC5994518/pdf/atm-06-10-173.pdf

Li, Y. (2021). Modern epigenetics methods in biological research. *Methods*, *187*, 104-113. https://doi.org/10.1016/j.ymeth.2020.06.022

Li, Y., Park, C., & Li, X. (2018). Base Modifications: Regulation of Stem Cell Functions and Diseases. *Stem Cells Int*, *2018*, 5402384. https://doi.org/10.1155/2018/5402384

Li, Y., Sun, H., Chen, Z., Xu, H., Bu, G., & Zheng, H. (2016). Implications of GABAergic Neurotransmission in Alzheimer's Disease. *Front Aging Neurosci*, *8*, 31. https://doi.org/10.3389/fnagi.2016.00031

Li, Y., & Tollefsbol, T. O. (2011). DNA methylation detection: bisulfite genomic sequencing analysis. *Methods Mol Biol*, *791*, 11-21. https://doi.org/10.1007/978-1-61779-316-5_2

Liu, H., Gooneratne, R., Huang, X., Lai, R., Wei, J., & Wang, W. (2015). A rapid in vivo zebrafish model to elucidate oxidative stress-mediated PCB126-induced apoptosis and developmental toxicity. *Free Radic Biol Med*, *84*, 91-102. https://doi.org/10.1016/j.freeradbiomed.2015.03.002

Liu, J., Xu, Y., Liao, G., Tu, H., Huang, Y., Peng, T., Chen, X., Huang, Z., Zhang, Y., Meng, X., & Zou, F. (2022). The role of ambra1 in Pb-induced developmental neurotoxicity in zebrafish. *Biochem Biophys Res Commun*, *594*, 139-145. https://doi.org/10.1016/j.bbrc.2021.12.084

Liu, M., Choi, D. Y., Hunter, R. L., Pandya, J. D., Cass, W. A., Sullivan, P. G., Kim, H. C., Gash, D. M., & Bing, G. (2010). Trichloroethylene induces dopaminergic neurodegeneration in Fisher 344 rats. *J Neurochem*, *112*(3), 773-783. https://doi.org/10.1111/j.1471-4159.2009.06497.x

Liu, S., Qiu, W., Li, R., Chen, B., Wu, X., Magnuson, J. T., Xu, B., Luo, S., Xu, E. G., & Zheng, C. (2023). Perfluorononanoic Acid Induces Neurotoxicity via Synaptogenesis Signaling in Zebrafish. *Environ Sci Technol*, *57*(9), 3783-3793. https://doi.org/10.1021/acs.est.2c06739

Liu, X., Zhang, R., & Jin, Y. (2020). Differential responses of larval zebrafish to the fungicide propamocarb: Endpoints at development, locomotor behavior and oxidative stress. *Sci Total Environ*, *731*, 139136. https://doi.org/10.1016/j.scitotenv.2020.139136

Lockwood, B., Bjerke, S., Kobayashi, K., & Guo, S. (2004). Acute effects of alcohol on larval zebrafish: a genetic system for large-scale screening. *Pharmacol Biochem Behav*, *77*(3), 647-654. https://doi.org/10.1016/j.pbb.2004.01.003

Macleod, D., Clark, V. H., & Bird, A. (1999). Absence of genome-wide changes in DNA methylation during development of the zebrafish. *Nat Genet*, *23*(2), 139-140. https://doi.org/10.1038/13767

MacMahon Copas, A. N., McComish, S. F., Fletcher, J. M., & Caldwell, M. A. (2021). The Pathogenesis of Parkinson's Disease: A Complex Interplay Between Astrocytes, Microglia, and T Lymphocytes? *Front Neurol*, *12*, 666737. https://doi.org/10.3389/fneur.2021.666737

Mahapatra, A., Gupta, P., Suman, A., Ray, S. S., Malafaia, G., & Singh, R. K. (2023). Unraveling the mechanisms of perfluorooctanesulfonic acid-induced dopaminergic neurotoxicity and microglial activation in developing zebrafish. *Sci Total Environ*, *887*, 164030. https://doi.org/10.1016/j.scitotenv.2023.164030

Majtnerová, P., & Roušar, T. (2018). An overview of apoptosis assays detecting DNA fragmentation. *Mol Biol Rep*, *45*(5), 1469-1478. https://doi.org/10.1007/s11033-018-4258-9

Martin, C. C., Laforest, L., Akimenko, M. A., & Ekker, M. (1999). A role for DNA methylation in gastrulation and somite patterning. *Developmental biology*, *206*(2), 189-205. https://doi.org/10.1006/dbio.1998.9105

Martinowich, K., & Lu, B. (2008). Interaction between BDNF and serotonin: role in mood disorders. *Neuropsychopharmacology*, *33*(1), 73-83. https://doi.org/10.1038/sj.npp.1301571

Martyn, C. N., Barker, D. J., Osmond, C., Harris, E. C., Edwardson, J. A., & Lacey, R. F. (1989). Geographical relation between Alzheimer's disease and aluminum in drinking water. *Lancet*, *1*(8629), 59-62.

Mathur, P., & Guo, S. (2011). Differences of acute versus chronic ethanol exposure on anxiety-like behavioral responses in zebrafish. *Behav Brain Res*, *219*(2), 234-239. https://doi.org/10.1016/j.bbr.2011.01.019

Mathur, S., Gawas, C., Ahmad, I. Z., Wani, M., & Tabassum, H. (2023). Neurodegenerative disorders: Assessing the impact of natural vs drug-induced treatment options. *Aging Med (Milton)*, *6*(1), 82-97. https://doi.org/10.1002/agm2.12243

McClenahan, P., Troup, M., & Scott, E. K. (2012). Fin-tail coordination during escape and predatory behavior in larval zebrafish. *PLoS One*, *7*(2), e32295. https://doi.org/10.1371/journal.pone.0032295

McGrath, P., & Seng, W. L. (2013). Use of zebrafish apoptosis assays for preclinical drug discovery. *Expert Opin Drug Discov*, *8*(10), 1191-1202. https://doi.org/10.1517/17460441.2013.825244

McKelvey-Martin, V. J., Green, M. H., Schmezer, P., Pool-Zobel, B. L., De Méo, M. P., & Collins, A. (1993). The single cell gel electrophoresis assay (comet assay): a European review. *Mutat Res*, *288*(1), 47-63. https://doi.org/10.1016/0027-5107(93)90207-v

McKeown, K. A., Downes, G. B., & Hutson, L. D. (2009). Modular laboratory exercises to analyze the development of zebrafish motor behavior. *Zebrafish*, *6*(2), 179-185. https://doi.org/10.1089/zeb.2008.0564

McLean, D. L., & Fetcho, J. R. (2004). Ontogeny and innervation patterns of dopaminergic, noradrenergic, and serotonergic neurons in larval zebrafish. *J Comp Neurol*, *480*(1), 38-56. https://doi.org/10.1002/cne.20280

Meldrum, B. S. (2000). Glutamate as a neurotransmitter in the brain: review of physiology and pathology. *J Nutr*, *130*(4S Suppl), 1007s-1015s. https://doi.org/10.1093/jn/130.4.1007S

Menelaou, E., Husbands, E. E., Pollet, R. G., Coutts, C. A., Ali, D. W., & Svoboda, K. R. (2008). Embryonic motor activity and implications for regulating motoneuron axonal pathfinding in zebrafish. *Eur J Neurosci*, *28*(6), 1080-1096. https://doi.org/10.1111/j.1460-9568.2008.06418.x

Millán-Zambrano, G., Burton, A., Bannister, A. J., & Schneider, R. (2022). Histone post-translational modifications — cause and consequence of genome function. *Nature Reviews Genetics*, *23*(9), 563-580. https://doi.org/10.1038/s41576-022-00468-7

Miller, D. B., & O'Callaghan, J. P. (2015). Biomarkers of Parkinson's disease: present and future. *Metabolism*, *64*(3 Suppl 1), S40-46. https://doi.org/10.1016/j.metabol.2014.10.030

Mirsaeidi, M., Gidfar, S., Vu, A., & Schraufnagel, D. (2016). Annexins family: insights into their functions and potential role in pathogenesis of sarcoidosis. *J Transl Med*, *14*, 89. https://doi.org/10.1186/s12967-016-0843-7

Mirzayans, R., & Murray, D. (2020). Do TUNEL and Other Apoptosis Assays Detect Cell Death in Preclinical Studies? *Int J Mol Sci*, *21*(23). https://doi.org/10.3390/ijms21239090

Miyata, K., Naito, M., Miyata, T., Mokuda, S., & Asahara, H. (2017). Bisulfite Sequencing for DNA Methylation Analysis of Primary Muscle Stem Cells. *Methods Mol Biol*, *1668*, 3-13. https://doi.org/10.1007/978-1-4939-7283-8_1

Monaco, A., Capriello, T., Grimaldi, M. C., Schiano, V., & Ferrandino, I. (2017). Neurodegeneration in zebrafish embryos and adults after cadmium exposure. *Eur J Histochem*, *61*(4), 2833. https://doi.org/10.4081/ejh.2017.2833

Morris, K. V. (2009). Non-coding RNAs, epigenetic memory and the passage of information to progeny. *RNA Biol*, *6*(3), 242-247. https://doi.org/10.4161/rna.6.3.8353

Mourabit, S., Fitzgerald, J. A., Ellis, R. P., Takesono, A., Porteus, C. S., Trznadel, M., Metz, J., Winter, M. J., Kudoh, T., & Tyler, C. R. (2019). New insights into organ-specific oxidative stress mechanisms using a novel biosensor zebrafish. *Environ Int*, *133*(Pt A), 105138. https://doi.org/10.1016/j.envint.2019.105138

Murphy, M. P., Bayir, H., Belousov, V., Chang, C. J., Davies, K. J. A., Davies, M. J., Dick, T. P., Finkel, T., Forman, H. J., Janssen-Heininger, Y., Gems, D., Kagan, V. E., Kalyanaraman, B., Larsson, N. G., Milne, G. L., Nyström, T., Poulsen, H. E., Radi, R., Van Remmen, H.,…Halliwell, B. (2022). Guidelines for measuring reactive oxygen species and oxidative damage in cells and in vivo. *Nat Metab*, *4*(6), 651-662. https://doi.org/10.1038/s42255-022-00591-z

Ncube, D., Tallafuss, A., Serafin, J., Bruckner, J., Farnsworth, D. R., Miller, A. C., Eisen, J. S., & Washbourne, P. (2022). A conserved transcriptional fingerprint of multi-neurotransmitter neurons necessary for social behavior. *BMC Genomics*, *23*(1), 675. https://doi.org/10.1186/s12864-022-08879-w

Neely, S. A., & Lyons, D. A. (2021). Insights Into Central Nervous System Glial Cell Formation and Function From Zebrafish. *Front Cell Dev Biol*, *9*, 754606. https://doi.org/10.3389/fcell.2021.754606

Ng, N. S., & Ooi, L. (2021). A Simple Microplate Assay for Reactive Oxygen Species Generation and Rapid Cellular Protein Normalization. *Bio Protoc*, *11*(1), e3877. https://doi.org/10.21769/BioProtoc.3877

Ngo, D. H., & Vo, T. S. (2019). An Updated Review on Pharmaceutical Properties of Gamma-Aminobutyric Acid. *Molecules*, *24*(15). https://doi.org/10.3390/molecules24152678

Ngo, V., & Duennwald, M. L. (2022). Nrf2 and Oxidative Stress: A General Overview of Mechanisms and Implications in Human Disease. *Antioxidants (Basel)*, *11*(12). https://doi.org/10.3390/antiox11122345

Ni, A., & Ernst, C. (2022). Evidence That Substantia Nigra Pars Compacta Dopaminergic Neurons Are Selectively Vulnerable to Oxidative Stress Because They Are Highly Metabolically Active. *Front Cell Neurosci*, *16*, 826193. https://doi.org/10.3389/fncel.2022.826193

Nikolac Perkovic, M., Videtic Paska, A., Konjevod, M., Kouter, K., Svob Strac, D., Nedic Erjavec, G., & Pivac, N. (2021). Epigenetics of Alzheimer's Disease. *Biomolecules*, *11*(2). https://doi.org/10.3390/biom11020195

Nomura, W. (2018). Development of Toolboxes for Precision Genome/Epigenome Editing and Imaging of Epigenetics. *Chem Rec*, *18*(12), 1717-1726. https://doi.org/10.1002/tcr.201800036

Norton, W., & Bally-Cuif, L. (2010). Adult zebrafish as a model organism for behavioural genetics. *BMC Neuroscience*, *11*(1), 90. https://doi.org/10.1186/1471-2202-11-90

O'Neill, L. P., VerMilyea, M. D., & Turner, B. M. (2006). Epigenetic characterization of the early embryo with a chromatin immunoprecipitation protocol applicable to small cell populations. *Nat Genet*, *38*(7), 835-841. https://doi.org/10.1038/ng1820

OECD. (1998). *Test No. 212: Fish, Short-term Toxicity Test on Embryo and Sac-Fry Stages*. https://doi.org/doi:https://doi.org/10.1787/9789264070141-en

OECD. (2008). *Test No. 407: Repeated Dose 28-day Oral Toxicity Study in Rodents*. https://doi.org/doi:https://doi.org/10.1787/9789264070684-en

OECD. (2012). *Test No. 305: Bioaccumulation in Fish: Aqueous and Dietary Exposure*. https://doi.org/doi:https://doi.org/10.1787/9789264185296-en

OECD. (2013a). *Test No. 210: Fish, Early-life Stage Toxicity Test*. https://doi.org/doi:https://doi.org/10.1787/9789264203785-en

OECD. (2013b). *Test No. 236: Fish Embryo Acute Toxicity (FET) Test*. https://doi.org/doi:https://doi.org/10.1787/9789264203709-en

OECD. (2018). *Test No. 408: Repeated Dose 90-Day Oral Toxicity Study in Rodents*. https://doi.org/doi:https://doi.org/10.1787/9789264070707-en

OECD. (2019). *Test No. 203: Fish, Acute Toxicity Test*. https://doi.org/doi:https://doi.org/10.1787/9789264069961-en

Olivares, C. I., Field, J. A., Simonich, M., Tanguay, R. L., & Sierra-Alvarez, R. (2016). Arsenic (III, V), indium (III), and gallium (III) toxicity to zebrafish embryos using a high-

throughput multi-endpoint in vivo developmental and behavioral assay. *Chemosphere*, *148*, 361-368. https://doi.org/10.1016/j.chemosphere.2016.01.050

Ortmann, J., Altenburger, R., Scholz, S., & Luckenbach, T. (2022). Photomotor response data analysis approach to assess chemical neurotoxicity with the zebrafish embryo. *Altex*, *39*(1), 82-94. https://doi.org/10.14573/altex.2004021

Oshima, E., Ishihara, T., Yokota, O., Nakashima-Yasuda, H., Nagao, S., Ikeda, C., Naohara, J., Terada, S., & Uchitomi, Y. (2013). Accelerated tau aggregation, apoptosis and neurological dysfunction caused by chronic oral administration of aluminum in a mouse model of tauopathies. *Brain Pathol*, *23*(6), 633-644. https://doi.org/10.1111/bpa.12059

Owens, D. F., & Kriegstein, A. R. (2002). Is there more to GABA than synaptic inhibition? *Nat Rev Neurosci*, *3*(9), 715-727. https://doi.org/10.1038/nrn919

Pal, M. M. (2021). Glutamate: The Master Neurotransmitter and Its Implications in Chronic Stress and Mood Disorders. *Front Hum Neurosci*, *15*, 722323. https://doi.org/10.3389/fnhum.2021.722323

Parlak, V. (2018). Evaluation of apoptosis, oxidative stress responses, AChE activity and body malformations in zebrafish (Danio rerio) embryos exposed to deltamethrin. *Chemosphere*, *207*, 397-403. https://doi.org/10.1016/j.chemosphere.2018.05.112

Parliament, E., & Council, E. (2010). DIRECTIVE 2010/63/EU on the protection of animals used for scientific purposes. *EU Official Journal*, *L276*.

Passani, M. B., Bacciottini, L., Mannaioni, P. F., & Blandina, P. (2000). Central histaminergic system and cognition. *Neurosci Biobehav Rev*, *24*(1), 107-113. https://doi.org/10.1016/s0149-7634(99)00053-6

Percário, S., da Silva Barbosa, A., Varela, E. L. P., Gomes, A. R. Q., Ferreira, M. E. S., de Nazaré Araújo Moreira, T., & Dolabela, M. F. (2020). Oxidative Stress in Parkinson's Disease: Potential Benefits of Antioxidant Supplementation. *Oxid Med Cell Longev*, *2020*, 2360872. https://doi.org/10.1155/2020/2360872

Petrovic, M., Farré, M., Eljarrat, E., Diaz, S., & Barceló, D. (2013). Chapter 14 - Environmental Analysis: Emerging Pollutants. In S. Fanali, P. R. Haddad, C. F. Poole, P. Schoenmakers, & D. Lloyd (Eds.), *Liquid Chromatography* (pp. 389-410). Elsevier. https://doi.org/https://doi.org/10.1016/B978-0-12-415806-1.00014-0

Pinheiro-da-Silva, J., & Luchiari, A. C. (2021). Embryonic ethanol exposure on zebrafish early development. *Brain Behav*, *11*(6), e02062. https://doi.org/10.1002/brb3.2062

Provensi, G., Costa, A., Izquierdo, I., Blandina, P., & Passani, M. B. (2020). Brain histamine modulates recognition memory: possible implications in major cognitive disorders. *Br J Pharmacol*, *177*(3), 539-556. https://doi.org/10.1111/bph.14478

Quiñonez-Silvero, C., Hübner, K., & Herzog, W. (2020). Development of the brain vasculature and the blood-brain barrier in zebrafish. *Developmental biology*, *457*(2), 181-190. https://doi.org/10.1016/j.ydbio.2019.03.005

Rana, S. V. (2008). Metals and apoptosis: recent developments. *J Trace Elem Med Biol*, *22*(4), 262-284. https://doi.org/10.1016/j.jtemb.2008.08.002

Reddy-Thootkur, M., Kraguljac, N. V., & Lahti, A. C. (2022). The role of glutamate and GABA in cognitive dysfunction in schizophrenia and mood disorders - A systematic review of magnetic resonance spectroscopy studies. *Schizophr Res*, *249*, 74-84. https://doi.org/10.1016/j.schres.2020.02.001

Reif, D. M., Truong, L., Mandrell, D., Marvel, S., Zhang, G., & Tanguay, R. L. (2016). High-throughput characterization of chemical-associated embryonic behavioral changes predicts teratogenic outcomes. *Arch Toxicol*, *90*(6), 1459-1470. https://doi.org/10.1007/s00204-015-1554-1

Ribble, D., Goldstein, N. B., Norris, D. A., & Shellman, Y. G. (2005). A simple technique for quantifying apoptosis in 96-well plates. *BMC Biotechnol*, *5*, 12. https://doi.org/10.1186/1472-6750-5-12

Rico, E. P., Rosemberg, D. B., Seibt, K. J., Capiotti, K. M., Da Silva, R. S., & Bonan, C. D. (2011). Zebrafish neurotransmitter systems as potential pharmacological and toxicological targets. *Neurotoxicol Teratol*, *33*(6), 608-617. https://doi.org/10.1016/j.ntt.2011.07.007

Rosa, J. G. S., Lima, C., & Lopes-Ferreira, M. (2022). Zebrafish Larvae Behavior Models as a Tool for Drug Screenings and Pre-Clinical Trials: A Review. *Int J Mol Sci*, *23*(12). https://doi.org/10.3390/ijms23126647

Rozov, S. V., Porkka-Heiskanen, T., & Panula, P. (2015). On the Role of Histamine Receptors in the Regulation of Circadian Rhythms. *PLoS One*, *10*(12), e0144694. https://doi.org/10.1371/journal.pone.0144694

S, S. V. (1941). Fluoreszenzmikroskopische Untersuchungen über die Aufnahme und Speicherung des Akridinorange durch lebende und tote Pflanzenzellen. *Protoplasma*, *36*, 469.

Sáez-Espinosa, P., Franco-Esclapez, C., Robles-Gómez, L., Silva, W., Romero, A., Immler, S., & Gómez-Torres, M. J. (2022). Morphological and ultrastructural alterations of zebrafish (Danio rerio) spermatozoa after motility activation. *Theriogenology*, *188*, 108-115. https://doi.org/10.1016/j.theriogenology.2022.05.025

Saint-Amant, L., & Drapeau, P. (1998). Time course of the development of motor behaviors in the zebrafish embryo. *J Neurobiol*, *37*(4), 622-632. https://doi.org/10.1002/(sici)1097-4695(199812)37:4<622::aid-neu10>3.0.co;2-s

Sales Cadena, M. R., Cadena, P. G., Watson, M. R., Sarmah, S., Boehm Ii, S. L., & Marrs, J. A. (2021). Zebrafish (Danio rerio) larvae show behavioral and embryonic development defects when exposed to opioids at embryo stage. *Neurotoxicol Teratol*, *85*, 106964. https://doi.org/10.1016/j.ntt.2021.106964

Santana, D. A., Smith, M. A. C., & Chen, E. S. (2023). Histone Modifications in Alzheimer's Disease. *Genes (Basel)*, *14*(2). https://doi.org/10.3390/genes14020347

Sarawagi, A., Soni, N. D., & Patel, A. B. (2021). Glutamate and GABA Homeostasis and Neurometabolism in Major Depressive Disorder. *Front Psychiatry*, *12*, 637863. https://doi.org/10.3389/fpsyt.2021.637863

Sayre, L. M., Perry, G., & Smith, M. A. (2008). Oxidative stress and neurotoxicity. *Chem Res Toxicol*, *21*(1), 172-188. https://doi.org/10.1021/tx700210j

Schmidt, R., Strähle, U., & Scholpp, S. (2013). Neurogenesis in zebrafish - from embryo to adult. *Neural Dev*, *8*, 3. https://doi.org/10.1186/1749-8104-8-3

Schnörr, S. J., Steenbergen, P. J., Richardson, M. K., & Champagne, D. L. (2012). Measuring thigmotaxis in larval zebrafish. *Behav Brain Res*, *228*(2), 367-374. https://doi.org/10.1016/j.bbr.2011.12.016

Schür, R. R., Draisma, L. W., Wijnen, J. P., Boks, M. P., Koevoets, M. G., Joëls, M., Klomp, D. W., Kahn, R. S., & Vinkers, C. H. (2016). Brain GABA levels across psychiatric disorders: A systematic literature review and meta-analysis of (1) H-MRS studies. *Hum Brain Mapp*, *37*(9), 3337-3352. https://doi.org/10.1002/hbm.23244

Searle, B., Müller, M., Carell, T., & Kellett, A. (2023). Third-Generation Sequencing of Epigenetic DNA. *Angew Chem Int Ed Engl*, *62*(14), e202215704. https://doi.org/10.1002/anie.202215704

Shi, Q., Yang, H., Chen, Y., Zheng, N., Li, X., Wang, X., Ding, W., & Zhang, B. (2023). Developmental Neurotoxicity of Trichlorfon in Zebrafish Larvae. *Int J Mol Sci*, *24*(13). https://doi.org/10.3390/ijms241311099

Shi, Q., Yang, H., Zheng, Y., Zheng, N., Lei, L., Li, X., & Ding, W. (2023). Neurotoxicity of an emerging organophosphorus flame retardant, resorcinol bis(diphenyl phosphate), in zebrafish larvae. *Chemosphere*, *334*, 138944. https://doi.org/10.1016/j.chemosphere.2023.138944

Shou, W. Z. (2020). Current status and future directions of high-throughput ADME screening in drug discovery. *J Pharm Anal*, *10*(3), 201-208. https://doi.org/10.1016/j.jpha.2020.05.004

Shrivastava, A. N., Triller, A., & Sieghart, W. (2011). GABA(A) Receptors: Post-Synaptic Co-Localization and Cross-Talk with Other Receptors. *Front Cell Neurosci*, *5*, 7. https://doi.org/10.3389/fncel.2011.00007

Smith, A. J., & Lilley, E. (2019). The Role of the Three Rs in Improving the Planning and Reproducibility of Animal Experiments. *Animals (Basel)*, *9*(11). https://doi.org/10.3390/ani9110975

Sobanska, M., Scholz, S., Nyman, A. M., Cesnaitis, R., Gutierrez Alonso, S., Klüver, N., Kühne, R., Tyle, H., de Knecht, J., Dang, Z., Lundbergh, I., Carlon, C., & De Coen, W. (2018). Applicability of the fish embryo acute toxicity (FET) test (OECD 236) in the regulatory context of Registration, Evaluation, Authorisation, and Restriction of Chemicals (REACH). *Environ Toxicol Chem*, *37*(3), 657-670. https://doi.org/10.1002/etc.4055

Somogyi, A., Rosta, K., Pusztai, P., Tulassay, Z., & Nagy, G. (2007). Antioxidant measurements. *Physiol Meas*, *28*(4), R41-55. https://doi.org/10.1088/0967-3334/28/4/r01

Sorrells, S., Toruno, C., Stewart, R. A., & Jette, C. (2013). Analysis of apoptosis in zebrafish embryos by whole-mount immunofluorescence to detect activated Caspase 3. *J Vis Exp*(82), e51060. https://doi.org/10.3791/51060

Spitz, D. R., & Oberley, L. W. (1989). An assay for superoxide dismutase activity in mammalian tissue homogenates. *Anal Biochem*, *179*(1), 8-18. https://doi.org/10.1016/0003-2697(89)90192-9

Stewart, A., Gaikwad, S., Kyzar, E., Green, J., Roth, A., & Kalueff, A. V. (2012). Modeling anxiety using adult zebrafish: a conceptual review. *Neuropharmacology*, *62*(1), 135-143. https://doi.org/10.1016/j.neuropharm.2011.07.037

Stewart, A. M., Gaikwad, S., Kyzar, E., & Kalueff, A. V. (2012). Understanding spatio-temporal strategies of adult zebrafish exploration in the open field test. *Brain Res*, *1451*, 44-52. https://doi.org/10.1016/j.brainres.2012.02.064

Strähle, U., Scholz, S., Geisler, R., Greiner, P., Hollert, H., Rastegar, S., Schumacher, A., Selderslaghs, I., Weiss, C., Witters, H., & Braunbeck, T. (2012). Zebrafish embryos as an alternative to animal experiments--a commentary on the definition of the onset of protected life stages in animal welfare regulations. *Reprod Toxicol*, *33*(2), 128-132. https://doi.org/10.1016/j.reprotox.2011.06.121

Strömqvist, M., Tooke, N., & Brunström, B. (2010). DNA methylation levels in the 5' flanking region of the vitellogenin I gene in liver and brain of adult zebrafish (Danio rerio)--sex and tissue differences and effects of 17alpha-ethinylestradiol exposure. *Aquat Toxicol*, *98*(3), 275-281. https://doi.org/10.1016/j.aquatox.2010.02.023

*Summary of the Toxic Substances Control Act*. (2023). https://www.epa.gov/laws-regulations/summary-toxic-substances-control-act

Sun, H. J., Zhang, J. Y., Wang, Q., Zhu, E., Chen, W., Lin, H., Chen, J., & Hong, H. (2019). Environmentally relevant concentrations of arsenite induces developmental toxicity and oxidative responses in the early life stage of zebrafish. *Environ Pollut*, *254*(Pt A), 113022. https://doi.org/10.1016/j.envpol.2019.113022

Sun, X., Yang, Q., Jing, M., Jia, X., Tian, L., & Tao, J. (2023). Environmentally relevant concentrations of organic (benzophenone-3) and inorganic (titanium dioxide nanoparticles) UV filters co-exposure induced neurodevelopmental toxicity in zebrafish. *Ecotoxicol Environ Saf*, *249*, 114343. https://doi.org/10.1016/j.ecoenv.2022.114343

Tan, J. K., Nazar, F. H., Makpol, S., & Teoh, S. L. (2022). Zebrafish: A Pharmacological Model for Learning and Memory Research. *Molecules*, *27*(21). https://doi.org/10.3390/molecules27217374

Tanner, C. M., & Goldman, S. M. (1996). Epidemiology of Parkinson's disease. *Neurol Clin*, *14*(2), 317-335. https://doi.org/10.1016/s0733-8619(05)70259-0

Teleanu, R. I., Niculescu, A. G., Roza, E., Vladâcenco, O., Grumezescu, A. M., & Teleanu, D. M. (2022). Neurotransmitters-Key Factors in Neurological and Neurodegenerative Disorders of the Central Nervous System. *Int J Mol Sci*, *23*(11). https://doi.org/10.3390/ijms23115954

Terrazas-Salgado, L., García-Gasca, A., Betancourt-Lozano, M., Llera-Herrera, R., Alvarado-Cruz, I., & Yáñez-Rivera, B. (2022). Epigenetic Transgenerational Modifications Induced by Xenobiotic Exposure in Zebrafish. *Front Cell Dev Biol*, *10*, 832982. https://doi.org/10.3389/fcell.2022.832982

Tiwari, S., Atluri, V., Kaushik, A., Yndart, A., & Nair, M. (2019). Alzheimer's disease: pathogenesis, diagnostics, and therapeutics. *Int J Nanomedicine*, *14*, 5541-5554. https://doi.org/10.2147/ijn.s200490

Tolosa, E., Garrido, A., Scholz, S. W., & Poewe, W. (2021). Challenges in the diagnosis of Parkinson's disease. *Lancet Neurol*, *20*(5), 385-397. https://doi.org/10.1016/s1474-4422(21)00030-2

Tönnies, E., & Trushina, E. (2017). Oxidative Stress, Synaptic Dysfunction, and Alzheimer's Disease. *J Alzheimers Dis*, *57*(4), 1105-1121. https://doi.org/10.3233/jad-161088

Torres-Ruiz, M., de Alba González, M., Morales, M., Martin-Folgar, R., González, M. C., Cañas-Portilla, A. I., & De la Vieja, A. (2023). Neurotoxicity and endocrine disruption caused by polystyrene nanoparticles in zebrafish embryo. *Science of The Total Environment*, *874*, 162406. https://doi.org/https://doi.org/10.1016/j.scitotenv.2023.162406

Tucker, B., & Lardelli, M. (2007). A rapid apoptosis assay measuring relative acridine orange fluorescence in zebrafish embryos. *Zebrafish*, *4*(2), 113-116. https://doi.org/10.1089/zeb.2007.0508

Tufi, S., Leonards, P., Lamoree, M., de Boer, J., Legler, J., & Legradi, J. (2016). Changes in Neurotransmitter Profiles during Early Zebrafish (Danio rerio) Development and after Pesticide Exposure. *Environ Sci Technol*, *50*(6), 3222-3230. https://doi.org/10.1021/acs.est.5b05665

Urbaniak, S. K., Boguszewska, K., Szewczuk, M., Kaźmierczak-Barańska, J., & Karwowski, B. T. (2020). 8-Oxo-7,8-Dihydro-2'-Deoxyguanosine (8-oxodG) and 8-Hydroxy-2'-

Deoxyguanosine (8-OHdG) as a Potential Biomarker for Gestational Diabetes Mellitus (GDM) Development. *Molecules*, *25*(1). https://doi.org/10.3390/molecules25010202

Valavanidis, A., Vlachogianni, T., & Fiotakis, C. (2009). 8-hydroxy-2' -deoxyguanosine (8-OHdG): A critical biomarker of oxidative stress and carcinogenesis. *J Environ Sci Health C Environ Carcinog Ecotoxicol Rev*, *27*(2), 120-139. https://doi.org/10.1080/10590500902885684

Valko, M., Morris, H., & Cronin, M. T. (2005). Metals, toxicity and oxidative stress. *Curr Med Chem*, *12*(10), 1161-1208. https://doi.org/10.2174/0929867053764635

van Engeland, M., Nieland, L. J., Ramaekers, F. C., Schutte, B., & Reutelingsperger, C. P. (1998). Annexin V-affinity assay: a review on an apoptosis detection system based on phosphatidylserine exposure. *Cytometry*, *31*(1), 1-9. https://doi.org/10.1002/(sici)1097-0320(19980101)31:1<1::aid-cyto1>3.0.co;2-r

van Ham, T. J., Mapes, J., Kokel, D., & Peterson, R. T. (2010). Live imaging of apoptotic cells in zebrafish. *Faseb j*, *24*(11), 4336-4342. https://doi.org/10.1096/fj.10-161018

Vaughan, M., & van Egmond, R. (2010). The use of the zebrafish (Danio rerio) embryo for the acute toxicity testing of surfactants, as a possible alternative to the acute fish test. *Altern Lab Anim*, *38*(3), 231-238. https://doi.org/10.1177/026119291003800310

Verma, R., Raj Choudhary, P., Kumar Nirmal, N., Syed, F., & Verma, R. (2022). Neurotransmitter systems in zebrafish model as a target for neurobehavioural studies. *Materials Today: Proceedings*, *69*, 1565-1580. https://doi.org/https://doi.org/10.1016/j.matpr.2022.07.147

Vorhees, C. V., Williams, M. T., Hawkey, A. B., & Levin, E. D. (2021). Translating Neurobehavioral Toxicity Across Species From Zebrafish to Rats to Humans: Implications for Risk Assessment. *Front Toxicol*, *3*, 629229. https://doi.org/10.3389/ftox.2021.629229

Wang, H., Mu, S., Zhang, F., Liu, H., Zhang, H., & Kang, X. (2015). Effects of Atrazine on the Development of Neural System of Zebrafish, Danio rerio. *Biomed Res Int*, *2015*, 976068. https://doi.org/10.1155/2015/976068

Wang, J., Wang, D., Hu, G., Yang, L., Yan, D., Wang, M., Serikuly, N., Alpyshov, E., Amstislavskaya, T. G., Demin, K. A., de Abreu, M. S., Zabegalov, K. N., & Kalueff, A.

V. (2020). A new method for vibration-based neurophenotyping of zebrafish. *J Neurosci Methods*, *333*, 108563. https://doi.org/10.1016/j.jneumeth.2019.108563

Wang, S., Bryan, C., Xie, J., Zhao, H., Lin, L. F., Tai, J. A. C., Horzmann, K. A., Sanchez, O. F., Zhang, M., Freeman, J. L., & Yuan, C. (2022). Atrazine exposure in zebrafish induces aberrant genome-wide methylation. *Neurotoxicol Teratol*, *92*, 107091. https://doi.org/10.1016/j.ntt.2022.107091

Wang, X. H., Souders, C. L., 2nd, Zhao, Y. H., & Martyniuk, C. J. (2018). Paraquat affects mitochondrial bioenergetics, dopamine system expression, and locomotor activity in zebrafish (Danio rerio). *Chemosphere*, *191*, 106-117. https://doi.org/10.1016/j.chemosphere.2017.10.032

Wang, Z., Li, K., Xu, Y., Song, Z., Lan, X., Pan, C., Zhang, S., Foulkes, N. S., & Zhao, H. (2023). Ferroptosis contributes to nickel-induced developmental neurotoxicity in zebrafish. *Sci Total Environ*, *858*(Pt 3), 160078. https://doi.org/10.1016/j.scitotenv.2022.160078

Waryah, C. B., Moses, C., Arooj, M., & Blancafort, P. (2018). Zinc Fingers, TALEs, and CRISPR Systems: A Comparison of Tools for Epigenome Editing. *Methods Mol Biol*, *1767*, 19-63. https://doi.org/10.1007/978-1-4939-7774-1_2

Weber, G. J., Sepúlveda, M. S., Peterson, S. M., Lewis, S. S., & Freeman, J. L. (2013). Transcriptome alterations following developmental atrazine exposure in zebrafish are associated with disruption of neuroendocrine and reproductive system function, cell cycle, and carcinogenesis. *Toxicol Sci*, *132*(2), 458-466. https://doi.org/10.1093/toxsci/kft017

Wilkinson, B. L., & Landreth, G. E. (2006). The microglial NADPH oxidase complex as a source of oxidative stress in Alzheimer's disease. *Journal of Neuroinflammation*, *3*(1), 30. https://doi.org/10.1186/1742-2094-3-30

Winata, C. L., Korzh, S., Kondrychyn, I., Zheng, W., Korzh, V., & Gong, Z. (2009). Development of zebrafish swimbladder: The requirement of Hedgehog signaling in specification and organization of the three tissue layers. *Developmental biology*, *331*(2), 222-236. https://doi.org/https://doi.org/10.1016/j.ydbio.2009.04.035

Wirbisky, S. E., Weber, G. J., Lee, J. W., Cannon, J. R., & Freeman, J. L. (2014). Novel dose-dependent alterations in excitatory GABA during embryonic development associated

with lead (Pb) neurotoxicity. *Toxicol Lett*, *229*(1), 1-8. https://doi.org/10.1016/j.toxlet.2014.05.016

Wirbisky, S. E., Weber, G. J., Schlotman, K. E., Sepúlveda, M. S., & Freeman, J. L. (2016). Embryonic atrazine exposure alters zebrafish and human miRNAs associated with angiogenesis, cancer, and neurodevelopment. *Food Chem Toxicol*, *98*(Pt A), 25-33. https://doi.org/10.1016/j.fct.2016.03.027

Wirbisky, S. E., Weber, G. J., Sepúlveda, M. S., Xiao, C., Cannon, J. R., & Freeman, J. L. (2015). Developmental origins of neurotransmitter and transcriptome alterations in adult female zebrafish exposed to atrazine during embryogenesis. *Toxicology*, *333*, 156-167. https://doi.org/10.1016/j.tox.2015.04.016

Wlodkowic, D., & Campana, O. (2021). Toward High-Throughput Fish Embryo Toxicity Tests in Aquatic Toxicology. *Environ Sci Technol*, *55*(6), 3505-3513. https://doi.org/10.1021/acs.est.0c07688

Wolf, J. C., & Segner, H. E. (2023). Hazards of current concentration-setting practices in environmental toxicology studies. *Crit Rev Toxicol*, *53*(5), 297-310. https://doi.org/10.1080/10408444.2023.2229372

Wolfle, T. L. (2003). 50 years of the Institute for Laboratory Animal Research (ILAR): 1953-2003. *Ilar j*, *44*(4), 324-337. https://doi.org/10.1093/ilar.44.4.324

Woo, K., & Fraser, S. E. (1995). Order and coherence in the fate map of the zebrafish nervous system. *Development*, *121*(8), 2595-2609. https://doi.org/10.1242/dev.121.8.2595

Wu, J., Basha, M. R., Brock, B., Cox, D. P., Cardozo-Pelaez, F., McPherson, C. A., Harry, J., Rice, D. C., Maloney, B., Chen, D., Lahiri, D. K., & Zawia, N. H. (2008). Alzheimer's disease (AD)-like pathology in aged monkeys after infantile exposure to environmental metal lead (Pb): evidence for a developmental origin and environmental link for AD. *J Neurosci*, *28*(1), 3-9. https://doi.org/10.1523/jneurosci.4405-07.2008

Wu, Y., Wang, J., Xia, Y., Tang, K., Xu, J., Wang, A., Hu, S., Wen, L., Wang, B., Yao, W., & Wang, J. (2023). Toxic effects of isofenphos-methyl on zebrafish embryonic development. *Ecotoxicol Environ Saf*, *254*, 114723. https://doi.org/10.1016/j.ecoenv.2023.114723

Xiang, C., Chen, H., Liu, X., Dang, Y., Li, X., Yu, Y., Li, B., Li, X., Sun, Y., Ding, P., & Hu, G. (2023). UV-aged microplastics induces neurotoxicity by affecting the neurotransmission

in larval zebrafish. *Chemosphere*, *324*, 138252. https://doi.org/10.1016/j.chemosphere.2023.138252

Xie, A., Gao, J., Xu, L., & Meng, D. (2014). Shared mechanisms of neurodegeneration in Alzheimer's disease and Parkinson's disease. *Biomed Res Int*, *2014*, 648740. https://doi.org/10.1155/2014/648740

Xiong, Y., Wang, C., Dong, M., Li, M., Hu, C., & Xu, X. (2023). Chlorphoxim induces neurotoxicity in zebrafish embryo through activation of oxidative stress. *Environ Toxicol*, *38*(3), 566-578. https://doi.org/10.1002/tox.23702

Yamashita, M., Mizusawa, N., Hojo, M., & Yabu, T. (2008). Extensive apoptosis and abnormal morphogenesis in pro-caspase-3 transgenic zebrafish during development. *J Exp Biol*, *211*(Pt 12), 1874-1881. https://doi.org/10.1242/jeb.012690

Yan, H., Tian, S., Slager, S. L., & Sun, Z. (2016). ChIP-seq in studying epigenetic mechanisms of disease and promoting precision medicine: progresses and future directions. *Epigenomics*, *8*(9), 1239-1258. https://doi.org/10.2217/epi-2016-0053

Yang, D., Lauridsen, H., Buels, K., Chi, L. H., La Du, J., Bruun, D. A., Olson, J. R., Tanguay, R. L., & Lein, P. J. (2011). Chlorpyrifos-oxon disrupts zebrafish axonal growth and motor behavior. *Toxicol Sci*, *121*(1), 146-159. https://doi.org/10.1093/toxsci/kfr028

Yang, L., Zhu, B., Zhou, S., Zhao, M., Li, R., Zhou, Y., Shi, X., Han, J., Zhang, W., & Zhou, B. (2023). Mitochondrial Dysfunction Was Involved in Decabromodiphenyl Ethane-Induced Glucolipid Metabolism Disorders and Neurotoxicity in Zebrafish Larvae. *Environ Sci Technol*, *57*(30), 11043-11055. https://doi.org/10.1021/acs.est.3c03552

Yang, Q., Deng, P., Xing, D., Liu, H., Shi, F., Hu, L., Zou, X., Nie, H., Zuo, J., Zhuang, Z., Pan, M., Chen, J., & Li, G. (2023). Developmental Neurotoxicity of Difenoconazole in Zebrafish Embryos. *Toxics*, *11*(4). https://doi.org/10.3390/toxics11040353

Yang, X., Wang, C., Yang, L., Zheng, Q., Liu, Q., Wawryk, N. J. P., & Li, X. F. (2022). Neurotoxicity and transcriptome changes in embryonic zebrafish induced by halobenzoquinone exposure. *J Environ Sci (China)*, *117*, 129-140. https://doi.org/10.1016/j.jes.2022.03.042

Yoon, M., Blaauboer, B. J., & Clewell, H. J. (2015). Quantitative in vitro to in vivo extrapolation (QIVIVE): An essential element for in vitro-based risk assessment. *Toxicology*, *332*, 1-3. https://doi.org/10.1016/j.tox.2015.02.002

Yoshida, Y., Umeno, A., & Shichiri, M. (2013). Lipid peroxidation biomarkers for evaluating oxidative stress and assessing antioxidant capacity in vivo. *J Clin Biochem Nutr*, *52*(1), 9-16. https://doi.org/10.3164/jcbn.12-112

Yu, H., Zhang, J., Chen, Y., Chen, J., Qiu, Y., Zhao, Y., Li, H., Xia, S., Chen, S., & Zhu, J. (2022). The adverse effects of fluxapyroxad on the neurodevelopment of zebrafish embryos. *Chemosphere*, *307*(Pt 1), 135751. https://doi.org/10.1016/j.chemosphere.2022.135751

Yu, T., Xu, X., Mao, H., Han, X., Liu, Y., Zhang, H., Lai, J., Gu, J., Xia, M., Hu, C., & Li, D. (2022). Fenpropathrin exposure induces neurotoxicity in zebrafish embryos. *Fish Physiol Biochem*, *48*(6), 1539-1554. https://doi.org/10.1007/s10695-022-01134-9

Yuan, H., Zheng, J. C., Liu, P., Zhang, S. F., Xu, J. Y., & Bai, L. M. (2007). Pathogenesis of Parkinson's disease: oxidative stress, environmental impact factors and inflammatory processes. *Neurosci Bull*, *23*(2), 125-130. https://doi.org/10.1007/s12264-007-0018-x

Zhao, G., Hu, J., Gao, M., Zhu, Y., & Hong, Y. (2022). Excessive selenium affects neural development and locomotor behavior of zebrafish embryos. *Ecotoxicol Environ Saf*, *238*, 113611. https://doi.org/10.1016/j.ecoenv.2022.113611

Zhao, W., Chen, Y., Hu, N., Long, D., & Cao, Y. (2024). The uses of zebrafish (Danio rerio) as an in vivo model for toxicological studies: A review based on bibliometrics. *Ecotoxicology and Environmental Safety*, *272*, 116023. https://doi.org/https://doi.org/10.1016/j.ecoenv.2024.116023

Zhao, Y., & Zhao, B. (2013). Oxidative stress and the pathogenesis of Alzheimer's disease. *Oxid Med Cell Longev*, *2013*, 316523. https://doi.org/10.1155/2013/316523

Zhou, J., Zhao, Y., Dai, J., & Zhang, K. (2023). Environmentally relevant concentrations of antidepressant mirtazapine impair the neurodevelopment of zebrafish (Danio rerio). *Ecotoxicol Environ Saf*, *262*, 115335. https://doi.org/10.1016/j.ecoenv.2023.115335

Zhu, B., He, W., Hu, S., Kong, R., & Yang, L. (2019). The fate and oxidative stress of different sized SiO(2) nanoparticles in zebrafish (Danio rerio) larvae. *Chemosphere*, *225*, 705-712. https://doi.org/10.1016/j.chemosphere.2019.03.091

Zhu, J., Huang, M., Liu, C., Wang, J., Zou, L., Yang, F., & Zhu, R. (2023). Curcumin protects against fenvalerate-induced neurotoxicity in zebrafish (Danio rerio) larvae through

inhibition of oxidative stress. *Ecotoxicol Environ Saf*, *264*, 115484. https://doi.org/10.1016/j.ecoenv.2023.115484

Zhu, J., Wang, C., Gao, X., Wang, L., Cao, S., Wu, Q., Qiao, S., Zhang, Z., & Li, L. (2019). Comparative effects of mercury chloride and methylmercury exposure on early neurodevelopment in zebrafish larvae. *RSC Adv*, *9*(19), 10766-10775. https://doi.org/10.1039/c9ra00770a

Zitka, O., Skalickova, S., Gumulec, J., Masarik, M., Adam, V., Hubalek, J., Trnkova, L., Kruseova, J., Eckschlager, T., & Kizek, R. (2012). Redox status expressed as GSH:GSSG ratio as a marker for oxidative stress in paediatric tumour patients. *Oncol Lett*, *4*(6), 1247-1253. https://doi.org/10.3892/ol.2012.931

# Chapter 3

# Developmental exposure of zebrafish to 1-Trichloromethyl-1,2,3,4-tetrahydro-beta-carboline (TaClo) elicits MPTP-like neurotoxicity


## Abstract

1-Trichloromethyl-1,2,3,4-tetrahydro-β-carboline (TaClo) is an endogenous metabolite of the industrial waste trichloroethylene (TCE) and has been implicated as a potent neurotoxicant in TCE-induced neurotoxicity. TaClo has been associated with Parkinson's disease (PD) due to its neurotoxic effects and structural resemblance to 1-methyl-4-phenyl-1,2,3,6-tetrahydropyridine (MPTP). Despite the similarities, limited studies have explored the comparative neurotoxicity of MPTP and TaClo within the same experimental models. Zebrafish (*Danio rerio*) are a powerful high throughput platform for neurotoxicology studies and have been used to evaluate TCE-associated developmental neurotoxicity; however, the role of TaClo in TCE-associated neurotoxicity in the zebrafish model is unknown. To address these gaps, we established an MPTP-induced PD zebrafish model and investigated the role of TaClo by comparing its neurotoxic effects with those of MPTP. We demonstrate that TaClo elicits MPTP-like neurotoxicity in the developmental zebrafish. We show that embryonic zebrafish exposed to TaClo exhibit neurobehavioral impairments, diencephalic dopaminergic neuronal damage, increased cellular apoptosis, astrocytic loss, microgliosis, and altered glutathione peroxidase activity levels. These findings provide important insights into the neurotoxic mechanisms of TaClo and emphasize the utility of developmental zebrafish as a model for studying TaClo-induced neurotoxicity. Our work contributes to environmental contaminants research in neurodegenerative diseases by providing evidence of the potential link between TaClo exposure and PD.

## 1. Introduction

1-Trichloromethyl-1,2,3,4-tetrahydro-beta-carboline (TaClo) is an endogenous metabolite of trichloroethylene (TCE), a volatile organic compound widely used as a solvent and detergent in industrial processes (Bringmann, God, Feineis, Wesemann, et al., 1995). TCE has been identified as an environmental contaminant and a potential risk factor for various diseases (Chiu et al., 2013). Although several countries have banned the use of TCE due to its toxic potential, it remains frequently detected in aquatic systems, air, and solid waste through industrial discharges (Dorsey et al., 2023; Wu & Schaum, 2000). While the US Environmental Protection Agency (EPA) classifies TCE as an environmentally hazardous waste and regulates the maximum contaminant level (MCL) for TCE in drinking water at 5 parts per billion (ppb) (ATSDR, 2020), TCE has been detected at approximately 350 Superfund sites across the United States, at levels often exceeding 1000 ppb in nearby groundwater (Dorsey et al., 2023). These findings raise significant environmental concerns and pose a potential threat to human health. Chronic environmental and occupational exposure to TCE linked to neurotoxicity, developmental toxicity, carcinogenicity, respiratory diseases, and reproductive toxicity (Chiu et al., 2013; Goldman et al., 2012; Wu & Schaum, 2000; Wu et al., 2022). Occupational TCE exposure has been implicated as a possible risk factor in the development of Parkinson's disease (PD) (Dorsey et al., 2023; Gash et al., 2008; Liu et al., 2010). While several metabolites and mechanisms have been proposed to explain TCE's neurotoxic effects, TaClo, formed when chloral hydrate reacts with endogenous tryptamine, is suggested to be a potent neurotoxicant responsible for the development of neurotoxicity (Bringmann et al., 1999; Sharma et al., 2017).

Although there are limited human studies, one study detected TaClo in the brains of mice orally exposed to TCE for 8 months (Liu et al., 2018). Several studies reported TaClo as a highly cytotoxic substance capable of inducing apoptosis in human neuroblastoma cells (Akundi et al., 2003; Sharma et al., 2017). TaClo's neurotoxicity has also been described in rodent models with neurotoxic effects similar to those reported in human PD (Liu et al., 2010). Rats injected with TaClo exhibited motor dysfunction, nigrostriatal mitochondrial impairment, oxidative stress, microglial activation, and, most importantly, a significant reduction in dopaminergic neurons, which is a hallmark pathological finding for diagnosing human PD (Liu et al., 2010).

Concerningly, it is speculated that chronic TCE exposure may produce sufficient TaClo concentrations in the brain to cause significant dopaminergic neuronal damage (Liu et al., 2018).

While previous studies have proposed a link to PD development, much of TaClo's research has focused exclusively on the neurotoxic effects triggered by TaClo and assumes a mechanism similar to 1-methyl-4-phenyl-1,2,3,6-tetrahydropyridine (MPTP) due to TaClo's structural and chemical similarity to MPTP (Kalyn et al., 2019; J. Zhang et al., 2022). MPTP is a well-known neurotoxicant that induces PD-like syndrome in various animal models and has been largely applied to investigate the mechanisms underlying PD (Meredith & Rademacher, 2011; Omar et al., 2023b; Smeyne & Jackson-Lewis, 2005). Limited studies have explored the comparative neurotoxic effects of MPTP and TaClo within the same experimental models.

The zebrafish model (*Danio rerio*) is a valuable platform for neurotoxicology research (Biechele-Speziale et al., 2023; Chia et al., 2022; Yin & Horzmann, 2024). To date, studies have generated MPTP-induced PD-like models in both developmental and adult zebrafish to study environmental neurotoxic chemicals and their pathophysiology (Haojia Dong et al., 2022; McKinley et al., 2005; Omar et al., 2023b). MPTP-treated zebrafish exhibit several hallmark features of PD, including reduced locomotion, downregulation of dopaminergic markers, mitochondrial dysfunction, elevated reactive oxygen species (ROS), increased apoptosis, and decreased dopamine levels (Bashirzade et al., 2022; Omar et al., 2023b; Razali et al., 2024; Verma et al., 2022). Beyond their utility in neurotoxicity studies, zebrafish models are well-suited for high-throughput screening of environmental neurotoxicants due to their small size, inexpensive, high fecundity, early-stage transparency, and rapid development (Horzmann & Freeman, 2016; Sáez-Espinosa et al., 2022; Schmidt et al., 2013). Despite the advantages, we found TaClo has not yet been studied in zebrafish models. Previous research has demonstrated the environmentally relevant concentrations of TCE, ranging from 5 ppb to 500 ppb, induced developmental toxicity and neurotoxic effects in developmental zebrafish (Horzmann et al., 2020). However, unlike TCE, TaClo is not regulated, and it is completely unknown whether concentrations of TaClo, at levels comparable to or higher than those of TCE-regulated environmental exposure, can induce similar toxic effects in developmental zebrafish.

Therefore, to advance our understanding of using zebrafish as an experimental model for TaClo toxicity research and its link to PD, we exposed developmental zebrafish to TaClo at concentrations anchored to the TCE regulatory levels. Additionally, we established a MPTP-induced PD model in larval zebrafish to compare and explore key roles and similarities in mode of action at behavioral, phenotypic, enzymatic, cellular, and molecular levels. We hypothesized that the developmental zebrafish model would be a valuable platform for TaClo toxicity studies and that the neurotoxic effects of TaClo will be comparable to those observed in the MPTP-induced PD zebrafish model. Our study expands the value of zebrafish as a model for investigating environmental neurotoxins and strengthens the link between TaClo and MPTP, making a valuable contribution to the research on environmental contaminants and their potential impact on neurodegenerative diseases.

## 2. Materials and methods

### *2.1 Ethics statement*

This study was reviewed and approved by the Institutional Animal Care and Use Committee at Auburn University (protocol numbers: 2021-3912, 2022-4087, and 2024-5380). All experiments were conducted strictly in accordance with the Guide for the Care and Use of Laboratory Animals of the National Institutes of Health. Buffered Tricaine-S (ethyl m-amino benzoate methanesulfonate; Western Chemical Inc., Ferndale, WA) was used for anesthesia (0.1 mg/mL) and euthanasia (0.4 mg/mL) throughout the study.

### *2.2 Chemicals*

A 50 mM (8,662,500 ppb, molar mass: 173.25 g/mol) stock solution of 1-methyl-4-phenyl-1,2,3,6-tetrahydropyridine (MPTP) (99.94%, CAS# 23007-85-4, Selleck Chemicals, USA) was prepared in distilled water and stored at -20°c until use. The working solution of MPTP was further diluted in artificial aquaria water. The artificial aquaria water was prepared using reverse osmosis filtered water with sea salt (Aquaneering Inc., San Diego, CA, USA) added to a conductivity of 500–600 µS and pH 7.0–7.5. The artificial aquaria water served as a

control in all experiments. A 100,000,000 ppb stock solution of 1-trichloromethyl-1,2,3,4-tetrahydro-beta-carboline (TaClo) (CAS# 6649-90-7, Exclusive Chemistry, San Diego, CA, USA) was freshly prepared at the time of exposure by dissolving it in dimethylsulfoxide (DMSO) (CAS# 67-68-5, VWR®, USA). The working solution of TaClo was subsequently diluted from the stock solution in aquaria water to achieve a final vehicle concentration of either 0.1% DMSO for most experiments or 0.001% DMSO for the visual motor response test.

*2.3 Zebrafish husbandry, breeding, and chemical exposure*

Adult-specific, pathogen-free wild-type AB strain zebrafish (*Danio rerio*) sourced originally from the Sinnhuber Aquatic Research Laboratory at Oregon State University (Corvallis, OR, USA) and were maintained in a ZS660 Stand Alone system (Auburn University; Aquaneering Inc., San Diego, CA, USA) on a photoperiod of 14-hour light:10-hour dark cycles. Water quality was consistently maintained at a temperature of 26–28°C, pH at 7.3–7.5, and conductivity at 550–650 µS/cm. Adult zebrafish were monitored twice daily and were fed with a mixture of Golden Pearls 500–800 mm (Artemia International LLC., Fairview, TX, USA), Zeigler adult zebrafish food (Zeigler Bros Inc., Gardners, PA, USA), and live brine shrimp (Artemia International LLC.). For breeding, female and male zebrafish were paired in a 1:1 ratio, with a maximum of six adults per 1-L breeding tank, and were separated overnight by transparent dividers. Artificial plants were added to the female side to stimulate spawning. The dividers were removed the following morning, and embryos were collected one hour after mating. Only fertilized, non-coagulated embryos exhibiting synchronous division at the 4-8 cell stage were selected and sorted into groups of 50 embryos per petri dish for each chemical treatment. Sample size selection for each assay was determined based on previous studies with similar toxicological (Horzmann et al., 2020), behavioral (Horzmann et al., 2020), morphological (Ahkin Chin Tai et al., 2021), enzymatic (Pompermaier et al., 2022), and imaging experiments (Soman et al., 2019) and was calculated with Minitab 18 software (Minitab LLC., State College, PA). Survival and hatching percentages were assessed in three biological replicates, with 50 embryos per treatment per replicate. Six biological replicates, each containing 24 larvae at 120 hours post-fertilization (hpf) per treatment group, were used for larval heart rate analysis and morphological assessments. Larval neurobehavioral evaluations were conducted using ten

biological replicates of zebrafish at 24 hpf (photomotor response test) or 120 hpf (visual motor response test), with each replicate consisting of 24 larvae per treatment. Whole-mount *in situ* hybridization assay was performed on three biological replicates of 30 larvae at 120 hpf per treatment per replicate, while whole-mount immunofluorescence assays were conducted with three biological replicates of 30 zebrafish each at different developmental stages (24 hpf, 48 hpf, 72 hpf, 96 hpf, and 120 hpf) per treatment per replicate. Additionally, six biological replicates of up to 50 larvae at 120 hpf were used to detect oxidative stress (reactive oxygen species and antioxidant enzymatic activity) and gene expression (quantitative polymerase chain reaction). A schematic diagram of the chemical exposure and experimental design is presented in **Figure 3-1**.

*2.4 Developmental toxicity endpoints*

The lethal concentration 50 (*LC50*) assay, heart rate analysis, and body morphological measurements were performed on 120 hpf zebrafish as previously described (Horzmann et al., 2020).

*2.4.1 Lethal concentration 50 (LC50) assay*

Fertilized zebrafish embryos were incubated with static vehicle (0.1% DMSO) and 0-100 parts per million (ppm) TaClo at 28.5°C for 5 days. Survival and hatching percentages were monitored daily and recorded to calculate $LC_{50}$. Hatching was determined by releasing the larvae from chorions. Mortality was defined by the presence of embryonic coagulation or the absence of heartbeat when examined under a stereomicroscope (VWR®, USA).

*2.4.2 Heart rate analysis*

Heart rate was assessed in 120 hpf larvae treated with static vehicle (0.1% DMSO) and TaClo (0, 5, 50, and 500 ppb) exposure from 1-120 hpf. In brief, anesthetized larvae were positioned in lateral recumbency under an Olympus SZX10, and a 30-second video was recorded using an Olympus DP22 camera connected to cellSens Entry software (Olympus Corporation, Center Valley, Pennsylvania). Cardiotoxicity parameters, including beats per second (BPS) and beats per minute (BPM), were quantified by the Noldus DanioScope (Noldus Information Technology, Wageningen, Netherlands) cardiology module.

*2.4.3 Body morphological assessment*

Following the heart rate recording, the same replicates of the anesthetized TaClo-treated larvae were then subjected to body morphological measurement. Larvae were positioned in dorsal and lateral recumbency, and the following parameters were measured: body length, head length, head width, eye diameter, jaw length, otolith width, and pericardial area. Additionally, the ratios of head length to body length and head width to body length were calculated. Previous studies have shown that MPTP-treated zebrafish larvae developed pericardial edema (citation), curved tails, anemia, and jaw protrusions. To determine whether similar body malformations occurred at 120 hpf after MPTP exposure, larvae were treated with static concentrations of 0-100 μM MPTP. Both measurements (TaClo) and body malformations evaluations (MPTP) were captured using an Olympus SZX10 stereomicroscope, connected to an Olympus DP22 camera and cellSens Entry software (Olympus Corporation, Center Valley, Pennsylvania).

*2.5 Neurotoxicity endpoints*

*2.5.1 Neurobehavioral tests*

The photomotor response test and visual motor response test were conducted on 120 hpf larvae according to the protocols established in a previous study (Horzmann et al., 2020) and both tests were performed between 10 am to 12 pm Central Standard time (CST, USA).

*2.5.1.1 Embryonic photomotor response (PMR) test*

A PMR test was conducted to monitor light-induced embryonic responses in zebrafish at 24-30 hpf (Ortmann et al., 2022). Briefly, embryonic zebrafish treated with static MPTP (1.75 μM; 303.2 ppb, molar mass: 173.25 g/mol), vehicle (0.1% DMSO), and TaClo (0, 5, 50, 500 ppb) were placed in the dark for 30 seconds, with two 1-second light stimuli at the 10-second and 20-second marks. The activity and movement of the embryos were recorded using an Olympus SZX10 stereomicroscope, Olympus DP22 camera, and cellSens Entry software (Olympus Corporation, Center Valley, Pennsylvania). Embryonic neurobehavioral endpoints, including burst activity, inactivity, total burst duration, mean burst duration, inactivity duration, burst count, and burst count per minute, were analyzed using the Noldus DanioScope software embryonic activity module (Noldus Information Technology, Wageningen, Netherlands).

*2.5.1.2 Larval visual motor response (VMR) test*

The VMR test was performed on 120 hpf larvae following exposure to 1-120 hpf MPTP, vehicle (0.001% DMSO), and TaClo (0, 5, 50, and 500 ppb). To identify the optimal DMSO concentration for the VMR assay, we exposed zebrafish embryos to six concentrations of DMSO (0.001%, 0.01%, 0.1%, 0.5%, and 1% v/v). Our results revealed a U-shaped bimodal dose-response curve, with DMSO concentrations of 0.01%, 0.1%, and 0.5% inducing a significant reduction in locomotor activity (velocity and distance moved in 120 hpf larvae **(Figure 3-2 A-B).** We further found that DMSO at 0.001%, 0.01%, 0.1%, 0.5%, and 1% did not impact PMR results compared to the control (burst activity, mean burst duration, total burst duration, mean burst count, inactivity, and inactivity duration) **(Figure 3-2 C-H)**. Treated zebrafish larvae were placed in a 96-well plate and incubated at 28°C in a Noldus DanioVision Observation Chamber (Noldus Information Technology, Wageningen, Netherlands). Larval activity tracks were recorded using the Noldus White Light Routine, which, after 10 minutes of acclimation in the dark, alternated between 10-minute dark and light cycles for 50 minutes. The collected data were analyzed using a Noldus EthoVision XT 14 software (Noldus Information Technology, Wageningen, Netherlands) to calculate movement parameters, including total distance moved, velocity, time spent moving, turn angle, angular velocity, mean meander, and turning direction.

*2.6 Whole-mount in situ hybridization assay (WISH)*

While zebrafish share significant neuroanatomical similarities with mammals, they lack substantia nigra (Lal & Kawakami, 2022). However, zebrafish ventral diencephalon (vDC) is widely recognized as homologous to the mammalian striatum (Lal & Kawakami, 2022). Additionally, numerous studies have confirmed that the dopaminergic neuronal loss in the vDC regions is responsible for locomotor deficits (Xi et al., 2011). To assess dopaminergic neuronal expression in the vDC of treated zebrafish larvae, we purchased a plasmid (Addgene plasmid #53764) carrying solute carrier family 6 member 3 (*slc6a3*) sequences, known as dopamine transporter (*dat*), for *in situ* RNA probe synthesis. The plasmid was then amplified and purified using the Wizard® Plus SV Minipreps DNA Purification System (Promega, USA), and further digested with KpnI (Promega, USA) and NotI (Promega, USA) restriction enzymes. Both antisense and sense digoxigenin (DIG)-labeled RNA probes were generated using the DIG RNA

labeling kit (Roche Diagnostics, Germany), following the manufacturer's instruction. WISH was performed according to Thisse et al. with minor modifications (Thisse & Thisse, 2008). Briefly, 120 hpf zebrafish after exposure to static treatments of MPTP (1.75 µM), vehicle (0.001% DMSO), or TaClo (0, 5, 50, 500 ppb) were euthanized and fixed overnight in 4% paraformaldehyde (PFA) at 4°C. Following fixation, larvae were then washed in PBST (PBS+0.1% Tween 20), depigmented with 1% $H_2O_2$ (VWR®, USA) and 1% KOH (Fisher Scientific, USA), and sequentially dehydrated in methanol/PBST (25%, 50%, 75%, and 100%) before being stored at -20°C in 100% methanol (VWR®, USA) overnight. Larvae were then subsequentially rehydrated, washed in PBST, and permeabilized with proteinase K (VWR®, USA) at a final concentration of 10 µg/ml for 10 mins. After PBST washes, larvae were post-fixed with 4% PFA for 20 mins. The prehybridization and hybridization processes were conducted at 65°C, followed by washes in 2X SSC and 0.2X SSC buffer (Promega, USA). Hybridized larvae were detected with sheep anti-digoxigenin-AP Fab fragments (dilution 1:5000, Milipore Sigma, USA). The color staining was carried out with a chromogen substrate NBT and BCIP (Milipore Sigma, USA) until the desired staining intensity was reached. Image acquisition was conducted using a Keyence BZ-x810 fluorescence microscope at the magnification of 20x in a 1 µm interval within a 100 µm range (Keyence Corp., Osaka, Japan). The *slc6a3/dat*-positive signal was analyzed with Qupath software (http://qupath.github.io).

*2.7 Whole mount immunofluorescence assay (WIFA)*

To evaluate protein expression related to dopaminergic neurons, apoptosis, and astrocytes in the vDC of treated zebrafish larvae, we selected tyrosine hydroxylase (TH) as a marker for dopaminergic neurons, caspase-3 as a marker for apoptosis, and glial fibrillary acidic protein (GFAP) as a marker for astrocytes in wild-type AB strain zebrafish. Additionally, Tg(mpeg1.1:mCherry) zebrafish embryos (generously provided by Dr. Jennifer Panizzi) were used to assess microglial expression. In brief, to evaluate dopaminergic neuronal expression at different developmental stages following exposure to MPTP (1.75 µM), vehicle (0.001% DMSO), and TaClo (0, 5, 50, 500 ppb) during 1–24 hpf, 1–48 hpf, 1–72 hpf, 1–96 hpf, and 1–120 hpf, zebrafish larvae at each stage were collected, euthanized, and fixed in 4% sucrose/4% PFA at 4°C overnight. Fixed larvae were washed in PBST (PBS + 0.3% Tween 20) and

depigmented using 3% $H_2O_2$ (VWR®, USA) and 0.5% KOH (Fisher Scientific, USA). Depigmented larvae were sequentially dehydrated in methanol-PBST gradients and stored in 100% methanol (VWR®, USA) at -20°C for at least one night. Larvae were sequentially rehydrated, washed in PBST, and permeabilized with proteinase K (VWR®, USA) at a final concentration of 10 µg/ml for 15 minutes (48 hpf) or 30 minutes (72 hpf, 96 hpf, and 120 hpf). Permeabilized larvae were then washed in PBST, post-fixed in 4% PFA for 20 minutes, blocked for at least 1 hour, and incubated overnight at 4°C with a primary antibody against tyrosine hydroxylase (Millipore Sigma, #AB152). For 24 hpf zebrafish, larvae were manually dechorionated after fixation, and steps, including depigmentation, permeabilization, and post-fixation, were omitted. The following day, larvae were washed in PBST and incubated with Alexa Fluor™ 488-conjugated secondary antibodies (Thermo Fisher Scientific, #A-11034) for 2 hours. After additional PBST washes, larvae were mounted in 100% glycerol for imaging. Image acquisition was performed using a Keyence BZ-x810 fluorescence microscope at 40x magnification with a 1 µm interval within a 100 µm range (Keyence Corp., Osaka, Japan). Positive signals were analyzed using QuPath software (http://qupath.github.io). Double WIFA was performed to investigate the expression levels of apoptosis, microglia, and astrocytes, specifically in vDC, with tyrosine hydroxylase (TH) primary antibody serving as a marker to highlight dopaminergic neurons. The following primary antibodies were used double WIFA: tyrosine hydroxylase (Millipore Sigma, #MAB318), caspase-3 (BD Pharmingen™, #559565), anti-mCherry (Abcam, #ab167453), and glial fibrillary acidic protein (GFAP; Agilent Dako, #Z0334). The secondary antibodies included Alexa Fluor™ 488 (Thermo Fisher Scientific, #A-11029) and Alexa Fluor™ 647 (Thermo Fisher Scientific, #A-21244). Detailed information on antibody specifications and dilutions is provided in **Table 3-1**.

*2.8 Flow cytometric analysis*

Flow cytometric analysis was conducted to evaluate cellular and mitochondrial reactive oxygen species (ROS) levels, as well as mitochondrial membrane potential, in zebrafish at 120 hpf following exposure to MPTP (1.75 µM), vehicle (0.001% DMSO), and TaClo (0, 5, 50, 500 ppb). Single-cell preparation was performed as previously described with minor modifications (Mugoni et al., 2014). Prepared single-cell suspension was incubated in the dark for 30 mins with

the following probe dyes and concentrations: CellROX® Green Reagent (10 µM; Invitrogen™, CAS C10444), MitoSox™ Red (5 µM; Invitrogen™, CAS M36008), and MitoTracker™ Deep Red FM (1 µM; Invitrogen™, CAS M22426). LIVE/DEAD™ Fixable Near IR (876) (Invitrogen™, CAS L34982) was co-incubated to determine the cellular viability. The stained cells were analyzed using a flow cytometer (CytoFLEX LX, Beckman, USA) at the Auburn University Flow Cytometry and High-Speed Cell Sorting Laboratory Core Facility (RRID:SCR_025507). For each experiment, 10,000 events were acquired, and data analysis was performed using FlowJo software (FlowJo™ v10, FlowJo, LLC, Ashland, CA) to measure mean fluorescence intensity (MFI) and cell count.

*2.9 Antioxidantive enzymatic activity*

Total antioxidative enzymatic activity of superoxide dismutase (cytosolic and mitochondrial SOD), catalase (CAT), glutathione (GSH), glutathione disulfide (GSSG), and glutathione peroxidase (GPX) was measured through commercial kits (Cayman, Ann Arbor, Michigan, USA). Sample preparation followed methods described methods with minor modifications (Pompermaier et al., 2022). In brief, a pool of 120 hpf zebrafish larvae treated with MPTP (1.75 µM), vehicle (0.001% DMSO), and TaClo (0, 5, 50, 500 ppb) were euthanized using ice water (Leary et al., 2013), rinsed with PBS, and homogenized in ice-cold 50 mM Tris-HCl buffer (CAS# 1185-53-1, Thermo Fisher Scientific, USA). The homogenates were snap-frozen in liquid nitrogen and stored at -80°C until analysis. Total protein concentrations were determined using the Pierce™ Bradford Plus Protein Assay Kit (Thermo Scientific™), and absorbance was measured using a Microplate reader (Infinite® M200 PRO Multimode Microplate Reader, Tecan, Switzerland). The antioxidative enzymatic activities were normalized to the total protein content for each sample. Assays were performed according to the manufacturer's instructions (Cayman, Ann Arbor, Michigan, USA). The following commercial kits were used: Catalase Assay Kit (707002), Superoxide Dismutase Assay Kit (706002), Glutathione Reductase Assay Kit (703202), and Glutathione S-Transferase Assay Kit (703302). Absorbance for SOD, CAT, GSH, and GSSG assays was measured using the Infinite® M200 PRO Multimode Microplate Reader (Tecan, Switzerland), while GPX activity was assessed using the BioTek Synergy HTX Multimode Reader (Winooski, VT, USA). The minimum protein concentrations required for

antioxidant enzymatic activity detection in treated larvae were as follows: 0.32 mg/ml for cytosolic SOD, 0.29 mg/ml for mitochondrial SOD, 0.3 mg/ml for CAT, 0.32 mg/ml for GSH and GSSG, and 1.4 mg/ml for GPX.

*2.10 Gene expression*

Total RNA extraction and cDNA synthesis were performed as previously described (Peterson & Freeman, 2009). RNA quality and quantity were assessed using NanoDrop 1000 Spectrophotometer V3.8 (Thermo Fisher Scientific, Waltham Massachusetts, US). Gene expression was evaluated using quantitative polymerase chain reaction (q-PCR) according to MIQE guidelines (Bustin et al., 2009). Expression levels of 18 genes were performed using zebrafish-specific primers (purchased from Integrated DNA Technologies, Inc. USA) **(Table 3-2)** and PowerTrack™ SYBR Green Master Mix (Applied Biosystems™, USA) on a QuantStudio™ 7 Flex Real-Time PCR System (Thermo Fisher, Waltham, MA, USA). Final Gene expression was quantified using the $2^{-\Delta\Delta Ct}$ method with normalization to the reference *b-actin* gene (Livak & Schmittgen, 2001).

*2.11 Zebrafish neurochemical processing for HPLC-ECD analysis*

Samples for the neurotransmitter detection were submitted to Isakson Center for Neurological Disease Research at University of Georgia (Dr. Anumantha G. Kanthasamy's lab) and the experiment was performed by Dr. Piyush Padhi and Dr. Anumantha G. Kanthasamy.

For neurochemical analysis, a pool of 30 larvae per treatment per group were stored in antioxidant buffer (Sodium Metabisulfite (5 mg/mL); 70% Perchloric acid (0.196 M); EDTA (5 mg/mL; water (HPLC-grade, 0.2 mM filtered); isoproterenol (416 ng/mL)) as described previously (1-5). Samples were thawed on ice before tissue homogenization with a tissue grinder (Fisher Scientific) followed by sonication for 6 cycles with 30-sec pulses followed by 30-sec spacing using a Q700 Sonicator (QSonica L.L.C). The samples were centrifuged at 14,200 x g for 10 min, transferred to Spin-X Nylon centrifuge tube filters, and then subjected to a second

centrifugation cycle at the same respective setting. The filter was discarded, and the samples were stored at -80°C until HPLC sample injection.

*2.12 HPLC-ECD Method Validation, Chromatographic conditions, and performance*

A commercial mobile phase (MDTM, Cat# NC9777698, Thermo Scientific) was used for tissue neurochemical analysis. For plasma analysis, a home-made mobile phase (sodium dihydrogen phosphate, monohydrate (75 mM, Sigma); 1-octanesulfonic acid sodium salt (1.7 mM, Sigma); triethylamine (TEA, 100 µL/L, Sigma); EDTA tetrasodium tetrahydrate (25 µM, Sigma); acetonitrile (10% v/v, Sigma), adjusted to pH of 3 with phosphoric acid; water (HPLC-grade, 0.2 mM filtered)) was utilized to achieve optimum L-DOPA, BZ, and ISO signal-to-noise ratio. The assay was established using a previously validated method for HPLC-EC detection to detect norepinephrine (NE, Sigma - A9512), 3,4-Dihydroxyphenylacetic acid (DOPAC, Sigma - 850217), dopamine (DA, Sigma - H8502), 5-hydroxyindoleacetic acid (5-HIAA, Sigma - H8876), serotonin (5-HT, Sigma - H9523), and isoproterenol (ISO, Sigma – 1351005) in plasma and tissue lysates (1-5). The preliminary analyses aimed at detecting serotonin in whole larval tissue (a pooled sample of 30 larvae at 120 hpf) failed to yield a detectable signal **(Figure 3-3)**. Therefore, in this study, we focused on measuring the levels of DOPAC, norepinephrine, dopamine, and 5-HIAA. Samples were loaded in the auto-sampler (Thermo Scientific WPS-3000TSL) and injected at a volume of 20 µL. The analytes were separated isocratically with commercial mobile phase by reversed-phase C-18 column (ZORBAX Eclipse Plus 4.6x100 mm, Agilent) at 0.6 mL/min for 21 min (pump, ISO-3100 SD, Thermo Scientific). Detection of L-DOPA, NE, DOPAC, DA, 5-HIAA, ISO and 5-HT were performed by ECD (CoulArray 5600A, ESA) using the following potentials (Channel 1: 350mV (ESA Guard cell, 5020), Channel 3: -150 mV and CH4: +220 mV (ESA Microdialysis cell, 5014B). Method development and data integration and analysis were performed using Chromeleon (v. 7.1.3) and ESA CoulArray Software (v. 3.10). A 9-point standard curve with the following concentrations: 2.5, 5, 10, 15, 20, 25, 50, 100, 250 ng/mL was generated, and the peak-area for the respective analytes determined the concentration.

*2.11 Statistical analysis*

Statistical and graphic analyses were conducted using GraphPad Prism 10.0.2 software (GraphPad Software Inc., La Jolla, CA, USA). All data were first assessed for normality and equal variance using the Shapiro–Wilk test. For normally distributed data, an unpaired t-test was used for two-group comparisons, while a one-way analysis of variance (ANOVA) followed by Tukey's post-hoc test was applied for comparisons involving more than two groups. Non-normally distributed data were analyzed using the Mann–Whitney test for two-group comparisons or the Kruskal–Wallis test followed by Dunn's multiple comparisons test for more than two groups. All values were expressed as the mean ± standard deviation (SD), and statistical significances are noted as * $p \leq 0.05$, ** $p \leq 0.01$, *** $p \leq 0.001$, and **** $p \leq 0.0001$.

## 3. Results

*3.1 1.75 μM MPTP significantly impacts embryonic neurobehavior and diminishes the larval locomotor activity and dopaminergic neuronal expression at the ventral diencephalon (vDC)*

To determine the optimal MPTP concentration for inducing a Parkinson's disease model in zebrafish without causing phenotypic abnormalities, we exposed zebrafish embryos to MPTP at concentrations ranging from 1 to 100 μM in a dose finding experiment. We assessed the neurotoxicity using PMR and VMR assays and evaluated dopaminergic neuronal expression in the vDC through WISH and WIFA analyses. Additionally, to ensure that locomotion assessments were not affected by morphological abnormalities, we examined and recorded the presence of morphological abnormalities including pericardial edema, curved tails, and jaw protrusions in the treated larvae. We found that the zebrafish embryos exposed to 1.75 μM MPTP exhibited significantly altered PMR parameters compared to the control group, including reduced burst activity ($p \leq 0.0001$) **(Figure 3-4A)**, total burst duration ($p \leq 0.0001$) **(Figure 3-4B)**, mean burst duration ($p \leq 0.0001$) **(Figure 3-4C)**, burst count ($p \leq 0.0001$) **(Figure 3-4D)**, and burst count per minute ($p \leq 0.0001$) **(Figure 3-4E)**. Additionally, we observed the treated larvae exposed to the same MPTP concentration demonstrated significantly shorter movement distances ($p \leq 0.0001$) **(Figure 3-4F, H)** and reduced velocity ($p \leq 0.0001$) **(Figure 3-4G)** in the VMR assay. Moreover, a significantly diminished relative *slc6a3/dat* expression ($p \leq 0.0001$) **(Figure 3-4I, J)** and

tyrosine hydroxylase expression at vDC were found after 1.75 μM MPTP exposure ($p \leq 0.0001$) **(Figure 3-4I, K)**. Lastly, we found larvae were phenotypically normal in the same MPTP concentration. Our data demonstrate that 1.75 μM MPTP does not cause larval morphological changes but significantly triggers neurotoxicity in both embryonic and larval stages, resembling the findings reported in MPTP-induced Parkinson's disease zebrafish models.

*3.2 TaClo (5, 50, 500 ppb) does not cause morphologic changes and altered heart rate*

The $LC_{50}$ of TaClo had not yet been investigated in zebrafish models. To investigate its toxic potency, we exposed zebrafish embryos to a range of 0–100 ppm TaClo and monitored mortality daily to calculate the LC50. We determined the LC50 of TaClo at 120 hpf was 7.89 ppm **(Figure 3-5A)**. Previous studies have reported that larvae exposed to environmentally relevant concentrations of TCE affected hatching percentage, displayed morphological changes, and altered heart rate (Horzmann et al., 2020). We then asked whether TCE's metabolite, TaClo, produced similar developmental and cardiac toxicity in zebrafish larvae at concentrations comparable to TCE's regulatory and environmental levels. We monitored survival and hatching percentages daily, examined larval body morphology, and analyzed heart rate at 120 hpf. Our findings showed that TaClo (5, 50, and 500 ppb) did not cause significant alterations in these endpoints **(Figure 3-5B-C, Figure 3-6 A-K)**. Taken together, our results suggest that, unlike its parent compound TCE, TaClo does not have a significant impact on developmental or cardiac toxicity.

*3.3 Exposure to 5 ppb TaClo and 1.75 μM MPTP resulted in locomotion reduction and neuronal loss in the diencephalic regions of DC2, DC4/5, and DC6 at vDC*

Next, we investigated if TaClo would trigger neurotoxic impacts similar to those previously reported in TCE on larval zebrafish. A study indicated TCE significantly altered embryonic photomotor responses (5, 50, 500 ppb) and larval visual motor behaviors (500 ppb) (Horzmann et al., 2020). To investigate TaClo's neurotoxicity, we performed PMR and VMR assays to monitor neurobehavioral alterations and utilized WISH and WIFA to assess dopaminergic neuronal expression in the vDC. Our results confirm our expectation that TaClo

exerts neurotoxic effects on developmental zebrafish. Notably, we found it was the lowest concentration of TaClo (5 ppb) among the treated groups that induced the most significant changes across PMR, VMR, WISH, and WIFA assays. In the PMR test, embryonic zebrafish exposed to 5 ppb TaClo exhibited the highest and significantly increased burst activity ($p \leq 0.05$)**(Figure 3-7A)**, total burst duration ($p \leq 0.05$)**(Figure 3-7B)**, burst count ($p \leq 0.01$)**(Figure 3-7C)**, and burst count per minute ($p \leq 0.01$) **(Figure 3-7D)** among the exposed groups. Moreover, we observed the larvae exposed to the same concentration of TaClo (5 ppb) exhibited the shortest distance moved compared to control ($p \leq 0.01$) and vehicle groups ($p \leq 0.05$) **(Figure 3-7E)** with less recorded movement tracks **(Figure 3-7F)**. Finally, when comparing the relative dopaminergic neuronal cell numbers in the vDC, we found that 5 ppb TaClo-treated larvae exhibited the lowest *slc6a3/dat*-labeled cell numbers compared to the vehicle group (0.001% DMSO) ($p \leq 0.01$) **(Figure 3-7H)** and the most reduced TH-labeled cell numbers among all treated groups ($p \leq 0.001$) **(Figure 3-7I)**, indicating that TaClo and MPTP elicited similar neurotoxic effects on the treated larvae in neurobehavior and dopaminergic neurons in the vDC.

Previous studies have indicated specific larval diencephalic neuronal populations were sensitive to MPTP treatment (Kalyn et al., 2019; Xi et al., 2011). To investigate the impact of 1.75 μM MPTP and 5 ppb TaClo exposure on diencephalic neuronal populations (DC) and to identify the time window for both chemicals to exert neurotoxicity, we exposed embryonic zebrafish to 1.75 μM MPTP and 5 ppb TaClo and collected at 24 hpf, 48 hpf, 72 hpf, 96 hpf, and 120 hpf for WIFA analysis. We found that TaClo-treated larvae first exhibited a significant reduction in dopaminergic neurons within the vDC at 72 hpf ($p \leq 0.05$), followed by MPTP-exposed larvae at 96 hpf ($p \leq 0.001$). This reduction persisted in both groups through 120 hpf ($p \leq 0.001$) **(Figure 3-8A, C)**. To further investigate which DC is vulnerable to 5 ppb TaClo and 1.75 μM MPTP, we focused on DC1, DC2 and 4/5, DC3, and DC6 and assessed neuronal expression at 72 hpf, 96 hpf, and 120 hpf. Our analysis revealed that DC2 and 4/5 exhibited significantly fewer TH-labelled neurons in both treated groups at 96 hpf and 120 hpf **(Figure 3-8E-F)**, while no significant changes were observed in other DC populations **(Figure 3-8E-F)**. Additionally, we evaluated the *slc6a3/dat*-labeled DC populations at 120 hpf **(Fig. 3-7G-H)** and found that, in addition to DC2 and 4/5, DC6 also had significant dopaminergic neuronal loss in

both treatment groups **(Figure 3-8B)**. Collectively, our results suggest that 5 ppb TaClo acts as a neurotoxicant in the developmental zebrafish model and may share similar neurotoxic mechanisms with 1.75 μM MPTP against dopaminergic neurons.

*3.4 TaClo and MPTP influence diencephalic cellular apoptosis, astrocytic loss, and microgliosis of 120 hpf larvae*

Previous *in vitro* studies have demonstrated that TaClo induces cellular apoptosis and astrocytic loss (Akundi et al., 2003; Rausch et al., 1995). Additionally, increased microglial activation has been reported in murine models (Yang et al., 2019). These findings align with mechanisms underlying MPTP-induced neurotoxicity and are proposed to increase the vulnerability of nigral dopaminergic neurons to degenerative processes (Lee et al., 2019). To further investigate whether 5ppb TaClo and 1.75 μM MPTP trigger similar responses in the developmental zebrafish model, we took a forward phenotypic approach and performed double WIFA focusing on cellular interaction with dopaminergic neurons within vDC regions in 120 hpf larvae. We found 5 ppb TaClo and 1.75 μM MPTP treated groups had significantly increased numbers of caspase-3 labeled apoptotic bodies compared to vehicle and control groups ($p \leq 0.0001$) **(Figure 3-9A-B)**. Significantly higher caspase 3 immunolabeled apoptotic bodies were also observed in the 50 ppb treated group ($p \leq 0.01$ to vehicle and control) **(Figure 3-9 A-B)**. While not observed in the 1.75 μM MPTP-treated group, larvae exposed to 5 ppb ($p \leq 0.0001$) and 50 ppb TaClo ($p \leq 0.001$) exhibited significantly reduced GFAP-positive astrocytic density compared to the vehicle (0.001% DMSO) group **(Figure 3-9A, C)**. Finally, both 5 ppb TaClo ($p \leq 0.001$) and 1.75 μM MPTP ($p \leq 0.0001$) treated 120 hpf Tg(mpeg1.1:mCherry) larvae demonstrated significantly higher microglial density in relation to vehicle (0.001% DMSO), with 1.75 μM MPTP having the highest microglial density **(Figure 3-9D-E)**. Taken together, these findings suggest that exposure to 5 ppb TaClo and 1.75 μM MPTP could initiate diencephalic cellular apoptosis and glial response along with dopaminergic neurodegeneration.

*3.5 500 ppb TaClo and 1.75 μM MPTP alter glutathione peroxidase activity in larval zebrafish*

Mitochondrial dysfunction and imbalanced oxidative stress have been linked to dopaminergic neuronal death following exposure to TaClo and MPTP (Bajpai et al., 2013; Hung & Lee, 1998; Sriram et al., 1997; Yang et al., 2019). Therefore, we next directed our attention to exploring ROS levels, mitochondrial membrane potential, and antioxidative enzymatic levels in larvae treated with TaClo and MPTP. First, we performed flow cytometry to determine whether TaClo and MPTP stimulate ROS production and inhibit mitochondrial activity in the treated larvae. Surprisingly, we found no significant differences in cellular ROS, mitochondrial ROS, or mitochondrial membrane potential in the whole zebrafish larvae among the treated groups **(Figure 3-10)**. Next, we detected antioxidant enzymatic activity, although no significant alterations were observed in cytosolic and mitochondrial SOD, CAT, GSH, and GSSH activity levels **(Figure 3-11A-E)**, we noted the larvae exposed to 1.75 μM MPTP had the lowest normalized GPX activity across five-time points measured every minute **(Figure 3-12A)** with a significantly reduced overall GPX activity among the treated groups **(Figure 3-12B)**. Interestingly, embryonic zebrafish treated with 500 ppb TaClo had the overall highest GPX activity among the treated groups **(Figure 3-12B)**. Overall, our findings suggest that GPX activity plays a key role in mediating oxidative stress following TaClo and MPTP exposure in developmental zebrafish models.

*3.6 TaClo and MPTP upregulate microglial mRNA expression in larvae*

Our findings thus far demonstrate that TaClo and MPTP modulate the protein expression of diencephalic dopaminergic neurons, caspase-3, GFAP, and mpeg1.1, as well as alter GPX activity levels. Notably, 5 ppb TaClo-induced neurotoxicity recapitulates the effects observed in 1.75 μM MPTP-treated larvae, aligning with previously established MPTP-induced Parkinson's zebrafish models. To further investigate whether mRNA expression is similarly altered, we targeted genes related to dopaminergic neurons, microglia, astrocytes, antioxidant enzymes, apoptotic pathways, and Parkinson's disease-related genes. As expected, both 5 ppb TaClo and 1.75 μM MPTP significantly upregulated macrophage-expressed gene (*mpeg*) in the whole zebrafish larvae compared to the vehicle (0.001% DMSO) and control groups **(Figure 3-13A)**.

However, no significant changes were observed in the expression of the other 17 tested genes **(Figure 3-13B-R).**

*3.7 MPTP induced 5-HIAA depletion in 120 hpf zebrafish*

To investigate the impact of TaClo or 1.75 μM MPTP on neurotransmitter levels, we measured norepinephrine, DOPAC, dopamine, and 5-HIAA in 120 hpf larvae following early-life exposure. We observed a significant reduction in 5-HIAA levels in the 1.75 μM MPTP-treated group compared to controls **(Figure 3-14)**. However, no significant differences in norepinephrine, DOPAC, or dopamine levels were detected in either the TaClo-treated groups (5, 50, and 500 ppb) or the MPTP-treated group. Additionally, no significant differences in 5-HIAA levels were observed across all TaClo exposure concentrations. These findings suggest 1.75 μM MPTP may influence the serotoninergic pathway.

## 4. Discussion

This study investigates the developmental neurotoxicity of TaClo in the zebrafish model by evaluating neurobehavior, phenotype, antioxidative enzymatic activity, and genetic expression. Overall, we found TaClo caused similar neurotoxic effects in larval zebrafish to those previously reported from *in vitro* studies and murine models. In addition, our analyses closely aligned with findings from MPTP-induced PD zebrafish models. Specifically, we found that TaClo-treated embryonic zebrafish displayed reduced locomotor activity with dopaminergic neuronal damage, accompanied by cellular apoptosis, astrocytic dysfunction, and microgliosis in the vDC region. Notably, these findings were detected in the larvae exposed to 5 ppb TaClo, a concentration anchored to the EPA-regulated maximum contamination level for TCE in drinking water. Together, this is the first study to investigate the neurotoxic effects of TaClo in the zebrafish model. Our study demonstrates that TaClo elicits MPTP-like neurotoxicity in the developmental zebrafish and supports a potential link to PD.

In our study, we first sought to establish a chemical-induced Parkinson's disease model in developmental zebrafish. MPTP is considered an important neurotoxicant in human PD research due to its ability to selectively target substantia nigral dopaminergic neurons in mammalians (AlShimemeri et al., 2022; Dauer & Przedborski, 2003; Jagmag et al., 2015; Wasel & Freeman, 2020). Although other studies have used MPTP in larval zebrafish models to demonstrate locomotor and dopaminergic neuronal impairments, standardized exposure protocols have not yet been established (Haojia Dong et al., 2022; Lam et al., 2005; Xi et al., 2011). Earlier studies suggested that a concentration of 1000 μM MPTP is required to induce significant locomotor deficits and dopaminergic neuron loss in the diencephalic complex at 5 dpf in Turku strain zebrafish (Sallinen et al., 2009). Notably, larvae exposed to this high MPTP concentration remained phenotypically normal (Sallinen et al., 2009). However, Kalyn et al. found dopaminergic neuronal loss at 7 dpf in Tg(dat:eGFP) zebrafish and that an MPTP concentration over 250 μM not only triggered a significant reduction in total distance traveled and velocity, but also induced marked cardiac malformations and tail curvature (Kalyn et al., 2019). A recent study identified that following exposure to a low concentration of 1 μM MPTP, 120 hpf larvae exhibited significant reductions in swimming distance and speed without notable body malformations (Haojia Dong et al., 2022). However, their study found no significant reduction in dopaminergic neurons in the brain at 72 hpf and 120 hpf, except for a transient reduction observed at 96 hpf (Haojia Dong et al., 2022). In our study, we found 1.75 μM MPTP had no influence on larval body morphology, but impaired locomotor activity and induced dopaminergic neuronal damage at 120 hpf larvae. Overall, these results demonstrate the complexity of establishing MPTP-induced PD models in developmental zebrafish with variations observed in zebrafish strain, exposure age, and exposure duration.

Methodological differences may also explain some of the differences reported in the literature. It is likely zebrafish strain differences may influence the neurotoxic response to MPTP exposure. For example, one study observed that TU strain zebrafish exhibited fewer deleterious neurotoxic effects from embryonic alcohol exposure compared to AB strain (Mahabir et al., 2014). There is also a concern that earlier MPTP exposure may inhibit dopaminergic neurogenesis (McKinley et al., 2005). Some studies initiated MPTP treatment at 24 hpf in

manually dechorionated zebrafish embryos, as dopaminergic neurons first appear at 18-24 hpf (20-23 somite stage) in the diencephalon region (Guo et al., 1999). However, other studies have demonstrated that MPTP exposure prior to complete dopaminergic neuronal differentiation did not impede dopaminergic neuronal development (McKinley et al., 2005). Similarly, in our study, we exposed embryonic zebrafish at the 4-8 cell stage without dechorionation and examined dopaminergic neuronal expression at a 24-hour interval until 120 hpf. Our results showed the main diencephalic neuronal populations were present as early as 24 hpf (DC2, 4), with additional populations (DC5) observed at 48 hpf and that there were no significant differences in the numbers of dopaminergic neurons between the 1.75 μM MPTP-treated groups and the control at 24 hpf and 48 hpf. These findings suggest that 1.75 μM MPTP administration at 0 dpf does not impact dopaminergic neurogenesis. Additionally, in our study, the presence of the chorion during MPTP administration did not appear to influence its neurotoxic effects. However, the exposure duration at specific developmental windows may play a critical role in MPTP's ability to exert neurotoxicity. Dong et al. identified 48-96 hpf as a particularly sensitive window for MPTP toxicity after testing different developmental windows between 8-96 hpf (Haojia Dong et al., 2022). Exposure to 1 μM MPTP during this sensitive window resulted in a transient dopaminergic neuronal loss at 96 hpf and also led to long-lasting neurotoxic effects in adult zebrafish (Haojia Dong et al., 2022; H. Dong et al., 2022). Consistent with their observation, we observed the initial onset of dopaminergic neuronal cellular loss began at 96 hpf (Fig. 4A). Given that the complexity of MPTP-induced PD modeling in zebrafish is influenced by multiple factors, it is crucial to consider these factors during experimental design, including the zebrafish strain, exposure concentration, and, importantly, the developmental stage of exposure. These variables can significantly impact the outcomes and reproducibility of MPTP-induced neurotoxicity studies and should be carefully optimized to enhance the reliability and translational relevance of zebrafish models for Parkinson's disease research.

While previous studies have reported the neurotoxic effects of TaClo with *in vitro* studies and in murine models, its toxic potency has been rarely described (Liu et al., 2018; Sharma et al., 2017; Yang et al., 2019). Kean et al. studied TCE and its metabolites' toxicity on SH-SY5Y cell line and midbrain neurons and found TaClo was comparatively more toxic than TCE (Keane,

2013). In their study, while TCE was not determined to be toxic in either the SH-SY5Y cell line or midbrain neurons, the lethal dose 50 ($LD_{50}$) for TaClo was 100 μM in the SH-SY5Y cell line and 100-150 SH-SY5Y μM in midbrain neurons (Keane, 2013). Consistent with the previous observations, we found TaClo ($LC_{50}$ 7.89 ppm) to be more toxic than its parent compound TCE ($LC_{50}$ 68.98 ppm) (Horzmann et al., 2020) in 120 hpf larvae. These results suggest that TaClo has higher toxic potency than its parent compound. Although the US EPA established 5 ppb as the maximal containment level (MCL) of TCE in drinking water, previous studies have shown that environmentally relevant concentrations of TCE can induce developmental, cardiac toxicity, or neurotoxic effects in developmental zebrafish (Horzmann et al., 2020; Huang et al., 2020). Horzmann et al. reported 5 ppb TCE altered PMR and caused head malformation and altered heart rate in 120 hpf larvae (Horzmann et al., 2020). In another study, Huang et al. observed that 10 ppb TCE exposure led to cardiac malformations in 3 dpf larvae (Huang et al., 2020). However, in our experiments, we found no developmental malformations or cardiac function defects following exposure to TaClo at levels comparable to or higher than the regulatory limit of TCE. While researchers have proposed TaClo, rather than TCE, as the primary neurotoxicant responsible for triggering neurotoxic effects, the concentration of TaClo required to elicit these effects remains unclear (Dorsey et al., 2023; Liu et al., 2018).

To address this question, we exposed embryonic zebrafish to TaClo and evaluated neurotoxicity by assessing locomotor activity and dopaminergic neuronal expression. First, we assessed PMR, which is a non-visual behavior triggered by the stimulation of photoreceptors located in the hindbrain of the developing zebrafish embryo in response to high-intensity white light stimulus (Kokel et al., 2013; Ortmann et al., 2022). This assay has been frequently used to screen and differentiate compounds with uncharacterized toxicity and is considered a valuable tool for detecting neuroactive substances with various modes of action (Kokel & Peterson, 2011). Notably, it has been found that compounds with the same or similar mechanisms of action induce the same activity (hyp-or hyperactivity) (Carbaugh et al., 2020). A previous study reported hypoactivity in embryos treated with TCE at concentrations of 5, 50, and 500 ppb (Horzmann et al., 2020). Similarly, in our study, embryos exposed to 1.75 μM MPTP (303.2 ppb, molar mass: 173.25 g/mol) exhibited hypoactivity compared to controls. However, despite being a metabolite

of TCE and structurally resembling MPTP, 5 ppb TaClo induced a hyperactive response compared to the vehicle control (0.1% DMSO). Our PMR analysis results support that TCE, TaClo, and MPTP are neuroactive compounds. However, the observed differences in their PMR responses may suggest that their mechanisms of action may diverge, potentially involving different receptors, enzymes, or neuronal circuits. Many neuroactive compounds exhibit complex dose-dependent responses (Reif et al., 2016). While 1.75 μM MPTP-treated embryos showed a hypoactive reaction, it is likely that the effects of MPTP could vary with different concentrations, leading to distinct outcomes at lower versus higher doses. In the future, to better understand the full range of MPTP's effects and its PMR response in comparison to other neuroactive chemicals, testing multiple concentrations of MPTP in PMR assay would provide more comprehensive information.

DMSO is commonly used as a solvent for compounds in zebrafish embryo toxicity screening, as its relatively low toxicity in this model compared to other solvents (Hoyberghs et al., 2021). However, there is ongoing controversy regarding the impact of DMSO concentration on larval zebrafish locomotor activity (Chen et al., 2011). A wide range of DMSO concentrations (0.001%–0.64%) has been reported in larval zebrafish behavioral assays (Hedge et al., 2023). However, earlier studies demonstrated 0.01% DMSO could significantly alter locomotor activity and induce hyperactivity at 144 hpf (Chen et al., 2011). In contrast, a recent study argued that developmental exposure to only DMSO concentrations 0.5% or higher influences locomotor activity in light-dark larval neurobehavioral tests (Hedge et al., 2023). In our study, we found that embryos exposed to 0.01% and 0.5% DMSO showed a pronounced reduction in locomotor activity at the larval stage. We first applied 0.1% DMSO as a vehicle in PMR and VMR assays. While the PMR responses were similar to the control group, we observed a significant reduction in locomotor activity in 120 hpf larvae treated with 0.1% DMSO. Prior studies have suggested that these discrepancies could be attributed to the anxiolytic or anesthetic effects of DMSO (Sackerman et al., 2010); though the underlying mechanism of action remains unclear. Taken together, we suggest the use of DMSO as a vehicle solvent should be approached with caution, and conducting a pilot study is strongly recommended, as even low concentrations of DMSO can potentially lead to false-positive or false-negative results for tested compounds. In our study,

while 0.1% DMSO did not affect survival, hatching percentage, body morphology, heart rate, or PMR, it significantly influenced VMR results. This highlights the critical importance of carefully selecting and validating solvent concentrations in zebrafish neurobehavioral assays. Based on our findings, we suggest using 0.001% DMSO as a solvent in zebrafish neurobehavioral studies, particularly in research related to PD.

Previous research has demonstrated that TaClo initiates progressive and substantial neurodegeneration along with behavioral deficits in rats (Keane et al., 2019; Yang et al., 2019). Consistent with these findings, we observed that 5 ppb TaClo significantly decreased locomotor activity in 120 hpf zebrafish larvae and caused marked dopaminergic neuronal loss in the vDC. Our findings are similar to those observed in zebrafish models of MTPT-induced PD and our MPTP-induced PD larval zebrafish model (Haojia Dong et al., 2022; McKinley et al., 2005). While TaClo and MPTP share chemical and structural similarities, limited studies have directly compared their neurotoxic mechanisms of action. Previous studies have reported a 39–70% reduction in dopaminergic neurons in the vDC of MPTP-treated zebrafish larvae exhibiting hypolocomotion (Haojia Dong et al., 2022; McKinley et al., 2005; Xi et al., 2011). In our study, we observed 1.75 μM MPTP-treated larvae with a significantly decreased locomotor activity had an approximately 20.5% (compared to control, WISH), 27.8% (compared to vehicle, WISH), 18% (compared to control, WIFA), and 20.1% (compared to vehicle, WIFA) reduction in dopaminergic neurons in the vDC **(Table 3-3)**. Strikingly, the 5 ppb TaClo-treated larvae with a reduced distance moved were also found to have approximately 14.6% (compared to vehicle, WISH), 28.1% (compared to vehicle, WIFA), and 25.1% (compared to control, WIFA) dopaminergic neuronal reduction. Interestingly, by evaluating the dopaminergic loss every 24 hours, our results show that 5 ppb TaClo induces a more rapid dopaminergic neuronal loss (72 hpf) than 1.75 μM MPTP (96 hpf). These findings highlight a correlation between dopaminergic neuronal loss and impaired locomotor activity in developmental zebrafish, where a minimum reduction of 14.6–28.1% in dopaminergic neurons is associated with decreased distance moved. In addition, our results support that TaClo is a neurotoxicant in the developmental zebrafish model and exhibits neurotoxic effects comparable to MPTP at both the behavioral and dopaminergic neuronal levels. Moreover, 5 ppb TaClo appears to exert a faster neurotoxic effect

on dopaminergic neurons at the vDC than 1.75 μM MPTP, suggesting there may be some differences in mechanism despite the similar phenotypic effects.

Previous researchers have indicated that MPTP not only causes a pronounced reduction in the number of dopaminergic neurons but also selectively targets specific diencephalic neuronal populations (Sallinen et al., 2009; Wen et al., 2008; Xi et al., 2011). Eight TH-labeling catecholaminergic populations in the diencephalon (DC1-DC8) have been identified in 120 hpf zebrafish larvae (Rink & Wullimann, 2002). Among these regions, DC2 and DC4, corresponding to the periventricular posterior tuberculum and posterior tuberculum in the adult zebrafish brain, are considered to be equivalent to the mammalian substantia nigra neurons (Matsui & Sugie, 2017; Tay et al., 2011). Previous studies have reported that DC2/DC4-6 are particularly susceptible to MPTP toxicity and the loss of DC2 and DC4 likely contributes to motor dysfunction (Ilin et al., 2021; Sallinen et al., 2009; Wen et al., 2008; Xi et al., 2011). In accordance with our findings, a significant reduction in *slc6a3*/*dat* neuronal expression was observed in both DC2/4,5 and DC6, along with a loss of DC2/4,5 in TH-labeled cells in 1.75 μM MPTP and 5 ppb TaClo-treated 120 hpf larvae. When we examined specific DC populations at 24 hpf, 48 hpf, 72 hpf, 96 hpf, and 120 hpf, our analyses revealed that DC2/4,5 TH immunoreactive neuronal populations in particular exhibited a significant reduction at 96 hpf and 120 hpf in both 5 ppb TaClo and 1.75 μM MPTP treated larvae. First, our data suggest that, in addition to structural similarities, MPTP and TaClo share comparable modes of neurotoxicity by targeting the same diencephalic neuronal populations. Additionally, we observed a grossly remarkable loss of DC6 neurons in WISH at 120 hpf in 5 ppb TaClo and 1.75 μM MPTP exposed larvae. Although the reduction in DC6 neurons was not as significant in WIFA images, there appeared to be fewer neuronal numbers in this population compared to controls. Further imaging analyses confirmed that the loss of DC6 was more pronounced in WISH than larvae in WIFA. One possible explanation for this discrepancy is the use of targeted markers. Dopamine transporter and tyrosine hydroxylase are the markers commonly used to identify dopaminergic neurons in zebrafish models (Du et al., 2016; Filippi et al., 2010; Holzschuh et al., 2001; Xi et al., 2011). However, unlike the dopamine transporter, which specifically labels dopaminergic neurons, tyrosine hydroxylase catalyzes the synthesis of dopamine and other catecholamines

(Holzschuh et al., 2001). As a result, tyrosine hydroxylase labeling cells may include a broad range of catecholaminergic neurons. A prior study found that DC2 and DC4 neuronal populations were mainly dopaminergic, while other catecholaminergic neurons predominate in DC1, DC3, DC5, and DC6 populations (Du et al., 2016). Therefore, it is likely that the DC6 neuronal population contains not only dopaminergic neurons but also other catecholaminergic neurons, which could lead to a less specific detection of dopaminergic neurons when using tyrosine hydroxylase as a marker. Lastly, similar to 1.75 μM MPTP, we found that 5 ppb TaClo exposure prior to dopaminergic neuronal development does not appear to inhibit dopaminergic neurogenesis. Additionally, similar to MPTP, the presence of the chorion during TaClo exposure does not seem to prevent TaClo's neurotoxic effects. Overall, our study demonstrated TaClo elicits MPTP-like neurotoxicity in developmental zebrafish, characterized by impaired locomotor activity and a significant reduction in specific diencephalic neuronal populations. These findings further support the potential link between TaClo exposure and its contribution to PD development.

Upon investigating the neurotoxic effects, we observed that TaClo exposure induced bimodal concentration-response curves in the PMR and VMR behavioral assays and in the dopaminergic neuronal cell number assay, with the lowest concentration (5 ppb) exhibited the most drastic response. Bimodal dose responses are frequently reported in toxicology and pharmacology, at levels ranging from molecular to phenotypic and refer to dose-response relationships where a substance elicits two distinct and often opposing effects at different dose levels (Calabrese, 2013; Coral et al., 2021). Several studies have suggested this phenomenon arises from a dual mechanism of action involving different cellular or tissue responses (Coral et al., 2021; Yao et al., 2020).

To better understand the reason behind the bimodal responses in our study, we analyzed possible pathways by evaluating apoptosis, antioxidative enzymatic activity and genetic expression. In previous studies, researchers observed that 600 μM MPTP significantly inhibited mitochondrial complex I and increased inducible nitric oxide synthase (iNOS) in 3 dpf larvae with the most impact in the diencephalon (Díaz-Casado et al., 2016). Qin et al., 2024 observed

that activities of SOD, CAT, and GSH significantly decreased following five days of 70 MPTP μM treatment (Qin et al., 2024). Chen et al., 2021 observed that 400 MPTP μM triggered decreased GPX activity (Chen et al., 2021). Lastly, studies found 1 μM MPTP induced significant apoptosis at the dopaminergic neuronal regions (Haojia Dong et al., 2022). While limited studies have been performed in the zebrafish model, previous studies confirmed that TaClo inhibited complex I of the mitochondrial respiratory chain, induced ROS, and activated caspase-3 levels in rodent models (Keane et al., 2019; Yang et al., 2019). Consistent with previous observations, we observed a higher number of caspase-3 apoptotic bodies within the vDC in larvae treated with 1.75 μM MPTP and 5 ppb TaClo. Additionally, the 1.75 μM MPTP-treated larvae exhibited the lowest GPX activity, while the 500 ppb TaClo exposure group showed the highest GPX activity levels. In contrast to prior studies, we found no significant differences in mitochondrial membrane potential or cellular and mitochondrial ROS levels in the treated larvae. Despite the lack of other significant alterations, we propose that both TaClo and 1.75 μM MPTP may still induce ROS production and alter mitochondrial membrane potential, as the altered GPX activity observed in 500 ppb TaClo and 1.75 μM MPTP. GPX is an important antioxidant enzyme that maintains ROS homeostasis by regulating intracellular $H_2O_2$ levels and maintaining GSH/GSSG balance (Zhang et al., 2020). While diencephalic dopaminergic neurons were most affected at 5 ppb TaClo and 1.75 μM MPTP, we also observed an increased apoptotic level in 50 ppb exposed larvae. Moreover, both 5 ppb and 50 ppb treated larvae exhibited significantly decreased astrocytic expression. Taken together, these findings may suggest that TaClo and MPTP treatment may induce oxidative stress. The surge in GPX activity at 500 ppb TaClo appears to counteract cellular ROS damage. In contrast, the lack of protection from GPX in the TaClo (5 and 50 ppb) MPTP-treated larvae may ultimately contribute to cellular damage. We then questioned why, unlike previous MPTP studies in zebrafish models, alterations in ROS levels and mitochondrial dysfunction were not observed, despite the significant dopaminergic neuronal damage following TaClo and MPTP treatment. Dıaz-Casado et al., 2016 detected increased mitochondrial complex I activity in homogenized larvae following exposure to 600 μM MPTP (Díaz-Casado et al., 2016). However, this concentration caused widespread loss of dopaminergic neurons (DC1-7), leaving only a small population in the locus coeruleus intact (Díaz-Casado et al., 2016). In another study, the researchers found a significant increase in ROS generation in zebrafish larvae with an approximately 30% diencephalic dopaminergic neuronal

loss following 50 μM MPTP exposure (Ren et al., 2022). In contrast to our study, we observed an approximately 18% diencephalic dopaminergic neuronal loss in the MPTP-treated zebrafish larvae. We propose that the relatively lower level of neuronal damage may explain the lack of significant changes in mitochondrial membrane potential and ROS observed in our study. Another possible explanation is that, in the flow cytometry analysis, 10,000 cells were evaluated from pooled zebrafish larvae to detect ROS and mitochondrial membrane potential. We speculate that the relatively small proportion of diencephalic dopaminergic neurons compared to the total cell population in the larval body may have limited their representation in the analysis. Several studies have utilized whole zebrafish larvae in MPTP or PD research to evaluate ROS and mitochondrial function. However, based on our findings, we recommend that future studies focus specifically on the larval diencephalon to obtain more specific results.

While imbalanced oxidative stress and mitochondrial dysfunction have been incriminated, additional factors, such as microglial and astrocytic dysfunction, have also been suggested to contribute to dopaminergic neuronal damage in MPTP and TaClo-treated models (Lee et al., 2019; Rausch et al., 1995; Yang et al., 2019; Yasuda et al., 2008). Under physiological conditions, microglia and astrocytes are essential for dopaminergic neuronal protection (Yasuda et al., 2008). However, it has been reported that microglia and astrocytes modulate neuroinflammatory activities and are involved in the pathological process in the nigrostriatal system following MPTP administration (Kohutnicka et al., 1998). Previous research of glial alterations after MPTP exposure has been primarily performed in rodent models (Huang et al., 2017; Yasuda et al., 2008). Mice increased the number and size of Iba1-labeled microglial cells and GFAP-positive astrocytes in the striatum following MPTP administration (Huang et al., 2017). A study has demonstrated that TaClo not only caused oxidative stress and reduced mitochondrial membrane potential, but also resulted in elevated Iba1 mRNA expression detected in the nigrostriatal system (Yang et al., 2019). Earlier studies reported TaClo exposure led to 50% loss of tyrosine hydroxylase immunoreactive neurons and resulted in a 50% cellular reduction in astrocyte culture of C57/B16 mouse mesencephalon (Rausch et al., 1995). In our study, 5 ppb TaClo and 1.75 μM MPTP treated larvae had a significant increase in microglial density at the ventral diencephalon which appeared to center on dopaminergic neuronal regions. In addition,

these larvae showed the lowest astrocytic density among all the treated groups, with immunofluorescence loss appearing largely in the DC3 neuronal population (equivalent to paraventricular organ). Although we did not observe a significant microgliosis, 1.75 μM MPTP-treated larvae appeared to have a higher microglial density in comparison to the control group. While MPTP and TaClo are structurally and chemically similar, it is unknown whether they elicit opposite responses in astrocytes. A study found that TCE inhibited neural progenitor cells from differentiating into astrocytes (Rausch et al., 1995). Therefore, it is likely that TaClo utilizes a different mechanism from MPTP to modulate astrocytic function. Lastly, no significant alterations in mRNA expression levels were observed in the screening of 16 genes, except for *mpeg* (macrophage expressed gene 1), which codes for perforin-2 and is found in monocytic lineage cells like microglia. A transcriptomic analysis may be beneficial to unravel potential mechanisms. Overall, our findings highlight that imbalanced oxidative stress and glial responses contribute to MPTP and TaClo neurotoxicity in the developmental zebrafish model. These findings also provide some evidence to explain the bimodal dose effect observed in the TaClo-treated groups.

Lastly, we assessed neurotransmitter levels of DOPAC, dopamine, norepinephrine, and 5-HIAA in 120 hpf zebrafish larvae. Among these, only 5-HIAA was significantly decreased in the 1.75 μM MPTP-treated group. 5-HIAA, the primary metabolite of serotonin degradation, is considered a stable biomarker for overall serotonin production (Burks & Bao, 2016). Previous studies investigating the effects of MPTP on 5-HIAA levels have reported region-specific and variable results. For example, MPTP administration has been shown to increase 5-HIAA levels in the mouse striatum. (Fukuda et al., 1988); however, Yang et al. reported that intraperitoneal MPTP injection significantly reduced serotonin (5-HT) and its metabolite 5-HIAA in the prefrontal cortex and hippocampus (R. Yang et al., 2023). Similarly, Maiti et al. demonstrated that subcutaneous MPTP administration did not alter absolute 5-HT levels in the striatum or prefrontal cortex but significantly decreased the 5-HIAA/5-HT ratio (Maiti et al., 2016). Moreover, Previous studies have reported that depletion of 5-HIAA in the cortex may be associated with anxiety-like behaviors in MPTP-treated mice (R. Yang et al., 2023). Taken together, our findings suggest that 1.75 μM MPTP affects the serotonergic system, and the

observed locomotor deficits may not be solely attributed to dopaminergic neuronal loss but may also involve decreased 5-HIAA levels and the potential manifestation of anxiety-like behaviors. In addition, we propose that exposure to 1.75 μM MPTP imposes stress on zebrafish. Previous studies have indicated that the serotonergic system is highly sensitive to stress, which can lead to its hypofunction (Dankoski et al., 2014). Stressors can also indirectly modulate brain neurotransmitters, resulting in reductions of 5-HIAA, dopamine, and DOPAC levels (de Abreu et al., 2021).

## 5. Conclusions and future direction

In summary, this study aimed to investigate TaClo-induced neurotoxicity in the developmental zebrafish model. We also sought to address gaps in understanding the underlying mechanisms of neurotoxicity by comparing the toxicity of TaClo to MPTP neurotoxicity. Our study identified TaClo as a neurotoxicant that elicits phenotypic MPTP-like neurotoxicity in the developmental zebrafish model. Utilizing this model, we observed that alterations in antioxidative enzymatic activity and glial responses induced by MPTP and TaClo play critical roles in behavioral changes and dopaminergic neuronal damage. These findings closely align with observations previously reported in rodent models. Interestingly, we found the lowest concentration of TaClo, 5 ppb, elicited the most pronounced response. Future studies should focus on the neurotoxic impact of metabolic TaClo after exposure to its parent compounds. Although additional work is necessary to understand how TaClo impacts dopaminergic neurons, we believe this is the first study using the developmental zebrafish model to investigate the neurotoxic impact of TaClo and compare it with MPTP. In addition, this paper makes a valuable contribution to environmental contaminants research by providing evidence of the potential link between TaClo exposure and PD.

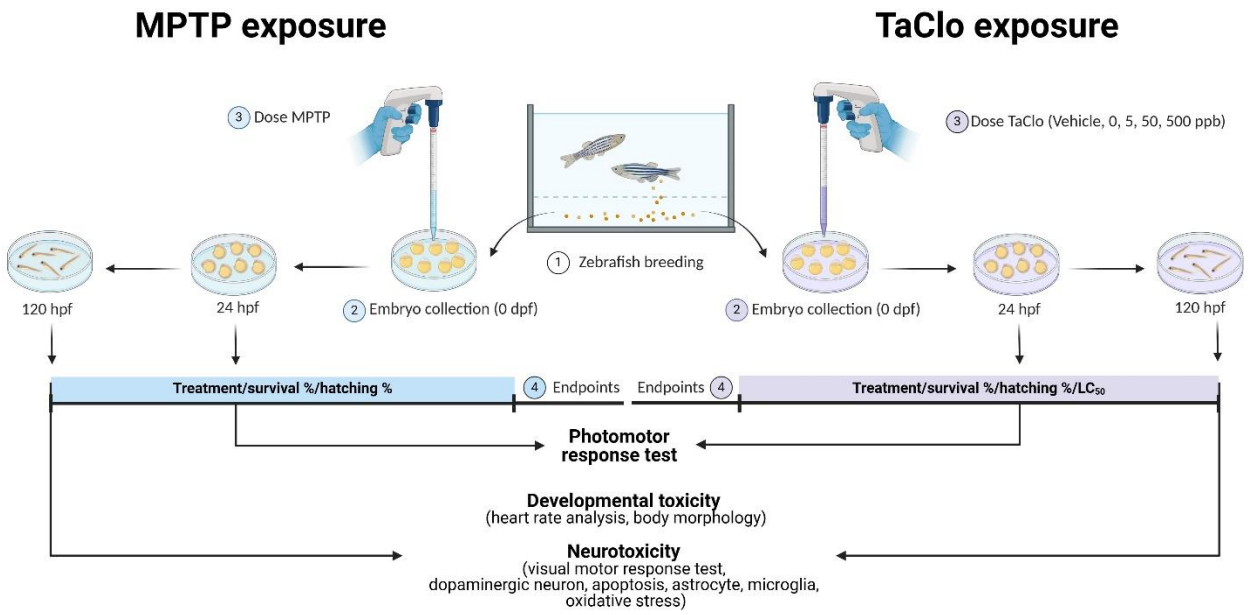


**Figure 3-1. Experimental design of 1-trichloromethyl-1,2,3,4-tetrahydro-beta-carboline (TaClo) and 1-methyl-4-phenyl-1,2,3,6-tetrahydropyridine (MPTP) exposures in the developmental zebrafish model**

① Adult wild-type AB strain zebrafish (Danio rerio) were first bred to obtain embryos for chemical exposure. ② Fertilized embryos were collected immediately and ③ exposed to MPTP, TaClo, or vehicle (dimethyl sulfoxide, DMSO) until 24 hours post-fertilization (hpf) or 120 hpf. ④ Developmental toxicity endpoints included survival and hatching percentages (1-120 hpf, MPTP and TaClo), lethal concentration 50 (LC50) (1-120 hpf, TaClo), body morphology assessments (120 hpf, MPTP and TaClo), and heart rate (120 hpf, TaClo). Neurotoxicity was assessed using the photomotor response test (24 hpf, MPTP and TaClo) and the visual motor response behavioral tests, and evaluation of dopaminergic neurons, apoptosis, astrocyte, microglia, and oxidative stress in 120 hpf MPTP or TaClo-treated larvae.

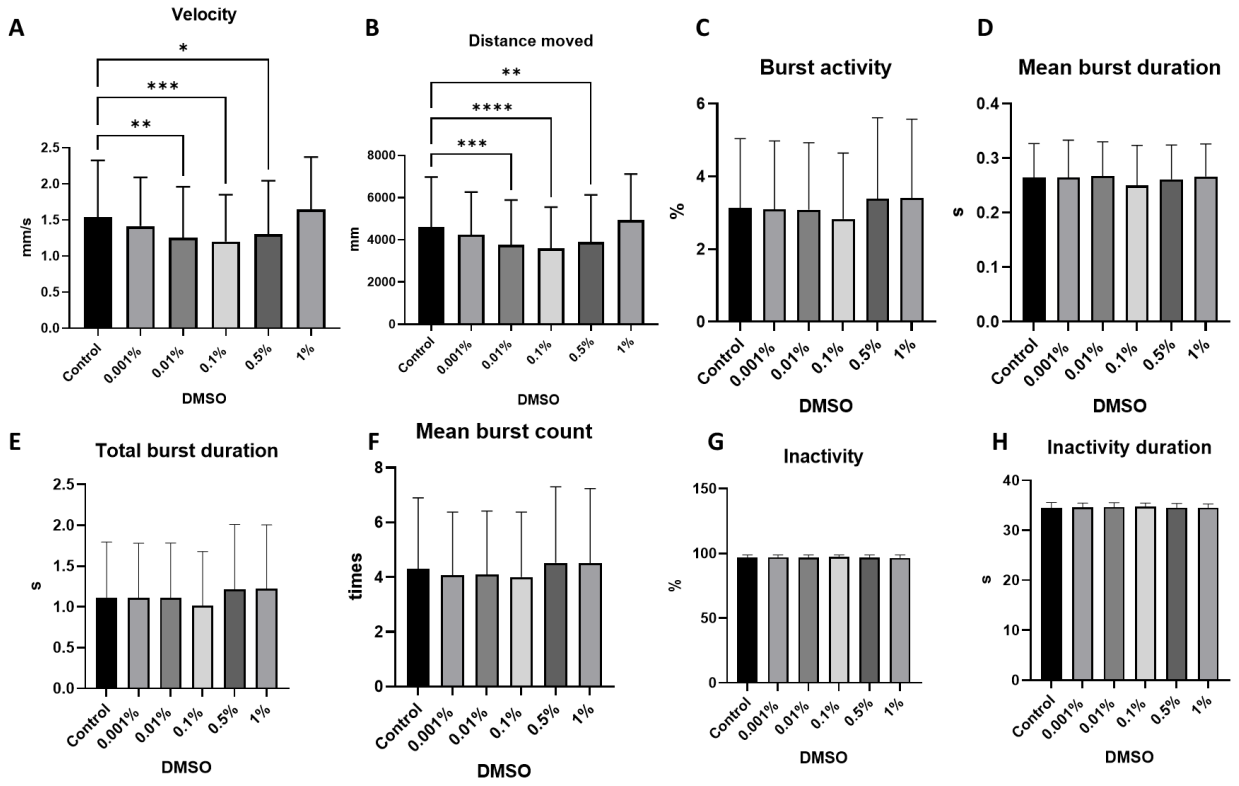


**Figure 3-2. Visual motor response test and photomotor response test**

Visual motor response test and photomotor response test result in different Dimethyl sulfoxide (DMSO) concentrations DMSO concentrations of 0.01%, 0.1%, and 0.5% inducing a significant reduction in locomotor activity (velocity and distance moved) in 120 hpf larvae (A and B). 0.001%, 0.01%, 0.1%, 0.5%, and 1% did not impact PMR results compared to the control in burst activity (C), mean burst duration (D), total burst duration (E), mean burst count (F), inactivity (G), and inactivity duration (H). All data were analyzed using Kruskal-Wallis test, followed by Dunn's multiple comparison test. *$p \leq 0.05$, **$p \leq 0.001$, and ****$p \leq 0.0001$. Error bars represent standard deviation.

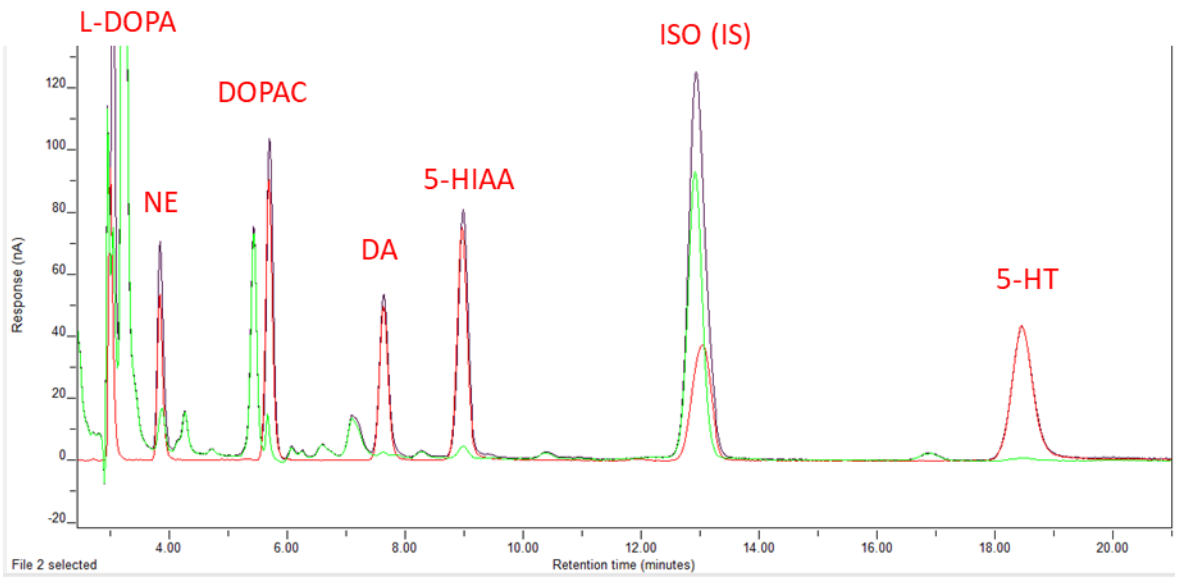


**Figure 3-3. HPLC-ECD neurotransmitter detection on 120 hours-post fertilization zebrafish larvae**

HPLC-EC detection to detect tyrosine and tryptophan-based metabolites Levodopa, (L-DOPA, Sigma - D9628), norepinephrine (NE, Sigma - A9512), 3,4-Dihydroxyphenylacetic acid (DOPAC, Sigma - 850217), dopamine (DA, Sigma - H8502), 5-hydroxyindoleacetic acid (5-HIAA, Sigma - H8876), serotonin (5-HT, Sigma - H9523), and isoproterenol (ISO, Sigma – 1351005) in tissue lysates. Image is provided by Dr. Piyush Padhi and Dr. Anumantha G. Kanthasamy at the Isakson Center for Neurological Disease Research at the University of Georgia. Red: standard; Green: spike; Blue: sample.

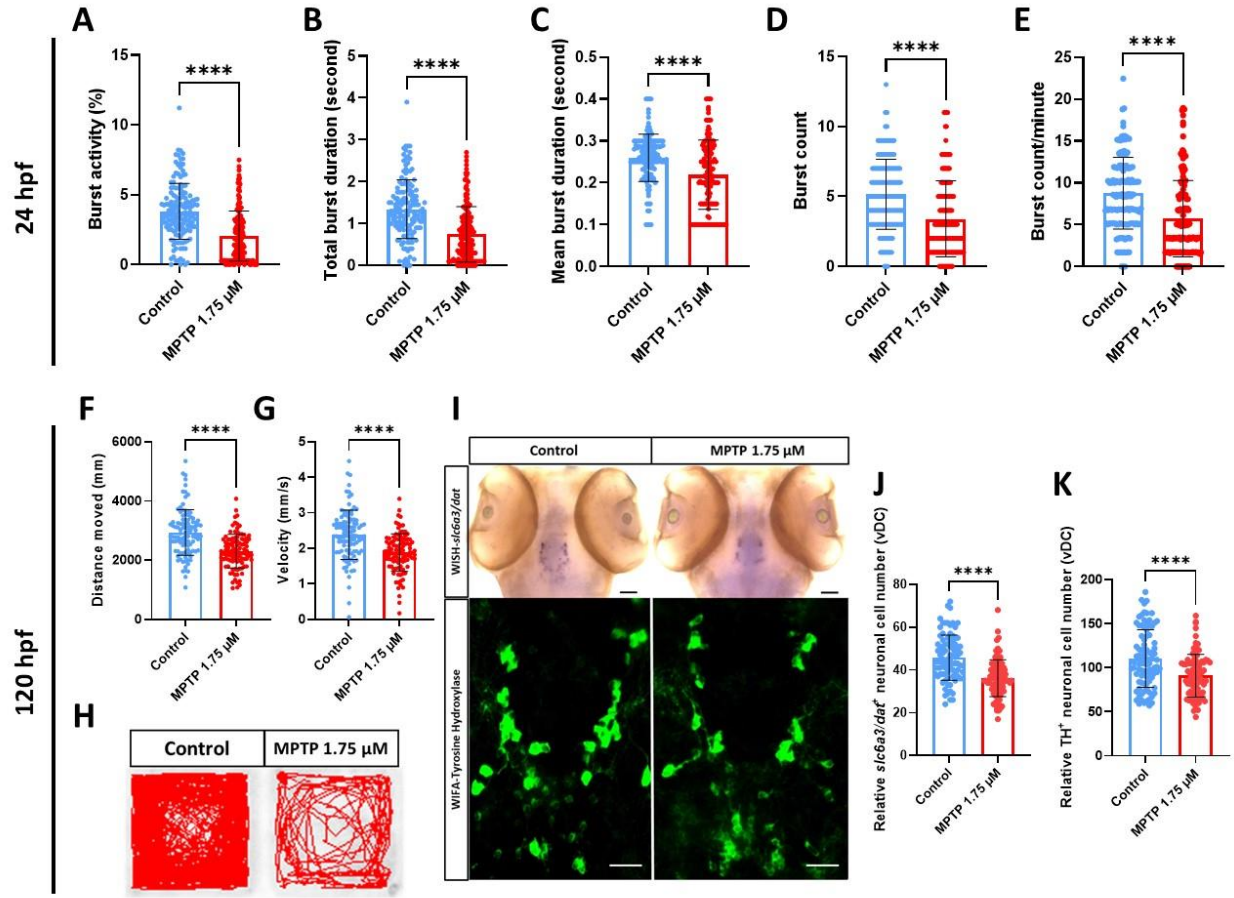


**Figure 3-4. Neurotoxic effects on 1.75 µM MPTP-treated developmental zebrafish**

Embryonic zebrafish exposed to 1.75 µM MPTP at 24 hours post-fertilization (hpf) displayed significantly reduced burst activity (%) (A), total burst duration (B), mean burst duration (C), burst count (D), and burst count/minute (E). Visual motor response test (F-H). Larval zebrafish exposed to 1.75 µM MPTP at 120 hpf had significantly shorter distance moved (mm) (F) and decreased velocity (mm/s)(G). A representative track diagram of the 120 hpf larvae from the control (0 µM) and 1.75 µM MPTP groups, obtained from an hour of video tracking, showed reduced movement distance in the 1.75 µM MPTP-treated larvae (H). Relative dopaminergic neuronal expression in ventral diencephalon (vDC) of 120 hpf larva (I-K). Upper panel: Whole mount in situ hybridization (WISH) assay using slc6a3 (solute carrier family 6 member 3)/dat (dopamine transporter) probes to label dopaminergic neurons. Lower panel: Whole mount immunofluorescence (WIFA) assay using tyrosine hydroxylase (TH) antibody to highlight dopaminergic neurons. Black scale bar=50 µm (WISH); white scale bar=20 µm (WIFA) (I). 1.75 µM MPTP triggered significant relative *slc6a3* (*dat*) (J) and TH (K) labeled dopaminergic neuronal cell loss at the vDC region compared to the control group (0 µM). Data are expressed as mean ± standard deviation. All data were analyzed using unpaired t test or Mann-Whitney U test. ****$p \leq 0.0001$.

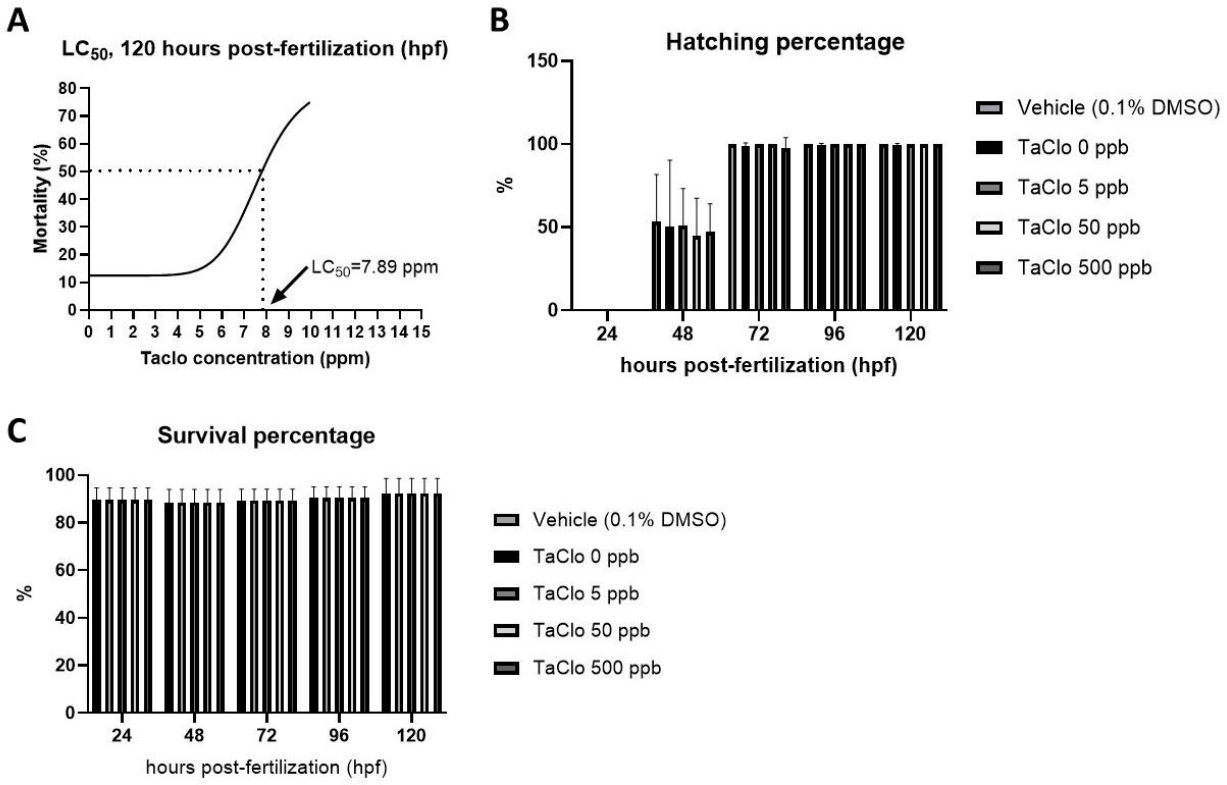


**Figure 3-5. Lethal concentration 50 and hatching and survival percentage in 120 hours post-fertilization after TaClo (vehicle, 0, 5, 50, 500 ppb) exposure**

Lethal concentration 50 at 120 hpf of TaClo was 7.89 parts per million (ppm) (A). No significant alterations were noted in hatching percentage (B) and survival percentage (C) following 5, 50, or 500 ppb TaClo treatment. Three biological replicates, with 50 embryos per treatment per replicate. Error bars represent standard deviation.

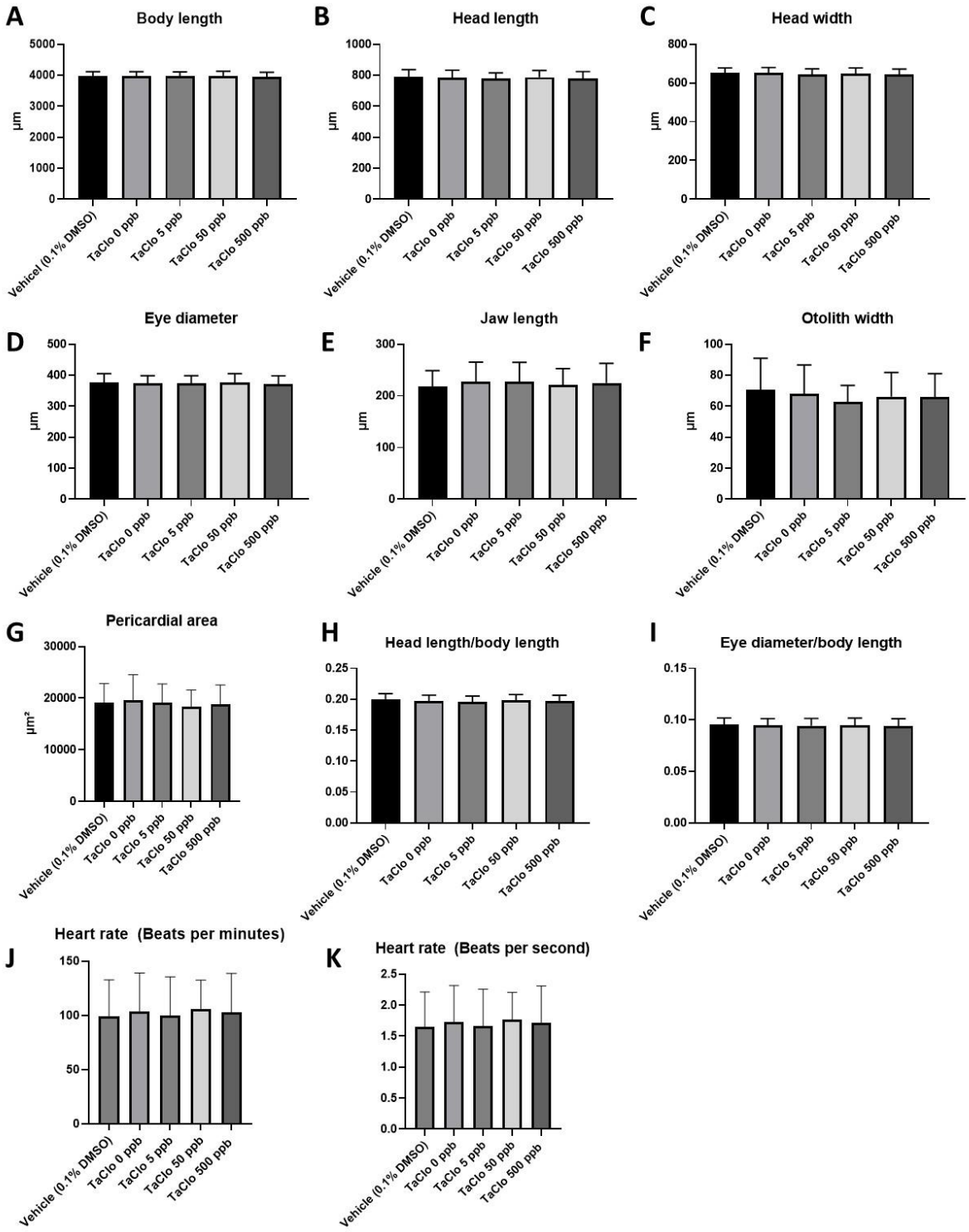


**Figure 3-6. Body morphology and cardiac function evaluation in 120 hpf larvae after TaClo (vehicle, 0, 5, 50, 500 ppb) exposure**

No body malformations were observed in body length (A), head length (B), head width (C), eye diameter (D), jaw length (E), otolith width (F), pericardia area (G), head length/body length (H), and eye diameter/body length (I). No significant changes were found in heart rate analyses, including beats per minute (J) and beats per second (K). Six biological replicates, with 24 larvae per treatment per replicate. Error bars represent standard deviation. All data were analyzed using Kruskal-Wallis test, followed by Dunn's multiple comparison test.

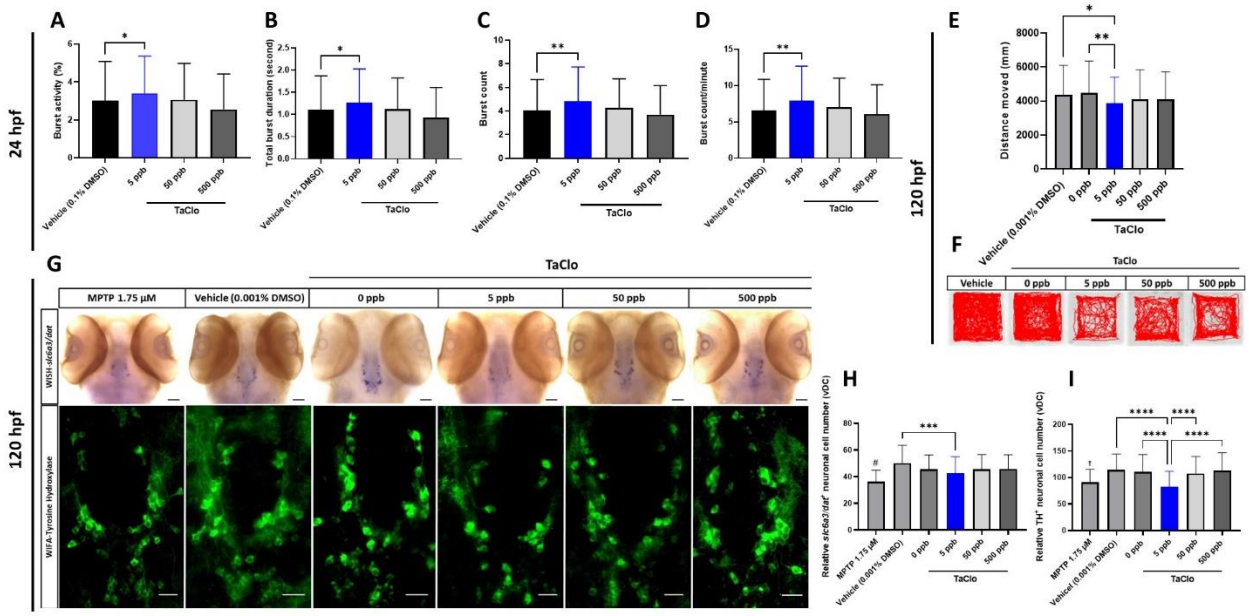


**Figure 3-7. 5 pp TaClo elicits MPTP-like neurotoxicity in zebrafish at embryonic and larval stages. Photomotor response test (A-D)**

Embryonic zebrafish at 24 hours post-fertilization (hpf) treated with 5 ppb TaClo exhibited increased burst activity (%)(A), total burst duration (second) (B), burst count (C), and burst count/minute (D). Visual motor response test (E-F). Zebrafish larvae at 120 hpf displayed the lowest distanced moved (mm) compared to control and vehicle control groups (E). A representative 30-minute video track diagram of the 120 hpf larvae showed reduced movement distance in the 1.75 µM MPTP-and TaClo treated larvae (F). Relative dopaminergic neuronal expression in the ventral diencephalon (vDC) of 120 hpf larva (G-H). Upper panel: Whole mount in situ hybridization (WISH) assay using *slc6a3* (solute carrier family 6 member 3)*/dat* (dopamine transporter) probes to label dopaminergic neurons. Lower panel: Whole mount immunofluorescence (WIFA) assay using tyrosine hydroxylase (TH) antibody to highlight dopaminergic neurons. Black scale bar=50 µm (WISH); white scale bar=20 µm (WIFA) (G). 5 ppb TaClo triggered significant relative *slc6a3/dat* labeled dopaminergic neuronal cell loss compared to vehicle (0.001% DMSO) (H) and a marked reduction of TH labeled dopaminergic neuronal cellular numbers at the vDC region compared to vehicle, 50 ppb TaCLO, and 500 ppb TaClo. #: In the WISH assay, 1.75 µM MPTP exposed larvae had the significantly lowest *slc6a3*(*dat*) neuronal cellular numbers compared to vehicle (0.001% DMSO, $p \leq 0.0001$), control (TaClo 0 ppb, $p \leq 0.0001$), TaClo 5 ppb ($p \leq 0.01$), TaClo 50 ppb ($p \leq 0.0001$), and TaClo 500 ppb ($p \leq 0.0001$) (H). †: In the WIFA assay, 1.75 µM MPTP exposed larvae had the significantly lowest TH neuronal cellular numbers compared to vehicle (0.001% DMSO, $p \leq 0.0001$), control (TaClo 0 ppb, $p \leq 0.01$), 50 ppb TaClo ($p \leq 0.05$), and 500 ppb TaClo ($p \leq 0.001$)(I). Data are expressed as mean ± standard deviation. All data were analyzed using Kruskal-Wallis test,

followed by Dunn's multiple comparison test. *$p \leq 0.05$, **$p \leq 0.001$, ***$p \leq 0.001$, and ****$p \leq 0.0001$.

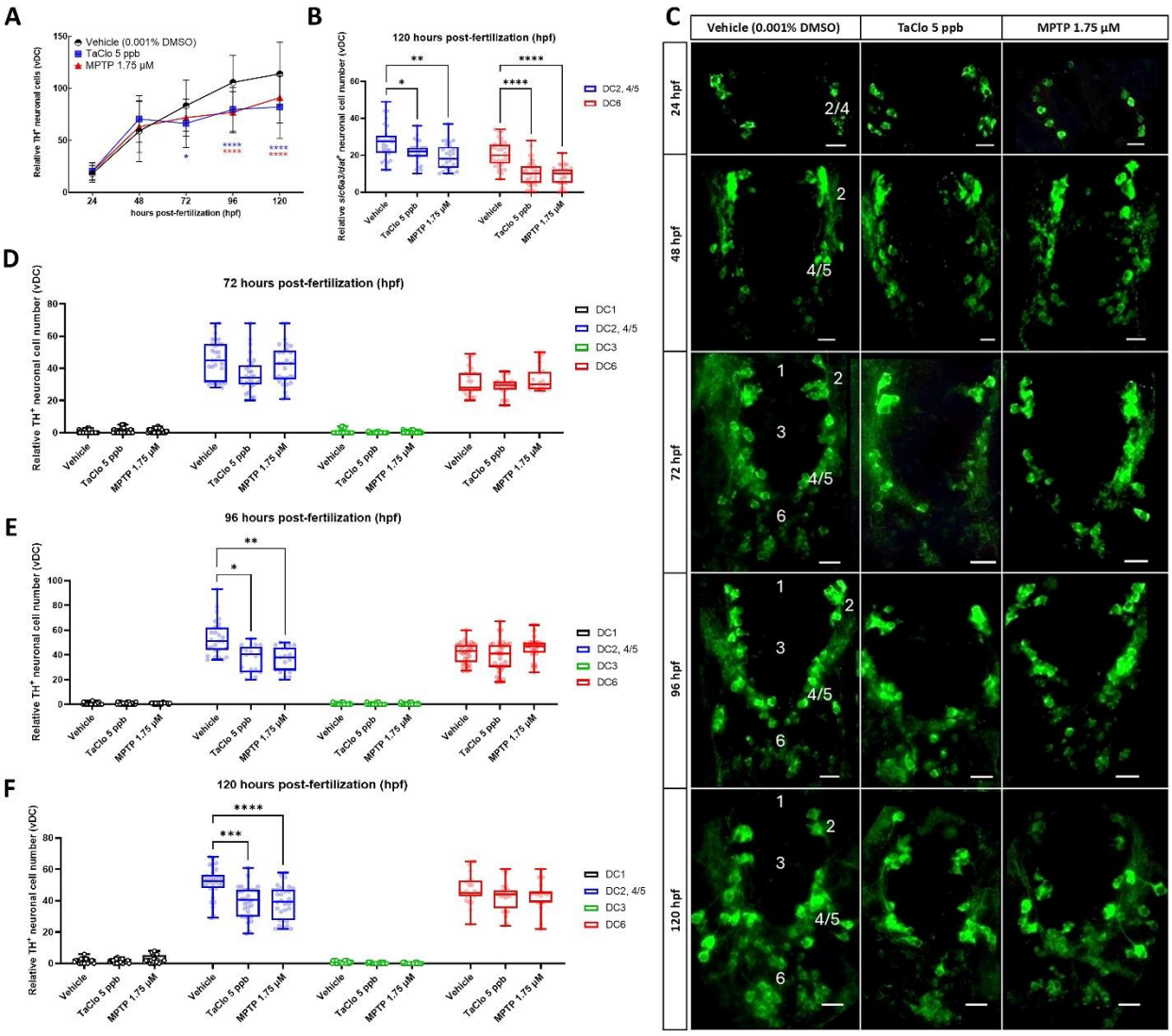


**Figure 3-8. 5 ppb and 1.75 µM MPTP time course study shows the neurotoxic impacts on diencephalic neuronal populations**

Embryonic zebrafish were exposed to 5 ppb and 1.75 µM MPTP with samples collected at 24 hours post-fertilization (hpf), 48 hpf, 72 hpf, 96 hpf, and 120 hpf for whole mount immunofluorescence assay (WIFA) and stained with anti-tyrosine hydroxylase (TH) antibody. Significant reductions in TH-immunoreactive neurons were first observed at 72 hpf in the 5 ppb TaClo group, followed by the 1.75 µM MPTP group at 96 hpf, with both reductions persisting through 120 hpf (A). Whole-mount *in situ* hybridization assay (WISH) analysis at 120 hpf revealed that *slc6a3/dat*-labeled diencephalic neuronal populations DC2, DC4/5, and DC6 were particularly vulnerable to 5 ppb TaClo and 1.75 µM MPTP exposure (B). Time course WIFA imaging of TH-immunoreactive cells within ventral diencephalon at different developmental stages following vehicle (0.001% DMSO), 5 ppb TaClo, and 1.75 µM MPTP exposure. Numbers (DC1-6) indicate different diencephalic neuronal populations (Du et al., 2016), scale bar=20 µm

(C). WIFA analysis at 72 hpf showed no significant differences in DC1, DC2 and DC4/5, DC3, and DC6 among treatment groups (D). WIFA analyses at 96 hpf (E) and 120 hpf (F) revealed significant reductions in TH-immunoreactive neurons within DC2 and DC4/5 following exposure to 5 ppb TaClo and 1.75 μM MPTP. Data are expressed as mean ± standard deviation. All data were analyzed using Kruskal-Wallis test, followed by Dunn's multiple comparison test. *$p \leq 0.05$, **$p \leq 0.001$, ***$p \leq 0.001$, and ****$p \leq 0.0001$.

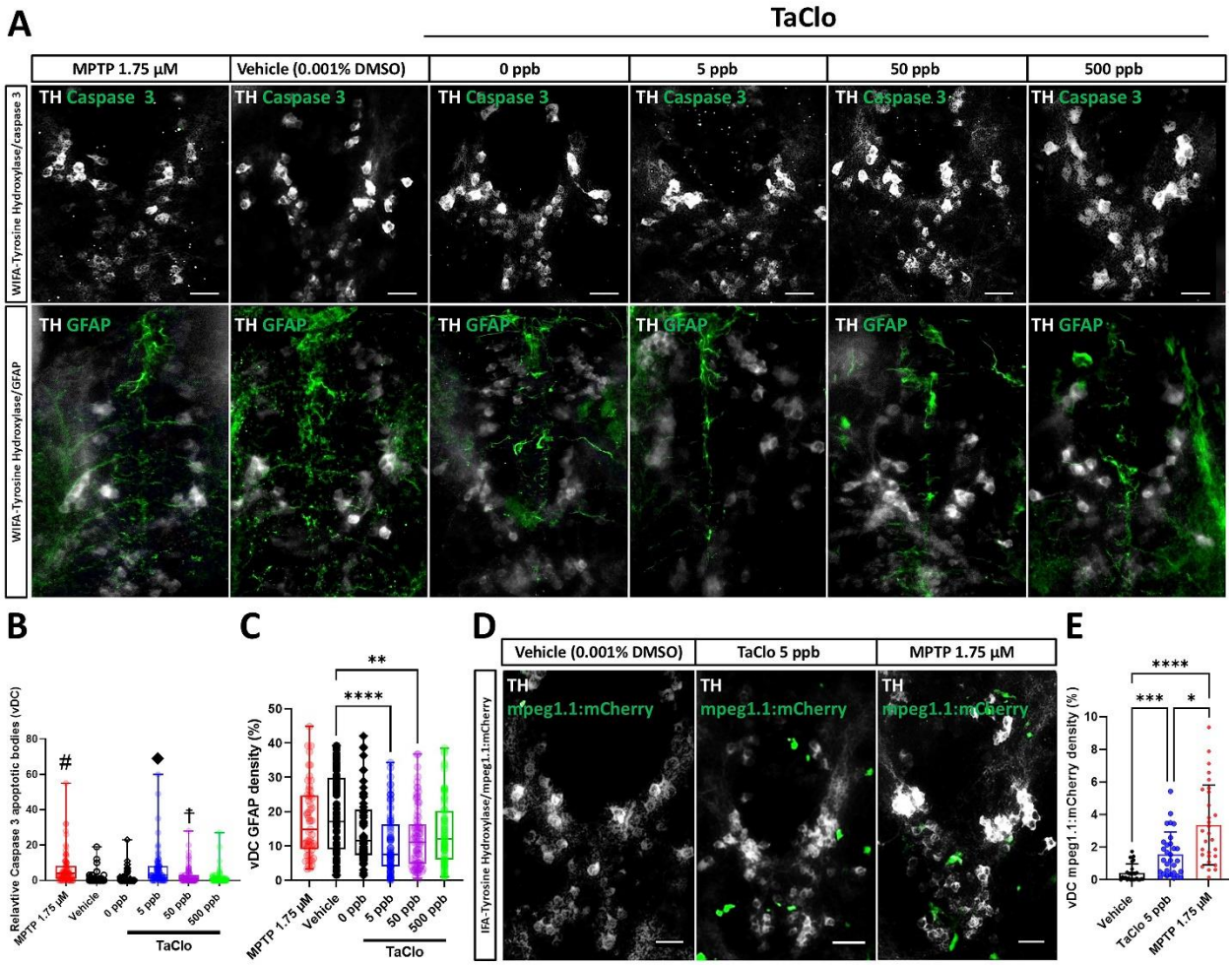


**Figure 3-9. TaClo and MPTP mediate activated apoptosis, astrocytic dysfunction, and microgliosis at the ventral diencephalon (vDC) in 120 hpf larvae**

Representative double whole mount immunofluorescence images of tyrosine hydroxylase (TH) (upper and lower panel), caspase 3 (upper panel), and glial fibrillary acidic protein (GFAP) (lower panel) in 1.75 µM MPTP, vehicle (0.001% DMSO), and TaClo (0, 5, 50, 500 ppb) exposure groups, TH-positive cells and caspase 3/GFAP positive cells are shown in white and green, respectively, scale bar=20 µm (A). #: 1.75 µM MPTP treatment induces significantly higher numbers of apoptotic bodies at the vDC compared to the vehicle and TaClo (0, 50, 500 ppb) ($p \leq 0.0001$) exposures in 120 hpf larvae. ♦ : 5 ppb TaClo exposure groups show a significant increase in apoptotic bodies at the vDC compared to the vehicle and TaClo (0, 50, 500 ppb) ($p \leq 0.0001$) exposures. †: 120 hpf larvae treated with 50 ppb TaClo produce more apoptotic bodies than the vehicle and 0 ppb TaClo ($p \leq 0.01$) exposures (B). Double WIFA imaging analysis on GFAP density at the vDC demonstrates TaClo triggers (5 ppb and 50 ppb) lower GFAP-immunoreactive astrocytic density than the vehicle group (C). Double immunostaining for red fluorescent protein (mCherry) and tyrosine hydroxylase (TH) in 120 hpf Tg(mpeg1.1:mCherry) larvae, TH-positive cells and mpeg1.1:mCherry positive cells are shown

in white and green, respectively, scale bar=20 μm (D). 5 ppb TaClo and 1.75 μM MPTP-exposed larvae show significantly higher levels of mpeg1.1:mCherry with the 1.75 μM MPTP group having the highest density (E). Data are expressed as mean ± standard deviation. All data were analyzed using Kruskal-Wallis test, followed by Dunn's multiple comparison test. *$p \leq 0.05$, **$p \leq 0.001$, ***$p \leq 0.001$, and ****$p \leq 0.0001$.

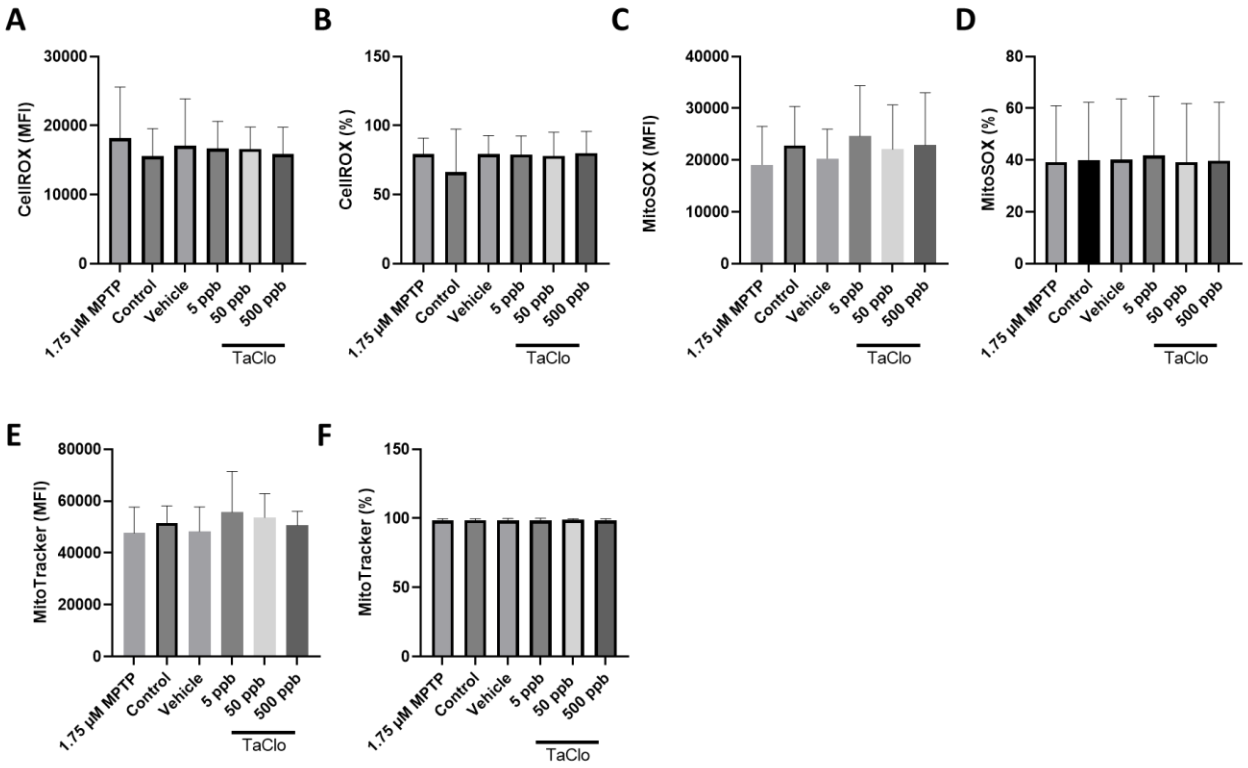


**Figure 3-10. Flow cytometry analysis on TaClo (5, 50, 500 ppb) and 1.75 µM MPTP exposure at 0-120 hpf**

No significant differences were observed in cellular ROS, mitochondrial ROS production, or mitochondrial membrane potential in 120 hpf zebrafish, as assessed by CellROX Green (A-B), MitoSOX Red (C-D), and MitoTracker Deep Red-based (E-F) flow cytometry, respectively. Quantitative analyses on median fluorescent intensity (MFI) and percentage of positive cells (%). Data are expressed as mean ± standard deviation. All data were analyzed using one-way ANOVA, followed by Tukey's multiple comparison test. *$p \leq 0.05$ and **$p \leq 0.001$.

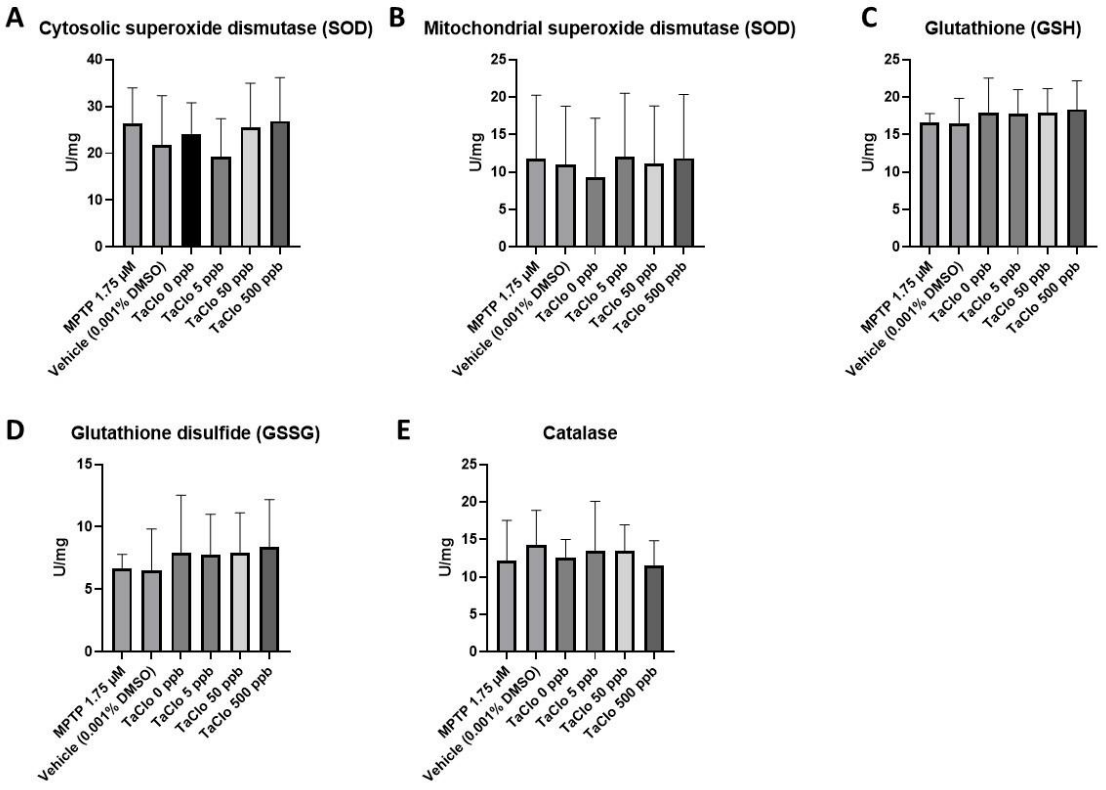


**Figure 3-11. Assessment of antioxidative enzymatic activity in 120 hpf larvae following TaClo (vehicle, 0, 5, 50, 500 ppb) and 1.75 µM MPTP exposure**

No significant alterations were observed in cytosolic superoxide dismutase (A), mitochondrial superoxide dismutase (B), glutathione (C), glutathione disulfide (D), and catalase activity (E) evaluation in 120 hpf larvae treated with TaClo (vehicle, 0, 5, 50, 500 ppb) and 1.75 µM MPTP. Six biological replicates, 40 to 50 pooled larvae per treatment per replicate. Error bars represent standard deviation. All data were analyzed using Kruskal-Wallis test, followed by Dunn's multiple comparison test.

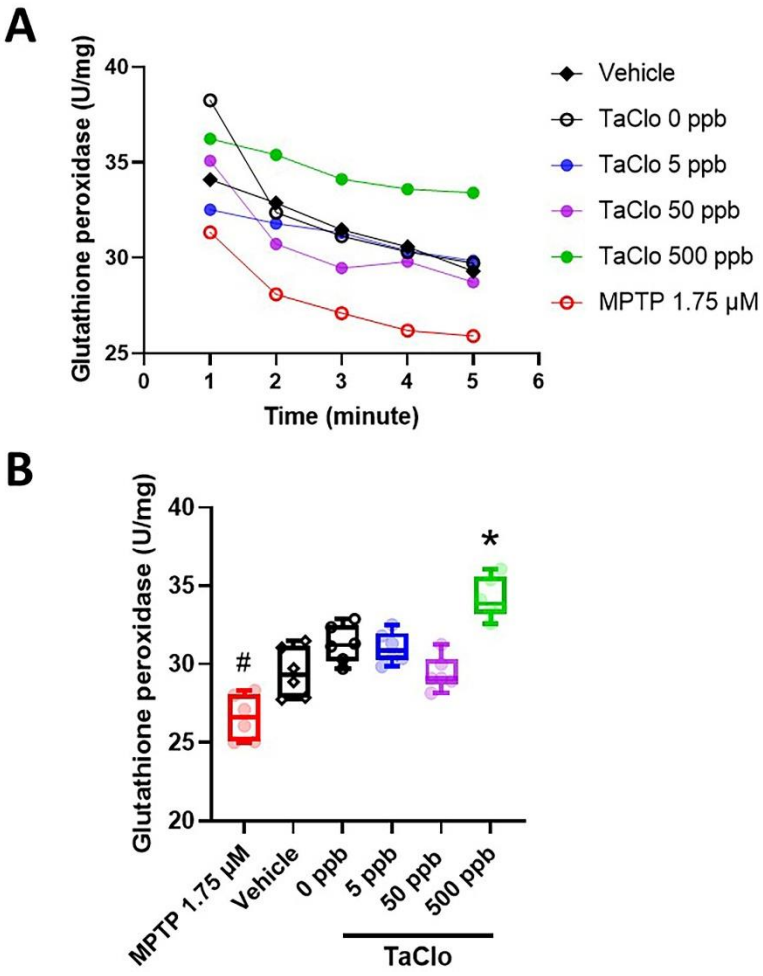


**Figure 3-12. Glutathione peroxidase (GPX) activity levels are altered in 120 hpf larvae exposed to TaClo and 1.75 µM MPTP larvae**

A schematic image of GPX activity across five time points measured every minute (1-5 minutes) in the vehicle (0.001% DMSO), TaClo (0, 5, 50, 500 ppb), and 1.75 µM MPTP treated larvae (A). #: the 1.75 µM MPTP exposed group show the lowest normalized GPX activity level across five minutes (A) and has the significantly lowest overall GPX activity compared to vehicle and 50 ppb TaClo ($p \leq 0.001$) and TaClo (0, 5, 500 ppb) ($p \leq 0.0001$) exposures. *: the 500 ppb TaClo exposure appears to exhibit high GPX activity through five minutes (A) and has the significantly highest overall GPX activity compared to the vehicle and 50 ppb TaClo ($p \leq 0.0001$) and TaClo (0, 5 ppb) ($p \leq 0.001$) exposures. All GPX data are normalized and are expressed as U (nmol/min/ml of protein)/mg. Data are expressed as mean ± standard deviation. All data were analyzed by one-way ANOVA test, followed by Tukey's post hoc test.

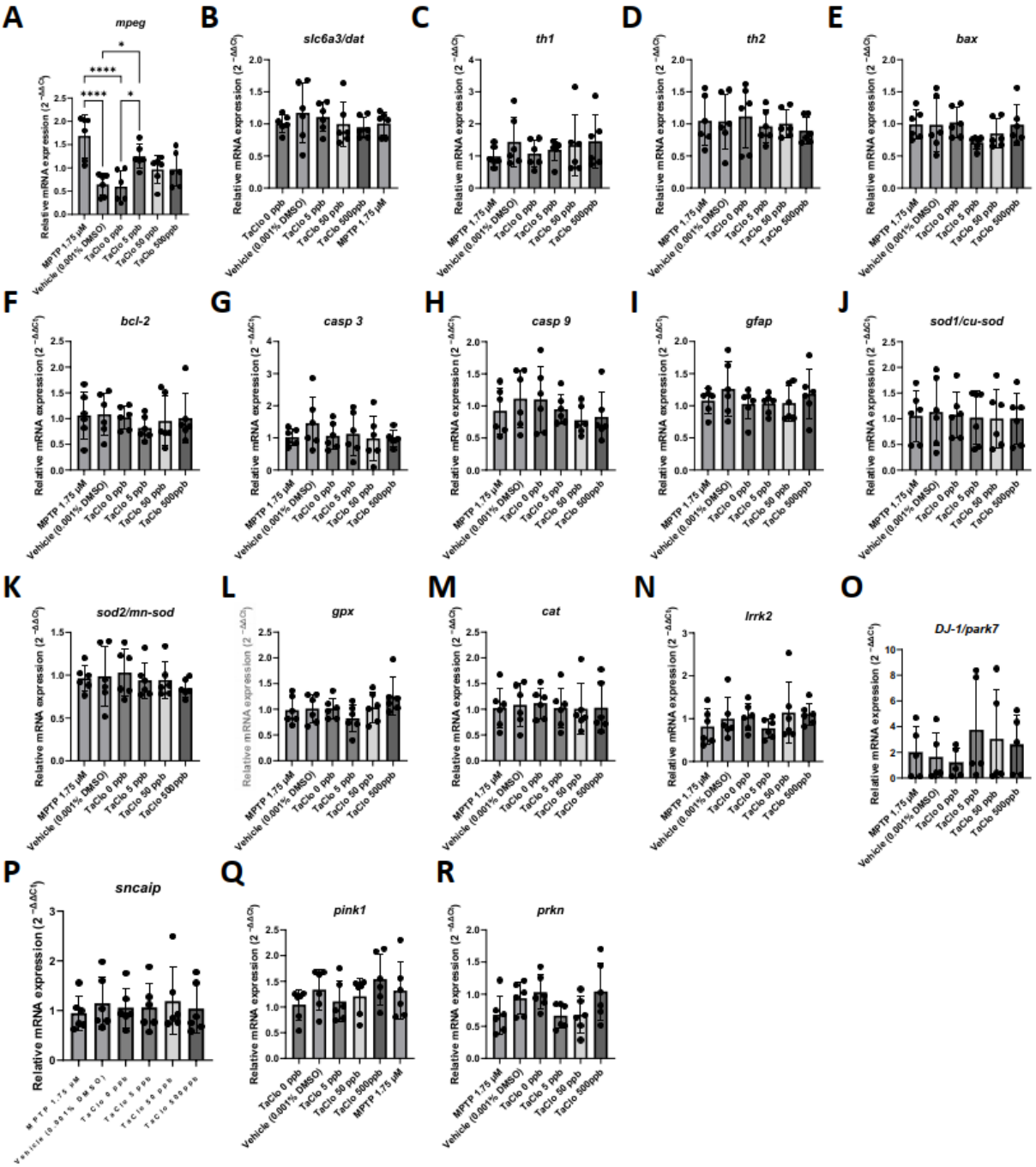


**Figure 3-13. Relative mRNA expression in TaClo (vehicle, 0, 5, 50, 500 ppb) and 1.75 µM MPTP-treated 120 hpf larvae**

5 ppb TaClo and 1.75 µM MPTP exposed larvae had a significantly higher *mpeg* (*macrophage-expressed gene*) mRNA expression than control and vehicle groups (A). Gene expression was not significantly different between groups for *slc6a3/dat* (B), *th1* (C), *th2* (D), *bax* (E), *bcl-2* (F), *casp 3* (G), *casp 9* (H), *gfap* (I), *sod1/cu-sod* (J), *sod2/mn-sod* (K), *gpx* (L), *cat* (M), *lrrk2* (N),

*DJ/park7* (O), *sncaip* (P), *pink1* (Q), and *parkn* (R). Six biological replicates, 40 to 50 pooled larvae per treatment per replicate. Error bars represent standard deviation. All data were analyzed using Kruskal-Wallis test, followed by Dunn's multiple comparison test. *$p \leq 0.05$, **$p \leq 0.001$, and ****$p \leq 0.0001$. *slc6a3 (solute carrier family 6 member 3)/dat (dopamine transporter), th1* (*tyrosine hydroxylase 1*), *th2* (*tyrosine hydroxylase 2*), *bax (BCL2 associated X), bcl2 (B-cell leukemia/lymphoma 2 protein), casp 3 (caspase 3), casp 9 (caspase 9), gfap* (*glial fibrillary acidic protein*), *sod1/cu-sod* (*Cu superoxide dismutase*), *sod2/mn-sod* (*manganese superoxide dismutase*), *gpx* (*glutathione peroxidase*), *cat (catalase), lrrk2* (*leucine-rich repeat kinase 2*), *sncaip* (*alpha interacting protein*), *pink 1(PTEN-induced putative kinase 1*), and *prkn* (*parkin RBR E3 ubiquitin protein ligase*).

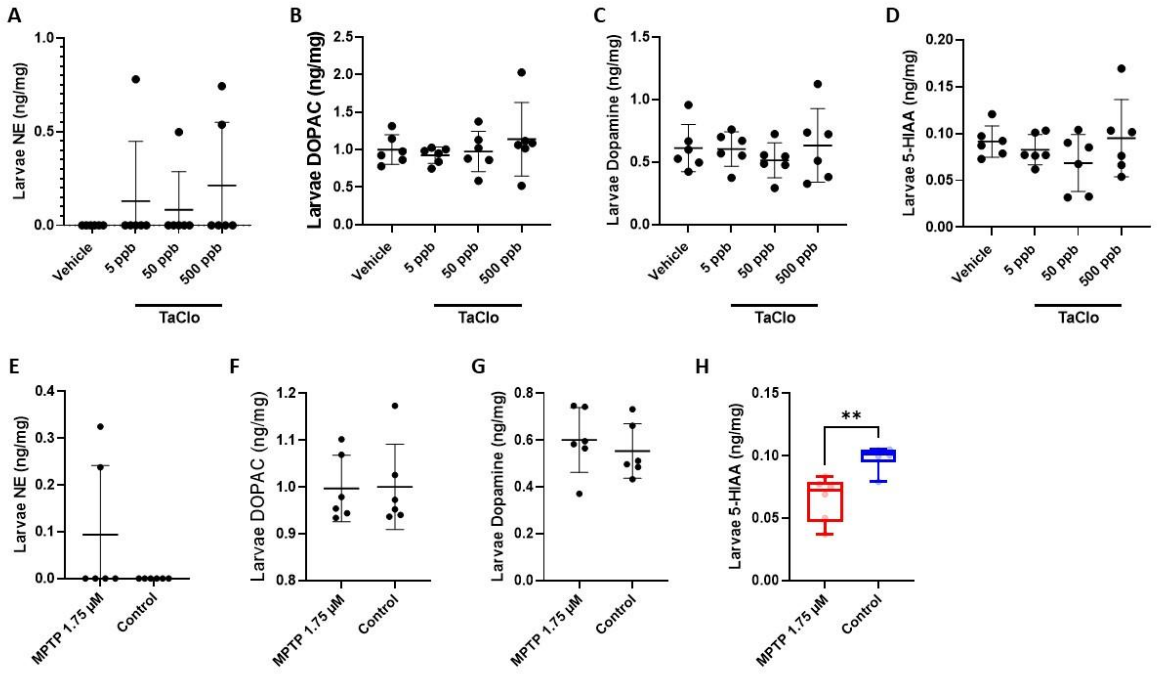


**Figure 3-14. Neurotransmitter levels in TaClo (vehicle, 0, 5, 50, 500 ppb) and 1.75 µM MPTP-treated 120 hpf larvae**

Norepinephrine, 3,4-Dihydroxyphenylacetic acid (DOPAC), dopamine, and 5-hydroxyindoleacetic acid (5-HIAA) levels were evaluated in the 120 hpf larval zebrafish. No significant differences of norepinephrine (A), DOPAC (B), dopamine (C), and 5-HIAA (D) in TaClo treated 120 hpf zebrafish. No significant differences of norepinephrine (E), DOPAC (F), and dopamine (G) in 1.75 µM MPTP treated 120 hpf zebrafish. Embryonic exposure to 1.75 µM MPTP resulted in significantly decreased 5-HIAA in the larvae (H) compared to the control group. Error bars represent standard deviation. ** significant difference from the control with $p \leq 0.01$. Data are expressed as mean ± standard deviation. All data were analyzed by one-way ANOVA test, followed by Tukey's post hoc test.

**Table 3-1. Commercially available antibodies labeling zebrafish proteins in this study**

| Primary antibody | Host | Antibody type | Antibody labeled | Dilution | Company/Catalog |
|---|---|---|---|---|---|
| Anti-mCherry antibody | Rabbit | Polyclonal IgG | cross-reacts with tdTomato and mOrange | 1:500 | Abcam/ab167453 |
| Caspase 3 | Rabbit | monoclonal IgG | active form caspase-3 | 1:500 | BD Pharmingen™/559565 |
| Glial Fibrillary Acidic Protein | Rabbit | Polyclonal | cytoskeleton in astrocytes | 1:500 | Agilent Dako/Z0334 |
| Tyrosine hydroxylase | Mouse | Monoclonal IgG1κ | catecholaminergic cells | 1:500 | Milipore sigma/MAB318 |
| Tyrosine hydroxylase | Rabbit | Polyclonal | catecholaminergic cells | 1:500 | Milipore sigma/AB152 |

| Secondary antibody | Host | Antibody type | Species Reactivity | Dilution | Company/Catalog |
|---|---|---|---|---|---|
| Alexa Fluor™ 488 | Goat | Polyclonal IgG (H+L) | Mouse | 1:500 | Thermofisher scientific/ # A-11029 |
| Alexa Fluor™ 488 | Goat | Polyclonal IgG (H+L) | Rabbit | 1:500 | Thermofisher scientific/ # A-11034 |
| Alexa Fluor™ 647 | Goat | Polyclonal IgG (H+L) | Rabbit | 1:500 | Thermofisher scientific/ # A-21244 |

**Table 3-2. List of primer pairs used for quantitative PCR reactions**

| Target genes | Gene target | Primer sequence (5'→3') | GeneBank (Accession number) | Reference |
|---|---|---|---|---|
| *slc6a3 (solute carrier family 6 member 3)/dat (dopamine transporter)* | dopaminergic neurons | Forward: CGTCACCAACGGTGGAATCTA<br>Reverse: TGCCGATGGCCTCAATTAGTA | NM_131755.1 | (Chen et al., 2012) |
| *th1* (*tyrosine hydroxylase 1*) | dopamine biosynthetic process | Forward: GACGGAAGATGATCGGAGACA<br>Reverse: CCGCCATGTTCCGATTTCT | NM_131149.1 | (Chen et al., 2012) |
| *th2* (*tyrosine hydroxylase 2*) | dopamine and serotonin biosynthetic process | Forward: CTCCAGAAGAGAATGCCACATG<br>Reverse: ACGTTCACTCTCCAGCTGAGTG | NM_001001829 | (Chen et al., 2012) |
| *bax (BCL2 associated X)* | apoptosis | Forward: AGTGTTTGCAGCAGATCGGAGATG<br>Reverse: TGACAAGGCGACAGGCAAAGTAGA | NM_131562.2 | (Ji et al., 2013) |
| *bcl2 (B-cell leukemia/lymphoma 2 protein)* | apoptosis | Forward: TCACTCGTTCAGACCCTCAT<br>Reverse: ACGCTTTCCACGCACAT | NM001030253 | (Di Paola et al., 2022) |
| *casp 3 (caspase 3)* | apoptosis | Forward: CCGCTGCCCATCACTA<br>Reverse: ATCCTTTCACGACCATCT | NM131877 | (Zhang et al., 2016) |
| *casp 9 (caspase 9)* | apoptosis | Forward: CTGAGGCAAGCCATAATCG<br>Reverse: AGAGGACATGGGAATAGCGT | NM_001007404.2 | (Zhang et al., 2016) |
| *gfap* (*glial fibrillary acidic protein*) | Astrocyte | Forward: GAAGCAGGAGGCCAATGACTATC<br>Reverse: GGACTCATTAGACCCACGGAGAG | NM_131373.2 | (Chen et al., 2020) |

| | | | | |
|---|---|---|---|---|
| *sod1/cu-sod* (*Cu superoxide dismutase*) | *superoxide dismutase* | Forward: CGCACTTCAACCCTCATGAC<br>Reverse: TGAATCACCATGGTCCTCCC | NM_131294.1 | (Al-Zahaby et al., 2023) |
| *sod2/mn-sod* (*manganese superoxide dismutase*) | *Mitochondrial superoxide dismutase* | Forward: CCGGACTATGTTAAGGCCATCT<br>Reverse: ACACTCGGTTGCTCTCTTTTCTCT | NM_199976 | (Alassaf et al., 2019) |
| *gpx* (*glutathione peroxidase*) | *glutathione peroxidase* | Forward: GGCACAACAGTCAGGGATTA<br>Reverse: CAGGACGGACGTATTTCAGA | NM_001007281.2 | (Saputra et al., 2024) |
| *cat (catalase)* | *catalase* | Forward: AGTTCCCTCTGATTCCTGTG<br>Reverse: ATGGCGATGTGTGTCTGG | NM_130912.2 | (Jaramillo et al., 2018) |
| *lrrk2* (*leucine-rich repeat kinase 2*) | Genes associated with PD | Forward: GGACCAGTCTAGACCGATGG<br>Reverse: CAAAATGTGTCCCGCTCTCG | NM_001201456.2 | (Ünal et al., 2023) |
| *DJ-1*/*park7* (*parkinson disease protein 7*) | Genes associated with PD | Forward: GGCCGGTAAAAGAGCGTTAG<br>Reverse: ACCCATGAGTCCTCCACTA | NM_001005938.1 | (Wang et al., 2017) |
| *sncaip* (*alpha interacting protein*) | Genes associated with PD | Forward: GACACGCATCCAGAAAACAAG<br>Reverse: GATCAGCTCCAGATTCTCCG | NM 001113636.2 | (Khalili et al., 2023) |
| *pink 1(PTEN-induced putative kinase 1*) | Genes associated with PD | Forward: GGCAATGAAGATGATGTGGAAC<br>Reverse: GGTCGGCAGGACATCAGGA | NM_001008628.1 | (Merhi et al., 2021) |
| *prkn* (*parkin RBR E3 ubiquitin protein ligase*) | Genes associated with PD | Forward: GAGGAGTTTCACGAGGGTCC<br>Reverse: TGAGTGGTTTTGGTGATGGTC | NM_001423707.1 | (Li et al., 2022) |
| *mpeg* (*macrophage-expressed gene*) | microglia | Forward: CCCACCAAGTGAAAGAGG<br>Reverse: GTGTTTGATTGTTTTCAATGG | NM_212737.1 | (Ferrero et al., 2021) |

| | | | | |
|---|---|---|---|---|
| *actb1*(*beta-actin*) | Housekeeping gene | Forward: ACCAACCTAAACCTCTCGAACA<br>Reverse: TCCTCCCCCTGTTAGACAACTA | NM_131031.2 | |

**Table 3-3. Relative dopaminergic neuronal cellular numbers in whole mount *in situ* hybridization and whole mount immunofluorescence assays at 5 days post-fertilization**

| | WISH<br>(mean ± standard deviation) | WIFA<br>(mean ± standard deviation) |
|---|---|---|
| Vehicle (0.001% DMSO) | 50.21±13.57 | 113.9±30.25 |
| Control | 45.58±10.76 | 107.4.6±32.26 |
| 5 ppb TaClo | 42.92±12.2 | 82±29.98 |
| 1.75 μM MPTP | 36.27±8.63 | 91.04±24.27 |

| | Dopaminergic neuronal percentage loss with hypoactivity | |
|---|---|---|
| | 5 ppb TaClo | 1.75 μM MPTP |
| Vehicle (0.001% DMSO) | 14.6% (WISH); 28.1% (WIFA) | 27.8% (WISH); 20.1% (WIFA) |
| Control | 25.1 (WIFA) | 20.5% (WISH); 18% (WIFA) |

WISH: whole mount *in situ* hybridization; WIFA: whole mount immunofluorescence assay

**References**


Ahkin Chin Tai, J. K., Horzmann, K. A., Franco, J., Jannasch, A. S., Cooper, B. R., & Freeman, J. L. (2021). Developmental atrazine exposure in zebrafish produces the same major metabolites as mammals along with altered behavioral outcomes. *Neurotoxicol Teratol*, *85*, 106971. https://doi.org/10.1016/j.ntt.2021.106971

Akundi, R. S., Hüll, M., Clement, H. W., & Fiebich, B. L. (2003). 1-trichloromethyl-1,2,3,4-tetrahydro-beta-carboline (TaClo) induces apoptosis in human neuroblastoma cell lines. *Ann N Y Acad Sci*, *1010*, 304-306. https://doi.org/10.1196/annals.1299.053

Al-Zahaby, S. A., Farag, M. R., Alagawany, M., Taha, H. S. A., Varoni, M. V., Crescenzo, G., & Mawed, S. A. (2023). Zinc Oxide Nanoparticles (ZnO-NPs) Induce Cytotoxicity in the Zebrafish Olfactory Organs via Activating Oxidative Stress and Apoptosis at the Ultrastructure and Genetic Levels. *Animals (Basel)*, *13*(18). https://doi.org/10.3390/ani13182867

Alassaf, M., Daykin, E. C., Mathiaparanam, J., & Wolman, M. A. (2019). Pregnancy-associated plasma protein-aa supports hair cell survival by regulating mitochondrial function. *Elife*, *8*. https://doi.org/10.7554/eLife.47061

AlShimemeri, S., Di Luca, D. G., & Fox, S. H. (2022). MPTP Parkinsonism and Implications for Understanding Parkinson's Disease. *Mov Disord Clin Pract*, *9*(1), 42-47. https://doi.org/10.1002/mdc3.13344

ATSDR. (2020). *Toxicological Profile for Trichloroethylene*. Public Health Service: Atalanta

Bajpai, P., Sangar, M. C., Singh, S., Tang, W., Bansal, S., Chowdhury, G., Cheng, Q., Fang, J. K., Martin, M. V., Guengerich, F. P., & Avadhani, N. G. (2013). Metabolism of 1-methyl-4-phenyl-1,2,3,6-tetrahydropyridine by mitochondrion-targeted cytochrome P450 2D6: implications in Parkinson disease. *J Biol Chem*, *288*(6), 4436-4451. https://doi.org/10.1074/jbc.M112.402123

Bashirzade, A. A. O., Cheresiz, S. V., Belova, A. S., Drobkov, A. V., Korotaeva, A. D., Azizi-Arani, S., Azimirad, A., Odle, E., Gild, E. V., Ardashov, O. V., Volcho, K. P., Bozhko, D. V., Myrov, V. O., Kolchanova, S. M., Polovian, A. I., Galumov, G. K., Salakhutdinov, N. F., Amstislavskaya, T. G., & Kalueff, A. V. (2022). MPTP-Treated Zebrafish Recapitulate 'Late-Stage' Parkinson's-like Cognitive Decline. *Toxics*, *10*(2). https://doi.org/10.3390/toxics10020069

Biechele-Speziale, D., Camarillo, M., Martin, N. R., Biechele-Speziale, J., Lein, P. J., & Plavicki, J. S. (2023). Assessing CaMPARI as new approach methodology for evaluating neurotoxicity. *Neurotoxicology*, *97*, 109-119. https://doi.org/10.1016/j.neuro.2023.05.013

Bringmann, G., God, R., Fähr, S., Feineis, D., Fornadi, K., & Fornadi, F. (1999). Identification of the dopaminergic neurotoxin 1-trichloromethyl-1,2, 3,4-tetrahydro-beta-carboline in human blood after intake of the hypnotic chloral hydrate. *Anal Biochem*, *270*(1), 167-175. https://doi.org/10.1006/abio.1999.4088

Bringmann, G., God, R., Feineis, D., Wesemann, W., Riederer, P., Rausch, W. D., Reichmann, H., & Sontag, K. H. (1995). The TaClo concept: 1-trichloromethyl-1,2,3,4-tetrahydro-beta-carboline (TaClo), a new toxin for dopaminergic neurons. *J Neural Transm Suppl*, *46*, 235-244.

Burks, M. L., & Bao, S. (2016). The 24-Hour Urinary 5-HIAA: A Simple Test With a Common Pitfall. *AACE Clinical Case Reports*, *2*(3), e186-e188. https://doi.org/https://doi.org/10.4158/EP15794CR

Bustin, S. A., Benes, V., Garson, J. A., Hellemans, J., Huggett, J., Kubista, M., Mueller, R., Nolan, T., Pfaffl, M. W., Shipley, G. L., Vandesompele, J., & Wittwer, C. T. (2009). The MIQE guidelines: minimum information for publication of quantitative real-time PCR experiments. *Clin Chem*, *55*(4), 611-622. https://doi.org/10.1373/clinchem.2008.112797

Calabrese, E. J. (2013). Biphasic dose responses in biology, toxicology and medicine: accounting for their generalizability and quantitative features. *Environ Pollut*, *182*, 452-460. https://doi.org/10.1016/j.envpol.2013.07.046

Carbaugh, C. M., Widder, M. W., Phillips, C. S., Jackson, D. A., DiVito, V. T., van der Schalie, W. H., & Glover, K. P. (2020). Assessment of zebrafish embryo photomotor response sensitivity and phase-specific patterns following acute- and long-duration exposure to neurotoxic chemicals and chemical weapon precursors. *J Appl Toxicol*, *40*(9), 1272-1283. https://doi.org/10.1002/jat.3984

Chen, J., Chen, Y., Zheng, Y., Zhao, J., Yu, H., Zhu, J., & Li, D. (2021). Protective Effects and Mechanisms of Procyanidins on Parkinson's Disease In Vivo and In Vitro. *Molecules*, *26*(18). https://doi.org/10.3390/molecules26185558

Chen, T. H., Wang, Y. H., & Wu, Y. H. (2011). Developmental exposures to ethanol or dimethylsulfoxide at low concentrations alter locomotor activity in larval zebrafish:

implications for behavioral toxicity bioassays. *Aquat Toxicol*, *102*(3-4), 162-166. https://doi.org/10.1016/j.aquatox.2011.01.010

Chen, Y. C., Baronio, D., Semenova, S., Abdurakhmanova, S., & Panula, P. (2020). Cerebral Dopamine Neurotrophic Factor Regulates Multiple Neuronal Subtypes and Behavior. *J Neurosci*, *40*(32), 6146-6164. https://doi.org/10.1523/jneurosci.2636-19.2020

Chen, Y. C., Sundvik, M., Rozov, S., Priyadarshini, M., & Panula, P. (2012). MANF regulates dopaminergic neuron development in larval zebrafish. *Developmental Biology*, *370*(2), 237-249. https://doi.org/10.1016/j.ydbio.2012.07.030

Chia, K., Klingseisen, A., Sieger, D., & Priller, J. (2022). Zebrafish as a model organism for neurodegenerative disease. *Front Mol Neurosci*, *15*, 940484. https://doi.org/10.3389/fnmol.2022.940484

Chiu, W. A., Jinot, J., Scott, C. S., Makris, S. L., Cooper, G. S., Dzubow, R. C., Bale, A. S., Evans, M. V., Guyton, K. Z., Keshava, N., Lipscomb, J. C., Barone, S., Jr., Fox, J. F., Gwinn, M. R., Schaum, J., & Caldwell, J. C. (2013). Human health effects of trichloroethylene: key findings and scientific issues. *Environ Health Perspect*, *121*(3), 303-311. https://doi.org/10.1289/ehp.1205879

Coral, J. A., Heaps, S., Glaholt, S. P., Karty, J. A., Jacobson, S. C., Shaw, J. R., & Bondesson, M. (2021). Arsenic exposure induces a bimodal toxicity response in zebrafish. *Environ Pollut*, *287*, 117637. https://doi.org/10.1016/j.envpol.2021.117637

Dankoski, E. C., Agster, K. L., Fox, M. E., Moy, S. S., & Wightman, R. M. (2014). Facilitation of serotonin signaling by SSRIs is attenuated by social isolation. *Neuropsychopharmacology*, *39*(13), 2928-2937. https://doi.org/10.1038/npp.2014.162

Dauer, W., & Przedborski, S. (2003). Parkinson's disease: mechanisms and models. *Neuron*, *39*(6), 889-909. https://doi.org/10.1016/s0896-6273(03)00568-3

de Abreu, M. S., Demin, K. A., Giacomini, A., Amstislavskaya, T. G., Strekalova, T., Maslov, G. O., Kositsin, Y., Petersen, E. V., & Kalueff, A. V. (2021). Understanding how stress responses and stress-related behaviors have evolved in zebrafish and mammals. *Neurobiol Stress*, *15*, 100405. https://doi.org/10.1016/j.ynstr.2021.100405

Di Paola, D., Capparucci, F., Lanteri, G., Crupi, R., Marino, Y., Franco, G. A., Cuzzocrea, S., Spanò, N., Gugliandolo, E., & Peritore, A. F. (2022). Environmental Toxicity

Assessment of Sodium Fluoride and Platinum-Derived Drugs Co-Exposure on Aquatic Organisms. *Toxics*, *10*(5). https://doi.org/10.3390/toxics10050272

Díaz-Casado, M. E., Lima, E., García, J. A., Doerrier, C., Aranda, P., Sayed, R. K., Guerra-Librero, A., Escames, G., López, L. C., & Acuña-Castroviejo, D. (2016). Melatonin rescues zebrafish embryos from the parkinsonian phenotype restoring the parkin/PINK1/DJ-1/MUL1 network. *J Pineal Res*, *61*(1), 96-107. https://doi.org/10.1111/jpi.12332

Dong, H., Mao, L., Bai, C., Ye, K., Wu, H., Lei, Y., Yu, S., Liu, Y., Tao, J., Pan, W., Xu, H., Lin, J., Zhu, J., & Dong, Q. (2022). Characterization of Developmental Neurobehavioral Toxicity in a Zebrafish MPTP-Induced Model: A Novel Mechanism Involving Anemia. *ACS Chemical Neuroscience*, *13*(13), 1877-1890. https://doi.org/10.1021/acschemneuro.2c00089

Dong, H., Wu, H., Bai, C., Ye, K., Mao, L., Lei, Y., Liu, Y., Xu, H., Lin, J., Zhu, J., & Dong, Q. (2022). Transient MPTP exposure at a sensitive developmental window altered gut microbiome and led to male-biased motor and social behavioral deficits in adult zebrafish. *Neurotoxicology*, *91*, 360-368. https://doi.org/10.1016/j.neuro.2022.06.008

Dorsey, E. R., Zafar, M., Lettenberger, S. E., Pawlik, M. E., Kinel, D., Frissen, M., Schneider, R. B., Kieburtz, K., Tanner, C. M., De Miranda, B. R., Goldman, S. M., & Bloem, B. R. (2023). Trichloroethylene: An Invisible Cause of Parkinson's Disease? *J Parkinsons Dis*, *13*(2), 203-218. https://doi.org/10.3233/jpd-225047

Du, Y., Guo, Q., Shan, M., Wu, Y., Huang, S., Zhao, H., Hong, H., Yang, M., Yang, X., Ren, L., Peng, J., Sun, J., Zhou, H., Li, S., & Su, B. (2016). Spatial and Temporal Distribution of Dopaminergic Neurons during Development in Zebrafish. *Front Neuroanat*, *10*, 115. https://doi.org/10.3389/fnana.2016.00115

Ferrero, G., Miserocchi, M., Di Ruggiero, E., & Wittamer, V. (2021). A csf1rb mutation uncouples two waves of microglia development in zebrafish. *Development*, *148*(1). https://doi.org/10.1242/dev.194241

Filippi, A., Mahler, J., Schweitzer, J., & Driever, W. (2010). Expression of the paralogous tyrosine hydroxylase encoding genes th1 and th2 reveals the full complement of dopaminergic and noradrenergic neurons in zebrafish larval and juvenile brain. *J Comp Neurol*, *518*(4), 423-438. https://doi.org/10.1002/cne.22213

Fukuda, H., Hara, K., Nakamura, S., Kimura, H., & Kameyama, M. (1988). 1-Methyl-4-phenyl-1,2,3,6-tetrahydropyridine (MPTP) enhances tryptophan hydroxylase activity in mouse striatum, but not in the frontal cortex. *Brain Res*, *449*(1-2), 399-402. https://doi.org/10.1016/0006-8993(88)91063-3

Gash, D. M., Rutland, K., Hudson, N. L., Sullivan, P. G., Bing, G., Cass, W. A., Pandya, J. D., Liu, M., Choi, D. Y., Hunter, R. L., Gerhardt, G. A., Smith, C. D., Slevin, J. T., & Prince, T. S. (2008). Trichloroethylene: Parkinsonism and complex 1 mitochondrial neurotoxicity. *Ann Neurol*, *63*(2), 184-192. https://doi.org/10.1002/ana.21288

Goldman, S. M., Quinlan, P. J., Ross, G. W., Marras, C., Meng, C., Bhudhikanok, G. S., Comyns, K., Korell, M., Chade, A. R., Kasten, M., Priestley, B., Chou, K. L., Fernandez, H. H., Cambi, F., Langston, J. W., & Tanner, C. M. (2012). Solvent exposures and Parkinson disease risk in twins. *Ann Neurol*, *71*(6), 776-784. https://doi.org/10.1002/ana.22629

Guo, S., Brush, J., Teraoka, H., Goddard, A., Wilson, S. W., Mullins, M. C., & Rosenthal, A. (1999). Development of noradrenergic neurons in the zebrafish hindbrain requires BMP, FGF8, and the homeodomain protein soulless/Phox2a. *Neuron*, *24*(3), 555-566. https://doi.org/10.1016/s0896-6273(00)81112-5

Hedge, J. M., Hunter, D. L., Sanders, E., Jarema, K. A., Olin, J. K., Britton, K. N., Lowery, M., Knapp, B. R., Padilla, S., & Hill, B. N. (2023). Influence of Methylene Blue or Dimethyl Sulfoxide on Larval Zebrafish Development and Behavior. *Zebrafish*, *20*(4), 132-145. https://doi.org/10.1089/zeb.2023.0017

Holzschuh, J., Ryu, S., Aberger, F., & Driever, W. (2001). Dopamine transporter expression distinguishes dopaminergic neurons from other catecholaminergic neurons in the developing zebrafish embryo. *Mech Dev*, *101*(1-2), 237-243. https://doi.org/10.1016/s0925-4773(01)00287-8

Horzmann, K. A., & Freeman, J. L. (2016). Zebrafish Get Connected: Investigating Neurotransmission Targets and Alterations in Chemical Toxicity. *Toxics*, *4*(3). https://doi.org/10.3390/toxics4030019

Horzmann, K. A., Portales, A. M., Batcho, K. G., & Freeman, J. L. (2020). Developmental toxicity of trichloroethylene in zebrafish (Danio rerio). *Environ Sci Process Impacts*, *22*(3), 728-739. https://doi.org/10.1039/c9em00565j

Hoyberghs, J., Bars, C., Ayuso, M., Van Ginneken, C., Foubert, K., & Van Cruchten, S. (2021). DMSO Concentrations up to 1% are Safe to be Used in the Zebrafish Embryo Developmental Toxicity Assay. *Front Toxicol*, *3*, 804033. https://doi.org/10.3389/ftox.2021.804033

Huang, D., Xu, J., Wang, J., Tong, J., Bai, X., Li, H., Wang, Z., Huang, Y., Wu, Y., Yu, M., & Huang, F. (2017). Dynamic Changes in the Nigrostriatal Pathway in the MPTP Mouse Model of Parkinson's Disease. *Parkinsons Dis*, *2017*, 9349487. https://doi.org/10.1155/2017/9349487

Huang, Y., Jiang, B., Xia, Y., Wang, J., Ji, C., Tong, J., Chen, T., & Jiang, Y. (2020). Downregulation of miR-133a contributes to the cardiac developmental toxicity of trichloroethylene in zebrafish. *Chemosphere*, *251*, 126610. https://doi.org/10.1016/j.chemosphere.2020.126610

Hung, H. C., & Lee, E. H. (1998). MPTP produces differential oxidative stress and antioxidative responses in the nigrostriatal and mesolimbic dopaminergic pathways. *Free Radic Biol Med*, *24*(1), 76-84. https://doi.org/10.1016/s0891-5849(97)00206-2

Ilin, V. A., Bai, Q., Watson, A. M., Volgushev, M., & Burton, E. A. (2021). Mechanism of Pacemaker Activity in Zebrafish DC2/4 Dopaminergic Neurons. *J Neurosci*, *41*(18), 4141-4157. https://doi.org/10.1523/jneurosci.2124-20.2021

Jagmag, S. A., Tripathi, N., Shukla, S. D., Maiti, S., & Khurana, S. (2015). Evaluation of Models of Parkinson's Disease. *Front Neurosci*, *9*, 503. https://doi.org/10.3389/fnins.2015.00503

Jaramillo, M. L., Pereira, A. G., Davico, C. E., Nezzi, L., Ammar, D., Müller, Y. M. R., & Nazari, E. M. (2018). Evaluation of reference genes for reverse transcription-quantitative PCR assays in organs of zebrafish exposed to glyphosate-based herbicide, Roundup. *Animal*, *12*(7), 1424-1434. https://doi.org/10.1017/s1751731117003111

Ji, W., Liang, H., Zhou, W., & Zhang, X. (2013). Apoptotic responses of zebrafish (Danio rerio) after exposure with microcystin-LR under different ambient temperatures. *J Appl Toxicol*, *33*(8), 799-806. https://doi.org/10.1002/jat.2735

Kalyn, M., Hua, K., Mohd Noor, S., Wong, C. E. D., & Ekker, M. (2019). Comprehensive Analysis of Neurotoxin-Induced Ablation of Dopaminergic Neurons in Zebrafish Larvae. *Biomedicines*, *8*(1). https://doi.org/10.3390/biomedicines8010001

Keane, P. (2013). *The Mechanism of Trichloroethylene Neurotoxicity and its Relation to Parkinsonism* Newcastle University].

Keane, P. C., Hanson, P. S., Patterson, L., Blain, P. G., Hepplewhite, P., Khundakar, A. A., Judge, S. J., Kahle, P. J., LeBeau, F. E. N., & Morris, C. M. (2019). Trichloroethylene and its metabolite TaClo lead to degeneration of substantia nigra dopaminergic neurones: Effects in wild type and human A30P mutant α-synuclein mice. *Neurosci Lett*, *711*, 134437. https://doi.org/10.1016/j.neulet.2019.134437

Khalili, A., Safarian, N., van Wijngaarden, E., Zoidl, G. S., Zoidl, G. R., & Rezai, P. (2023). Loss of Panx1 function in zebrafish alters motor behavior in a lab-on-chip model of Parkinson's disease. *J Neurosci Res*, *101*(12), 1814-1825. https://doi.org/10.1002/jnr.25241

Kohutnicka, M., Lewandowska, E., Kurkowska-Jastrzębska, I., Członkowski, A., & Członkowska, A. (1998). Microglial and astrocytic involvement in a murine model of Parkinson's disease induced by 1-methyl-4-phenyl-1,2,3,6-tetrahydropyridine (MPTP). *Immunopharmacology*, *39*(3), 167-180. https://doi.org/https://doi.org/10.1016/S0162-3109(98)00022-8

Kokel, D., Dunn, T. W., Ahrens, M. B., Alshut, R., Cheung, C. Y., Saint-Amant, L., Bruni, G., Mateus, R., van Ham, T. J., Shiraki, T., Fukada, Y., Kojima, D., Yeh, J. R., Mikut, R., von Lintig, J., Engert, F., & Peterson, R. T. (2013). Identification of nonvisual photomotor response cells in the vertebrate hindbrain. *J Neurosci*, *33*(9), 3834-3843. https://doi.org/10.1523/jneurosci.3689-12.2013

Kokel, D., & Peterson, R. T. (2011). Using the zebrafish photomotor response for psychotropic drug screening. *Methods Cell Biol*, *105*, 517-524. https://doi.org/10.1016/b978-0-12-381320-6.00022-9

Lal, P., & Kawakami, K. (2022). Integrated Behavioral, Genetic and Brain Circuit Visualization Methods to Unravel Functional Anatomy of Zebrafish Amygdala. *Front Neuroanat*, *16*, 837527. https://doi.org/10.3389/fnana.2022.837527

Lam, C. S., Korzh, V., & Strahle, U. (2005). Zebrafish embryos are susceptible to the dopaminergic neurotoxin MPTP. *Eur J Neurosci*, *21*(6), 1758-1762. https://doi.org/10.1111/j.1460-9568.2005.03988.x

Leary, S. L., Underwood, W. J., Anthony, R., Cartner, S. C., Corey, D., Grandin, T., Greenacre, C. B., Gwaltney-Bran, S., Mccrackin, M. A., Meyer, R. E., Miller, D. S., Shearer, J. K., & Yanong, R. P. E. (2013). AVMA Guidelines for the Euthanasia of Animals: 2013 Edition.

Lee, E., Hwang, I., Park, S., Hong, S., Hwang, B., Cho, Y., Son, J., & Yu, J. W. (2019). MPTP-driven NLRP3 inflammasome activation in microglia plays a central role in dopaminergic neurodegeneration. *Cell Death Differ*, *26*(2), 213-228. https://doi.org/10.1038/s41418-018-0124-5

Li, L., Chen, M., Liu, W., Tai, P., Liu, X., & Liu, J. X. (2022). Zebrafish cox17 modulates primitive erythropoiesis via regulation of mitochondrial metabolism to facilitate hypoxia tolerance. *Faseb j*, *36*(11), e22596. https://doi.org/10.1096/fj.202200829R

Liu, M., Choi, D. Y., Hunter, R. L., Pandya, J. D., Cass, W. A., Sullivan, P. G., Kim, H. C., Gash, D. M., & Bing, G. (2010). Trichloroethylene induces dopaminergic neurodegeneration in Fisher 344 rats. *J Neurochem*, *112*(3), 773-783. https://doi.org/10.1111/j.1471-4159.2009.06497.x

Liu, M., Shin, E. J., Dang, D. K., Jin, C. H., Lee, P. H., Jeong, J. H., Park, S. J., Kim, Y. S., Xing, B., Xin, T., Bing, G., & Kim, H. C. (2018). Trichloroethylene and Parkinson's Disease: Risk Assessment. *Mol Neurobiol*, *55*(7), 6201-6214. https://doi.org/10.1007/s12035-017-0830-x

Livak, K. J., & Schmittgen, T. D. (2001). Analysis of relative gene expression data using real-time quantitative PCR and the 2(-Delta Delta C(T)) Method. *Methods*, *25*(4), 402-408. https://doi.org/10.1006/meth.2001.1262

Mahabir, S., Chatterjee, D., & Gerlai, R. (2014). Strain dependent neurochemical changes induced by embryonic alcohol exposure in zebrafish. *Neurotoxicol Teratol*, *41*, 1-7. https://doi.org/10.1016/j.ntt.2013.11.001

Maiti, P., Gregg, L. C., & McDonald, M. P. (2016). MPTP-induced executive dysfunction is associated with altered prefrontal serotonergic function. *Behav Brain Res*, *298*(Pt B), 192-201. https://doi.org/10.1016/j.bbr.2015.09.014

Matsui, H., & Sugie, A. (2017). An optimized method for counting dopaminergic neurons in zebrafish. *PLoS One*, *12*(9), e0184363. https://doi.org/10.1371/journal.pone.0184363

McKinley, E. T., Baranowski, T. C., Blavo, D. O., Cato, C., Doan, T. N., & Rubinstein, A. L. (2005). Neuroprotection of MPTP-induced toxicity in zebrafish dopaminergic neurons. *Brain Res Mol Brain Res*, *141*(2), 128-137. https://doi.org/10.1016/j.molbrainres.2005.08.014

Meredith, G. E., & Rademacher, D. J. (2011). MPTP mouse models of Parkinson's disease: an update. *J Parkinsons Dis*, *1*(1), 19-33. https://doi.org/10.3233/jpd-2011-11023

Merhi, R., Kalyn, M., Zhu-Pawlowsky, A., & Ekker, M. (2021). Loss of parla Function Results in Inactivity, Olfactory Impairment, and Dopamine Neuron Loss in Zebrafish. *Biomedicines*, *9*(2). https://doi.org/10.3390/biomedicines9020205

Mugoni, V., Camporeale, A., & Santoro, M. M. (2014). Analysis of oxidative stress in zebrafish embryos. *J Vis Exp*(89). https://doi.org/10.3791/51328

Omar, N. A., Kumar, J., & Teoh, S. L. (2023). Parkinson's disease model in zebrafish using intraperitoneal MPTP injection. *Front Neurosci*, *17*, 1236049. https://doi.org/10.3389/fnins.2023.1236049

Ortmann, J., Altenburger, R., Scholz, S., & Luckenbach, T. (2022). Photomotor response data analysis approach to assess chemical neurotoxicity with the zebrafish embryo. *Altex*, *39*(1), 82-94. https://doi.org/10.14573/altex.2004021

Peterson, S. M., & Freeman, J. L. (2009). RNA isolation from embryonic zebrafish and cDNA synthesis for gene expression analysis. *J Vis Exp*(30). https://doi.org/10.3791/1470

Pompermaier, A., Tamagno, W. A., Alves, C., & Barcellos, L. J. G. (2022). Persistent and transgenerational effects of pesticide residues in zebrafish. *Comparative Biochemistry and Physiology Part C: Toxicology & Pharmacology*, *262*, 109461. https://doi.org/https://doi.org/10.1016/j.cbpc.2022.109461

Qin, F., Zhang, M., Wang, P., Dai, Z., Li, X., Li, D., Jing, L., Qi, C., Fan, H., Qin, M., Li, Y., Huang, L., & Wang, T. (2024). Transcriptome analysis reveals the anti-Parkinson's activity of Mangiferin in zebrafish. *Biomedicine & Pharmacotherapy*, *179*, 117387. https://doi.org/https://doi.org/10.1016/j.biopha.2024.117387

Rausch, W. D., Abdel-mohsen, M., Koutsilieri, E., Chan, W. W., & Bringmann, G. (1995). Studies of the potentially endogenous toxin TaClo (1-trichloromethyl-1,2,3,4-tetrahydro-beta-carboline) in neuronal and glial cell cultures. *J Neural Transm Suppl*, *46*, 255-263.

Razali, K., Kumar, J., & Mohamed, W. M. Y. (2024). Characterizing the adult zebrafish model of Parkinson's disease: a systematic review of dynamic changes in behavior and physiology post-MPTP administration. *Front Neurosci*, *18*, 1432102. https://doi.org/10.3389/fnins.2024.1432102

Reif, D. M., Truong, L., Mandrell, D., Marvel, S., Zhang, G., & Tanguay, R. L. (2016). High-throughput characterization of chemical-associated embryonic behavioral changes predicts teratogenic outcomes. *Arch Toxicol*, *90*(6), 1459-1470. https://doi.org/10.1007/s00204-015-1554-1

Ren, Q., Jiang, X., Zhang, S., Gao, X., Paudel, Y. N., Zhang, P., Wang, R., Liu, K., & Jin, M. (2022). Neuroprotective effect of YIAEDAER peptide against Parkinson's disease like pathology in zebrafish. *Biomed Pharmacother*, *147*, 112629. https://doi.org/10.1016/j.biopha.2022.112629

Rink, E., & Wullimann, M. F. (2002). Development of the catecholaminergic system in the early zebrafish brain: an immunohistochemical study. *Brain Res Dev Brain Res*, *137*(1), 89-100. https://doi.org/10.1016/s0165-3806(02)00354-1

Sackerman, J., Donegan, J. J., Cunningham, C. S., Nguyen, N. N., Lawless, K., Long, A., Benno, R. H., & Gould, G. G. (2010). Zebrafish Behavior in Novel Environments: Effects of Acute Exposure to Anxiolytic Compounds and Choice of Danio rerio Line. *Int J Comp Psychol*, *23*(1), 43-61. https://pmc.ncbi.nlm.nih.gov/articles/PMC2879659/pdf/nihms195915.pdf

Sáez-Espinosa, P., Franco-Esclapez, C., Robles-Gómez, L., Silva, W., Romero, A., Immler, S., & Gómez-Torres, M. J. (2022). Morphological and ultrastructural alterations of zebrafish (Danio rerio) spermatozoa after motility activation. *Theriogenology*, *188*, 108-115. https://doi.org/10.1016/j.theriogenology.2022.05.025

Sallinen, V., Torkko, V., Sundvik, M., Reenilä, I., Khrustalyov, D., Kaslin, J., & Panula, P. (2009). MPTP and MPP+ target specific aminergic cell populations in larval zebrafish. *J Neurochem*, *108*(3), 719-731. https://doi.org/10.1111/j.1471-4159.2008.05793.x

Saputra, F., Kishida, M., & Hu, S. Y. (2024). Oxidative stress induced by hydrogen peroxide disrupts zebrafish visual development by altering apoptosis, antioxidant and estrogen related genes. *Sci Rep*, *14*(1), 14454. https://doi.org/10.1038/s41598-024-64933-5

Schmidt, R., Strähle, U., & Scholpp, S. (2013). Neurogenesis in zebrafish - from embryo to adult. *Neural Dev*, *8*, 3. https://doi.org/10.1186/1749-8104-8-3

Sharma, R. K., Candelario-Jalil, E., Feineis, D., Bringmann, G., Fiebich, B. L., & Akundi, R. S. (2017). 1-Trichloromethyl-1,2,3,4-tetrahydro-beta-carboline (TaClo) Alters Cell Cycle Progression in Human Neuroblastoma Cell Lines. *Neurotox Res*, *32*(4), 649-660. https://doi.org/10.1007/s12640-017-9782-1

Smeyne, R. J., & Jackson-Lewis, V. (2005). The MPTP model of Parkinson's disease. *Molecular Brain Research*, *134*(1), 57-66. https://doi.org/https://doi.org/10.1016/j.molbrainres.2004.09.017

Soman, S. K., Bazała, M., Keatinge, M., Bandmann, O., & Kuznicki, J. (2019). Restriction of mitochondrial calcium overload by mcu inactivation renders a neuroprotective effect in zebrafish models of Parkinson's disease. *Biol Open*, *8*(10). https://doi.org/10.1242/bio.044347

Sriram, K., Pai, K. S., Boyd, M. R., & Ravindranath, V. (1997). Evidence for generation of oxidative stress in brain by MPTP: in vitro and in vivo studies in mice. *Brain Res*, *749*(1), 44-52. https://doi.org/10.1016/s0006-8993(96)01271-1

Tay, T. L., Ronneberger, O., Ryu, S., Nitschke, R., & Driever, W. (2011). Comprehensive catecholaminergic projectome analysis reveals single-neuron integration of zebrafish ascending and descending dopaminergic systems. *Nat Commun*, *2*, 171. https://doi.org/10.1038/ncomms1171

Thisse, C., & Thisse, B. (2008). High-resolution in situ hybridization to whole-mount zebrafish embryos. *Nat Protoc*, *3*(1), 59-69. https://doi.org/10.1038/nprot.2007.514

Ünal, İ., Cansız, D., Sürmen, M. G., Sürmen, S., Sezer, Z., Beler, M., Üstündağ Ü, V., Güzel, E., Alturfan, A. A., & Emekli-Alturfan, E. (2023). Identification of molecular network of gut-brain axis associated with neuroprotective effects of PPARδ-ligand erucic acid in rotenone-induced Parkinson's disease model in zebrafish. *Eur J Neurosci*, *57*(4), 585-606. https://doi.org/10.1111/ejn.15904

Verma, R., Raj Choudhary, P., Kumar Nirmal, N., Syed, F., & Verma, R. (2022). Neurotransmitter systems in zebrafish model as a target for neurobehavioural studies. *Materials Today: Proceedings*, *69*, 1565-1580. https://doi.org/https://doi.org/10.1016/j.matpr.2022.07.147

Wang, Y., Liu, W., Yang, J., Wang, F., Sima, Y., Zhong, Z. M., Wang, H., Hu, L. F., & Liu, C. F. (2017). Parkinson's disease-like motor and non-motor symptoms in rotenone-treated zebrafish. *Neurotoxicology*, *58*, 103-109. https://doi.org/10.1016/j.neuro.2016.11.006

Wasel, O., & Freeman, J. L. (2020). Chemical and Genetic Zebrafish Models to Define Mechanisms of and Treatments for Dopaminergic Neurodegeneration. *Int J Mol Sci*, *21*(17). https://doi.org/10.3390/ijms21175981

Wen, L., Wei, W., Gu, W., Huang, P., Ren, X., Zhang, Z., Zhu, Z., Lin, S., & Zhang, B. (2008). Visualization of monoaminergic neurons and neurotoxicity of MPTP in live transgenic zebrafish. *Dev Biol*, *314*(1), 84-92. https://doi.org/10.1016/j.ydbio.2007.11.012

Wu, C., & Schaum, J. (2000). Exposure assessment of trichloroethylene. *Environ Health Perspect*, *108 Suppl 2*(Suppl 2), 359-363. https://doi.org/10.1289/ehp.00108s2359

Wu, Z., Man, Q., Niu, H., Lyu, H., Song, H., Li, R., Ren, G., Zhu, F., Peng, C., Li, B., & Ma, X. (2022). Recent advances and trends of trichloroethylene biodegradation: A critical review. *Front Microbiol*, *13*, 1053169. https://doi.org/10.3389/fmicb.2022.1053169

Xi, Y., Yu, M., Godoy, R., Hatch, G., Poitras, L., & Ekker, M. (2011). Transgenic zebrafish expressing green fluorescent protein in dopaminergic neurons of the ventral diencephalon. *Dev Dyn*, *240*(11), 2539-2547. https://doi.org/10.1002/dvdy.22742

Yang, R., Ye, S., Zhang, S., Huang, H., Zhang, Y., Yang, Y., Xie, S., He, L., Yang, Y., & Shi, J. (2023). Serotonin and dopamine depletion in distinct brain regions may cause anxiety in 1-methyl-4-phenyl-1,2,3,6-tetrahydropyridine-treated mice as a model of early Parkinson's disease. *Neuroreport*, *34*(11), 551-559. https://doi.org/10.1097/wnr.0000000000001922

Yang, Y., Pang, B., Liu, Z., Li, J., Zhang, Z., Zhang, R., Hou, X., Guo, H., Chi, L., Pang, Q., & Xin, T. (2019). 1-Trichloromethyl-1,2,3,4-tetrahydro-beta-carboline (TaClo) Induces the Apoptosis of Dopaminergic Neurons via Oxidative Stress and Neuroinflammation. *Oxid Med Cell Longev*, *2019*, 1292891. https://doi.org/10.1155/2019/1292891

Yao, C. H., Wang, L., Stancliffe, E., Sindelar, M., Cho, K., Yin, W., Wang, Y., & Patti, G. J. (2020). Dose-Response Metabolomics To Understand Biochemical Mechanisms and Off-Target Drug Effects with the TOXcms Software. *Anal Chem*, *92*(2), 1856-1864. https://doi.org/10.1021/acs.analchem.9b03811

Yasuda, Y., Shimoda, T., Uno, K., Tateishi, N., Furuya, S., Yagi, K., Suzuki, K., & Fujita, S. (2008). The effects of MPTP on the activation of microglia/astrocytes and cytokine/chemokine levels in different mice strains. *Journal of Neuroimmunology*, *204*(1), 43-51. https://doi.org/https://doi.org/10.1016/j.jneuroim.2008.08.003

Yin, J. H., & Horzmann, K. A. (2024). Embryonic Zebrafish as a Model for Investigating the Interaction between Environmental Pollutants and Neurodegenerative Disorders. *Biomedicines*, *12*(7). https://doi.org/10.3390/biomedicines12071559

Zhang, J., Hao, H., Wu, X., Wang, Q., Chen, M., Feng, Z., & Chen, H. (2020). The functions of glutathione peroxidase in ROS homeostasis and fruiting body development in Hypsizygus marmoreus. *Appl Microbiol Biotechnol*, *104*(24), 10555-10570. https://doi.org/10.1007/s00253-020-10981-6

Zhang, J., Sun, B., Yang, J., Chen, Z., Li, Z., Zhang, N., Li, H., & Shen, L. (2022). Comparison of the effect of rotenone and 1-methyl-4-phenyl-1,2,3,6-tetrahydropyridine on inducing chronic Parkinson's disease in mouse models. *Mol Med Rep*, *25*(3). https://doi.org/10.3892/mmr.2022.12607

Zhang, Y., Liu, K., Hassan, H. M., Guo, H., Ding, P., Han, L., He, Q., Chen, W., Hsiao, C. D., Zhang, L., & Jiang, Z. (2016). Liver Fatty Acid Binding Protein Deficiency Provokes Oxidative Stress, Inflammation, and Apoptosis-Mediated Hepatotoxicity Induced by Pyrazinamide in Zebrafish Larvae. *Antimicrob Agents Chemother*, *60*(12), 7347-7356. https://doi.org/10.1128/aac.01693-16

# Chapter 4

# Early-life 1-Trichloromethyl-1,2,3,4-tetrahydro-beta-carboline (TaClo) and 1-Methyl-4-phenyl-1,2,3,6-tetrahydropyridine (MPTP) exposure induces long-term neurotoxicity in adult zebrafish (*Danio rerio*)


## Abstract

1-Trichloromethyl-1,2,3,4-tetrahydro-beta-carboline (TaClo), a metabolite of the industrial solvent trichloroethylene (TCE), has been implicated as a primary neurotoxicant in TCE-induced neurotoxicity and the development of Parkinson's disease. Previously, we demonstrated that TaClo induces MPTP-like neurotoxicity in larval zebrafish, characterized by neurobehavioral impairments, diencephalic neuronal loss, and altered neuroinflammatory and antioxidant enzymatic activity. However, the long-term effects of early-life exposure to TaClo and MPTP remain largely unexplored. To understand whether early-life exposure to TaClo and MPTP could result in long-lasting neurotoxicity in zebrafish models. We exposed embryonic zebrafish to TaClo (0, 5, 50, 500 ppb), vehicle (0.001% DMSO), or 1.75 μM MPTP from 0 to 5 days post-fertilization, then transferred to chemical-free aquaria and maintained until 6 months post-fertilization (mpf). We found that MPTP exposure led to reduced locomotion and increased female-biased anxiety-like behavior at 6 mpf. Additionally, both MPTP and TaClo (5 and 500 ppb) induced persistent and progressive diencephalic neurodegeneration. Furthermore, we identified imbalanced oxidative stress in the 6 mpf zebrafish brains following early-life exposure to MPTP and TaClo. Our findings demonstrate that transient early-life exposure to TaClo and MPTP results in long-lasting neurotoxicity. Finally, our work highlights the potential health risks associated with environmental TCE contamination.

## 1. Introduction

Trichloroethylene (TCE) is a volatile organic compound widely used in industrial and commercial processes (Chiu et al., 2013). Despite the U.S. Environmental Protection Agency (EPA) banning its use due to significant health risks, TCE remains a widespread environmental contaminant, persisting in groundwater and Superfund sites across the United States (Chiu et al., 2013; Dorsey et al., 2023). Occupational exposure to TCE has been linked to neurotoxicity and the development of Parkinson's disease (PD) (Gash et al., 2008; Keane et al., 2019). 1-Trichloromethyl-1,2,3,4-tetrahydro-β-carboline (TaClo), one of the TCE *in vivo* metabolites, has been implicated as a primary neurotoxicant contributing to TCE-induced neurotoxicity (Bringmann et al., 1999; Yang et al., 2019). Our previous work in Chapter 3 demonstrated that TaClo induced 1-methyl-4-phenyl-1,2,3,6-tetrahydropyridine (MPTP)-like neurotoxicity in larval zebrafish models. Specifically, we found that both TaClo and MPTP selectively targeted larval diencephalic dopaminergic neurons, triggered neuroinflammatory responses, and altered antioxidative enzymatic activities, with mechanisms that closely resemble those proposed in human PD.

Early life environmental exposure is a critical concern due to the potential long-lasting effects on an individual's health and development in the later life stages (Boekelheide et al., 2012; Maitre et al., 2021). Previous studies have demonstrated that embryonic exposure to environmental chemicals could result in long-term neurotoxicity in adult zebrafish (Gao et al., 2017; Glazer & Brennan, 2021; Moreira et al., 2024; Z. Wang et al., 2022). For example, exposure to Benzo[a]Pyrene from 1–96 hours post-fertilization (hpf) in zebrafish has been shown to reduce locomotor activity and neurotransmitter levels, induce dopaminergic neurodegeneration, and increase cell apoptosis in the adult zebrafish brain (Gao et al., 2017). Embryonic zebrafish exposed to environmental levels of lead from 2-120 hpf exhibited impaired neurodevelopment, neurobehavioral disorders, alterations in the neurotransmitter system, and reduced neuronal density in the midbrain optic tectum, persisting through larval to adult life stages (Z. Wang et al., 2022). Exposure to environmentally relevant concentrations of Benzophenone-3 from 6–96 hpf altered antioxidative enzymatic and neurotransmission responses in larval zebrafish, with these changes persisting into adulthood, along with increased

anxiety-like behavior and reduced social behavior (Moreira et al., 2024). Early-life exposure to low concentrations of 5-96 hpf methylmercury exposure resulted in long-term behavioral alterations, including increased anxiety and impaired locomotor activity. Additionally, it disrupted the expression of neural stress-response genes associated with the hypothalamus-pituitary-interrenal axis and the dopaminergic system (Glazer & Brennan, 2021).

Despite many studies that have demonstrated the long-lasting neurotoxicity of early-life environmental exposure in zebrafish models, research on TaClo and MPTP remains limited. This is concerning, as our previous work in Chapter 3 has shown that TaClo at 5 ppb (comparable to EPA-regulated TCE exposure levels in drinking water) and low concentration of MPTP (1.75 μM) induced neurotoxicity in zebrafish larvae. Therefore, to investigate whether early-life exposure to TaClo and MPTP could result in persistent neurotoxicity into adulthood, we expanded on our previous work to advance our understanding of the long-term effects of these chemicals in zebrafish models. We observed neurotoxicity that included locomotor deficits, altered anxiety behaviors, and irreversible, progressive diencephalic neurodegeneration in adult zebrafish. Additionally, we identified underlying mechanisms similar to those observed at the larval stage. Our study highlights the long-term neurotoxic risks of early-life exposure to TaClo and MPTP and underscores the potential health risks of environmental TCE contamination.

## 2. Materials and methods

### *2.1 Ethics statement*

This study was approved by the Institutional Animal Care and Use Committee at Auburn University (protocol numbers: 2021-3912, 2022-4087, and 2024-5380) and conducted in compliance with the National Institutes of Health Guide for the Care and Use of Laboratory Animals. Euthanasia was performed using buffered Tricaine-S (ethyl m-amino benzoate methanesulfonate; Western Chemical Inc., Ferndale, WA) at a concentration of 0.4 mg/mL or an ice bath, according to the experimental requirements (Leary et al., 2013).

*2.2 Chemicals*

A 50 mM (8,662,500 ppb, molar mass: 173.25 g/mol) MPTP stock solution was prepared by dissolving 1-methyl-4-phenyl-1,2,3,6-tetrahydropyridine (MPTP) (99.94%, CAS#: 23007-85-4, Selleck Chemicals, USA) in distilled water and stored at -20°c until use. 1.75 µM MPTP (303.1875 ppb, molar mass: 173.25 g/mol) working solution was freshly prepared by diluting the stock solution in aquaria water prior to the experiment. Aquaria water was made using reverse osmosis-filtered water supplemented with sea salt (Aquaneering Inc., San Diego, CA, USA) to achieve a conductivity of 500–600 µS and a pH of 7.0–7.5, and it served as a negative control in all experiments. The 100,000,000 ppb stock solution of 1-trichloromethyl-1,2,3,4-tetrahydro-beta-carboline (TaClo) (CAS#: 6649-90-7, Exclusive Chemistry, San Diego, CA, USA) was freshly prepared by dissolving it in dimethylsulfoxide (DMSO) (CAS#: 67-68-5, VWR®, USA). The working solution of TaClo was subsequently diluted from the stock solution in aquaria water to obtain a final vehicle concentration of 0.001% DMSO.

*2.3 Zebrafish husbandry and chemical exposure*

Adult-specific, pathogen-free wild-type AB strain zebrafish (Danio rerio) were obtained from the Sinnhuber Aquatic Research Laboratory at Oregon State University (Corvallis, OR, USA). The purchased zebrafish were housed in a ZS660 Stand Alone system (Auburn University; Aquaneering Inc., San Diego, CA, USA) under a controlled 14-hour light/10-hour dark photoperiod. Water parameters were consistently maintained at 26–28°C, with a pH of 7.3–7.5 and conductivity between 550–650 µS/cm. Adult zebrafish were monitored twice daily and fed a combination of Golden Pearls 500–800 mm (Artemia International LLC., Fairview, TX, USA), Zeigler adult zebrafish food (Zeigler Bros Inc., Gardners, PA, USA), and live brine shrimp (Artemia International LLC.). Sample size selection for each assay was guided by prior research involving similar toxicological (Horzmann et al., 2022), behavioral (Horzmann et al., 2022), enzymatic (Tamagno et al., 2022), imaging studies (Vijayanathan et al., 2022), neurotransmitter detection (Wirbisky et al., 2014), and genetic expression (S. Wang et al., 2022) and was calculated using Minitab 18 software (Minitab LLC., State College, PA, USA). Neurobehavioral tests were assessed in eight biological replicates, with 10 zebrafish per treatment per sex per replicate. Three biological replicates, each containing 6 zebrafish brains,

were used for double immunofluorescence assay, flow cytometric analysis, antioxidative enzymatic activity, and gene expression. A schematic diagram overview of the chemical exposure and experimental regime is presented in **Figure 4-1.**

*2.4 Neurotoxicity endpoints*

*2.4.1 Neurobehavioral tests*

The novel tank test and open field test were conducted following previously established protocols with minor modifications (Fontana et al., 2020; Horzmann et al., 2021). Both tests were performed between 9:00 AM and 6:00 PM Central Standard Time (CST, USA) on 6-month-old zebrafish that had undergone early-life exposure (1–120 hpf) to 1.75 μM MPTP, vehicle (0.001% DMSO), or TaClo (0, 5, 50, and 500 ppb). To minimize the influence of sex differences on locomotor activity and anxiety levels, female and male zebrafish from each treatment group were tested separately (Philpott et al., 2012). Before testing, zebrafish were acclimated for 10 minutes in a 1-L transparent polycarbonate holding tank (22.38 × 11.11 cm, 8.41 cm water depth, ZHCT100, Aquaneering Inc., San Diego, CA, USA) filled with aquaria water to a depth of 8 cm. The holding tank was maintained in a water bath at 28°C throughout the test period. Neurobehavioral testing began with the novel tank test, followed by the open field test. After the novel tank test, zebrafish were returned to the holding tank for a recovery period of 80–160 minutes before the next test. All behavioral recordings were captured using a digital camera (Basler acA1300-60gm GigE camera, Japan) and analyzed with EthoVision XT 14 video tracking and analysis software (Noldus Information Technology BV, Wageningen, the Netherlands).

*2.4.1.2 Novel tank test*

In brief, individual fish were placed into a 1.8-L clear polycarbonate testing tank (7.46 x 33.49 cm, 15.24 water depth, ZT180, Aquaneering Inc., San Diego, CA, USA) filled with aquaria water to a depth of 12 cm. The testing tank was divided into an upper zone and a bottom zone at the midpoint of the aquaria water level. The camera was positioned horizontally to capture the testing arena. Zebrafish were transferred from the holding tank to the testing tank using a net, and the movement was immediately recorded for a 10-min period. Parameters used

to assess locomotor activity and anxiety levels included distance moved, velocity, mobility, time spent moving, time spent in the upper and bottom zones, frequency of zone entries, and latency to enter the upper or bottom zones.

*2.4.1.2 Open field test*

Briefly, individual fish were placed into a 35-cm-diameter, white ceramic, circular arena with a wall height of 6 cm, filled with aquaria water to a depth of 2 cm. The arena was divided into outer and inner zones with a camera positioned above the testing arena and oriented downward to record the fish's movements. Zebrafish were transferred from the holding tank to the testing tank using a net and the video was immediately recorded after the fish was detected. Each fish's movement was tracked for a 10-minute period. Parameters used to assess locomotor activity and anxiety levels included distance moved, velocity, mobility, time spent moving, time spent in the outer and inner zones, frequency of zone entries, and latency to enter the inner and outer zones.

*2.5 Double immunofluorescence assay (IFA)*

Zebrafish at 6 mpf that had underwent early-life exposure to 1-120 hpf MPTP (1.75 μM), vehicle (0.001% DMSO), or TaClo (0, 5, 50, and 500 ppb) were euthanized by immersing in aquaria water containing 0.4% Tricane, followed by decapitation. Heads with brains were fixed in 4% paraformaldehyde (PFA) at 4°C overnight. Subsequently, brains were dissected out and post-fixed in 4% PFA for an additional 20 min at room temperature, followed by three washes in PBST (PBS + 0.3% Tween 20). Brain specimens were cryosectioned at 10 μm sagittal thickness using a cryostat (Microm HM550, Thermo Scientific, USA), with sections collected on charged slides (RANKIN, USA) and stored at −80°C until staining. Before staining, sections were thawed, rehydrated in PBST, and subjected to antigen retrieval using Diva or Reveal Decloaker (Biocare Medical, USA) at 80°C for 30 minutes in a Decloaking Chamber™ NxGen (Biocare Medical, USA). Following PBST washes, sections were blocked for at least 1 hour at room temperature. To evaluate protein expression in the brain, we selected tyrosine hydroxylase as a marker for dopaminergic neurons, caspase-3 as a marker for apoptosis, lymphocyte cytosolic protein 1 (L-plastin) as a marker for macrophages, and glial fibrillary acidic protein (GFAP) as a

marker for astrocytes. The pretreated sections were incubated overnight at 4°C with a primary antibody against tyrosine hydroxylase (Millipore Sigma, #MAB318) and L-plastin (GeneTex, Cat No.GTX124420) or anti-caspase 3 (BD Pharmingen™, #559565), or glial fibrillary acidic protein (Agilent Dako, #Z0334). The following day, tissue specimens were washed in PBST and co-incubated with Alexa Fluor™ 488-conjugated secondary antibodies (Thermo Fisher Scientific, #A-11029) and Alexa Fluor™ 647 (Thermo Fisher Scientific, #A-21244) for 2 hours in dark at room temperature. After additional PBST washes, tissue specimens were mounted in an antifade mounting medium with DAPI (H-2000, VECTASHIELD®, Vector Laboratories) for imaging. Image acquisition was performed using a Keyence BZ-x810 fluorescence microscope at 20x magnification with a 1 µm interval within a 10 µm range (Keyence Corp., Osaka, Japan). Positive signals at the telencephalon, diencephalon, parvocellular preoptic nucleus, posterior tuberculum, paraventricular organ, posterior tuberal nucleus, caudal zone of periventricular hypothalamus, and rhombencephalon were analyzed using QuPath software (http://qupath.github.io). Detailed information on antibody specifications and dilutions is provided in **Table 4-1.**

*2.6 Flow cytometric analysis*

We selected flow cytometry to assess cellular and mitochondrial reactive oxygen species (ROS) levels as well as mitochondrial membrane potential in adult zebrafish brains. Brain samples were collected from 6-month-old zebrafish that had undergone early-life exposure to MPTP (1.75 µM), vehicle (0.001% DMSO), and TaClo (0, 5, 50, and 500 ppb) and were subjected to single-cell preparation prepared with Papain dissociation system (Worthington Biochemical). Single-cell suspension was incubated in the dark for 30 mins with the following probe dyes and concentrations: CellROX® Green Reagent (5 µM; Invitrogen™, CAS#: C10444), MitoSox™ Red (10 µM; Invitrogen™, CAS#: M36008), and MitoTracker™ Deep Red FM (1 µM; Invitrogen™, CAS#: M22426). LIVE/DEAD™ Fixable Near IR (876) (Invitrogen™, CAS#: L34982) was co-incubated to determine the cellular viability. The stained cells were analyzed using a CytoFLEX LX flow cytometer (Beckman, USA) at the Auburn University Flow Cytometry and High-Speed Cell Sorting Laboratory Core Facility (RRID: SCR_025507). For each experiment, 10,000 events were acquired, and data analysis was

conducted using FlowJo™ v10 software (FlowJo, LLC, Ashland, CA) to assess mean fluorescence intensity (MFI) and percentage (%).

*2.7 Antioxidative enzymatic activity*

We measured the total antioxidative enzymatic activity of superoxide dismutase (cytosolic and mitochondrial SOD), catalase (CAT), glutathione (GSH), glutathione disulfide (GSSG), and glutathione peroxidase (GPX) in the brains of treated adult zebrafish. Sample preparation for total antioxidative enzymatic activity evaluation followed previously described methods with minor modifications (Pompermaier et al., 2022). Briefly, 6-month-old zebrafish were euthanized using an ice bath (Leary et al., 2013). Brains were collected, rinsed with PBS, and homogenized in ice-cold 50 mM Tris-HCl buffer (CAS# 1185-53-1, Thermo Fisher Scientific, USA). The homogenates were snap-frozen in liquid nitrogen and stored at -80°C until analysis. Total protein concentrations were determined using the Pierce™ Bradford Plus Protein Assay Kit (Thermo Scientific™), and absorbance was measured with a Microplate reader (Infinite® M200 PRO Multimode Microplate Reader, Tecan, Switzerland). Total antioxidative enzymatic activity was measured by commercial kits and assays were performed according to the manufacturer's instructions (Cayman, Ann Arbor, Michigan, USA). The following commercial kits were used: Catalase Assay Kit (707002), Superoxide Dismutase Assay Kit (706002), Glutathione Reductase Assay Kit (703202), and Glutathione S-Transferase Assay Kit (703302). Absorbance for SOD, CAT, GSH, and GSSG assays was measured using the Infinite® M200 PRO Multimode Microplate Reader (Tecan, Switzerland), and GPX activity was assessed with the BioTek Synergy HTX Multimode Reader (BioTek Instruments, Winooski, VT, USA). The minimum protein concentrations required for antioxidant enzymatic activity detection in treated adult zebrafish brains were as follows: 0.07 mg/ml for cytosolic SOD, 0.16 mg/ml for mitochondrial SOD, 0.3 mg/ml for CAT, 0.17 mg/ml for GSH and GSSG, and 0.22 mg/ml for GPX. The antioxidative enzymatic activities were normalized to the total protein content for each sample.

*2.8 Gene expression*

For 6 mpf zebrafish brain, a single brain was homogenized with Pellet Mixers and Cordless Motor (VWR) in TRIzol (Thermo Fisher Scientific, USA). RNA was isolated and purified with RNeasy MinElute clean up kit (Qiagen, USA). Total RNA extraction and cDNA synthesis of the brains were performed following previously established protocols (Peterson & Freeman, 2009). RNA integrity and concentration were assessed using a NanoDrop 1000 Spectrophotometer V3.8 (Thermo Fisher Scientific, Waltham, MA, USA). Quantitative real-time polymerase chain reaction (qRT-PCR) was conducted to evaluate gene expression. Expression levels of 18 target genes were analyzed using zebrafish-specific primers (Integrated DNA Technologies, Inc., USA) **(Table 3-2, Chapter 3)**. Reactions were carried out using PowerTrack™ SYBR Green Master Mix (Applied Biosystems™, USA) on a QuantStudio™ 7 Flex Real-Time PCR System (Thermo Fisher Scientific, Waltham, MA, USA). Gene expression levels were quantified using the $2^{-\Delta\Delta CT}$ method (Livak and Schmittgen, 2001), with normalization to the housekeeping β-actin gene (Bustin et al., 2009).

*2.9 Zebrafish neurochemical processing for HPLC-ECD analysis, HPLC-ECD Method Validation, Chromatographic conditions, and performance*

Samples for the neurotransmitter detection were submitted to Isakson Center for Neurological Disease Research at University of Georgia (Dr. Anumantha G. Kanthasamy's lab) and the experiment was performed by Dr. Piyush Padhi and Dr. Anumantha G. Kanthasamy.

For neurochemical analysis, the testing methods and HPLC-ECD analysis were similar as previously described in Chapter 2. Briefly, 6 mpf zebrafish brains were stored in antioxidant buffer, followed by homogenization, and sonication. The samples were centrifuged at 14,200 x g for 10 min, transferred to Spin-X Nylon centrifuge tube filters, and then subjected to a second centrifugation cycle at the same respective setting. The filter was discarded, and the samples were stored at -80°C until HPLC sample injection. Samples were subjected to HPLC-EC detection to detect norepinephrine (NE, Sigma - A9512), 3,4-Dihydroxyphenylacetic acid (DOPAC, Sigma - 850217), dopamine (DA, Sigma - H8502), 5-hydroxyindoleacetic acid (5-

HIAA, Sigma - H8876), and isoproterenol (ISO, Sigma – 1351005) in plasma and tissue lysates (1-5). The preliminary analyses aimed at detecting serotonin (5-HT) in whole larval tissue (a pooled sample of 30 larvae at 120 hpf) failed to yield a detectable signal **(Figure 4-2)**. Therefore, in this study, we focused on measuring the levels of DOPAC, norepinephrine, dopamine, and 5-HIAA.

*2.10 Statistical analysis*

Statistical and graphic analyses were conducted using GraphPad Prism 10.0.2 software (GraphPad Software Inc., La Jolla, CA, USA). All data were first assessed for normality and equal variance using the Shapiro–Wilk test. For normally distributed data, an unpaired t-test was used for two-group comparisons, while a one-way analysis of variance (ANOVA) followed by Tukey's post-hoc test was applied for comparisons involving more than two groups. Non-normally distributed data were analyzed using the Mann–Whitney test for two-group comparisons or the Kruskal–Wallis test followed by Dunn's multiple comparisons test for more than two groups. Results are presented as mean ± standard deviation (SD), with statistical significance indicated as follows: * $p \leq 0.05$, ** $p \leq 0.01$, *** $p \leq 0.001$, and **** $p \leq 0.0001$.

## 3. Results

*3.1 1.75 μM MPTP significantly impacts locomotor activities and increases female-biased anxiety-like behavior in adult zebrafish*

Our previous study in Chapter 3 found that 5 ppb TaClo induced MPTP-like neurotoxicity during both the embryonic and larval stages, with alterations in photomotor responses at 24 hpf and a significant decrease in the distance moved at 120 hpf. To assess whether early-life exposure to TaClo and MPTP led to persistent neurobehavioral deficits in adulthood, novel tank tests and open field tests were conducted on adult zebrafish to evaluate the locomotor activity and anxiety levels. We found in the novel tank test that male zebrafish exposed to 1.75 μM MPTP at the embryonic stage exhibited significantly reduced velocity ($p \leq 0.05$) **(Figure 4-3A)**, distance moved ($p \leq 0.001$) **(Figure 4-3B)**. Whereas, we found female adult zebrafish exhibiting a higher anxiety level by demonstrating a reduced frequency at the top

($p \leq 0.05$) **(Figure 4-3C)**, shorter cumulative duration at the top ($p \leq 0.001$) **(Figure 4-3D)**, and a higher latency from bottom to top ($p \leq 0.001$) **(Figure 4-3E)** in the novel tank test. Lastly, in the two-dimensional heat map of zebrafish swimming trajectory, we observed that MPTP-treated female zebrafish had more frequency at the bottom in the novel tank test **(Figure 4-3F)**. No significant alterations were observed in the novel tank test for the TaClo-treated group, and no significant changes in locomotor activity or anxiety levels were noted in the open field test in both TaClo and MPTP-treated groups. Our data demonstrate that transient exposure of zebrafish from 1-120 hpf to 1.75 μM MPTP resulted in neurobehavioral deficits during the larval stage that persisted into adulthood. Additionally, our findings suggest that 1.75 μM MPTP is an effective anxiolytic agent in female adult zebrafish. No significant neurobehavioral alterations were found in TaClo or 1.75 μM MPTP treated groups, including velocity, distance moved, acceleration (minimum and maximum), movement (moving cumulative duration, not moving cumulative duration, top frequency, top cumulative duration, top latency to first, bottom frequency, bottom cumulative duration, zone transition from top to bottom frequency, zone transition from top to bottom latency to first, zone transition from bottom to top frequency, zone transition from bottom to top latency to first, mean activity, activity frequency, mobility (body fill), mobility state (highly mobile, frequency), mobility state (highly mobile, cumulative duration, mobility state (mobile, frequency), mobility state (mobile, cumulative duration), mobility state (immobile, frequency), mobility state (immobile, cumulative duration), and rotation frequency in both female **(Figure 4-4)** and male **(Figure 4-5)** in novel tank test (NTT). No significant neurobehavioral alterations were found in TaClo or 1.75 μM MPTP treated groups, including velocity, distance moved, acceleration (minimum and maximum), movement (moving cumulative duration, not moving cumulative duration, acceleration state, movement, inner and outer frequency, and mobility state in both female **(Figure 4-6)** and male **(Figure 4-7)** in TaClo treated groups in open field test (OPF).

*3.2 Early life exposure to TaClo or MPTP results in irreversible and progressive diencephalic neurodegeneration in adult zebrafish*

In our previous work (Chapter 3), we found that 5 ppb TaClo and 1.75 μM MPTP selectively targeted larval diencephalic neuronal populations (DC) at DC2, DC4/5, and DC6 in

addition to impairing locomotor activity. Previous studies have suggested that the loss of DC2 and DC4 likely contributes to motor dysfunction in zebrafish larvae (Ilin et al., 2021; Sallinen et al., 2009; Wen et al., 2008; Xi et al., 2011). Therefore, we proposed that the diencephalic neuronal loss induced by 5 ppb TaClo and 1.75 μM MPTP contributed to the decreased locomotion at the larval stage. In this study, we observed that 1.75 μM MPTP exposure continued to impact locomotion and increase female-biased anxiety-like behavior in adulthood. This raised the question of whether adult zebrafish exposed to MPTP during early development still exhibited similar diencephalic degeneration or whether other brain regions were also affected. To address these questions, we examined the expression of the tyrosine hydroxylase (TH) immunolabeling neurons within each brain region **(Figure 4-8)**, including the telencephalon, diencephalon, and rhombencephalon. However, no significant differences in relative TH-highlighted neuronal density were observed in telencephalon **(Figure 4-9A)**, diencephalon **(Figure 4-9B**), and rhombencephalon **(Figure 4-9C)**. Next, we then focused on the diencephalon and specifically analyzed the TH-highlighted neuronal density in the parvocellular preoptic nucleus (PPa), periventricular pretectal nucleus (PPv), posterior tuberculum (PT), periventricular nucleus of the posterior tuberculum (TPp), DC2 and DC4, paraventricular organ (PVO), posterior tuberal nucleus (PTN), and caudal zone of periventricular hypothalamus (HC). While there were no significant differences in the PPa **(Figure 4-10A-B)**, PPV **(Figure 4-10A, C)**, PTN **(Figure 4-10A, D)**, and HC regions **(Figure 4-10A, E)**, we found that both 5 ppb TaClo and 1.75 μM MPTP led to a significant reduction in the relative density of TH immunolabeling neurons compared to the vehicle and control groups in the TPp **(Figure 4-11A-B)** and DC2/4 **(Figure 4-11A,C)**. Additionally, the analysis of the PVO **(Figure 4-11A, D)** and PT regions **(Figure 4-11A, E)** revealed that not only 5 ppb TaClo and 1.75 μM MPTP, but also 500 ppb TaClo, significantly decreased TH immunolabeling neuronal numbers compared to the vehicle group. These findings suggest that the damage to diencephalic neurons at the larval stage following TaClo and MPTP exposure is irreversible and persists into adulthood. Additionally, the diencephalic neurodegeneration appears not to directly link to hypoactivity or anxiety-like behavior in adult zebrafish.

*3.3 Early-life exposure to TaClo and MPTP does not influence diencephalic cellular apoptosis and glial responses in adult zebrafish*

In Chapter 3, we previously observed that exposure to 5 ppb TaClo and 1.75 μM MPTP increased diencephalic apoptosis and microgliosis, as well as induced astrocytic loss in 120 hpf larvae exposed to 5 ppb TaClo. Furthermore, our present study revealed that persistent diencephalic neuronal damage in adult zebrafish at the posterior tuberculum. Therefore, we questioned whether this persistent neuronal loss was linked to ongoing apoptosis and accompanied by neuroinflammatory responses. To answer this question, we took a forward phenotypic approach and performed double IFA targeting the telencephalon, diencephalon, and rhombencephalon, as well as the posterior tuberculum. However, we found there were no significant differences in caspase-3 labeled apoptotic bodies **(Figure 4-9 E-F, Figure 4-12A-B)**, LCP-labeled macrophages **(Figure 4-9 G-I, Figure 4-12A, C)**, and GFAP-highlighted astrocytes **(Figure 4-9 J-L, Figure 4-12A, D)** in the examined brain regions. Taken together, our data show that microglial and astrocytic responses resolve over time, and neither cellular apoptosis persists into adulthood following early-life exposure to TaClo and MPTP.

*3.4. Embryonic exposure to TaClo and MPTP induced persistent oxidative stress in adult zebrafish*

Our previous findings in Chapter 3 showed significant alterations in GPX activity in 0-120 hpf TaClo (500 ppb) and 1.75 μM MPTP-treated larvae. Imbalanced oxidative stress and mitochondrial dysfunction have been suggested as mechanisms of neurodegeneration in response to TaClo and MPTP exposure (Bajpai et al., 2013; Hung & Lee, 1998; Yang et al., 2019). Therefore, we next directed our attention to exploring whether oxidative stress or mitochondrial dysfunction could be the underlying mechanisms contributing to continuous and progressive diencephalic neurodegeneration observed in the adult zebrafish brain. Similar to our previous study, we first performed flow cytometry to evaluate the cellular and mitochondrial ROS levels as well as mitochondrial membrane potential in the adult zebrafish brain. In contrast to our previous larval model, we found that the adult zebrafish brain in the 500 ppb TaClo-treated group exhibited the highest MitoSox MFI compared to the vehicle group ($p \leq 0.05$) **(Figure 4-13A)**. Furthermore, we observed that the 500 ppb TaClo group also had the highest ratio of

mitochondrial ROS to active mitochondrial activity compared to both the vehicle and TaClo (5 and 50 ppb) groups ($p \leq 0.01$) **(Figure 4-13B)**. However, no significant differences were found in CellROX (MFI and percentage of positive cells), MitoSOX (percentage of positive cells), and MitoTracker (MFI and percentage of positive cells) **(Figure 4-14A-E).** Next, we evaluated antioxidative enzymatic activity in the adult zebrafish brain. Although no significant alterations were observed in the cytosolic and mitochondrial SOD, CAT, GSH, and GSSH activity levels **(Fig. 4-15A-D)**, we found that 1.75 µM MPTP significantly increased catalase activity compared to the control group ($p \leq 0.001$) **(Figure 4-16A)**. The 5 ppb and 500 ppb TaClo group exhibited the highest normalized GPX activity across five-time points measured every minute **(Figure 4-16B)**, with significantly higher GPX activity compared to the vehicle and control groups **(Figure 4-16C)**. Collectively, our results suggest that early-life exposure to TaClo and MPTP induces persistent oxidative stress in the adult zebrafish brain, which may contribute to the ongoing diencephalic neurodegeneration.

*3.5 mRNA expression is not fully regulated by early-life TaClo and MPTP exposure*

Our findings thus far demonstrate that early-life exposure to TaClo and MPTP modulates the protein expression of diencephalic dopaminergic neurons and alters catalase and GPX activity levels in adult zebrafish. In our previous work, we observed that 5 ppb TaClo and 1.75 µM MPTP significantly upregulated macrophage-expressed gene (*mpeg*) in 0-120 hpf treated zebrafish larvae. To further investigate whether mRNA expression was similarly regulated, we employed a molecular approach to analyze key genes associated with dopaminergic neurons, microglia, astrocytes, antioxidant enzymes, apoptotic pathways, and Parkinson's disease-related mechanisms. However, no significant changes were observed in the expression of all the tested genes **(Figure 4-17A-Q)**. This result suggests that the long-term neurotoxic effects of early-life TaClo and MPTP exposure may not be mediated through these pathways.

*3.6 1.75 µM MPTP impacts DOPAC levels in adult zebrafish brain*

To determine whether neurotransmitter levels are altered following exposure and whether the changes observed in 120 hpf zebrafish larvae after early-life exposure to 1.75 µM MPTP

persist into adulthood, we measured the levels of DOPAC, dopamine, norepinephrine, and 5-HIAA in the 6 mpf zebrafish brains. We found that only the 1.75 μM MPTP-treated group exhibited a significant increase in DOPAC levels **(Figure 4-18F)**. No significant differences in dopamine or norepinephrine were observed in either the TaClo-treated groups (5, 50, and 500 ppb) or the 1.75 μM MPTP group **(Figure 4-18A-C, E, G)**. Additionally, 5-HIAA levels in the brains of 6 mpf zebrafish exposed to TaClo (5, 50, and 500 ppb) did not differ significantly from control groups **(Figure 4-18D)**.

## 4. Discussion

This study extends our previous research on TaClo-induced MPTP-like Parkinson's larval models by investigating whether transient early-life exposure to TaClo and MPTP leads to long-lasting neurotoxic effects in adult zebrafish. Our findings indicate that early-life exposure to TaClo and MPTP resulted in persistent neurotoxic effects. Specifically, we observed impaired locomotor activity, anxiety-like behaviors, irreversible and progressive diencephalic neuronal damage, and ongoing oxidative stress in adult zebrafish. Overall, our study provides insights into the potential mechanisms through which early-life environmental exposure influences later-life neurotoxicity in zebrafish. In addition, our results highlight the need for awareness of TCE contamination in Superfund sites and its associated neurotoxic risks.

In our previous work (Chapter 3), we demonstrated that TaClo elicited MPTP-like neurotoxicity Parkinson's disease larval model. In this model, we found zebrafish larvae following the 1-120 hpf exposure to 5 ppb TaClo and 1.75 μM MPTP had significant locomotor deficits and a profound adverse effect on diencephalic neurons with increased apoptosis, microgliosis, and increased antioxidant enzymatic activity in addition to astrocytic loss following 5 ppb TaClo exposure. While previous studies have identified the larval ventral diencephalon as homologous to the mammalian substantia nigra, its correspondence in adulthood remains controversial (Lal & Kawakami, 2022). However, the adult diencephalic region is still largely considered a homolog of the mammalian substantia nigra, as the ascending dopaminergic projections from the diencephalic posterior tuberculum (PT) to the subpallium resemble the

mammalian nigrostriatal pathway. Earlier studies indicated that part of the dopaminergic cell population (periventricular nucleus of posterior tuberculum, TPp) within the PT is the strongest candidate for zebrafish homolog of substantia nigra (Panula et al., 2010; Rink & Wullimann, 2002). More recent studies have suggested that the dopaminergic neurons within the PT, including the TPp, as well as the diencephalic clusters (DC)2 and DC4, are correlated with the nigrostriatal projection (Ilin et al., 2021). One study specifically proposed that DC2 and DC4 dopaminergic neurons of PT in adult zebrafish are structurally equivalent to human substantia nigra (Matsui & Sugie, 2017). Several studies have identified the embryonic dopaminergic neuronal populations and their corresponding counterparts in adulthood. Rink et al. suggested that embryonic DC1 and DC3 may give rise to adult TPp and paraventricular organ (PVO) neurons (Rink & Wullimann, 2002). However, Brown et al. indicated that larval DC2 and adult DC2, larval DC3 and adult PVO, and larval DC4 and adult DC4 are related. In contrast, larval DC1 and adult TPp were not found to be related, and adult TPp may develop later than 55 hpf (Agnihotri et al., 2019). Limited studies have explored the neurotoxic impact of TaClo and MPTP in adulthood following early-life exposure. However, research has shown that the diencephalon is not the only brain region affected by MPTP. For instance, Omar et al. observed a significant reduction in tyrosine hydroxylase-positive dopaminergic neurons in the preoptic region, ventral thalamus, subpallium, TPp, and PVO of the diencephalon following intraperitoneal MPTP injection in adult zebrafish (Omar et al., 2023a). Kalyn et al. exposed MPTP to adult zebrafish through cerebroventricular microinjection and observed reduced dopaminergic neurons in the olfactory bulb and telencephalon (Kalyn & Ekker, 2021). Therefore, we analyzed each brain region, including the telencephalon, diencephalon, and rhombencephalon in our study. Additionally, we specifically examined the expression of TH-positive neurons, apoptosis, microglia, and astrocytes in the PPa, PPv, TPp, PVO, PT, PTN, and caudal zone of periventricular hypothalamus (HC). Similar to our previous work in the larval zebrafish model in Chapter 3, we found that exposure to 5 ppb TaClo and 1.75 μM MPTP resulted in a relative reduction of TH+ labeled neurons in the TPp, DC2/4, PVO, and PT regions. Additionally, exposure to 500 ppb TaClo led to a relative decrease in TH-positive neuronal relative numbers in the PVO and PT. These findings suggest that transient exposure to TaClo and MPTP immersion during embryonic development leads to irreversible and persistent neuronal damage limited to the diencephalon.

Imbalanced oxidative stress and mitochondrial dysfunction have been implicated as key factors contributing to dopaminergic neuronal damage in MPTP and TaClo-treated models. In our previous work, although cellular and mitochondrial ROS levels were not significantly altered, we observed a significant increase in GPX activity in 500 ppb TaClo-treated larvae, whereas MPTP-treated larvae exhibited a decrease in GPX activity in Chapter 3. Interestingly, in the brains of treated adult zebrafish, we not only observed increased GPX activity in those exposed to TaClo (5 and 500 ppb), but also an increase in catalase enzymatic activity in the 1.75 μM MPTP-treated brains. Additionally, mitochondrial ROS levels were elevated in the brains of 500 ppb TaClo-treated zebrafish. While the exact mechanisms underlying the persistent mitochondrial dysfunction and altered antioxidative enzymatic activity remain unclear, it is possible that this imbalance in oxidative stress contributes to the irreversible and ongoing neuronal damage in the diencephalon of adult zebrafish.

Previous studies have indicated that, unlike mammals, zebrafish do not exhibit chronic inflammation or glial scar formation following brain injuries (Caldwell et al., 2019; Zambusi & Ninkovic, 2020). Consistent with these findings, we observed no significant alterations in the protein expression of apoptosis, microglial, or astrocytic responses in the diencephalon of TaClo and MPTP-treated adult zebrafish. Taken together, our results suggest that exposure to TaClo and MPTP from 1–120 hpf induced glial responses in the ventral diencephalon at 120 hpf, which resolved by 6 months post-exposure. Microgliosis, apoptosis, astrogliosis, and neurogenesis have been identified as key factors contributing to zebrafish's remarkable ability to regenerate neurons in both larval and adult stages (Chen et al., 2024). For example, Ohnmacht et al. demonstrated that microglia played a role in neurogenesis following spinal ablation in larval zebrafish(Ohnmacht et al., 2016). Caldwell et al. demonstrated that a microglial response is essential for the regeneration of new dopaminergic neurons from diencephalic ependymo-radial glial progenitor cells in adult zebrafish (Caldwell et al., 2019). In their study, they performed intraventricular injections of 6 hydroxydopamine (6-OHDA) to ablate dopaminergic neurons in specific regions of the TH immunolabeling neuronal population 5/6 (corresponding to the posterior part of the parvocellular preoptic nucleus for region 5, and the anterior intermediate, ventrolateral, and ventromedial thalamic nuclei for region 6). The results revealed localized

microgliosis at neuronal population 5/6 within 12 hours post-injection. Furthermore, regeneration of the TH immunolabeling neuronal population in regions 5/6 was observed, with neuron numbers reaching levels comparable to those of age-matched controls at 540 days post-injection (Caldwell et al., 2019). Vijayanathan et al. explored dopaminergic neuron regeneration in adult zebrafish by injecting 6-OHDA at the posterior tuberculum-hypothalamus (PT-Hyp) junction in sexually mature male zebrafish. This resulted in an over 85% loss of diencephalic dopaminergic neurons, accompanied by apoptosis at 3 days post-lesion. The study also suggested that astrocytes play a crucial role in supporting regenerative processes by guiding proliferative cells following neural loss (Vijayanathan et al., 2022). In contrast to our study, although we observed diencephalic apoptosis and microgliosis in 120 hpf larvae following TaClo and MPTP exposure, along with a loss of diencephalic astrocytes in 1-120 hpf TaClo-exposed larvae, we found no regenerated neurons, but an irreversible and continuous neuronal loss, in treated zebrafish at 6 months post-exposure. It is possible that astrocytic loss observed in the TaClo-treated larvae inhibited neuronal regeneration. However, it appears that the neuronal regenerative process is complex and may involve a combination of factors, such as stem cell activation, overexpression of genes related to oxidative stress, or activation of specific genes associated with regeneration(Caldwell et al., 2019; Chen et al., 2024).

Our previous work (Chapter 3) revealed that 120 hpf larvae with diencephalic neuronal loss exhibited significant locomotor deficits following 1–120 hpf exposure to 5 ppb TaClo and 1.75 μM MPTP. In our present work, we found the MPTP-treated larval models continued to demonstrate hypo-locomotor activity in both 6-month-old female and male zebrafish. Additionally, females exhibited increased anxiety levels in the novel tank test. Similar to our study, Dong et al. reported that transient MPTP exposure at 1 μM during the sensitive developmental window of 48–96 hpf led to male-biased hypoactivity, with reduced fast swim bouts and social behavioral deficits in 6-month-old zebrafish(H. Dong et al., 2022). Moreover, Dong et al. further observed that 48–96 hpf MPTP exposure induced gut microbiome dysbiosis in larval and adult zebrafish, increasing susceptibility to pathogenic *Vibrio* colonization. Although they did not confirm whether *Vibrio* influenced the MPTP-induced hypoactivity in larval and adult zebrafish, recent studies have suggested that chemical exposure in zebrafish can

alter the gut microbiome. This dysbiosis may, in turn, modulate locomotion and anxiety-related behaviors in both larval and adult zebrafish through the gut-brain axis(Stagaman et al., 2024). For example, Zhang et al. found that zebrafish exposure to environmental fluorene-9-bisphenol (BHPF) altered gut microbiome diversity and further contributed to an imbalance in neurotransmission, behavioral inhibition, and altered social behaviors (Zhang et al., 2024). Stagaman et al. demonstrated that benzo[a]pyrene (BaP) influenced variation in the gut microbiome, impacting -developmental neurobehavioral toxicity in larval zebrafish (Stagaman et al., 2024). Therefore, it is likely that the transient MPTP exposure in embryonic zebrafish alters the gut microbiome diversity, which in turn affects locomotor activity and anxiety-related behaviors. It will be of interest for future studies to focus on investigating the relationship between TaClo and MPTP exposure, changes in the gut microbiome, and neurobehavioral deficits.

In a previous study, Dong et al. reported male-biased locomotor deficits and impaired social behavior in adult zebrafish following MPTP exposure during the larval stage (H. Dong et al., 2022). However, our findings indicate that locomotor deficits occurred in both males and females, with an additional increase in anxiety levels observed in female groups. The reason why only MPTP-treated female adult zebrafish exhibited a pronounced anxiety level in our study remains unclear. MPTP is a well-recognized neurotoxicant used to induce PD models in various animal species (Sarath Babu et al., 2016). It selectively targets dopaminergic neurons, leading to reduced locomotor activity and decreased dopamine levels, which can further influence anxiety-related behaviors (Sy et al., 2010). Previous studies have suggested that dopaminergic neurons in female rats are generally less vulnerable to degeneration-inducing factors compared to those in males (Bispo et al., 2019). In addition, estrogen is believed to be a protective factor against PD and perhaps explains why the risk of PD development is twice as high in men than in women (Cerri et al., 2019). However, while women have a lower risk of developing PD, they tend to experience faster disease progression (Cerri et al., 2019). Some studies have also found a higher prevalence of leucine-rich repeat kinase 2 (LRRK2) mutations in women than in men, suggesting that if LRRK2-carrier women have a greater genetic load, suggesting that women who carry LRRK2 mutations may have a greater genetic load and could develop the disease earlier or

experience more rapid progression (Cattaneo & Pagonabarraga, 2025; Cerri et al., 2019). Neurochemical imbalances, hormonal differences, and genetic variations in response to MPTP exposure may contribute to this anxiety-like behavior. Future studies should focus on sex-specific neurotransmitters, hormonal influences, and genetic analyses to better understand this correlation. Overall, our results suggest that MPTP serves as an anxiogenic agent, with females being more susceptible to its effects and exhibiting heightened anxiety responses.

In our current work, we found that only MPTP-treated adult zebrafish exhibited impaired locomotor activity and anxiety alterations, despite both TaClo (5 and 500 ppb) and 1.75 μM MPTP causing similar distribution of TH immunolabeling neuronal loss in the PT of the adult ventral diencephalon. In addition, we wondered if the severity of the TH immunolabeling neuronal loss might affect the outcomes of behaviors; however, we found no significant difference in the $TH^+$ neuronal loss among TaClo (5 and 500 ppb) and 1.75 μM MPTP treated adult zebrafish at TPp, DC2/4, PVO, and PT regions **(Table 4-2)**. We thus wondered if the diencephalic neurodegeneration may be sufficient to induce motor dysfunction in larvae, but not in adult zebrafish. More specifically, the question remains whether the damaged diencephalic regions are the only areas responsible for triggering locomotor deficits, or if other factors may be involved. A previous study has demonstrated the reduction of dopaminergic neurons within the diencephalon in adult zebrafish following MPTP intraperitoneally injection exhibiting reduced swimming speed and travel distance (Omar et al., 2023a). However, one study found that adult zebrafish following MPTP intraventricular microinjection showed decreased velocity and total distance but with reduced dopaminergic neurons rather in the diencephalon but in the olfactory bulb in addition to the telencephalon (Kalyn & Ekker, 2021). Moreover, one study inoculated MPTP to adult zebrafish found a significant reduction of TH immunolabeling neurons in the optic tectum with bradykinesia, dyskinesia, and decreased swimming movement (Sarath Babu et al., 2016). Furthermore, it has been demonstrated that even with the cellular loss in TH immunolabeling neuronal populations 5/6, 11 (corresponding to TPp), and 12 (corresponding to PTN), the authors did not detect significant alterations in locomotor activity nor anxiety level changes in the open field test, novel tank test, and light and dark test in the treated adult zebrafish (Caldwell et al., 2019). Taken together, we conclude that diencephalic TH immunolabeling

neuronal loss may not necessarily trigger locomotor deficits and anxiety alterations in adult zebrafish. Unlike larval zebrafish, adult zebrafish may require additional factors or more complex mechanisms to elicit these behavioral changes. Moreover, it is likely that MPTP not only impairs larval diencephalic dopaminergic neurons but may also target different mechanisms during exposure at the larval stage. Many factors may contribute to alterations in zebrafish locomotor activity. For example, following 1 μM MPTP exposure, Dong et al. observed significant dopaminergic neuronal loss in the retina of treated zebrafish larvae, accompanied by reduced locomotor activity (Haojia Dong et al., 2022). However, diencephalic motoneurons were reported to be unaffected in their study (Haojia Dong et al., 2022). Although the authors did not investigate the correlation between retinal dopaminergic neuronal loss and impaired locomotion, it is important to consider that dysfunction in dopaminergic signaling pathways in the retina could lead to visual abnormalities (Ribelayga et al., 2002; Syambani Ulhaq, 2020). In our study, we did not evaluate the TH immunolabeling neuronal expression in the retina at either the larval or adult stages. Future investigations into retinal responses to MPTP exposure would be of great interest to further understand potential contributions to locomotor deficits. Moreover, a previous study found that long-term exposure to environmentally realistic concentrations of Bisphenol S (BPS) impaired the stress function of the hypothalamic-pituitary-interrenal (HPI) axis and caused anxiety-like behavioral responses in zebrafish (Wei et al., 2020). It is possible that the HPI axis might also be targeted during MPTP exposure at the larval stage, potentially contributing to the observed anxiety-like behavioral changes. Furthermore, the lateral line is essential for driving adult zebrafish locomotion and has been linked to various behavioral responses, including prey detection, obstacle or predator avoidance, and schooling behavior (Ghysen & Dambly-Chaudière, 2004). As zebrafish mature into adulthood, the lateral line system becomes larger and more intricate, contributing significantly to sensory processing and the coordination of movement (Ghysen & Dambly-Chaudière, 2004; Thomas et al., 2015). Abreu et al. found acute peripheral lidocaine lateral line application induced anxiogenic-like effect in adult zebrafish (de Abreu et al., 2019). Han et al. found aminoglycoside-induced damage to the lateral line and muscles with locomotor behavioral changes in zebrafish (Han et al., 2020). Therefore, the disruption to the lateral line may play a significant role in altering both behavioral functions in adult zebrafish.

Lastly, we observed an increase in DOPAC levels in the brains of 6 mpf zebrafish following early-life exposure to 1.75 μM MPTP, without a persistent decrease in 5-HIAA levels that had been observed in 120 hpf larvae. We propose that this may represent a compensatory neuroadaptation. During early-life exposure, we observed reduced expression of diencephalic dopaminergic neurons and decreased 5-HIAA levels, suggesting dysregulation of both the dopaminergic and serotonergic systems. We propose that following MPTP withdrawal, surviving dopaminergic neurons may undergo plasticity-driven upregulation of dopamine turnover, resulting in enhanced dopamine metabolism to DOPAC. If continuous and persistent stress is superimposed during development or adulthood, it could further amplify DOPAC levels. Persistent stress is known to significantly influence dopamine dynamics; while it may initially increase dopamine release and turnover, prolonged exposure often leads to reduced dopamine availability and elevated DOPAC levels (de Abreu et al., 2021). This shift in dopamine metabolism may reflect compensatory mechanisms or impaired dopaminergic signaling (de Abreu et al., 2021; Mizoguchi et al., 2000). Moreover, previous studies investigating the effects of MPTP on dopamine and 5-HIAA levels have reported region-specific and variable outcomes. In our study, neurotransmitter levels were analyzed in whole-brain samples, which may have masked region-specific changes (Fukuda et al., 1988; R. Yang et al., 2023). Future studies should focus on dissecting specific brain regions to better resolve localized neurochemical alterations.

## 5. Conclusion

In conclusion, our study highlights the long-lasting neurotoxic effects of early-life exposure to TaClo, at concentrations comparable to the EPA-regulated levels of TCE, and low concentrations of MPTP in the zebrafish model. These findings underscore the potential environmental risks associated with TCE exposure, which may contribute to neurodegenerative conditions in the long term.

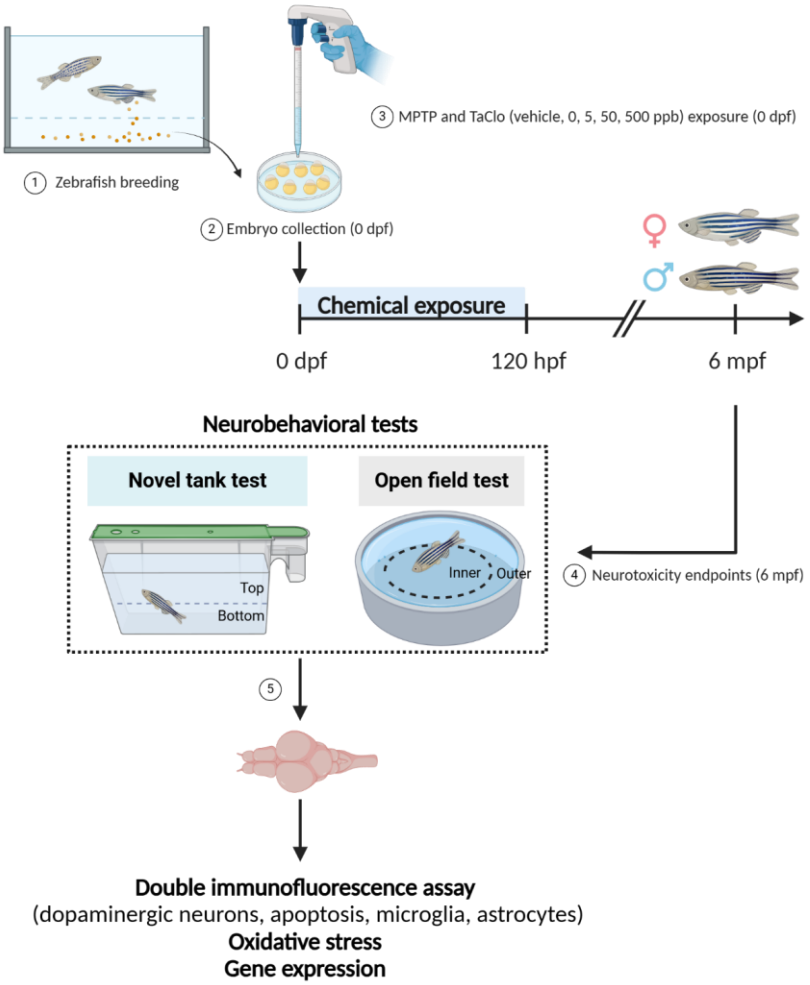


**Figure 4-1. Schematic overview of the experimental regime**

① Adult wild-type AB strain zebrafish (*Danio rerio*) were bred to obtain embryos for chemical exposure. ② Fertilized embryos at 0 days post-fertilization (dpf) were collected and ③ exposed to 1.75 μM 1-methyl-4-phenyl-1,2,3,6-tetrahydropyridine (MPTP), 1-trichloromethyl-1,2,3,4-tetrahydro-beta-carboline (TaClo) (0, 5, 50, 500 ppb), or vehicle (dimethyl sulfoxide, 0.001% DMSO) until 120 hours post-fertilization (hpf). 120 hpf treated zebrafish were rinsed and raised with chemical-free aquaria water and maintained until 6 months post-fertilization (mpf) for neurotoxicity evaluation. ④ 6 mpf female and male zebrafish were subjected to neurobehavioral tests, including novel tank test and open field test. ⑤ Following the neurobehavioral tests, zebrafish were euthanized, and the brains were removed for double immunofluorescence assays to investigate protein expressions of dopaminergic neurons, apoptosis, microglia, and astrocytes. Additionally, brains were collected for oxidative stress and genetic expression evaluation.

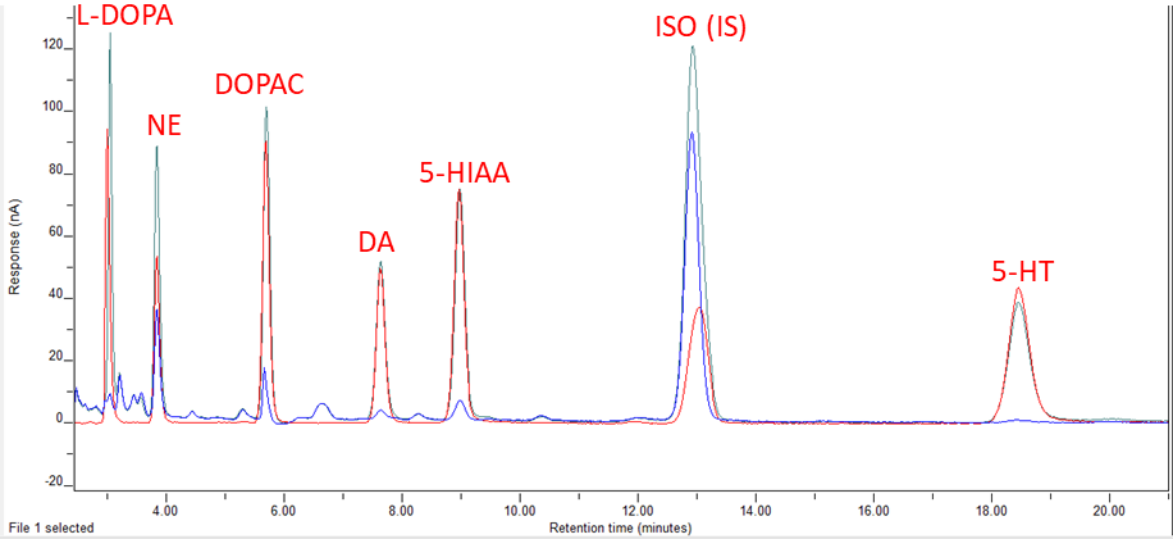


**Figure 4-2. HPLC-ECD neurotransmitter detection on 6 months-post fertilization zebrafish brain**

HPLC-EC detection to detect tyrosine and tryptophan-based metabolites Levodopa, (L-DOPA, Sigma - D9628), norepinephrine (NE, Sigma - A9512), 3,4-Dihydroxyphenylacetic acid (DOPAC, Sigma - 850217), dopamine (DA, Sigma - H8502), 5-hydroxyindoleacetic acid (5-HIAA, Sigma - H8876), serotonin (5-HT, Sigma - H9523), and isoproterenol (ISO, Sigma – 1351005) in tissue lysates. Image is provided by Dr. Piyush Padhi and Dr. Anumantha G. Kanthasamy at the Isakson Center for Neurological Disease Research at the University of Georgia. Red: standard; Green: spike; Blue: sample.

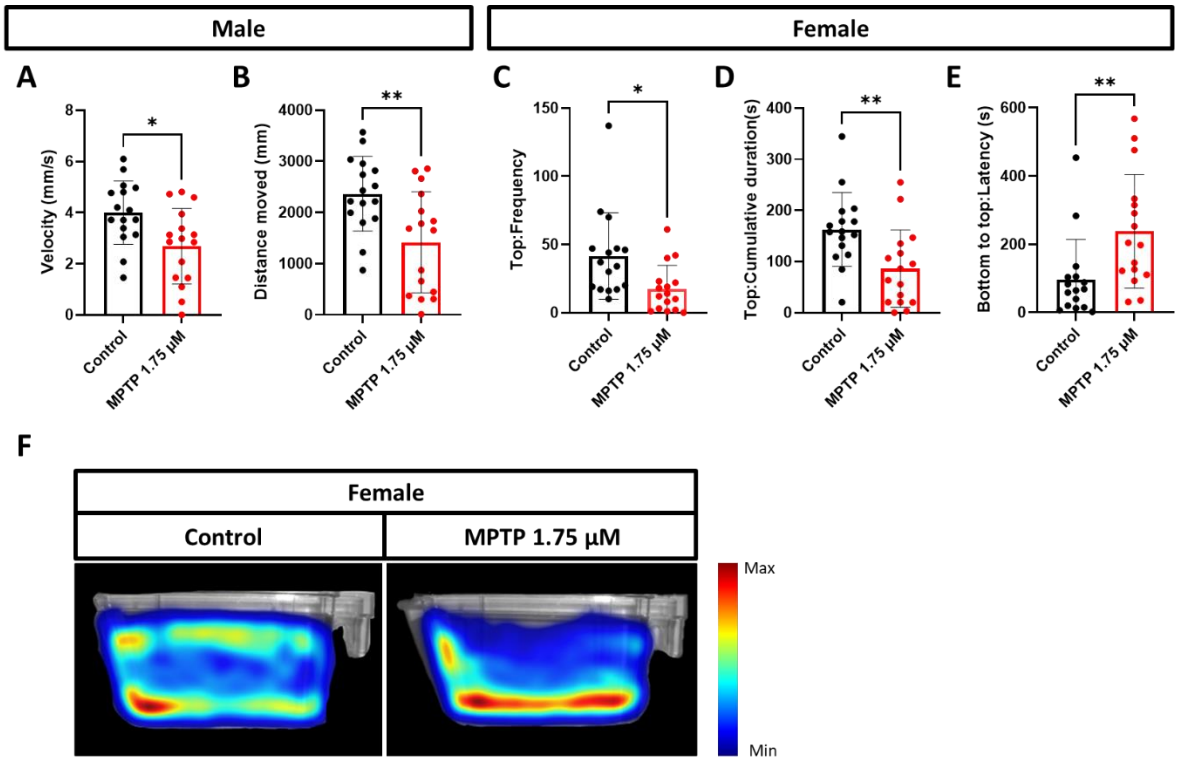


**Figure 4-3. Developmental exposure to 1.75 µM MPTP impaired locomotor activities and increased anxiety levels in 6-month-old zebrafish. (A-F, novel tank test).**

Early 1.75 µM MPTP exposure on male zebrafish displayed significantly reduced velocity (mm/s) (A), distance moved (mm) (B). Female zebrafish were observed with a significant reduced in frequency (C) and cumulative time (D) at the top, and an increase in latency from bottom to top (E). Data are expressed as mean ± standard deviation. All data were analyzed using an unpaired t-test or Mann-Whitney U test. *$p \leq 0.005$ and **$p \leq 0.01$. A representative 2D heat map of female zebrafish swimming trajectory for 10 mins following early life exposure to aquaria water (control) and 1.75 µM MPTP (F).

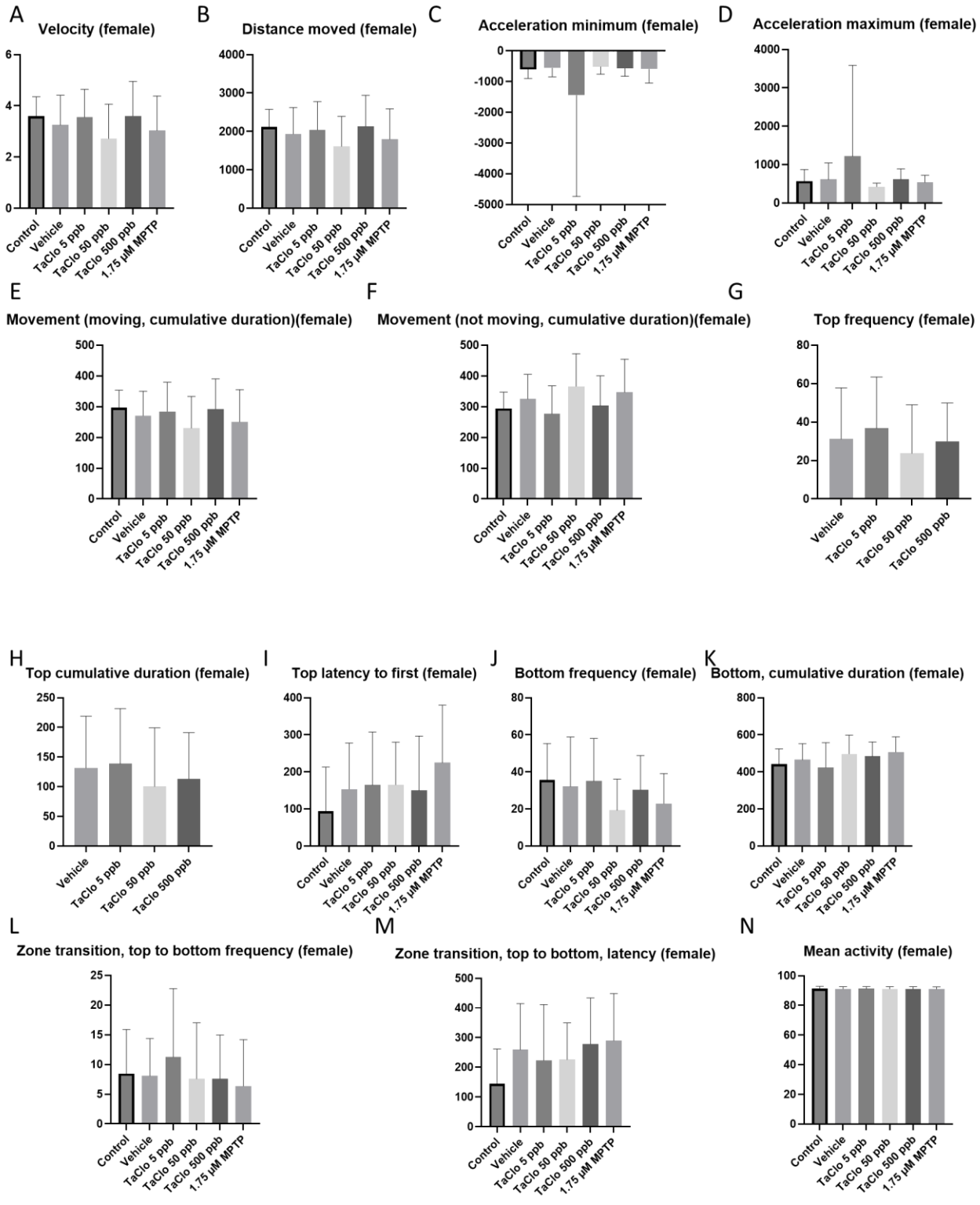
A
Velocity (female)
B
Distance moved (female)
C
Acceleration minimum (female)
D
Acceleration maximum (female)
E
Movement (moving, cumulative duration)(female)
F
Movement (not moving, cumulative duration)(female)
G
Top frequency (female)
H
Top cumulative duration (female)
I
Top latency to first (female)
J
Bottom frequency (female)
K
Bottom, cumulative duration (female)
L
Zone transition, top to bottom frequency (female)
M
Zone transition, top to bottom, latency (female)
N
Mean activity (female)
Control
Vehicle
TaClo 5 ppb
TaClo 50 ppb
TaClo 500 ppb
1.75 µM MPTP

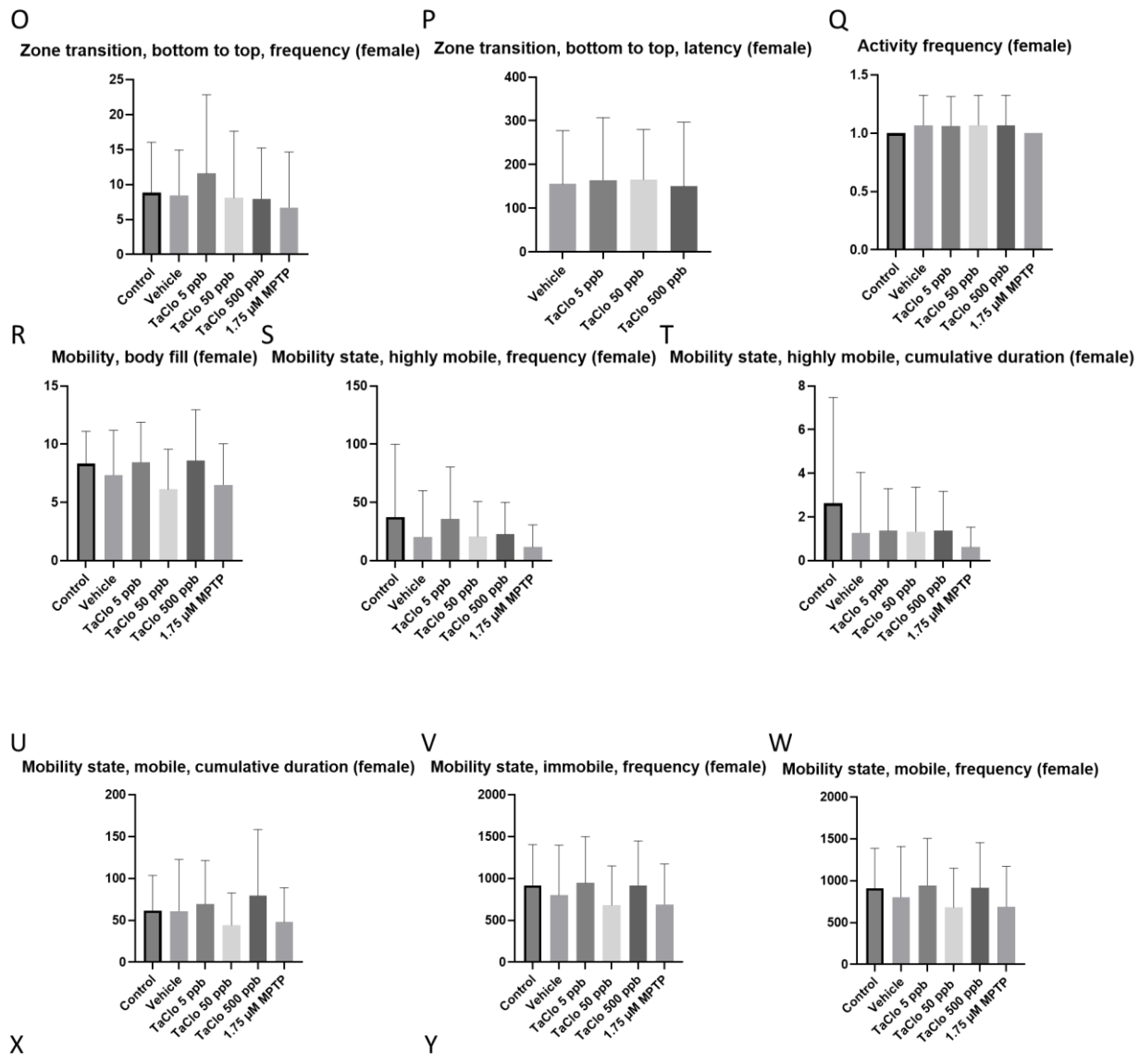


**Figure 4-4. Developmental exposure to TaClo and 1.75 µM MPTP in female in novel tank test (NTT) (A-Y, novel tank test)**

All data were analyzed using Kruskal-Wallis test, followed by Dunn's multiple comparison test.

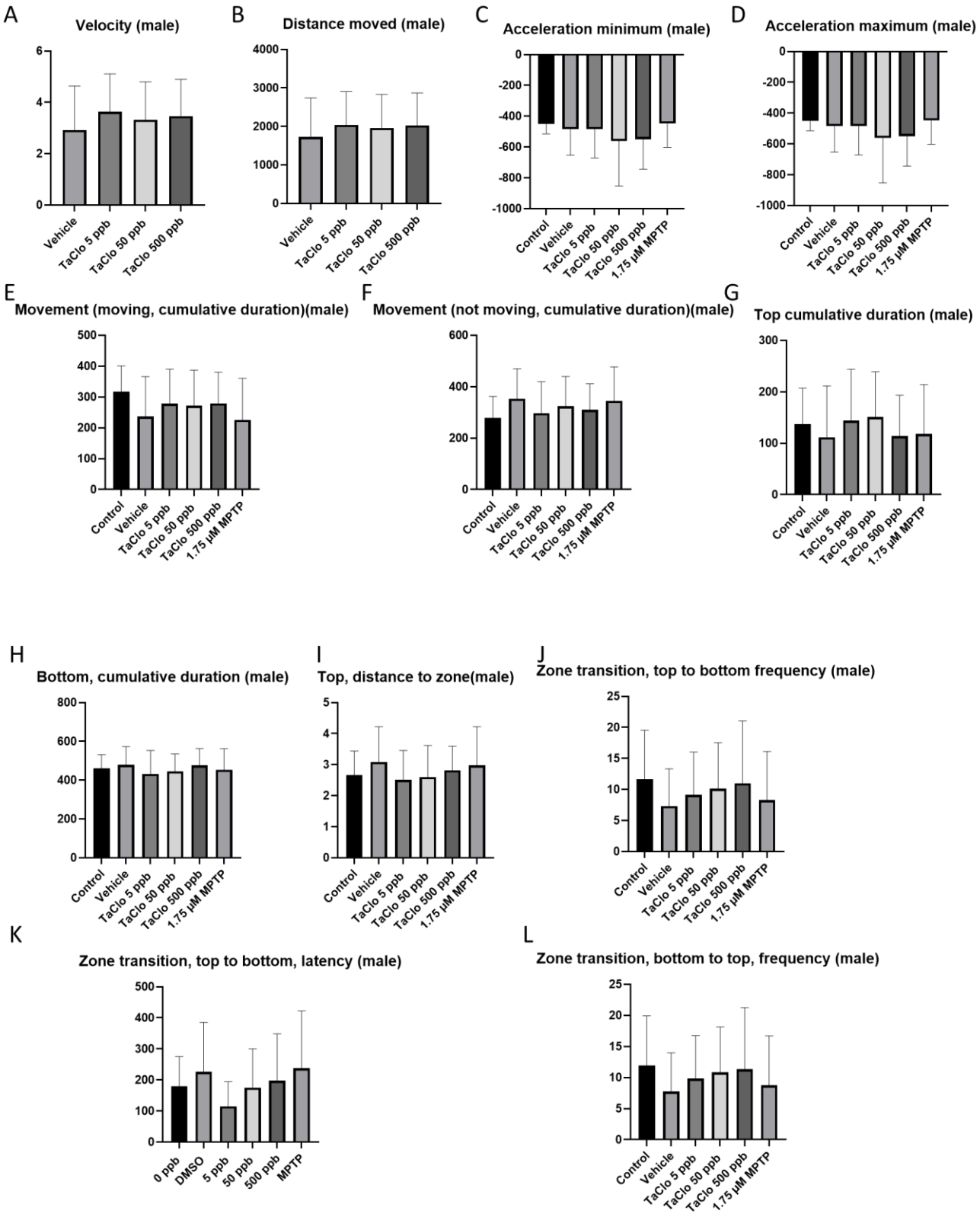
A
Velocity (male)
Vehicle
TaClo 5 ppb
TaClo 50 ppb
TaClo 500 ppb
B
Distance moved (male)
Vehicle
TaClo 5 ppb
TaClo 50 ppb
TaClo 500 ppb
C
Acceleration minimum (male)
Control
Vehicle
TaClo 5 ppb
TaClo 50 ppb
TaClo 500 ppb
1.75 µM MPTP
D
Acceleration maximum (male)
Control
Vehicle
TaClo 5 ppb
TaClo 50 ppb
TaClo 500 ppb
1.75 µM MPTP
E
Movement (moving, cumulative duration)(male)
Control
Vehicle
TaClo 5 ppb
TaClo 50 ppb
TaClo 500 ppb
1.75 µM MPTP
F
Movement (not moving, cumulative duration)(male)
Control
Vehicle
TaClo 5 ppb
TaClo 50 ppb
TaClo 500 ppb
1.75 µM MPTP
G
Top cumulative duration (male)
Control
Vehicle
TaClo 5 ppb
TaClo 50 ppb
TaClo 500 ppb
1.75 µM MPTP
H
Bottom, cumulative duration (male)
Control
Vehicle
TaClo 5 ppb
TaClo 50 ppb
TaClo 500 ppb
1.75 µM MPTP
I
Top, distance to zone(male)
Control
Vehicle
TaClo 5 ppb
TaClo 50 ppb
TaClo 500 ppb
1.75 µM MPTP
J
Zone transition, top to bottom frequency (male)
Control
Vehicle
TaClo 5 ppb
TaClo 50 ppb
TaClo 500 ppb
1.75 µM MPTP
K
Zone transition, top to bottom, latency (male)
0 ppb
DMSO
5 ppb
50 ppb
500 ppb
MPTP
L
Zone transition, bottom to top, frequency (male)
Control
Vehicle
TaClo 5 ppb
TaClo 50 ppb
TaClo 500 ppb
1.75 µM MPTP

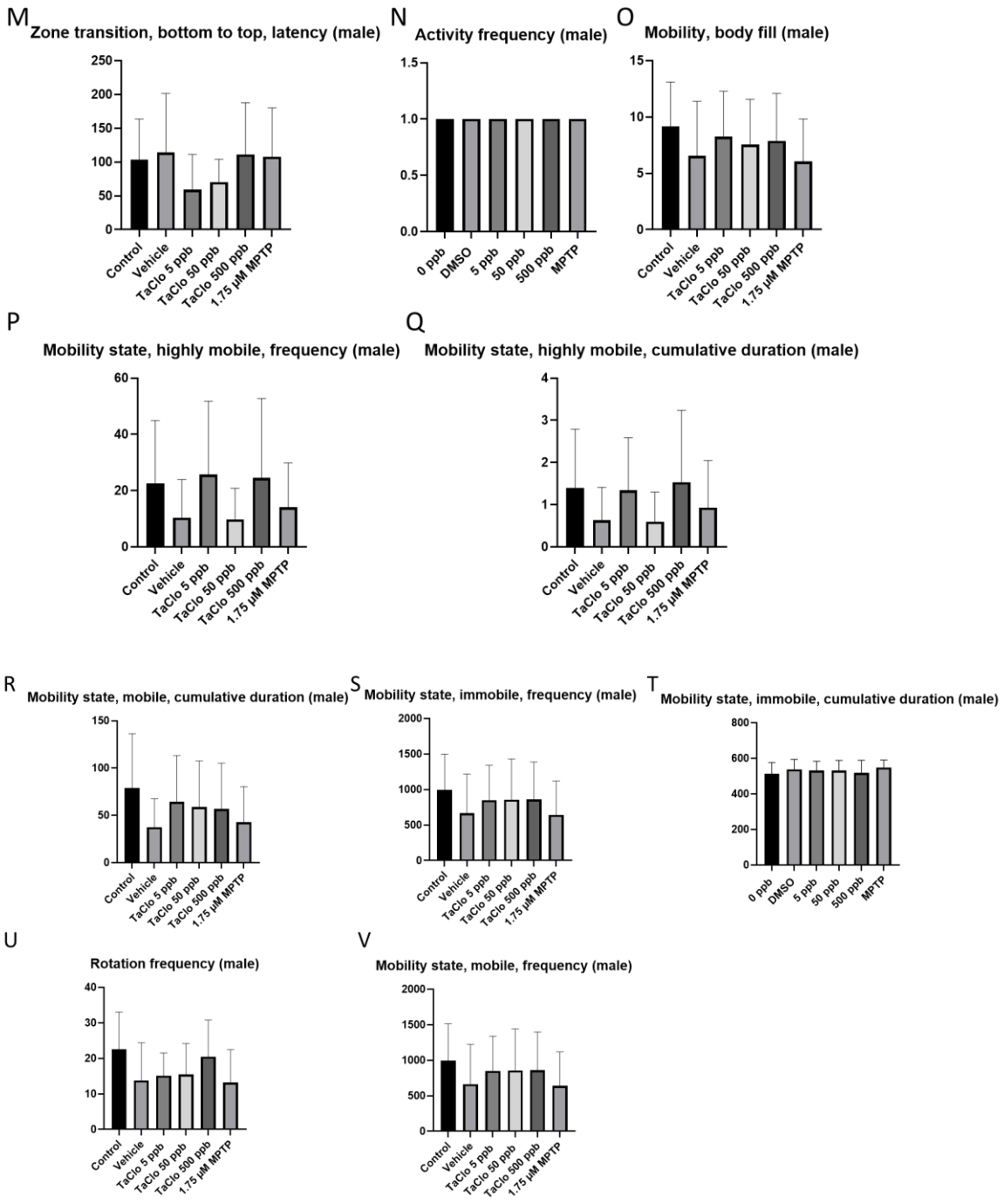


**Figure 4-5. Developmental exposure to TaClo and 1.75 µM MPTP in male in novel tank test (NTT) (A-V, novel tank test)**

All data were analyzed using Kruskal-Wallis test, followed by Dunn's multiple comparison test.

A

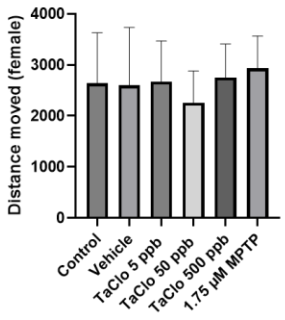
Distance moved (female)
Distance moved (female)
4000
3000
2000
1000
0
Control
Vehicle
TaClo 5 ppb
TaClo 50 ppb
TaClo 500 ppb
1.75 µM MPTP

B

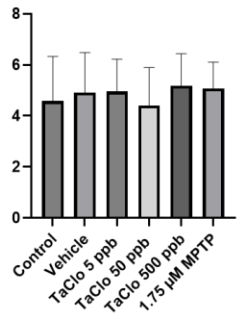
Velocity (female)
8
6
4
2
0
Control
Vehicle
TaClo 5 ppb
TaClo 50 ppb
TaClo 500 ppb
1.75 µM MPTP

C

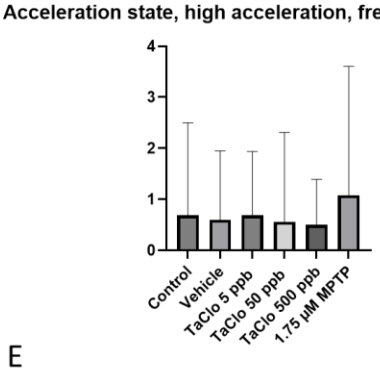
Acceleration state, high acceleration, frequency (female)
4
3
2
1
0
Control
Vehicle
TaClo 5 ppb
TaClo 50 ppb
TaClo 500 ppb
1.75 µM MPTP

D

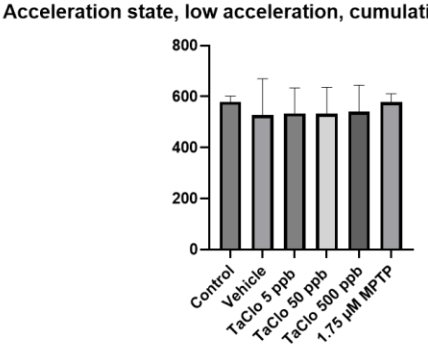
Acceleration state, low acceleration, cumulative duration (female)
800
600
400
200
0
Control
Vehicle
TaClo 5 ppb
TaClo 50 ppb
TaClo 500 ppb
1.75 µM MPTP

E

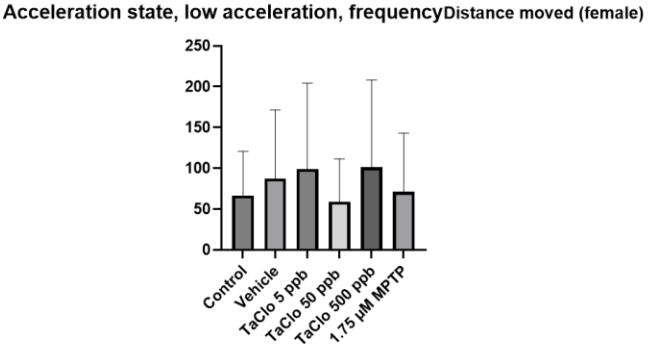
Acceleration state, low acceleration, frequency
Distance moved (female)
250
200
150
100
50
0
Control
Vehicle
TaClo 5 ppb
TaClo 50 ppb
TaClo 500 ppb
1.75 µM MPTP

F

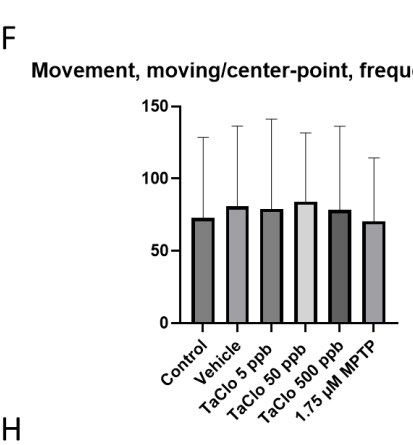
Movement, moving/center-point, frequency (female)
150
100
50
0
Control
Vehicle
TaClo 5 ppb
TaClo 50 ppb
TaClo 500 ppb
1.75 µM MPTP

G

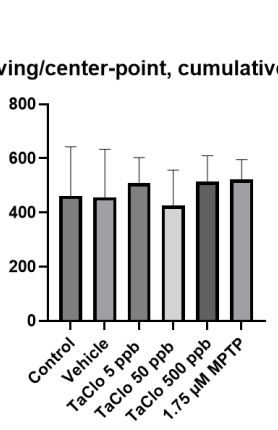
Movement, moving/center-point, cumulative duration (female)
800
600
400
200
0
Control
Vehicle
TaClo 5 ppb
TaClo 50 ppb
TaClo 500 ppb
1.75 µM MPTP

H

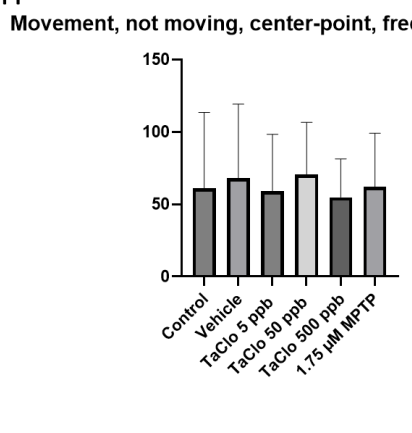
Movement, not moving, center-point, frequency (female)
150
100
50
0
Control
Vehicle
TaClo 5 ppb
TaClo 50 ppb
TaClo 500 ppb
1.75 µM MPTP

I

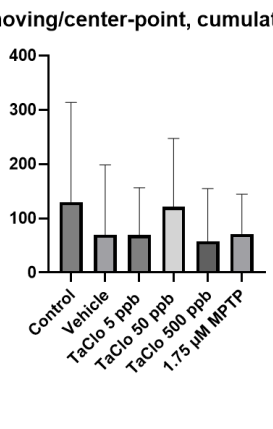
Movement, not moving/center-point, cumulative duration (female)
400
300
200
100
0
Control
Vehicle
TaClo 5 ppb
TaClo 50 ppb
TaClo 500 ppb
1.75 µM MPTP

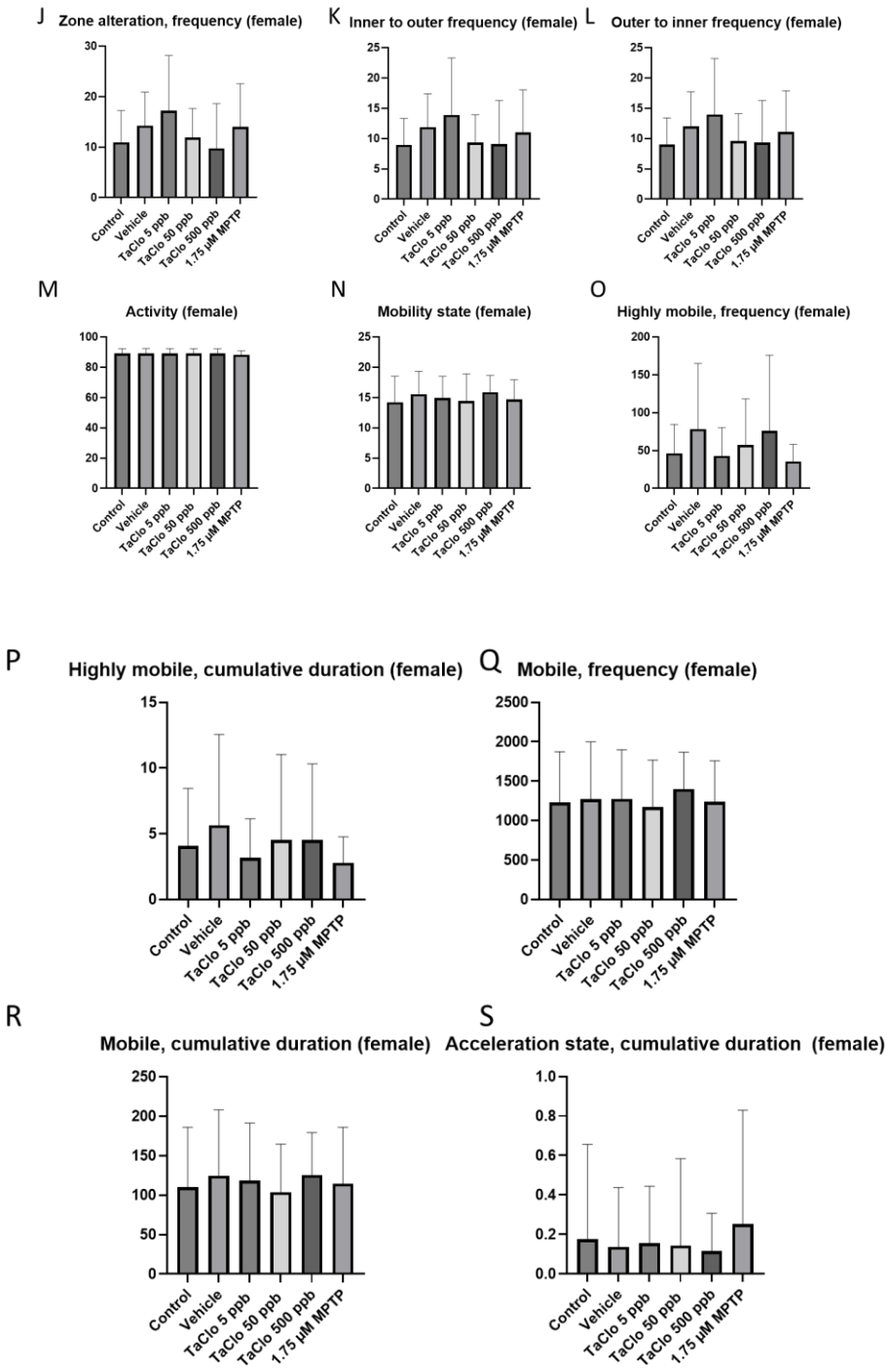


**Figure 4-6. Developmental exposure to TaClo and 1.75 µM MPTP in female in open field test (OPF) (A-S, open field test)**

All data were analyzed using Kruskal-Wallis test, followed by Dunn's multiple comparison test.

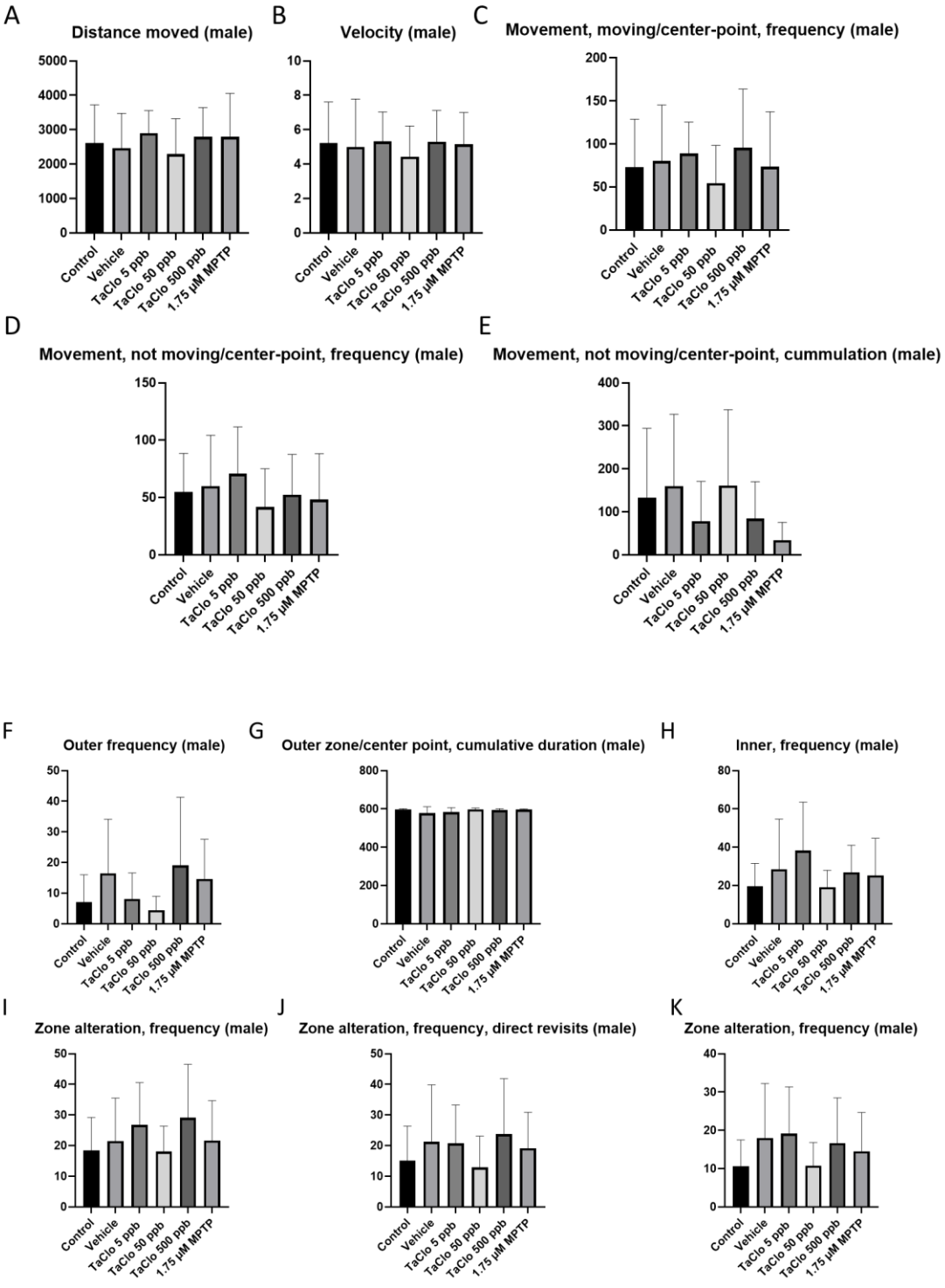
A
Distance moved (male)
5000
4000
3000
2000
1000
0
B
Velocity (male)
10
8
6
4
2
0
C
Movement, moving/center-point, frequency (male)
200
150
100
50
0
Control
Vehicle
TaClo 5 ppb
TaClo 50 ppb
TaClo 500 ppb
1.75 µM MPTP
D
Movement, not moving/center-point, frequency (male)
150
100
50
0
E
Movement, not moving/center-point, cummulation (male)
400
300
200
100
0
F
Outer frequency (male)
50
40
30
20
10
0
G
Outer zone/center point, cumulative duration (male)
800
600
400
200
0
H
Inner, frequency (male)
80
60
40
20
0
I
Zone alteration, frequency (male)
50
40
30
20
10
0
J
Zone alteration, frequency, direct revisits (male)
50
40
30
20
10
0
K
Zone alteration, frequency (male)
40
30
20
10
0

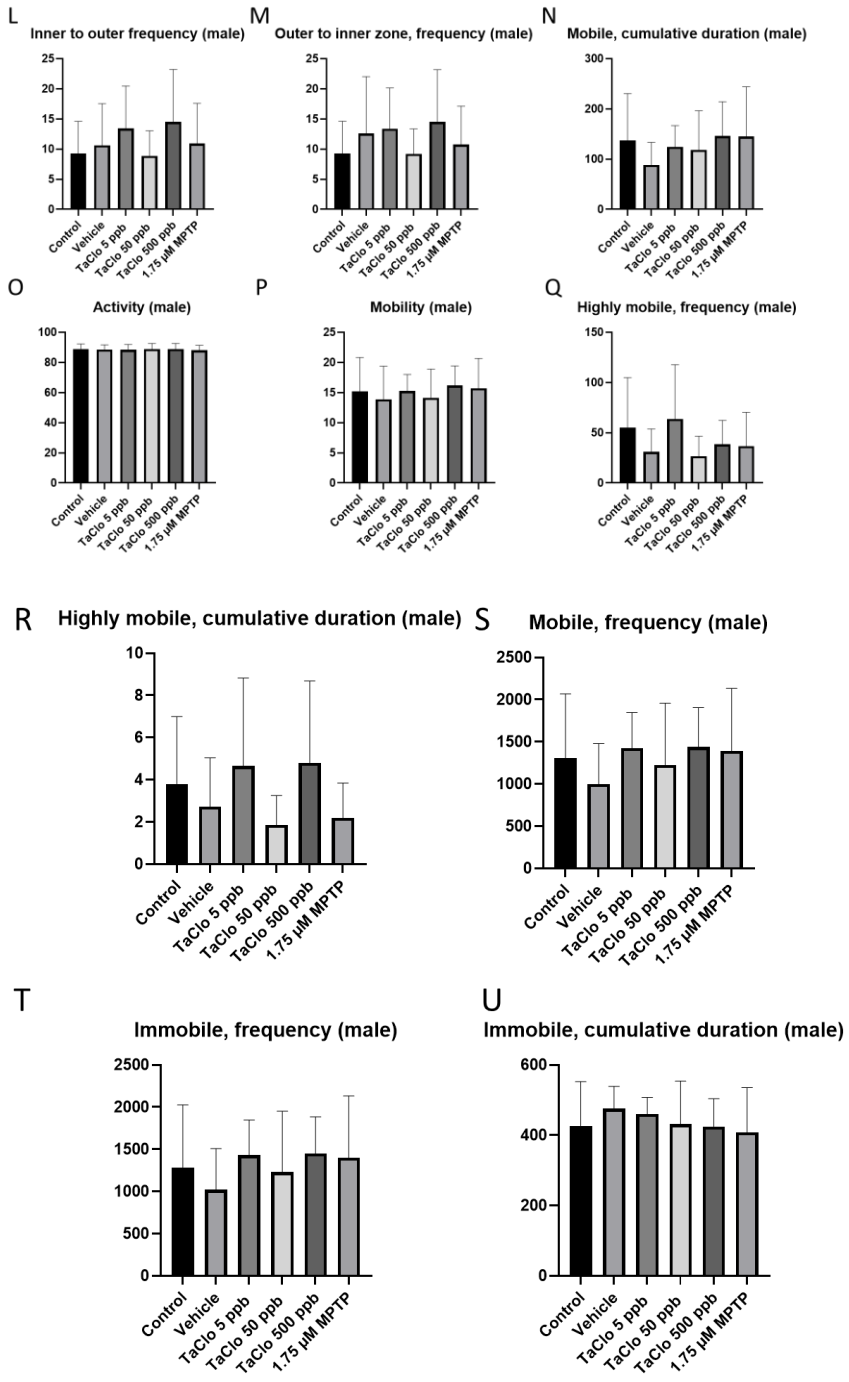


**Figure 4-7. Developmental exposure to TaClo and 1.75 µM MPTP in male in open field test, OPF) (A-U, open field test)**

All data were analyzed using Kruskal-Wallis test, followed by Dunn's multiple comparison test.

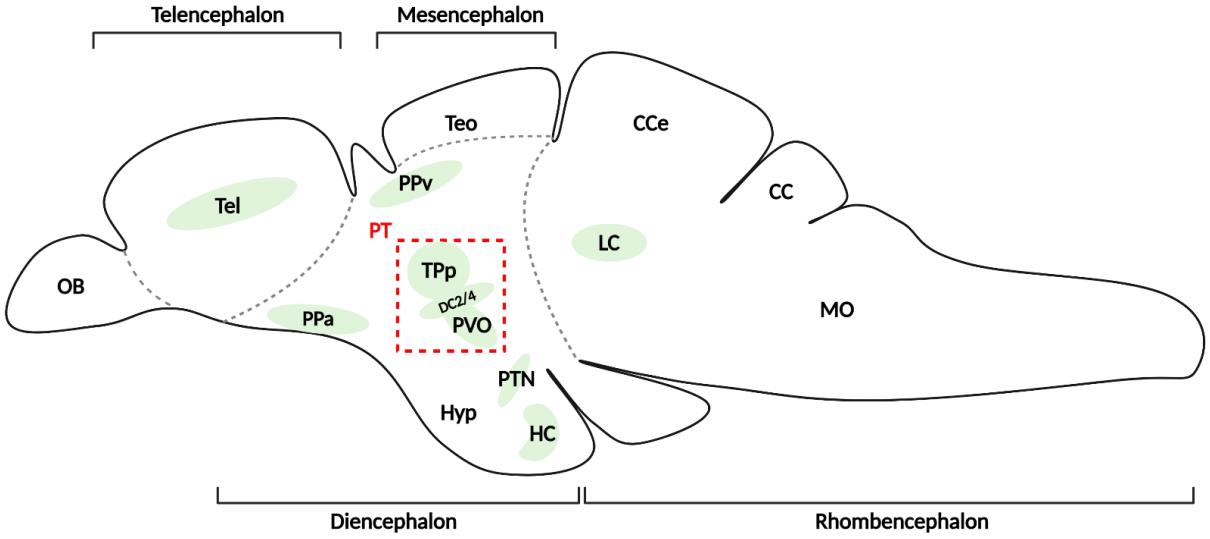


**Figure 4-8. Schematic representation of tyrosine hydroxylase-positive ($TH^+$) neuronal populations in the adult zebrafish brain**

The illustration depicts a sagittal section highlighting the distribution of $TH^+$ cells (oval green) selected in this study. OB: olfactory bulb; Tel: telencephalon. The diencephalon contains parvocellular preoptic nucleus (PPa), periventricular pretectal nucleus (PPv), posterior tuberculum (PT), periventricular nucleus of the posterior tuberculum (TPp), diencephalic neuronal clusters (DC) 2 and 4, paraventricular organ (PVO), posterior tuberal nucleus (PTN), hypothalamus (Hyp), and caudal zone of periventricular hypothalamus (HC). The mesencephalon includes tectum opticum (Teo). The rhombencephalon comprises corpus cerebelli (CCe), crista cerebellaris (CC), locus coeruleus (LC), and medulla oblongata (MO).

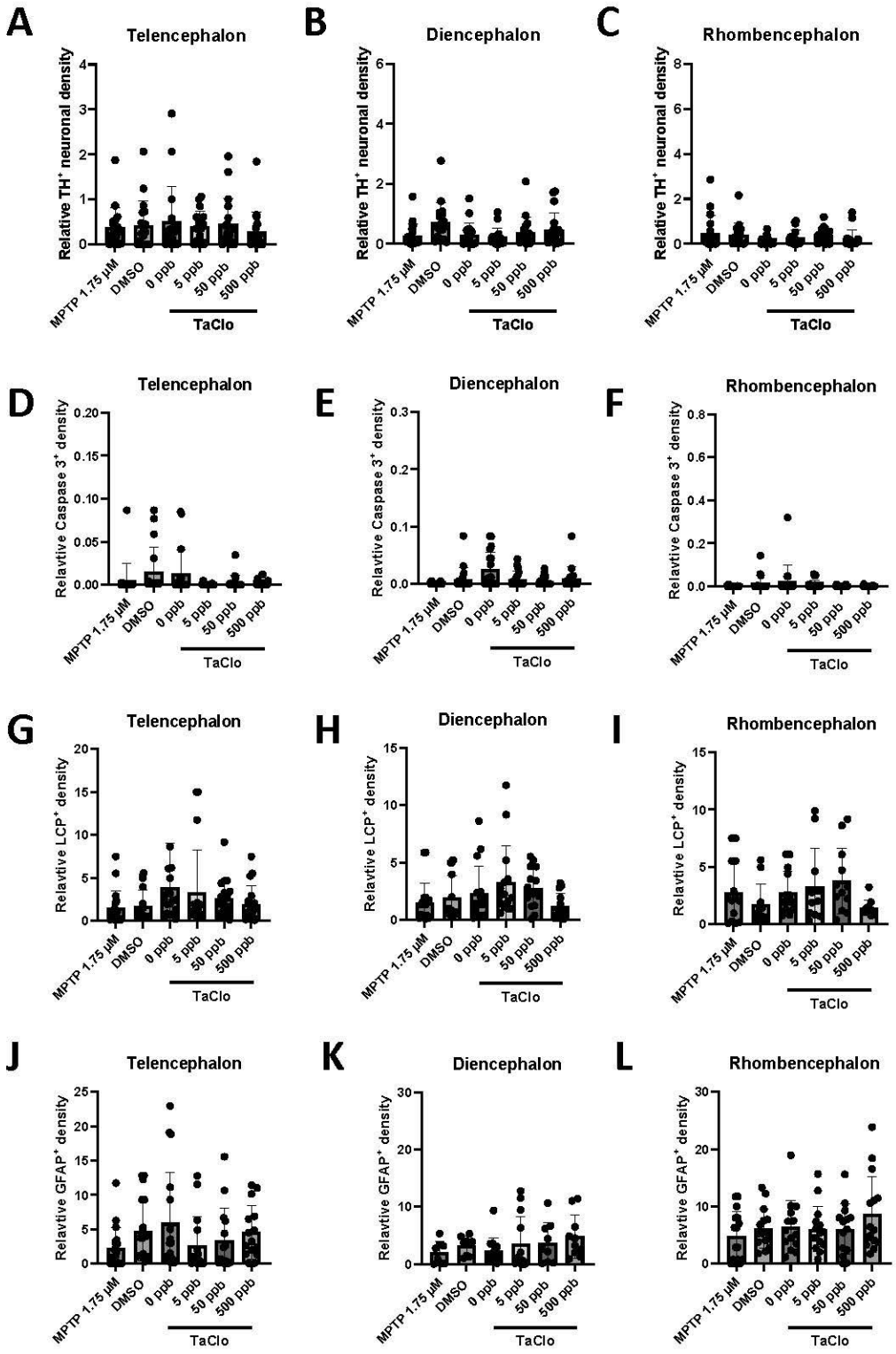


**Figure 4-9. Expression assessment of dopaminergic neurons, apoptosis, macrophages, and astrocytes at telencephalon, diencephalon, and rhombencephalon in 6 months post-fertilization zebrafish (mpf)**

Quantitative analysis of immunofluorescence images to assess the relative density of tyrosine hydroxylase ($TH^+$) labeled dopaminergic neurons, caspase-3 marked apoptotic bodies, lymphocyte cytosolic protein 1 (L-plastin/LCP) labeled macrophage, and glial fibrillary acidic protein (GFAP)-labeled astrocyte at telencephalon, diencephalon, and rhombencephalon. No significant differences in $TH^+$ dopaminergic neurons (A-C), apoptosis (D-F), macrophages (G-I), and astrocytes (J-L) were observed in 6 mpf zebrafish treated with 1-trichloromethyl-1,2,3,4-tetrahydro-beta-carboline (TaClo) and 1.75 μM 1-methyl-4-phenyl-1,2,3,6-tetrahydropyridine (MPTP) in each brain region. Six biological replicates, six subsamples per replicate per treatment. Error bars represent standard deviation. All data were analyzed using Kruskal-Wallis test, followed by Dunn's multiple comparison test.

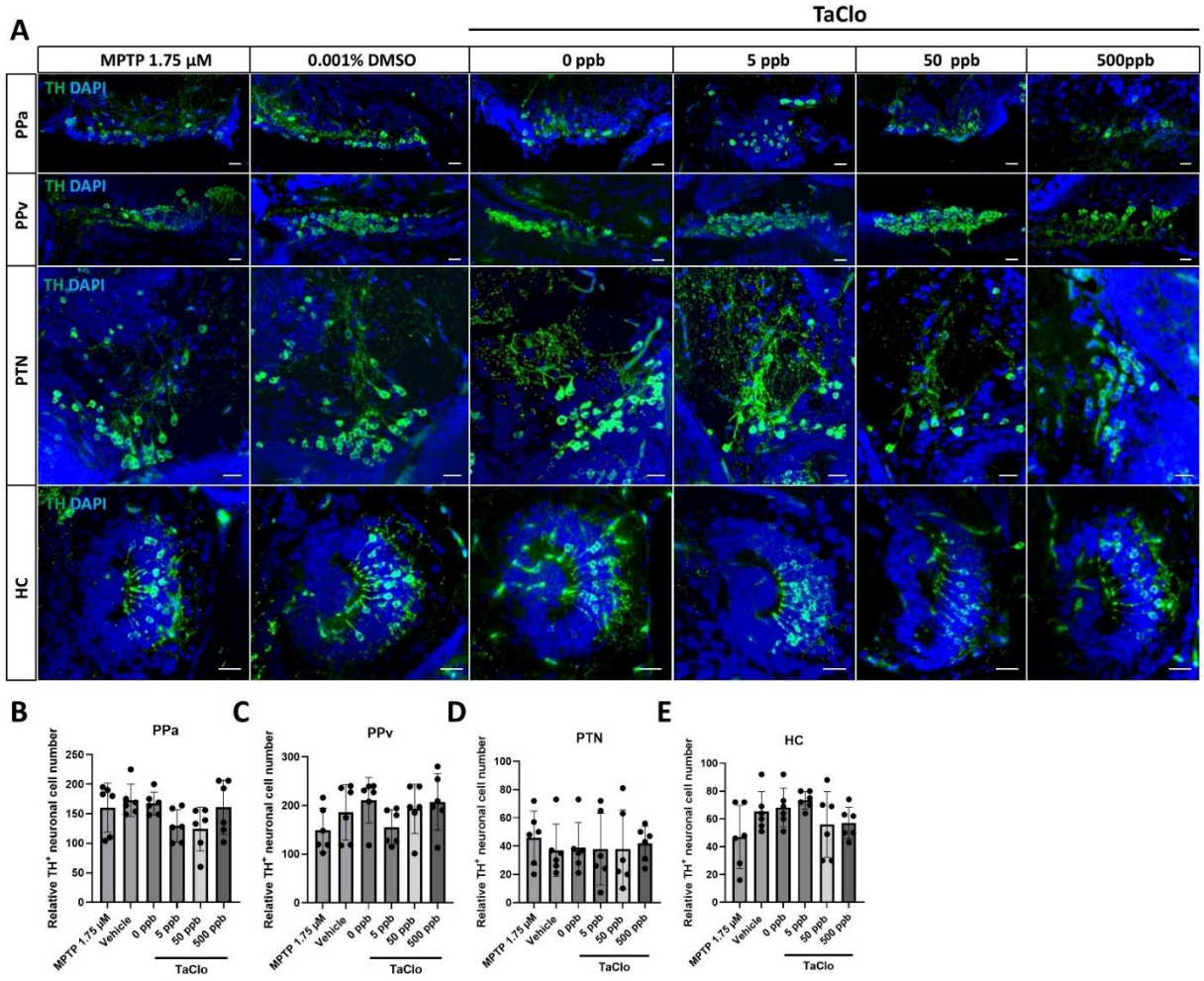


**Figure 4-10. TH$^+$ diencephalic dopaminergic neuronal expression in 6 mpf zebrafish**
Representative immunofluorescence images of TH in 1.75 µM MPTP, vehicle (0.001% DMSO), and TaClo (0, 5, 50, 500 ppb) exposure groups at the parvocellular preoptic nucleus (PPa), periventricular pretectal nucleus (PPv), posterior tuberal nucleus (PTN), and caudal zone of periventricular hypothalamus (HC). TH-positive cells are shown in green. DAPI-highlighted cell nuclei are marked in blue. PPa and PPv scale bar=20 µm. PTN and HC scale bar=100 µm (A). Image analysis of treated 6 mpf zebrafish diencephalon demonstrates no significant changes in relative TH+ dopaminergic neuron in PPa (B), PPv (C), PTN (D), and HC (E) among exposure groups. Six biological replicates, one subsample per replicate per treatment. Error bars represent standard deviation. All data were analyzed using Kruskal-Wallis test, followed by Dunn's multiple comparison test.

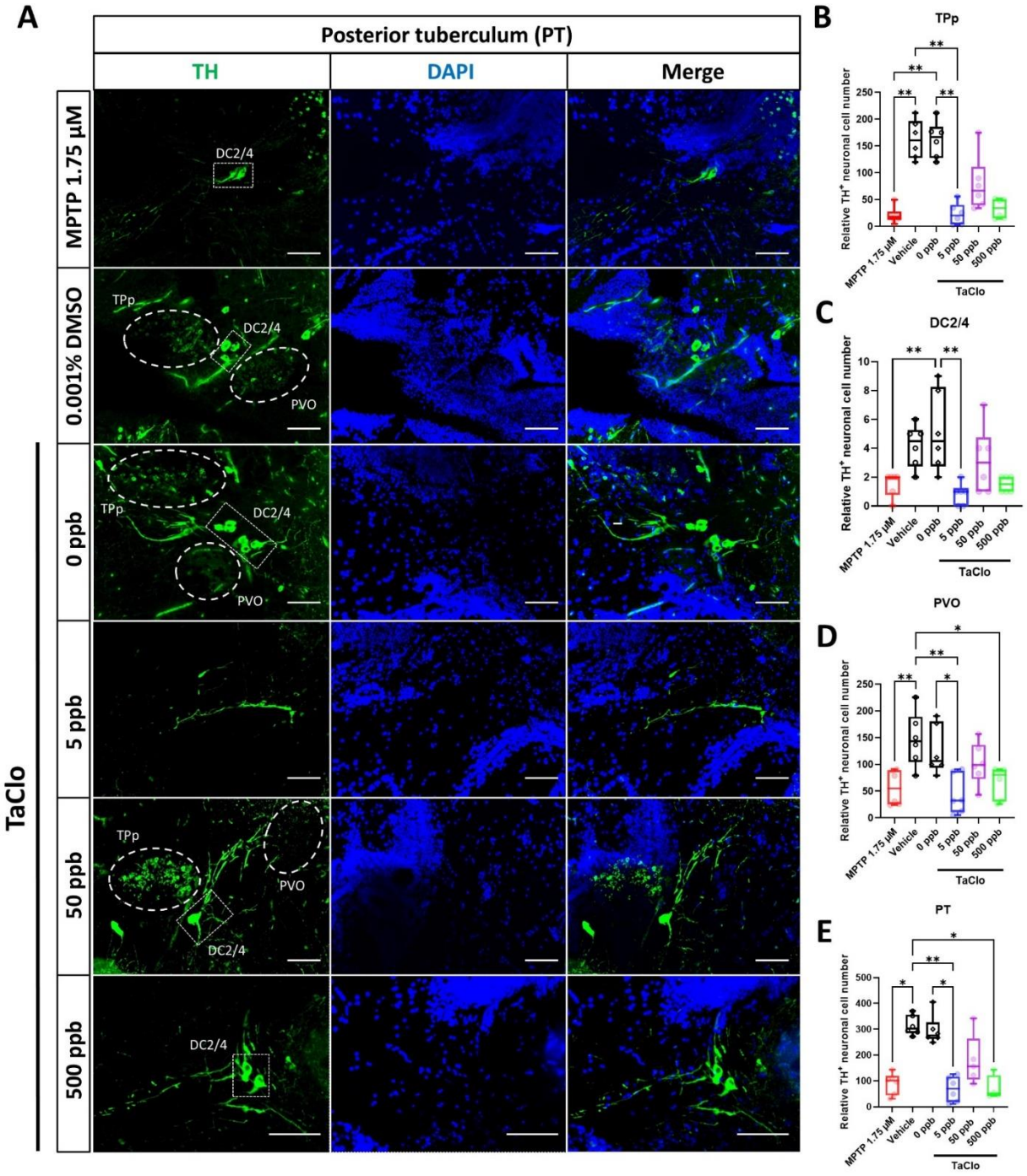
A
Posterior tuberculum (PT)
TH
DAPI
Merge
MPTP 1.75 μM
0.001% DMSO
0 ppb
5 ppb
50 ppb
500 ppb
TaClo
DC2/4
TPp
PVO
B
TPp
C
DC2/4
D
PVO
E
PT
Relative TH+ neuronal cell number
MPTP 1.75 μM
Vehicle
0 ppb
5 ppb
50 ppb
500 ppb
TaClo

**Figure 4-11. Early-life exposure to TaClo and MPTP led to persistent diencephalic neuronal damage into adulthood**

0-120 hpf embryonic zebrafish exposed to vehicle (0.001% DMSO), TaClo (0, 5, 50, 500 ppb), or 1.75 μM MPTP were assessed at 6 mpf for diencephalic $TH^+$ neuronal expression. Representative sagittal sections of the posterior tuberculum (PT) in immunofluorescence assay showing tyrosine hydroxylase labeling cells (TH, green) and cell nuclei (DAPI, blue). TPp and PVO neuronal populations are marked with an oval white dashed line. White square dashed lines highlight DC2/4 cells. Scale bar=100 μm (A). Quantitative analyses across neuronal populations at TPp (B), DC2/4 (C), PVO (D), and PT (E) showed that the relative TH+ dopaminergic neuronal numbers significantly decreased in TaClo (5 ppb) and MPTP at 6 mpf in TPp (B) and DC2/4 population (C) compared to the control (TaClo 0 ppb) and vehicle. Additionally, TaClo (5 ppb and 500 ppb) and MPTP treated zebrafish at 6 mpf showed significantly reduced relative TH+ dopaminergic neuronal numbers in PVO (D) and PT (E) regions compared to the control (TaClo 0 ppb) and vehicle. Data are expressed as mean ± standard deviation. All data were analyzed using Kruskal-Wallis test, followed by Dunn's multiple comparison test. *$p \leq 0.05$ and **$p \leq 0.001$.

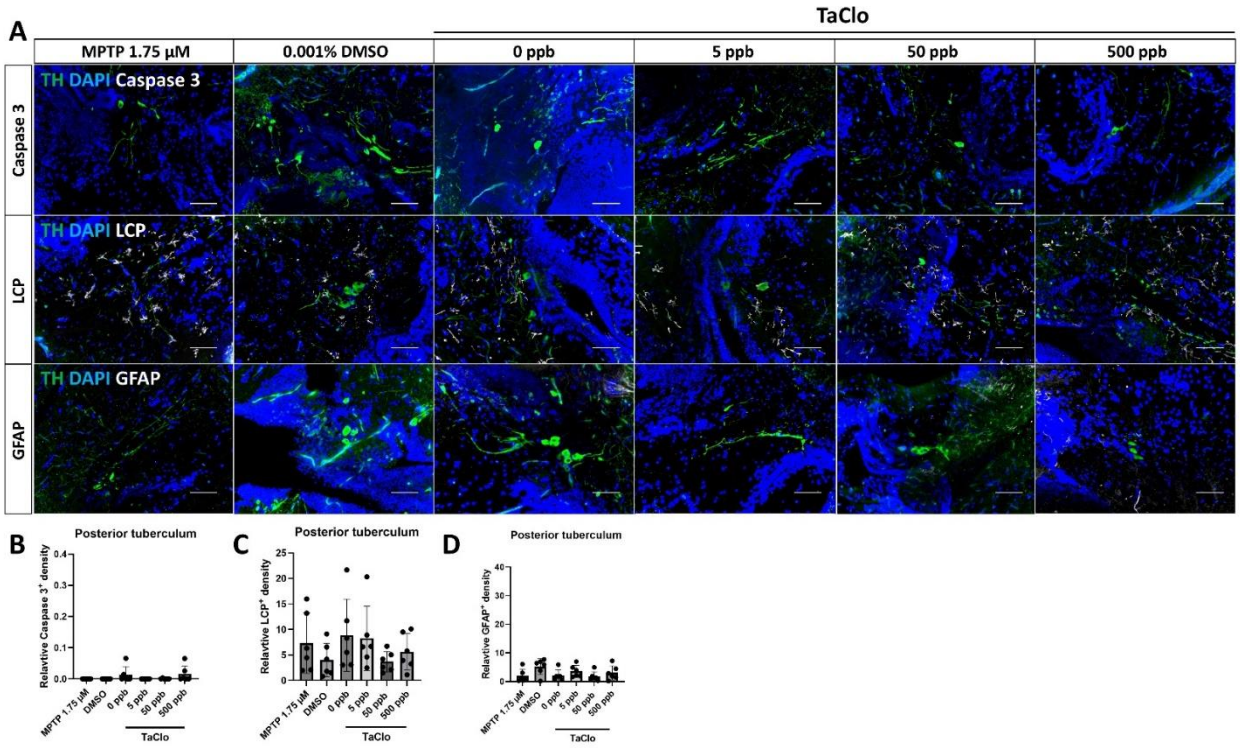


**Figure 4-12. Apoptosis and neuroinflammatory expression at posterior tuberculum (PT) at 6 mpf zebrafish**

Representative double immunofluorescence images of TH (upper, middle, and lower panel), caspase 3 (upper panel), L-plastin (LCP) (middle panel), and glial fibrillary acidic protein (GFAP) (lower panel) in 1.75 µM MPTP, vehicle (0.001% DMSO), and TaClo (0, 5, 50, 500 ppb) exposure groups at posterior tuberculum in 6 mpf zebrafish. TH-positive and caspase 3/LCP/GFAP-positive cells are shown in green and white, respectively. Cell nuclei are marked in white. Scale bar=100 µm (A). No significant changes of relative caspase-3 labeled apoptotic bodies (B), LCP-labeled macrophage (C), and GFAP-labeled astrocytes (D) are observed at PT in 6 mpf zebrafish. Six biological replicates, one subsample per replicate per treatment. Error bars represent standard deviation. All data were analyzed using Kruskal-Wallis test, followed by Dunn's multiple comparison test.

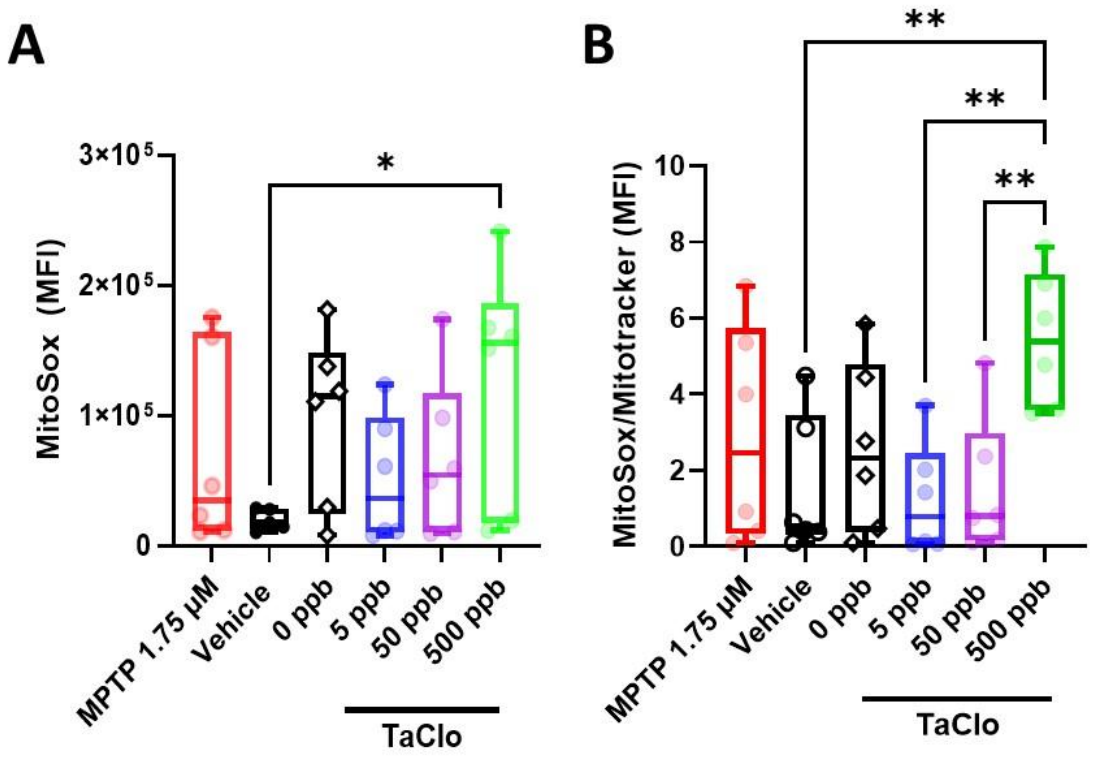


**Figure 4-13. TaClo (500 ppb) exposure at 0-120 hpf stimulated mitochondrial reactive oxygen species (ROS) generation in 6 mpf zebrafish brain**

MitoSox Red and Mitotracker Deep Red-based flow cytometric detection of mitochondrial ROS production and mitochondrial membrane potential in 6 mpf zebrafish brain, respectively. Quantitative analyses on median fluorescent intensity (MFI) demonstrated that 500 ppb TaClo exposure group showed a significant increase in mitochondrial ROS levels compared to vehicle (0.001% DMSO)(A) and an increased ratio of mitochondrial ROS level and mitochondrial membrane potential to vehicle group (B). Data are expressed as mean ± standard deviation. All data were analyzed using one-way ANOVA, followed by Tukey's multiple comparison test. *$p \leq 0.05$ and **$p \leq 0.001$.

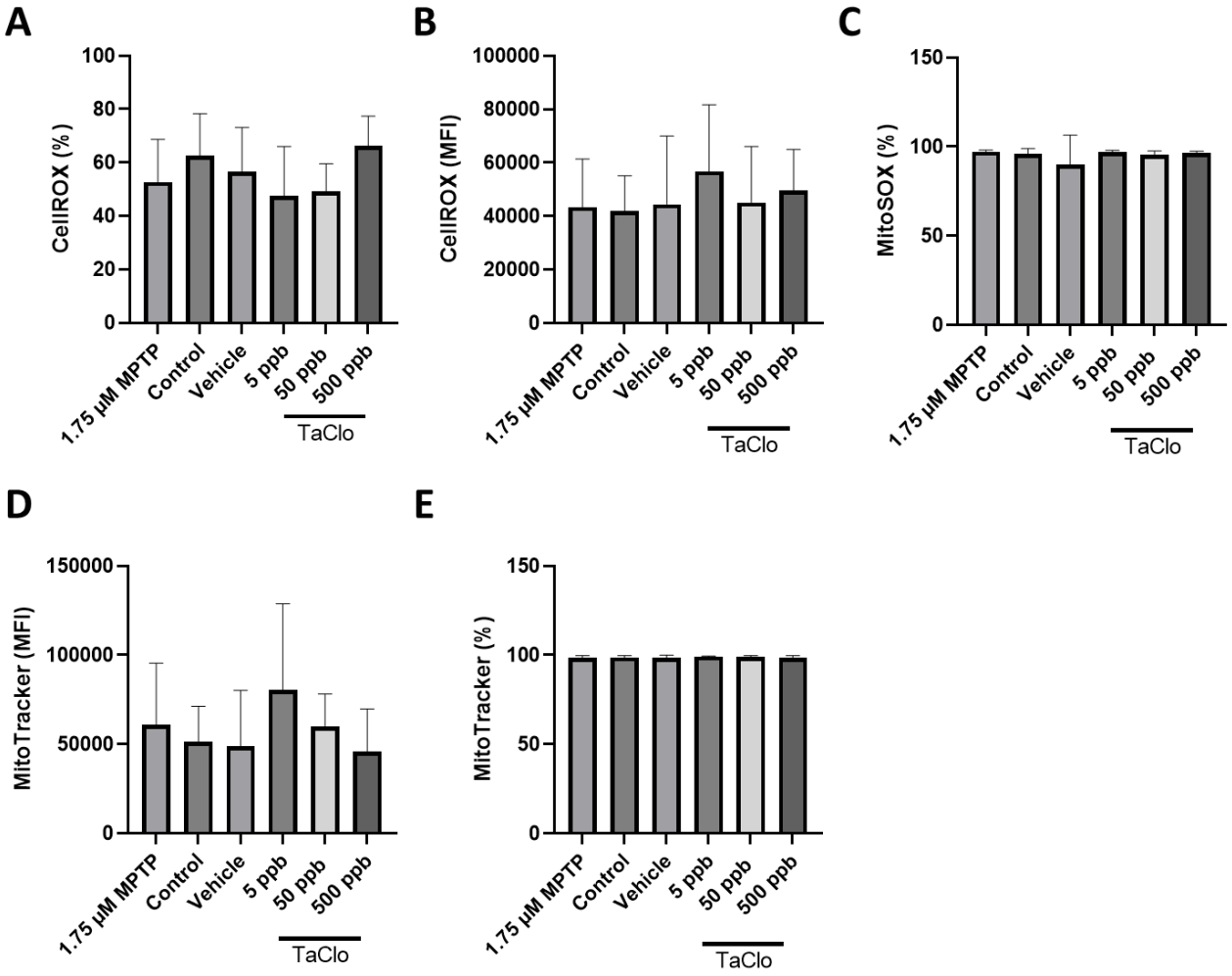


**Figure 4-14. Flow cytometry analysis of CellROX, MitoSox, and MitoTracker in 6 mpf zebrafish brain**

No significant differences were observed in early life TaClo (5, 50, 500 ppb) and 1.75 µM MPTP-treated 6 mpf zebrafish brain in CellRox (% and MPI) (A-B), MitoSox (%) (C), and MitoTracker (MFI and %) (E). Data are expressed as mean ± standard deviation. All data were analyzed using one-way ANOVA, followed by Tukey's multiple comparison test.

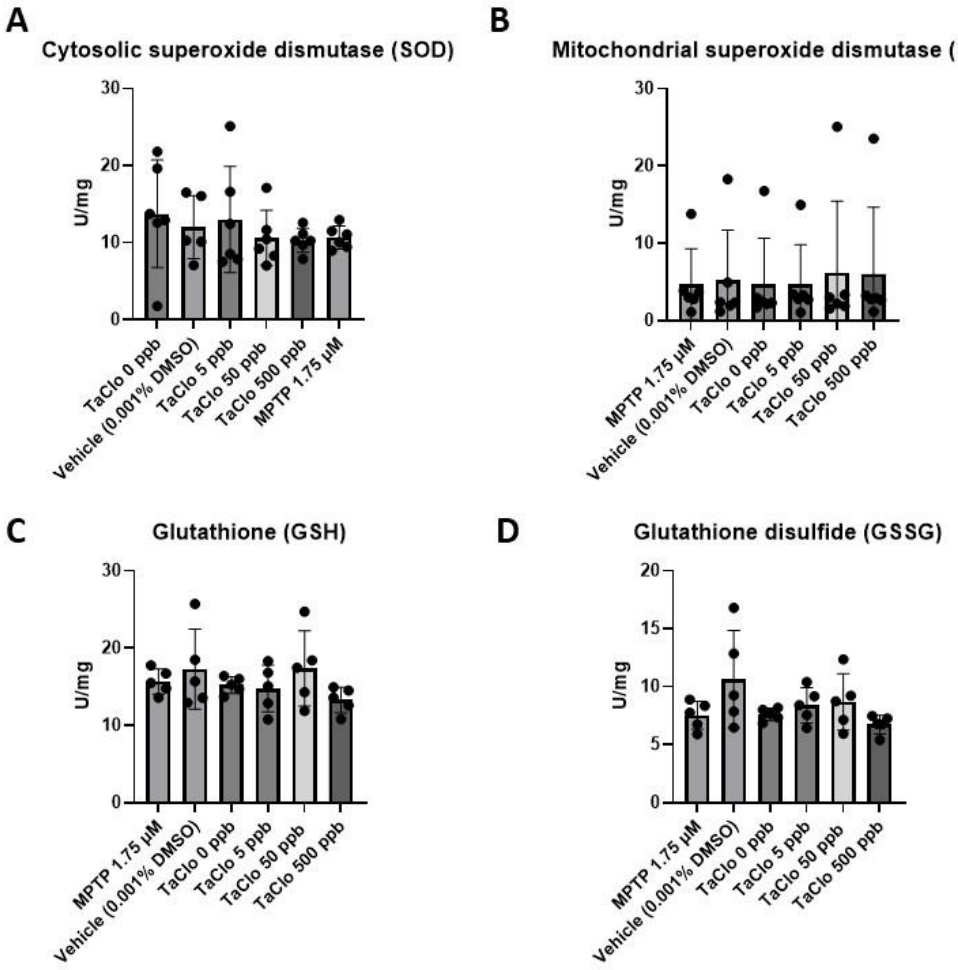


**Figure 4-15. Antioxidative enzymatic activity levels in 6 mpf zebrafish brain**

No significant alterations were observed in cytosolic superoxide dismutase (SOD) (A), mitochondrial superoxide dismutase (SOD)(B), glutathione (GSH)(C), and glutathione disulfide (GSSG)(D) in 6 mpf zebrafish brain following the embryonic exposure to TaClo (vehicle, 0, 5, 50, 500 ppb) and 1.75 µM MPTP. Six biological replicates, six subsamples per treatment per replicate. Error bars represent standard deviation. All antioxidative enzyme data are normalized and are expressed as U (nmol/min/ml of protein)/mg. All data were analyzed using Kruskal-Wallis test, followed by Dunn's multiple comparison test.

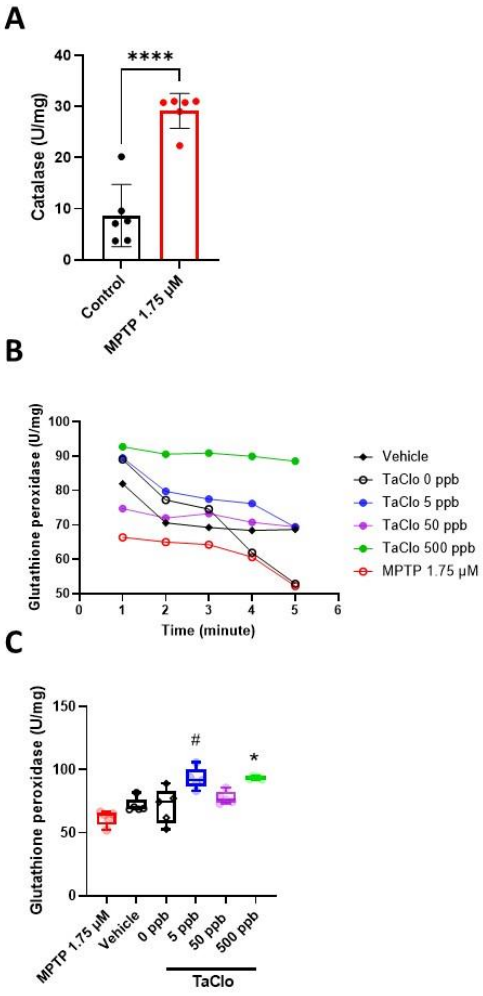


**Figure 4-16. Developmental exposure to TaClo and MPTP altered antioxidative enzymatic activities of catalase and glutathione peroxidase (GPX) levels in 6 mpf zebrafish brain**

6 mpf zebrafish brain demonstrated a higher catalase activity level in the 1.75 µM MPTP treated group compared to control ($p \leq 0.0001$)(A). A schematic image of GPX activity across five-time points measured every minute (1-5 minutes) (A) and the overall GPX activity levels (C) in the vehicle (0.001% DMSO), TaClo (0, 5, 50, 500 ppb), and 1.75 µM MPTP of 6 mpf zebrafish brain. TaClo (500 ppb) appeared to have the highest GPX level across five minutes (B). *: 500 ppb TaClo had a significantly elevated level compared to control (TaClo 0 ppb, $p \leq 0.001$), vehicle ($p \leq 0.001$), TaClo 50 ppb ($p \leq 0.05$), and 1.75 µM MPTP ($p \leq 0.0001$). #: TaClo 5 ppb exposed group showed an increased GPX activity compared to control ($p \leq 0.001$), vehicle ($p \leq 0.001$), 50 ppb TaClo ($p \leq 0.05$), and 1.75 µM MPTP ($p \leq 0.0001$). All catalase and GPX data are normalized and are expressed as U (nmol/min/ml of protein)/mg. Data are expressed as mean ± standard deviation. All data were analyzed by one-way ANOVA test, followed by Tukey's post hoc test.

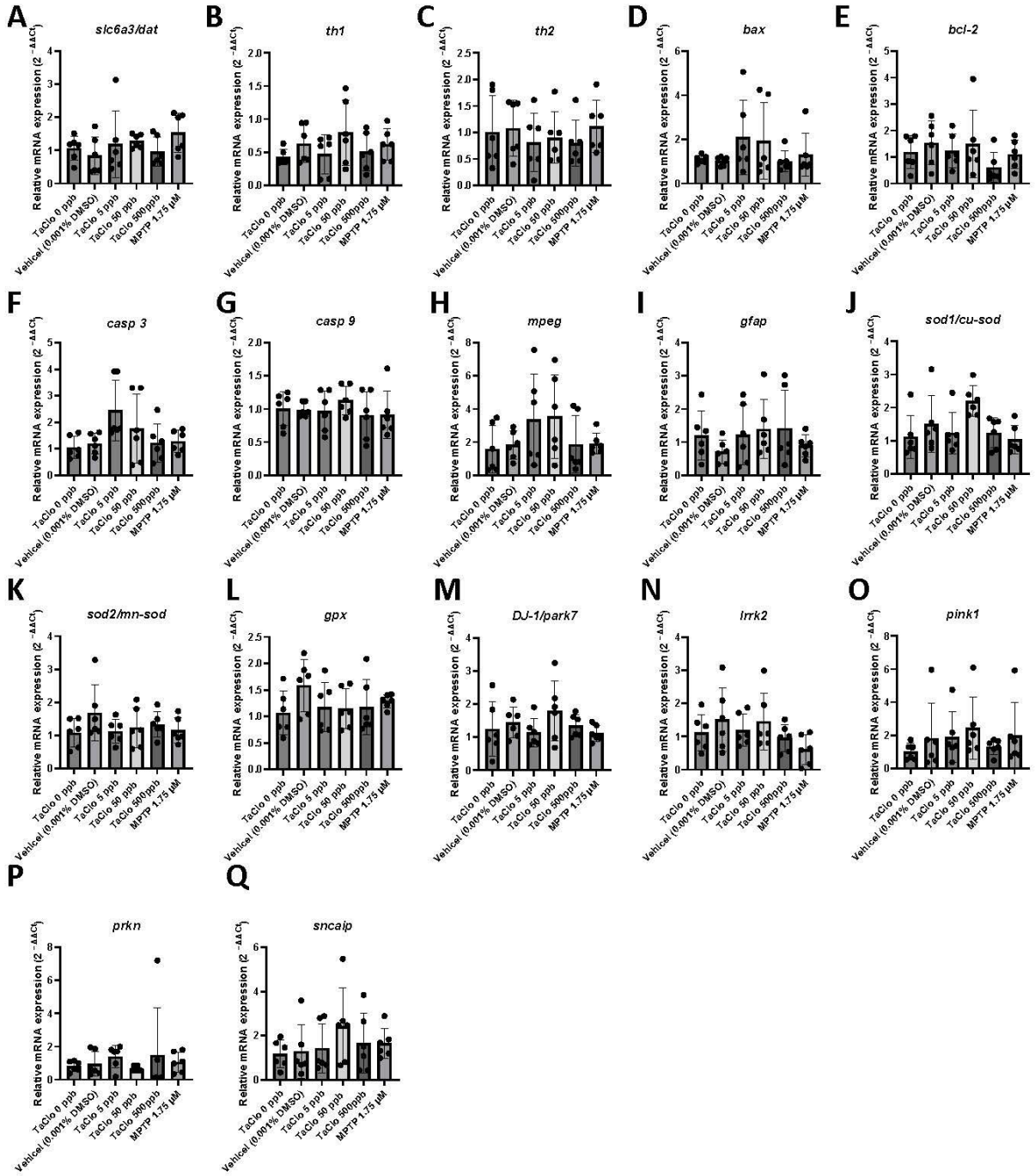


**Figure 4-17. Relative mRNA expression of 6 mpf zebrafish brain following embryonic exposure to TaClo (vehicle, 0, 5, 50, 500 ppb) and 1.75 µM MPTP**

No significant findings in *slc6a3/dat* (A), *th1* (B), *th2* (C), *bax* (D), *bcl-2* (E), *casp 3* (F), *casp 9* (G), *mpeg* (H), *gfap* (I), *sod1/cu-sod* (J), *sod2/mn-sod* (K), *gpx* (L), *DJ/park7* (M), *lrrk2* (N), *pink1* (O), *parkn* (P), and *sncaip* (Q). Six biological replicates, up to 50 larvae per treatment per replicate. Error bars represent standard deviation. All data were analyzed using Kruskal-Wallis

test, followed by Dunn's multiple comparison test. *slc6a3 (solute carrier family 6 member 3)/dat (dopamine transporter), th1* (*tyrosine hydroxylase 1*), *th2* (*tyrosine hydroxylase 2*), *bax (BCL2 associated X), bcl2 (B-cell leukemia/lymphoma 2 protein), casp 3 (caspase 3), casp 9 (caspase 9), mpeg (macrophage-expressed gene), gfap* (*glial fibrillary acidic protein*), *sod1/cu-sod* (*Cu superoxide dismutase*), *sod2/mn-sod* (*manganese superoxide dismutase*), *gpx* (*glutathione peroxidase*), *cat (catalase), lrrk2* (*leucine-rich repeat kinase 2*), *sncaip* (*alpha interacting protein*), *pink 1(PTEN-induced putative kinase 1*), and *prkn* (*parkin RBR E3 ubiquitin protein ligase*).

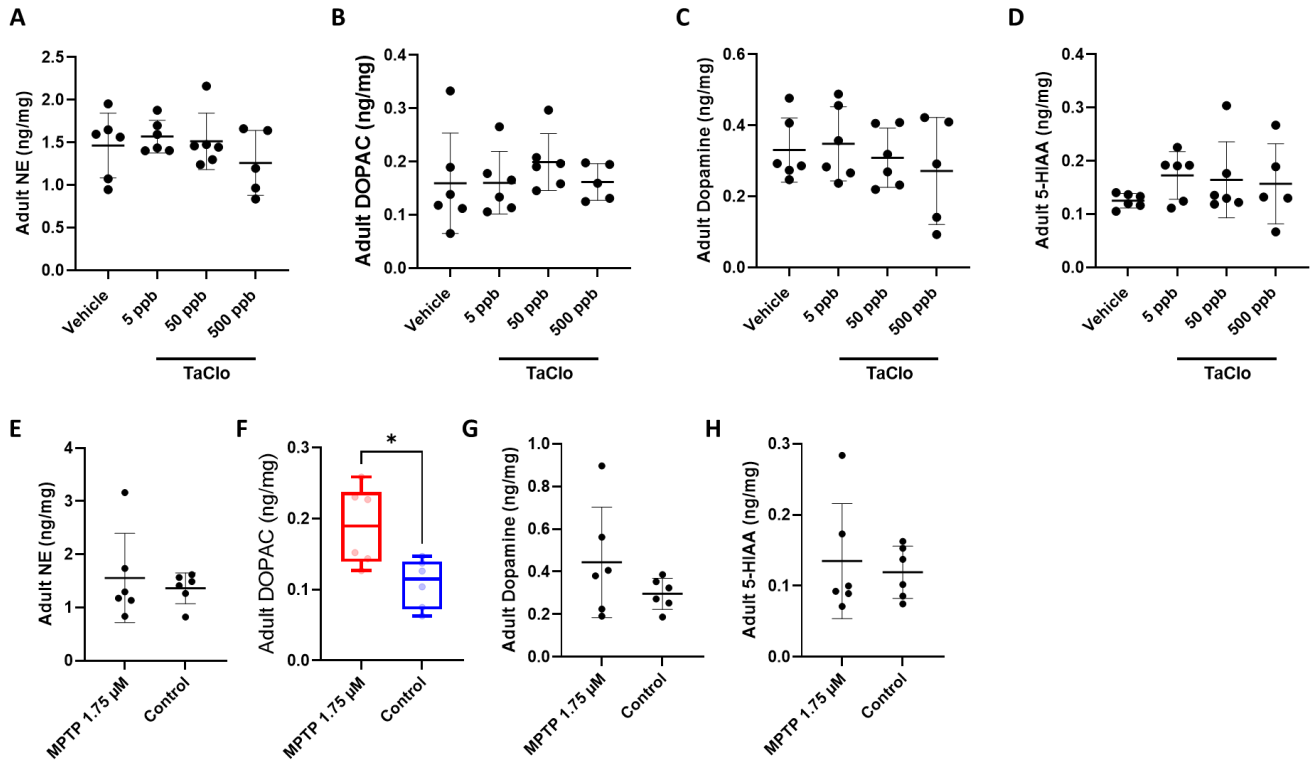


**Figure 4-18. Neurotransmitter levels in TaClo (vehicle, 0, 5, 50, 500 ppb) and 1.75 µM MPTP treated 6 mpf zebrafish brain**

Norepinephrine, 3,4-Dihydroxyphenylacetic acid (DOPAC), dopamine, and 5-hydroxyindoleacetic acid (5-HIAA) levels were evaluated in the 6 mpf zebrafish brain. No significant differences of norepinephrine (A), DOPAC (B), dopamine (C), and 5-HIAA (D) in TaClo treated 6 mpf zebrafish brain. No significant differences of norepinephrine (E), dopamine (G), and 5-HIAA (H) in 1.75 µM MPTP treated 6 mpf zebrafish brain. Embryonic exposure to 1.75 µM MPTP resulted in significantly increased in the 6 mpf zebrafish brain (F) compared to the control group. Error bars represent standard deviation. * significant difference from the control with $p \leq 0.05$. Data are expressed as mean ± standard deviation. All data were analyzed by one-way ANOVA test, followed by Tukey's post hoc test.

**Table 4-1. Commercially available antibodies labeling zebrafish protein in this study**

| Primary antibody | Host | Antibody type | Antibody labeled | Dilution | Company/Catalog |
|---|---|---|---|---|---|
| Anti-mCherry antibody | Rabbit | Polyclonal IgG | cross-reacts with tdTomato and mOrange | 1:500 | Abcam/ab167453 |
| Caspase 3 | Rabbit | monoclonal IgG | active form caspase-3 | 1:500 | BD Pharmingen™/559565 |
| Glial Fibrillary Acidic Protein | Rabbit | Polyclonal | cytoskeleton in astrocytes | 1:500 | Agilent Dako/Z0334 |
| Lymphocyte cytosolic protein 1 | Rabbit | | Pan-leukocyte | 1:500 | GeneTex/GTX124420 |
| Tyrosine hydroxylase | Mouse | Monoclonal IgG1κ | catecholaminergic cells | 1:500 | Milipore sigma/MAB318 |

| Secondary antibody | Host | Antibody type | Species Reactivity | Dilution | Company/Catalog |
|---|---|---|---|---|---|
| Alexa Fluor™ 488 | Goat | Polyclonal IgG (H+L) | Mouse | 1:500 | Thermofisher scientific/ # A-11029 |
| Alexa Fluor™ 647 | Goat | Polyclonal IgG (H+L) | Rabbit | 1:500 | Thermofisher scientific/ # A-21244 |

**Table 4-2. Relative tyrosine hydroxylase immunolabeling neuronal cellular numbers in immunofluorescence assay**

| | Control<br>(Mean ± Standard deviation) | Vehicle (0.001% DMSO)<br>(Mean ± Standard deviation) | 5 ppb TaClo<br>(Mean ± Standard deviation) | 500 ppb TaClo<br>(Mean ± Standard deviation) | 1.75 µM MPTP<br>(Mean ± Standard deviation) |
|---|---|---|---|---|---|
| Posterior tuberculum (PT) | 295.5 ± 56.3 | 314.5 ± 38.4 | 68.2 ± 48.9<br>(21.6% reduction to vehicle) | 71 ± 48.4<br>(22.6% reduction to vehicle) | 89.5 ± 41.8<br>(28.4% reduction to vehicle) |
| Periventricular nucleus of the posterior tuberculum (TPP) | 162 ± 33.8 | 162.3 ± 36.20 | 23.2 ± 20.3<br>14.3 to control<br>(14.27% reduction to vehicle) | | 21 ± 15.3<br>(12.96 % reduction to control)<br>(12.94 % reduction to vehicle) |
| Diencephalic neuronal population (DC) 2/4 | 5.2 ± 2.8 | 4.2 ± 1.5 | 0.8 ± 0.8<br>(16.1 % reduction to control) | | 1.5 ± 0.3<br>(0.29 to control) |
| Paraventricular organ (PVO) | 126.5 ± 46.06 | 147 ± 51.5 | 43.5 ± 36.9<br>(29.5 % reduction to vehicle) | 66.7 ± 30.0<br>(52.7% reduction to vehicle) | 56.7 ± 32.8<br>(44.8% reduction to vehicle) |

**References**


Agnihotri, S. K., Sun, L., Yee, B. K., Shen, R., Akundi, R. S., Zhi, L., Duncan, M. J., Cass, W. A., & Büeler, H. (2019). PINK1 deficiency is associated with increased deficits of adult hippocampal neurogenesis and lowers the threshold for stress-induced depression in mice. *Behavioural Brain Research*, *363*, 161-172. https://doi.org/https://doi.org/10.1016/j.bbr.2019.02.006

Bajpai, P., Sangar, M. C., Singh, S., Tang, W., Bansal, S., Chowdhury, G., Cheng, Q., Fang, J. K., Martin, M. V., Guengerich, F. P., & Avadhani, N. G. (2013). Metabolism of 1-methyl-4-phenyl-1,2,3,6-tetrahydropyridine by mitochondrion-targeted cytochrome P450 2D6: implications in Parkinson disease. *J Biol Chem*, *288*(6), 4436-4451. https://doi.org/10.1074/jbc.M112.402123

Bispo, J. M. M., Melo, J. E. C., Gois, A. M., Leal, P. C., Lins, L., Souza, M. F., Medeiros, K., Ribeiro, A. M., Silva, R. H., Marchioro, M., & Santos, J. R. (2019). Sex differences in the progressive model of parkinsonism induced by reserpine in rats. *Behav Brain Res*, *363*, 23-29. https://doi.org/10.1016/j.bbr.2019.01.041

Boekelheide, K., Blumberg, B., Chapin, R. E., Cote, I., Graziano, J. H., Janesick, A., Lane, R., Lillycrop, K., Myatt, L., States, J. C., Thayer, K. A., Waalkes, M. P., & Rogers, J. M. (2012). Predicting later-life outcomes of early-life exposures. *Environ Health Perspect*, *120*(10), 1353-1361. https://doi.org/10.1289/ehp.1204934

Bringmann, G., God, R., Fähr, S., Feineis, D., Fornadi, K., & Fornadi, F. (1999). Identification of the dopaminergic neurotoxin 1-trichloromethyl-1,2, 3,4-tetrahydro-beta-carboline in human blood after intake of the hypnotic chloral hydrate. *Anal Biochem*, *270*(1), 167-175. https://doi.org/10.1006/abio.1999.4088

Bustin, S. A., Benes, V., Garson, J. A., Hellemans, J., Huggett, J., Kubista, M., Mueller, R., Nolan, T., Pfaffl, M. W., Shipley, G. L., Vandesompele, J., & Wittwer, C. T. (2009). The MIQE guidelines: minimum information for publication of quantitative real-time PCR experiments. *Clin Chem*, *55*(4), 611-622. https://doi.org/10.1373/clinchem.2008.112797

Caldwell, L. J., Davies, N. O., Cavone, L., Mysiak, K. S., Semenova, S. A., Panula, P., Armstrong, J. D., Becker, C. G., & Becker, T. (2019). Regeneration of Dopaminergic Neurons in Adult Zebrafish Depends on Immune System Activation and Differs for

Distinct Populations. *J Neurosci*, *39*(24), 4694-4713. https://doi.org/10.1523/jneurosci.2706-18.2019

Cattaneo, C., & Pagonabarraga, J. (2025). Sex Differences in Parkinson's Disease: A Narrative Review. *Neurol Ther*, *14*(1), 57-70. https://doi.org/10.1007/s40120-024-00687-6

Cerri, S., Mus, L., & Blandini, F. (2019). Parkinson's Disease in Women and Men: What's the Difference? *J Parkinsons Dis*, *9*(3), 501-515. https://doi.org/10.3233/jpd-191683

Chen, J., Sanchez-Iranzo, H., Diotel, N., & Rastegar, S. (2024). Comparative insight into the regenerative mechanisms of the adult brain in zebrafish and mouse: highlighting the importance of the immune system and inflammation in successful regeneration. *Febs j*, *291*(19), 4193-4205. https://doi.org/10.1111/febs.17231

Chiu, W. A., Jinot, J., Scott, C. S., Makris, S. L., Cooper, G. S., Dzubow, R. C., Bale, A. S., Evans, M. V., Guyton, K. Z., Keshava, N., Lipscomb, J. C., Barone, S., Jr., Fox, J. F., Gwinn, M. R., Schaum, J., & Caldwell, J. C. (2013). Human health effects of trichloroethylene: key findings and scientific issues. *Environ Health Perspect*, *121*(3), 303-311. https://doi.org/10.1289/ehp.1205879

de Abreu, M. S., Demin, K. A., Giacomini, A., Amstislavskaya, T. G., Strekalova, T., Maslov, G. O., Kositsin, Y., Petersen, E. V., & Kalueff, A. V. (2021). Understanding how stress responses and stress-related behaviors have evolved in zebrafish and mammals. *Neurobiol Stress*, *15*, 100405. https://doi.org/10.1016/j.ynstr.2021.100405

de Abreu, M. S., Giacomini, A., Dos Santos, B. E., Genario, R., Marchiori, N. I., Rosa, L. G. D., & Kalueff, A. V. (2019). Effects of lidocaine on adult zebrafish behavior and brain acetylcholinesterase following peripheral and systemic administration. *Neurosci Lett*, *692*, 181-186. https://doi.org/10.1016/j.neulet.2018.11.004

Dong, H., Mao, L., Bai, C., Ye, K., Wu, H., Lei, Y., Yu, S., Liu, Y., Tao, J., Pan, W., Xu, H., Lin, J., Zhu, J., & Dong, Q. (2022). Characterization of Developmental Neurobehavioral Toxicity in a Zebrafish MPTP-Induced Model: A Novel Mechanism Involving Anemia. *ACS Chemical Neuroscience*, *13*(13), 1877-1890. https://doi.org/10.1021/acschemneuro.2c00089

Dong, H., Wu, H., Bai, C., Ye, K., Mao, L., Lei, Y., Liu, Y., Xu, H., Lin, J., Zhu, J., & Dong, Q. (2022). Transient MPTP exposure at a sensitive developmental window altered gut

microbiome and led to male-biased motor and social behavioral deficits in adult zebrafish. *Neurotoxicology*, *91*, 360-368. https://doi.org/10.1016/j.neuro.2022.06.008

Dorsey, E. R., Zafar, M., Lettenberger, S. E., Pawlik, M. E., Kinel, D., Frissen, M., Schneider, R. B., Kieburtz, K., Tanner, C. M., De Miranda, B. R., Goldman, S. M., & Bloem, B. R. (2023). Trichloroethylene: An Invisible Cause of Parkinson's Disease? *J Parkinsons Dis*, *13*(2), 203-218. https://doi.org/10.3233/jpd-225047

Fontana, B. D., Cleal, M., & Parker, M. O. (2020). Female adult zebrafish (Danio rerio) show higher levels of anxiety-like behavior than males, but do not differ in learning and memory capacity. *Eur J Neurosci*, *52*(1), 2604-2613. https://doi.org/10.1111/ejn.14588

Fukuda, H., Hara, K., Nakamura, S., Kimura, H., & Kameyama, M. (1988). 1-Methyl-4-phenyl-1,2,3,6-tetrahydropyridine (MPTP) enhances tryptophan hydroxylase activity in mouse striatum, but not in the frontal cortex. *Brain Res*, *449*(1-2), 399-402. https://doi.org/10.1016/0006-8993(88)91063-3

Gao, D., Wang, C., Xi, Z., Zhou, Y., Wang, Y., & Zuo, Z. (2017). Early-Life Benzo[a]Pyrene Exposure Causes Neurodegenerative Syndromes in Adult Zebrafish (Danio rerio) and the Mechanism Involved. *Toxicol Sci*, *157*(1), 74-84. https://doi.org/10.1093/toxsci/kfx028

Gash, D. M., Rutland, K., Hudson, N. L., Sullivan, P. G., Bing, G., Cass, W. A., Pandya, J. D., Liu, M., Choi, D. Y., Hunter, R. L., Gerhardt, G. A., Smith, C. D., Slevin, J. T., & Prince, T. S. (2008). Trichloroethylene: Parkinsonism and complex 1 mitochondrial neurotoxicity. *Ann Neurol*, *63*(2), 184-192. https://doi.org/10.1002/ana.21288

Ghysen, A., & Dambly-Chaudière, C. (2004). Development of the zebrafish lateral line. *Current Opinion in Neurobiology*, *14*(1), 67-73. https://doi.org/https://doi.org/10.1016/j.conb.2004.01.012

Glazer, L., & Brennan, C. H. (2021). Developmental Exposure to Low Concentrations of Methylmercury Causes Increase in Anxiety-Related Behaviour and Locomotor Impairments in Zebrafish. *Int J Mol Sci*, *22*(20). https://doi.org/10.3390/ijms222010961

Han, E., Ho Oh, K., Park, S., Chan Rah, Y., Park, H. C., Koun, S., & Choi, J. (2020). Analysis of behavioral changes in zebrafish (Danio rerio) larvae caused by aminoglycoside-induced damage to the lateral line and muscles. *Neurotoxicology*, *78*, 134-142. https://doi.org/10.1016/j.neuro.2020.03.005

Horzmann, K. A., Lin, L. F., Taslakjian, B., Yuan, C., & Freeman, J. L. (2021). Embryonic atrazine exposure and later in life behavioral and brain transcriptomic, epigenetic, and pathological alterations in adult male zebrafish. *Cell Biol Toxicol*, *37*(3), 421-439. https://doi.org/10.1007/s10565-020-09548-y

Horzmann, K. A., Lin, L. F., Taslakjian, B., Yuan, C., & Freeman, J. L. (2022). Anxiety-related behavior and associated brain transcriptome and epigenome alterations in adult female zebrafish exposed to atrazine during embryogenesis. *Chemosphere*, *308*(Pt 3), 136431. https://doi.org/10.1016/j.chemosphere.2022.136431

Hung, H. C., & Lee, E. H. (1998). MPTP produces differential oxidative stress and antioxidative responses in the nigrostriatal and mesolimbic dopaminergic pathways. *Free Radic Biol Med*, *24*(1), 76-84. https://doi.org/10.1016/s0891-5849(97)00206-2

Ilin, V. A., Bai, Q., Watson, A. M., Volgushev, M., & Burton, E. A. (2021). Mechanism of Pacemaker Activity in Zebrafish DC2/4 Dopaminergic Neurons. *J Neurosci*, *41*(18), 4141-4157. https://doi.org/10.1523/jneurosci.2124-20.2021

Kalyn, M., & Ekker, M. (2021). Cerebroventricular Microinjections of MPTP on Adult Zebrafish Induces Dopaminergic Neuronal Death, Mitochondrial Fragmentation, and Sensorimotor Impairments. *Front Neurosci*, *15*, 718244. https://doi.org/10.3389/fnins.2021.718244

Keane, P. C., Hanson, P. S., Patterson, L., Blain, P. G., Hepplewhite, P., Khundakar, A. A., Judge, S. J., Kahle, P. J., LeBeau, F. E. N., & Morris, C. M. (2019). Trichloroethylene and its metabolite TaClo lead to degeneration of substantia nigra dopaminergic neurones: Effects in wild type and human A30P mutant α-synuclein mice. *Neurosci Lett*, *711*, 134437. https://doi.org/10.1016/j.neulet.2019.134437

Lal, P., & Kawakami, K. (2022). Integrated Behavioral, Genetic and Brain Circuit Visualization Methods to Unravel Functional Anatomy of Zebrafish Amygdala. *Front Neuroanat*, *16*, 837527. https://doi.org/10.3389/fnana.2022.837527

Leary, S. L., Underwood, W. J., Anthony, R., Cartner, S. C., Corey, D., Grandin, T., Greenacre, C. B., Gwaltney-Bran, S., Mccrackin, M. A., Meyer, R. E., Miller, D. S., Shearer, J. K., & Yanong, R. P. E. (2013). AVMA Guidelines for the Euthanasia of Animals: 2013 Edition.

Maitre, L., Julvez, J., López-Vicente, M., Warembourg, C., Tamayo-Uria, I., Philippat, C., Gützkow, K. B., Guxens, M., Andrusaityte, S., Basagaña, X., Casas, M., de Castro, M., Chatzi, L., Evandt, J., Gonzalez, J. R., Gražulevičienė, R., Smastuen Haug, L., Heude, B.,

Hernandez-Ferrer, C.,…Vrijheid, M. (2021). Early-life environmental exposure determinants of child behavior in Europe: A longitudinal, population-based study. *Environ Int*, *153*, 106523. https://doi.org/10.1016/j.envint.2021.106523

Matsui, H., & Sugie, A. (2017). An optimized method for counting dopaminergic neurons in zebrafish. *PLoS One*, *12*(9), e0184363. https://doi.org/10.1371/journal.pone.0184363

Mizoguchi, K., Yuzurihara, M., Ishige, A., Sasaki, H., Chui, D. H., & Tabira, T. (2000). Chronic stress induces impairment of spatial working memory because of prefrontal dopaminergic dysfunction. *J Neurosci*, *20*(4), 1568-1574. https://doi.org/10.1523/jneurosci.20-04-01568.2000

Moreira, A. L. P., Souza, J., de Souza, J. F., Mamede, J. P. M., Farias, D., & Luchiari, A. C. (2024). Long-term effects of embryonic exposure to benzophenone-3 on neurotoxicity and behavior of adult zebrafish. *Sci Total Environ*, *908*, 168403. https://doi.org/10.1016/j.scitotenv.2023.168403

Ohnmacht, J., Yang, Y., Maurer, G. W., Barreiro-Iglesias, A., Tsarouchas, T. M., Wehner, D., Sieger, D., Becker, C. G., & Becker, T. (2016). Spinal motor neurons are regenerated after mechanical lesion and genetic ablation in larval zebrafish. *Development*, *143*(9), 1464-1474. https://doi.org/10.1242/dev.129155

Omar, N. A., Kumar, J., & Teoh, S. L. (2023). Neuroprotective effects of Neurotrophin-3 in MPTP-induced zebrafish Parkinson's disease model. *Front Pharmacol*, *14*, 1307447. https://doi.org/10.3389/fphar.2023.1307447

Panula, P., Chen, Y. C., Priyadarshini, M., Kudo, H., Semenova, S., Sundvik, M., & Sallinen, V. (2010). The comparative neuroanatomy and neurochemistry of zebrafish CNS systems of relevance to human neuropsychiatric diseases. *Neurobiol Dis*, *40*(1), 46-57. https://doi.org/10.1016/j.nbd.2010.05.010

Peterson, S. M., & Freeman, J. L. (2009). RNA isolation from embryonic zebrafish and cDNA synthesis for gene expression analysis. *J Vis Exp*(30). https://doi.org/10.3791/1470

Philpott, C., Donack, C. J., Cousin, M. A., & Pierret, C. (2012). Reducing the Noise in Behavioral Assays: Sex and Age in Adult Zebrafish Locomotion. *Zebrafish*, *9*(4), 191-194. https://doi.org/10.1089/zeb.2012.0764

Pompermaier, A., Tamagno, W. A., Alves, C., & Barcellos, L. J. G. (2022). Persistent and transgenerational effects of pesticide residues in zebrafish. *Comparative Biochemistry*

*and Physiology Part C: Toxicology & Pharmacology*, *262*, 109461. https://doi.org/https://doi.org/10.1016/j.cbpc.2022.109461

Ribelayga, C., Wang, Y., & Mangel, S. C. (2002). Dopamine mediates circadian clock regulation of rod and cone input to fish retinal horizontal cells. *J Physiol*, *544*(3), 801-816. https://doi.org/10.1113/jphysiol.2002.023671

Rink, E., & Wullimann, M. F. (2002). Development of the catecholaminergic system in the early zebrafish brain: an immunohistochemical study. *Brain Res Dev Brain Res*, *137*(1), 89-100. https://doi.org/10.1016/s0165-3806(02)00354-1

Sallinen, V., Torkko, V., Sundvik, M., Reenilä, I., Khrustalyov, D., Kaslin, J., & Panula, P. (2009). MPTP and MPP+ target specific aminergic cell populations in larval zebrafish. *J Neurochem*, *108*(3), 719-731. https://doi.org/10.1111/j.1471-4159.2008.05793.x

Sarath Babu, N., Murthy Ch, L., Kakara, S., Sharma, R., Brahmendra Swamy, C. V., & Idris, M. M. (2016). 1-Methyl-4-phenyl-1,2,3,6-tetrahydropyridine induced Parkinson's disease in zebrafish. *Proteomics*, *16*(9), 1407-1420. https://doi.org/10.1002/pmic.201500291

Stagaman, K., Alexiev, A., Sieler, M. J., Hammer, A., Kasschau, K. D., Truong, L., Tanguay, R. L., & Sharpton, T. J. (2024). The zebrafish gut microbiome influences benzo[a]pyrene developmental neurobehavioral toxicity. *Sci Rep*, *14*(1), 14618. https://doi.org/10.1038/s41598-024-65610-3

Sy, H.-N., Wu, S.-L., Wang, W.-F., Chen, C.-H., Huang, Y.-T., Liou, Y.-M., Chiou, C.-S., Pawlak, C. R., & Ho, Y.-J. (2010). MPTP-induced dopaminergic degeneration and deficits in object recognition in rats are accompanied by neuroinflammation in the hippocampus. *Pharmacology Biochemistry and Behavior*, *95*(2), 158-165. https://doi.org/https://doi.org/10.1016/j.pbb.2009.12.020

Syambani Ulhaq, Z. (2020). Dopamine D2 receptor influences eye development and function in Zebrafish. *Arch Soc Esp Oftalmol (Engl Ed)*, *95*(2), 84-89. https://doi.org/10.1016/j.oftal.2019.11.013 (El receptor de dopamina D2 influye en el desarrollo y la función del ojo en el pez cebra.)

Tamagno, W. A., Alves, C., Vanin, A. P., Bilibio, D., Varela, A. C. C., Mozzato, M. T., & Barcellos, L. J. G. (2022). Dietary transference of 17α-ethinylestradiol changes the biochemical and behavioral biomarkers in adult zebrafish (Danio rerio). *Comp Biochem Physiol C Toxicol Pharmacol*, *262*, 109472. https://doi.org/10.1016/j.cbpc.2022.109472

Thomas, E. D., Cruz, I. A., Hailey, D. W., & Raible, D. W. (2015). There and back again: development and regeneration of the zebrafish lateral line system. *Wiley Interdiscip Rev Dev Biol*, *4*(1), 1-16. https://doi.org/10.1002/wdev.160

Vijayanathan, Y., Hamzah, N. M., Lim, S. M., Lim, F. T., Tan, M. P., Majeed, A. B. A., & Ramasamy, K. (2022). Newly regenerated dopaminergic neurons in 6-OHDA-lesioned adult zebrafish brain proliferate in the Olfactory bulb and telencephalon, but migrate to, differentiate and mature in the diencephalon. *Brain Res Bull*, *190*, 218-233. https://doi.org/10.1016/j.brainresbull.2022.10.001

Wang, S., Bryan, C., Xie, J., Zhao, H., Lin, L. F., Tai, J. A. C., Horzmann, K. A., Sanchez, O. F., Zhang, M., Freeman, J. L., & Yuan, C. (2022). Atrazine exposure in zebrafish induces aberrant genome-wide methylation. *Neurotoxicol Teratol*, *92*, 107091. https://doi.org/10.1016/j.ntt.2022.107091

Wang, Z., Zhao, H., Xu, Y., Zhao, J., Song, Z., Bi, Y., Li, Y., Lan, X., Pan, C., Foulkes, N. S., & Zhang, S. (2022). Early-life lead exposure induces long-term toxicity in the central nervous system: From zebrafish larvae to juveniles and adults. *Sci Total Environ*, *804*, 150185. https://doi.org/10.1016/j.scitotenv.2021.150185

Wei, P., Zhao, F., Zhang, X., & Ru, S. (2020). Long-term exposure of zebrafish to bisphenol S impairs stress function of hypothalamic-pituitary-interrenal axis and causes anxiety-like behavioral responses to novelty. *Sci Total Environ*, *716*, 137092. https://doi.org/10.1016/j.scitotenv.2020.137092

Wen, L., Wei, W., Gu, W., Huang, P., Ren, X., Zhang, Z., Zhu, Z., Lin, S., & Zhang, B. (2008). Visualization of monoaminergic neurons and neurotoxicity of MPTP in live transgenic zebrafish. *Dev Biol*, *314*(1), 84-92. https://doi.org/10.1016/j.ydbio.2007.11.012

Wirbisky, S. E., Weber, G. J., Lee, J. W., Cannon, J. R., & Freeman, J. L. (2014). Novel dose-dependent alterations in excitatory GABA during embryonic development associated with lead (Pb) neurotoxicity. *Toxicol Lett*, *229*(1), 1-8. https://doi.org/10.1016/j.toxlet.2014.05.016

Xi, Y., Yu, M., Godoy, R., Hatch, G., Poitras, L., & Ekker, M. (2011). Transgenic zebrafish expressing green fluorescent protein in dopaminergic neurons of the ventral diencephalon. *Dev Dyn*, *240*(11), 2539-2547. https://doi.org/10.1002/dvdy.22742

Yang, R., Ye, S., Zhang, S., Huang, H., Zhang, Y., Yang, Y., Xie, S., He, L., Yang, Y., & Shi, J. (2023). Serotonin and dopamine depletion in distinct brain regions may cause anxiety in 1-methyl-4-phenyl-1,2,3,6-tetrahydropyridine-treated mice as a model of early Parkinson's disease. *Neuroreport*, *34*(11), 551-559. https://doi.org/10.1097/wnr.0000000000001922

Yang, Y., Pang, B., Liu, Z., Li, J., Zhang, Z., Zhang, R., Hou, X., Guo, H., Chi, L., Pang, Q., & Xin, T. (2019). 1-Trichloromethyl-1,2,3,4-tetrahydro-beta-carboline (TaClo) Induces the Apoptosis of Dopaminergic Neurons via Oxidative Stress and Neuroinflammation. *Oxid Med Cell Longev*, *2019*, 1292891. https://doi.org/10.1155/2019/1292891

Zambusi, A., & Ninkovic, J. (2020). Regeneration of the central nervous system-principles from brain regeneration in adult zebrafish. *World J Stem Cells*, *12*(1), 8-24. https://doi.org/10.4252/wjsc.v12.i1.8

Zhang, S., Mi, P., Luan, J., Sun, M., Zhao, X., & Feng, X. (2024). Fluorene-9-bisphenol acts on the gut-brain axis by regulating oxytocin signaling to disturb social behaviors in zebrafish. *Environ Res*, *255*, 119169. https://doi.org/10.1016/j.envres.2024.119169

# Chapter 5

# Comprehensive transcriptomic RNA-seq profiling uncovers new insights into early-life exposure to 1-Trichloromethyl-1,2,3,4-tetrahydro-beta-carboline (TaClo) and 1-Methyl-4-phenyl-1,2,3,6-tetrahydropyridine (MPTP) in zebrafish (*Danio rerio*)


## Abstract

Our previous studies demonstrated that early-life exposure to 1-Trichloromethyl-1,2,3,4-tetrahydro-β-carboline (TaClo) induces 1-Methyl-4-phenyl-1,2,3,6-tetrahydropyridine (MPTP)-like neurotoxicity in larval zebrafish (*Danio rerio*). Moreover, transient exposure to TaClo or MPTP during early development results in long-lasting neurotoxic effects in adulthood. While our earlier investigations primarily focused on phenotypic assessments to explore the mechanisms underlying these neurotoxic effects, the molecular pathways involved remain largely unexplored. In addition, transcriptomic RNA-sequencing analyses of TaClo- and MPTP-induced neurotoxicity have been rarely reported and are not well characterized in zebrafish models. To address this gap, we employed transcriptomic approaches to investigate the underlying mechanisms of neurotoxicity induced by early-life exposure to TaClo (5, 50, and 500 ppb) and 1.75 μM MPTP in 120-hour post-fertilization (hpf) larvae and 6-month post-fertilization (mpf) zebrafish brains. Our findings reveal that TaClo and MPTP elicit neurotoxicity through distinct mechanisms. In 120 hpf zebrafish, TaClo primarily disrupts cellular stress responses, whereas MPTP predominantly affects glutamatergic neurotransmission. TaClo exposure also induced maladaptive stress response during early development, followed by compensatory adaptation in adulthood. Notably, both compounds were found to affect pathways associated with systemic diseases beyond the nervous system. Together, this study provides the first comprehensive transcriptomic analysis of early-life TaClo and MPTP exposure across developmental stages in zebrafish, providing novel insights into their distinct neurotoxic mechanisms and potential systemic health implications.

## 1. Introduction

1-Trichloromethyl-1,2,3,4-tetrahydro-β-carboline (TaClo) is a metabolite of trichloroethylene (TCE) and has been identified as a potent neurotoxicant implicated in the development of neurotoxicity (Bringmann et al., 1999; Rausch et al., 1995). In addition, TaClo is structurally and chemically similar to 1-Methyl-4-phenyl-1,2,3,6-tetrahydropyridine (MPTP), a well-known neurotoxicant commonly used to induce Parkinson's disease (PD)-like symptoms in animal models (Bringmann, God, Feineis, Wesemann, et al., 1995; Keane et al., 2019; Liu et al., 2018). Therefore, TaClo has been associated with neurodegenerative diseases and is considered a potential contributor to the development of PD (Akundi et al., 2003; Bringmann, God, Feineis, Janetzky, et al., 1995; Grote et al., 1995; Rausch et al., 1995; Yang et al., 2019). Our previous studies demonstrated that early-life exposure to 1-Trichloromethyl-1,2,3,4-tetrahydro-β-carboline (TaClo) induces 1-Methyl-4-phenyl-1,2,3,6-tetrahydropyridine (MPTP)-like neurotoxicity in larval zebrafish (*Danio rerio*). Moreover, transient exposure to TaClo or MPTP during early development results in long-lasting neurotoxic effects in adulthood. In our previous studies (chapters 3 and chapter 4), we primarily focused on phenotypic assessments to investigate the mechanisms underlying these neurotoxic effects; however, the molecular aspects remain largely unexplored and underdiscussed.

Previous studies have utilized transcriptomic approaches along with the ingenuity pathway analysis to investigate the novel insights into the mechanisms underlying chemically induced effects in zebrafish models. For example, Lee et al. investigated the effects of embryonic lead (Pb) exposure on the adult zebrafish brain by performing transcriptomic analysis on brains of 12-month-old zebrafish exposed to 100 μg/L Pb during embryonic development. In adult female zebrafish, significant changes were observed in the expression of genes involved in neurological diseases and nervous system development and function. In contrast, adult males exhibited significant alterations in genes associated with cancer and tumor pathways (Lee et al., 2018). Ola et al. exposed embryos from 1 to 120 hours post-fertilization (hpf) to PFOA (perfluorooctanoic acid), PFHxA (perfluorohexanoic acid), and PFBA (perfluorobutanoic acid). Their study identified cancer as the top associated disease for PFOA exposure, while FXR/RXR activation emerged as a key canonical pathway for PFBA exposure. Furthermore, comparisons of

altered biological and molecular pathways in zebrafish exposed to PFOA aligned with findings from previous epidemiological studies and other animal model (Wasel et al., 2022). Horzmann et al. used transcriptomic approaches to investigate the effects of atrazine exposure during embryogenesis and observed significant changes in the female zebrafish brain. Transcriptomic profiling at 9 mpf female revealed altered gene expression pathways associated with organismal injury and cancer, with beta-estradiol and the estrogen receptor identified as key upstream regulators. Additionally, global brain DNA methylation analysis at 12 months post-fertilization (mpf) showed increased levels of 5-methylcytosine (5 mC) in females exposed to 0.3 ppb atrazine during embryogenesis (Horzmann et al., 2022). Fang et al. investigated transcriptomic changes in zebrafish embryos and larvae following exposure to benzo[a]pyrene (BaP). Adult zebrafish were exposed to 42.0–61.9 mg/L BaP for 7 days. Eggs were collected and either raised in control conditions or continuously exposed to BaP until 3.3 and 96 hpf. Functional ontology analysis using ingenuity pathway analysis revealed significant enrichment of disease pathways, including organismal death, growth failure, abnormal embryonic tissue morphology, congenital heart disease, and adverse neuritogenesis (Fang et al., 2015). However, transcriptomic RNA-sequencing analyses of TaClo- and MPTP-induced neurotoxicity remain rarely reported and are poorly characterized in zebrafish models.

Therefore, to address this gap and advance our understanding of zebrafish as a model for investigating underlying mechanisms, we employed transcriptomic approaches to explore the neurotoxicity induced by early-life exposure to TaClo (5, 50, and 500 ppb) and 1.75 μM MPTP in 120 hpf larvae and 6 mp adult zebrafish brains. We discovered that TaClo and MPTP elicit neurotoxicity through distinct mechanisms. We identified TaClo primarily disrupts cellular stress response and whereas MPTP predominantly affects glutamatergic neurotransmission. Moreover, we uncovered that TaClo and MPTP are not only neurotoxicants but also chemicals that induce multiple systemic diseases. Finally, our research work provides the first comprehensive transcriptomic analysis of early-life TaClo and MPTP exposure across developmental stages in zebrafish and advances novel insights into their distinct neurotoxic mechanisms and potential systemic health implications.

## 2. Materials and methods

### *2.1 Ethics statement*

All procedures were approved by the Institutional Animal Care and Use Committee at Auburn University (protocol numbers: 2021-3912, 2022-4087, and 2024-5380) and conducted in accordance with the National Institutes of Health Guide for the Care and Use of Laboratory Animals. Euthanasia was carried out using buffered Tricaine-S (ethyl m-amino benzoate methanesulfonate; Western Chemical Inc., Ferndale, WA) at a concentration of 0.4 mg/mL.

### *2.2 Zebrafish husbandry, chemical exposure, and experimental design*

Zebrafish husbandry, chemical preparation (stock and working solutions), and exposure protocols were previously described in Chapters 2 and 3. Briefly, adult-specific, pathogen-free wild-type AB strain zebrafish (*Danio rerio*) were obtained from the Sinnhuber Aquatic Research Laboratory at Oregon State University (Corvallis, OR, USA) and maintained in a ZS660 Stand-Alone system (Aquaneering Inc., San Diego, CA, USA) at Auburn University under a controlled 14-hour light/10-hour dark photoperiod. Adult zebrafish were bred and embryos were immediately collected for chemical exposure. The final concentrations of the test compounds were as follows: 1.75 μM 1-methyl-4-phenyl-1,2,3,6-tetrahydropyridine (MPTP), 0.001% dimethyl sulfoxide (DMSO), and 1-trichloromethyl-1,2,3,4-tetrahydro-β-carboline (TaClo) at 5 ppb, 50 ppb, and 500 ppb. Embryonic zebrafish were exposed until 120 hours post-fertilization (hpf). Following treatment, larvae were rinsed and raised in aquaria water (reverse osmosis-filtered water supplemented with Aquaneering sea salt) until 6 months post-fertilization (mpf). Samples for RNA extraction, Lexogen CORALL mRNA-Seq library preparation, and Ingenuity® Pathway Analysis (Qiagen, Redwood City, CA, USA) were collected at two timepoints: 120 hpf zebrafish larvae and individual 6 mpf adult zebrafish brains. Sample size selection for each assay was guided by prior research involving similar transcriptomic analysis (Dasgupta et al., 2021; McClure et al., 2023). For larvae, four biological replicates per group were used, each consisting of a pooled 120 hpf zebrafish larvae (up to 50 zebrafish larvae) per treatment. For adult zebrafish, four biological replicates were collected per treatment group. The four replicates include two male replicates and two female replicates. Each replicate per

treatment contained a 6 mpf zebrafish brain. A schematic diagram overview of the chemical exposure and experimental regime is presented in **Figure 5-1**.

*2.3 RNA isolation*

Total RNA extraction of the 120 hpf larvae and 6 mpf zebrafish brain was previously described in chapter 2 and chapter 3RNA integrity was assessed using the Agilent 4200 Bioanalyzer (Santa Clara, CA, USA), and RNA quality and concentration were evaluated with a NanoDrop 1000 Spectrophotometer V3.8 (Thermo Fisher Scientific, Waltham, MA, USA), following the manufacturers' instructions. Only RNA samples with a RNA Integrity Number (RIN) >8 were submitted for Lexogen CORALL mRNA-Seq library preparation and RNA sequencing (RNA-seq).

*2.4 RNA-seq data analysis and transcriptomic analysis*

RNA-seq data retrieved from Lexogen were imported into QIAGEN's Ingenuity® Pathway Analysis (IPA; Qiagen, Redwood City, CA, USA). Zebrafish gene identifiers were automatically mapped to their corresponding human orthologs using the IPA knowledge base. Differentially expressed genes (DEGs) were identified using a threshold of fold change > 1.5 and p-value < 0.05, and were used for subsequent analyses, including canonical pathway analysis, network analysis, upstream regulator analysis, disease and bio function analysis, and tox function analysis. Briefly, (1) Canonical Pathway Analysis identified significantly affected molecular pathways and predicted their activation or inhibition states using a z-score algorithm that compares the dataset to known pathway activity patterns. (2) Network Analysis constructed transcriptional networks to uncover regulatory relationships between signaling events and downstream gene expression changes. (3) Upstream Regulator Analysis predicted upstream molecules, including transcription factors, nuclear receptors, and microRNAs (miRNAs), that may be responsible for the observed gene expression changes. (4) Diseases and Bio functions analysis predicts activation or suppression of biological processes based on gene expression results, and (5) Tox functions predicted the effects of molecular changes in the dataset on downstream toxicological endpoints.

*2.5 Statistical analysis*

For all analyses conducted in this study, including canonical pathway, upstream regulatory analysis, disease and bio functions, and tox functions, QIAGEN IPA employed Fisher's exact test, with a p-value $< 0.05$ considered statistically significant. Activation or inhibition predictions were based on z-scores: positive z-scores indicated activation, while negative z-scores indicated inhibition. Moreover, z-scores $\geq 2$ were interpreted as statistically significant activation, and z-scores $\leq -2$ were considered statistically significant inhibition.

## 3. Results

*3.1 TaClo inhibits heat shock protein expression, stress responses, protein folding, and activates apoptosis and organismal death in larval zebrafish*

Our previous study demonstrated that TaClo induced MPTP-like neurotoxicity in 120 hpf zebrafish larvae (Chapter 3). Specifically, TaClo at 5 ppb significantly reduced locomotor activity and caused the most pronounced decrease in the expression of diencephalic dopaminergic neurons among all TaClo-treated groups. Furthermore, both 5 ppb and 50 ppb TaClo treatments resulted in the highest number of apoptotic bodies in the diencephalon. Collectively, these findings suggested a bimodal effect, with 5 ppb TaClo inducing the most severe neuronal damage. To investigate the mechanisms underlying this bimodal response, transcriptomic analysis was performed on 120 hpf zebrafish larvae treated with TaClo (5, 50, and 500 ppb) or 1.75 μM MPTP. We first identified the filtered DEGs in the treated larval zebrafish. Of the 59,466 uploaded Ensembl zebrafish gene IDs **(Table 5-1, Table 5-2, Table 5-3, Table 5-4, Table 5-5)**, IPA successfully mapped 32,410 to human orthologs, while 27,056 remained unmapped across the TaClo-treated groups (5, 50, and 500 ppb). In the 5 ppb TaClo-treated larvae, 55 DEGs were identified, including 15 upregulated and 40 downregulated genes. The 50 ppb TaClo group showed 57 DEGs, with 16 upregulated and 41 downregulated genes. In the 500 ppb TaClo group, 41 DEGs were filtered, comprising 12 upregulated and 29 downregulated genes. In contrast, larvae treated with 1.75 μM MPTP exhibited only 12 DEGs, including 5 upregulated and 7 downregulated genes **(Table 5-6)**. The relatively higher number of filtered DEGs in TaClo-treated larvae might suggest that TaClo exposure had a greater transcriptomic

impact on 120 hpf zebrafish than 1.75 μM MPTP. Volcano plots generated by QIAGEN IPA for each treatment group (TaClo and MPTP) are presented in **Figure 5-2**. To further investigate the mechanisms underlying the bimodal effects observed in zebrafish larvae treated with TaClo from 0 to 120 hpf, we uploaded the filtered DEGs from each TaClo treatment group (5, 50, and 500 ppb) into QIAGEN IPA for canonical pathway analysis. IPA predicted significant inhibition of several stress response-related pathways, including the cellular response to heat stress, HSP90 chaperone cycle for steroid hormone receptors in the presence of ligand, and the protein ubiquitination pathway **(Figure 5-3 and Table 5-7)**. In addition, the predicted z-scores for the cellular response to heat stress canonical pathway suggest a dose-dependent inhibitory effect, with the highest concentration of TaClo (500 ppb, z-score = –3.00) exhibiting a stronger predicted inhibition than 50 ppb (z-score = –2.83) and 5 ppb (z-score = –2.45) (**Table 5-8**). A similar trend was observed in the HSP90 chaperone cycle for steroid hormone receptors in the presence of ligand pathway, where 500 ppb TaClo (z-score = –2.89) showed a more pronounced inhibition than 50 ppb TaClo (z-score = –2.00) (**Table 5-8**). These findings prompted the question of whether the inhibition of the three canonical pathways observed in TaClo-treated larvae was mediated by shared DEGs across the different concentrations. To address this question, we performed network analysis on all TaClo- and 1.75 μM MPTP-treated groups. The analysis revealed that the cellular response to heat stress, HSP90 chaperone cycle for steroid hormone receptors in the presence of ligand, and protein ubiquitination pathway were primarily regulated by a common set of downregulated genes. Notably, the majority of these genes were associated with heat shock proteins (**Figure 5-4**). Moreover, several heat shock proteins, including HSP90AA1, HSPB1, HSP1L, DNAJB1, and FKBP4, were significantly associated with protein folding and post-translational modifications, such as protein refolding, aggregation, and ubiquitination **(Figure 5-5, Table 5-9)**. In addition, IPA predicted activation of apoptosis and organismal death in TaClo-treated larvae **(Table 5-10)**. However, none of these alterations were observed in 120 hpf zebrafish exposed to 1.75 μM MPTP **(Table 5-10)**. Collectively, our results suggest that TaClo (5, 50, and 500 ppb) functions as a stressor that disrupts heat shock protein expression, impairs stress response and protein folding, and promotes apoptotic and organismal death.

*3.2 50 ppb and 500 ppb TaClo activate Aryl Hydrocarbon receptor signaling and NRF-2 mediated oxidative stress response in larval zebrafish*

Our previous findings in chapter 3 demonstrated that 5 ppb TaClo exposure triggered the most severe neurotoxic effects in 120 hpf zebrafish larvae among all TaClo-treated groups. Additionally, our study in chapter 2 revealed 120 hpf zebrafish had a significantly increased glutathione peroxidase enzymatic activity following exposure to 500 ppb TaClo. Therefore, we next investigated whether other mechanisms may underlie the protective responses observed in TaClo-treated larvae against chemical-induced neurotoxicity. We identified two canonical pathways, Aryl Hydrocarbon receptor (AHR) signaling pathway (50 ppb TaClo z score=0.01; 500 ppb TaClo z score=0.58) and NRF-2 mediated oxidative stress response (50 ppb TaClo z score=0.01; 500 ppb TaClo z score=1.73), that were predicted to be activated in zebrafish larvae treated with 50 ppb and 500 ppb TaClo **(Figure 5-6)**. In the 500 ppb TaClo-treated group, multiple upstream regulators within the AHR signaling pathway were significantly altered, including AHR, AHR/ARNT (complex), AHR/ARNT/Aryl Hydrocarbon (complex), AHRR, and AHRR:ARNT. For example, AHR was predicted to be significantly activated (z-score = 2.3, p-vaue=8.11E-04), while AHR/ARNT (z-score = 1.41, p-value=1.66E-04). and AHR/ARNT/Aryl Hydrocarbon complexes (z-score = 1.41, p-value=1.93E-04) were also predicted to be activated Additionally, AHRR (z-score = –1, p-value=1.79E-03) and AHRR:ARNT (z-score = –1, p-value=1.79E-03) were predicted to be inhibited. In the NRF-2 mediated oxidative stress response canonical pathway, significant changes in upstream regulators were also observed in the 500 ppb group **(Figure 5-7).** For example, Kelch-like ECH-associated protein 1 (KEAP1), was predicted to be significantly inhibited (z-score = –2.82, p-value=1.27E-03), while NFE2L2 (NRF2) (z-score = 1.90, p-value=4.85E-07) and ACTIN (z-score=0.36, p-value=9.41E-16) were predicted to be activated. Additionally, upregulation of downstream target genes associated with oxidative stress protection, such as CYP1A1 ($log_2$ fold change=0.78; p-value=2.81E-06), CYP1B1($log_2$ fold change=0.84; p-value=3.58E-06), NQO1 ($log_2$ fold change=0.62; p-value=4.67E-05), and HMOX1($log_2$ fold change=0.69; p-value=4.22E-05), was observed exclusively in the 500 ppb TaClo-treated group **(Figure 5-8)**. Collectively, these findings suggest that both 50 ppb and 500 ppb TaClo activate the AHR signaling and NRF2-mediated oxidative stress response pathways, with 500 ppb TaClo exerting a stronger modulatory effect on the expression of downstream cytoprotective genes.

*3.3 1.75 μM MPTP upregulates glutamate transporter expression in larval zebrafish*

Intrigued by our previous findings that TaClo and 1.75 μM MPTP shared no overlapping canonical pathways related to cellular stress responses, yet produced similar neurotoxic phenotypes in larval zebrafish, we sought to investigate the molecular mechanisms underlying MPTP-driven neurotoxicity. In the 0–120 hpf 1.75 μM MPTP-treated group, we first identified SLC1A2 (solute carrier family 1 member 2), also known as EAAT2 (excitatory amino acid transporter 2), and GLUT1 (glucose transporter 1) as significantly upregulated ($\log_2$ fold change = 0.58; p-value = $9.41 \times 10^{-4}$). Second, several canonical pathways associated with neurotransmission were significantly impacted in the MPTP-treated group, including glutamate receptor signaling (p-value=0.03), trans-Golgi network vesicle budding (p-value=5.03E-04), SUMOylation of proteins (p-value=0.0155), and the neurotransmitter release cycle (p-value=1.79E-03). In addition, IPA identified slc1a2 as a key target molecule in both the glutamate receptor signaling and neurotransmitter release cycle pathways. Moreover, causal network analysis revealed several master regulators, such as glutamine synthetase (GLUL) (activated z score=1.414), glutamate metabotropic receptor 3 (GRM3) (activated z score=1), glutamate metabotropic receptor 5 (GRM5) (activated z score=1), and solute carrier family 17 member 7 (SLC17A7) (activated z score=1), also known as vesicular glutamate transporter 1 (VGLUT1), as significantly predicted activated, with slc1a2 the target molecule in our uploaded dataset. Furthermore, upstream regulator analysis further confirmed GRM3, GRM5, and SLC17A7 (VGLUT1) as significantly affected regulators with SLC1A2 as the targeted molecules. Lastly, disease and biofunction analysis indicated that 1.75 μM MPTP significantly affected lipid (activated z score=1.067) and cholesterol concentrations (activated z score=0.378), with SLC1A2 identified as a key molecule involved in these processes. Together, these findings suggest that 1.75 μM MPTP targets the glutamatergic synapse, modulates glutamatergic neurotransmission, and may exert neurotoxic effects through a mechanism distinct from that of TaClo.

*3.4 Developmental exposure to taclo suppresses stress responses in larvae but activates protective signaling pathways in adult zebrafish brain*

Based on the developmental origins of health and disease (DoHAD) concept, we hypothesized that embryonic exposure to TaClo (5, 50, 500 ppb) or 1.75 μM MPTP induced a long-lasting permanent change in larval zebrafish that persisted into adulthood. To test this hypothesis, we first identified significantly differentially expressed genes (DEGs) in adult zebrafish brains. Of the 59,466 uploaded Ensembl zebrafish gene IDs **(Table 5-11, Table 5-12, Table 5-13, Table 5-14, Table 5-15)**, IPA mapped 32,410 to human orthologs, while 27,056 remained unmapped in the TaClo-treated groups (5, 50, and 500 ppb). Following early-life exposure to 5 ppb TaClo, 35 DEGs were filtered, including 17 upregulated and 18 downregulated genes. The 50 ppb TaClo group exhibited 209 filtered DEGs, comprising 180 upregulated and 29 downregulated genes. In the 500 ppb TaClo-treated group, 82 filtered DEGs were identified, with 71 upregulated and 11 downregulated genes. Finally, the 1.75 μM MPTP-treated group showed 97 filtered DEGs, including 51 upregulated and 46 downregulated genes **(Table 5-16)**. Volcano plots for each treatment group are presented in **Figure 5-9**. Next, we used Venn diagrams to compare and identify overlapping DEGs between larvae and adult zebrafish brains in the TaClo-treated groups and the 1.75 μM MPTP-treated group. We found that heat shock protein beta-1 (HSPB1), NFKB Inhibitor Alpha (NFKBIA), and zinc finger protein 729 (ZNF729) were shared DEGs across the TaClo-treated groups (5, 50, and 500 ppb) in both 120 hpf larvae and 6 mpf adult brains **(Figure 5-10, Table 5-17)**. When analyzing individual TaClo concentrations, NFKBIA was the only overlapping gene in the 5 ppb group, while HSPB1 and zinc finger protein 729 were common in the 50 ppb group (**Figure 5-11**, **Table 5-17)**. No shared DEGs were identified in the 500 ppb TaClo group or the 1.75 μM MPTP-treated group **Figure 5-10, Figure 5-11**, **Table 5-17).** Both NFKBIA (5 ppb TaClo) and HSPB1 (50 ppb TaClo) were downregulated in 120 hpf larvae and remained downregulated in 6 mpf zebrafish brains (**Figure 5-10, Figure 5-11, Table 5-17).** Moreover, we found NFKB1A and HSPB1 played important roles in modulating apoptosis and organismal death in both larval and adult stages (**Figure 5-12, Figure 5-13**). For example, IPA predicted that downregulation of NFKBIA and HSPB1 in 120 hpf zebrafish was associated with activation of neuronal apoptosis and organismal death, whereas their upregulation in 6 mpf zebrafish brains was linked to inhibition of these processes (**Figure 5-12, Figure 5-13)**. In the 1.75 μM MPTP-treated groups, no prediction of apoptosis or organismal

death was observed in 120 hpf zebrafish larvae; however, activation of these processes was predicted in 6 mpf zebrafish brains (**Table 5-18)**. Earlier in this study, three canonical pathways, including cellular response to heat stress, HSP90 chaperone cycle for steroid hormone receptors in the presence of ligand, and protein ubiquitination pathway, were significantly inhibited in 0–120 hpf TaClo-treated larvae. However, these inhibitory effects were not observed in 6 mpf zebrafish brains; instead, several stress-related canonical pathways, such as serotonin receptor signaling (z-score = 2.52, p-value=1.62E-06), calcium signaling (z-score = 0.70, p-value=1.80E-07), and G-protein coupled receptor signaling (z-score = 0.58, p-value=0.05), were predicted to be activated. Taken together, our findings support the hypothesis that developmental exposure to TaClo induces permanent molecular changes; however, these changes differ between larval and adult stages, with suppressed stress responses during early development and activation of protective signaling pathways in adulthood.

*3.5 TaClo and MPTP exposure link to neurological disorders and systemic diseases*

Our previous study in Chapter 3 demonstrated that larval zebrafish exposed to 5 ppb TaClo or 1.75 μM MPTP exhibited locomotor deficits. A subsequent study in Chapter 4 revealed that embryonic exposure to 1.75 μM MPTP resulted in sex-specific behavioral alterations in adulthood, with male zebrafish displaying reduced locomotor activity and females exhibiting increased anxiety levels. To investigate whether TaClo and MPTP exposures contribute to a broader range of neurological and systemic disorders, we analyzed our RNA-seq datasets using QIAGEN IPA software to predict related diseases and biological functions. First, analysis of neurological disease-related predictions revealed distinct effects of TaClo and MPTP in 120 hpf zebrafish (**Table 5-19, Table 5-20**, **Table 5-21, Table 5-22, Table 5-23, Table 5-24)**. For example, TaClo exposure was largely associated with central nervous system solid tumors, glioma and brain tumors, and central nervous system cancers **(Table 5-20)**. Additionally, IPA predicted an inhibition of neurological lesion formation **(Table 5-20)**. In contrast, exposure to 1.75 μM MPTP significantly affected nervous system development and function, with predicted impacts on synaptic transmission in hippocampal neurons, synaptic vesicle recycling, astrocyte activation, and endocytosis of synaptic vesicles **(Table 5-21).** Moreover, IPA identified strong associations between MPTP exposure and psychological disorders, such as mood disorders,

major affective disorder, depressive disorder, anxiety disorders, and social anxiety disorder **(Table 5-22)**. In the 6 mpf zebrafish brain, IPA analysis predicted TaClo exposure exhibited a significant inhibition of several neurological diseases, including abnormal neuronal morphology, neurodegeneration, neuronal degeneration, and ataxia **(Table 5-23)**. However, IPA also predicted inhibition of the development of neuroglia, proliferation of neuronal cells, neurotransmission, and synaptic neurotransmission **(Table 5-24)**. In the 1.75 μM MPTP treated group, several aspects of nervous system development and function were predicted to be activated in, such as development of neurons, branching of neurons, neuritogenesis, neurotransmission, and synaptic transmission **(Table 5-25)**. Moreover, behaviors, such as, cognition, learning, social behavior, memory, and anxiety**,** were predicted to be activated **(Table 5-26)**. Next, we then directed our focus to identifying other diseases and biological functions, beyond neurological disorders, that may be influenced by TaClo and MPTP exposure. In 120 hpf zebrafish, the top five disease categories predicted following TaClo exposure were cancer, organismal injury and abnormalities, gastrointestinal disease, neurological disease, and reproductive system disorders **(Table 5-27).** In contrast, exposure to 1.75 μM MPTP was predicted to significantly affect organismal injury and abnormalities, psychological disorders, gastrointestinal disease, hepatic system disease, and connective tissue disorders **(Table 5-28)**. In the 6 mpf zebrafish brain, the top five predicted disease categories in the TaClo-treated group were cancer, organismal injury and abnormalities, gastrointestinal disease, neurological disease, and endocrine system disorders **(Table 5-29)**. For the MPTP-treated adult group, IPA predicted associations with cancer, organismal injury and abnormalities, gastrointestinal disease, hematological disease, and endocrine system disorders **(Table 5-30)**. Collectively, our results suggest that TaClo and MPTP are not only neurotoxicants but also chemicals that can trigger a broader range of systemic diseases.

## 4. Discussion

This study investigates the roles of TaClo and MPTP in neurotoxicity using transcriptomic RNA-seq data in zebrafish models. Overall, our findings demonstrate that TaClo and MPTP elicit neurotoxic effects through distinct mechanisms. Specifically, at the larval stage, TaClo primarily disrupts cellular stress responses, whereas MPTP affects glutamatergic neurotransmission. Additionally, TaClo-exposed zebrafish exhibited a maladaptive stress

response during early development, followed by a compensatory adaptation in adulthood. Moreover, early-life MPTP exposure, aligned with the developmental origins of health and disease hypothesis, was associated with an increased risk of anxiety-related disorders in adulthood. Furthermore, both compounds were found to influence broader systemic diseases beyond the nervous system. Taken together, this is the first comprehensive transcriptomic study to characterize early-life exposure to TaClo and MPTP across developmental stages in zebrafish models.

In response to exposure to various harmful stressors, such as hypoxia, free radicals, or environmental and chemical factors, cells or organisms activate a cellular defense mechanism known as “heat shock response”. This response is a highly conserved physiologic process and plays an important role in maintaining cellular homeostasis under stress conditions. Upon activation, the heat shock response protects cells from stress-induced protein damage by triggering the expression of a specific set of genes and proteins known as heat shock genes or heat shock proteins (HSPs) (Arrigo, 2017; Kowalczyk et al., 2018; Zuehlke et al., 2015). Overexpression of HSPs and their co-chaperones plays a role in stress adaptation, cell survival, hormone signaling, or apoptosis. For example, HSPs are a molecular chaperone that promotes the folding of de novo synthesized or incorrectly folded proteins, protecting neuronal proteins with aberrant aggregation from accumulating toxic aggregates. Moreover, HSP90 plays a central role in regulating the chaperone cycle that modulates the activity, conformation, and subcellular localization of steroid hormone receptors (SHRs)**.** In the presence of ligands, HSP90 assists in receptor activation and promotes the transcription of hormone-responsive genes involved in stress adaptation and cellular signaling. Furthermore, HSPs cooperate with quality control mechanisms, the ubiquitin proteasome system and autophagy, to identify and target misfolded and/or aggregated proteins toward degradation to prevent toxic and disease-related protein accumulation. Through these protective mechanisms, HSPs play a critical role in counteracting protein aggregation associated with neurodegenerative diseases, such as Alzheimer's disease and Parkinson's disease (Backe et al., 2022; Hoter et al., 2018). Chemical stressors, such as trichlorethylene (TCE) and MPTP have been shown to regulate HSPs at the cellular level. For example, Ou et al. demonstrated that exposure to 5 μM TCE reduced the interaction between

HSP90 and endothelial nitric oxide synthase in bovine coronary endothelial cells. The authors further suggested that this dysregulation may contribute to the TCE-induced impairment of bovine coronary endothelial cells (Ou et al., 2003). Freyaldenhoven et al. found $MPP^+$, the active metabolite of MPTP, triggered an increase in HSP70 synthesis in the Chinese hamster ovary (CHO) cell line and suggested the HSP played a neuroprotective role in MPTP-induced neurotoxicity (Freyaldenhoven & Ali, 1997). Despite the previous research on TCE and MPTP, the interaction between TaClo or MPTP and HSPs has been rarely investigated in zebrafish models. In our study, we observed several HSPs that was known for their roles in protein misfolding aggregation, protection against oxidative stress, and regulation of apoptosis during stress response, such as HSPB1, HSPA4, HSPA1L, HSP90AA1, DNAJB1, FKBP4, SUGT1, SERPINH1, and HIKESHI were significantly downregulated in TaClo-treated, but not in MPTP-exposed, larval zebrafish (Arrigo, 2017; Ito & Nagata, 2017; Kose et al., 2012; Kowalczyk et al., 2018; Monistrol et al., 2025; Pare et al., 2013; Yan et al., 2012; Zuehlke et al., 2015). Additionally, these changes were largely associated with the inhibition of cellular response to heat stress, HSP90 chaperone cycle for steroid hormone receptors in the presence of ligand, or protein ubiquitination canonical pathway. Moreover, IPA reported that the downregulation of these HSPs was associated with protein folding or post-translational modification of protein. As we further investigated apoptosis of neurons and organismal death following 0–120 hpf TaClo exposure, we found that these HSPs played a significant role in promoting both processes. Therefore, using larval zebrafish as a model, we propose that TaClo, acts as a "suppressive stressor" that downregulates the HSPs expression and inhibits the cellular stress responses. This suppression may directly or indirectly impact protein folding or post-translational modification of protein, resulting in the accumulation of misfolded or aggregated proteins. Such accumulation can trigger apoptosis of neurons and further contribute to neurodegeneration and the development of neurological disease **(Figure 5-14)**. Furthermore, our transcriptomic analysis may help explain the loss of diencephalic dopaminergic neurons (5 ppb TaClo), the presence of apoptotic bodies observed in the diencephalon (5 ppb and 50 ppb TaClo), and the locomotor deficits (5 ppb TaClo) in the treated 120 hpf zebrafish in our previous study.

In the current study, we found TaClo not only inhibited cellular stress responses in treated larval zebrafish but also activated the AHR signaling pathway and the NRF2-mediated oxidative stress response canonical pathways. The AHR signaling pathway detects and responds to environmental toxins by regulating xenobiotic metabolism and detoxification, while the NRF2-mediated oxidative stress response coordinates cellular antioxidant and anti-inflammatory responses. Together, these pathways cooperate and cross-regulate to maintain cellular defense against oxidative and chemical stress. AHR is a cytosolic, ligand-activated transcription factor widely expressed across various cell types. Upon binding to a ligand, AHR undergoes a conformational change, dissociates from the cytosolic complex, and translocates to the nucleus and dimerizes with the AHR nuclear translocator (ARNT) to form a functional transcription factor complex (AHR/ARNT complex). AHR/ARNT complex binds to xenobiotic response elements (XRE) in the regulatory regions of AHR target genes, leading to the transcriptional activation of genes involved in xenobiotic metabolism, ligand degradation, phase I xenobiotic-metabolizing enzymes, such as CYP1A1, CYP1B1, IDO1, and TDO2. Additionally, AHR/ARNT complex activates the transcription of aryl hydrocarbon receptor repressor (AHRR), which acts as a negative feedback regulator by competing with AHR for ARNT binding (AHRR:ARNT complexes) to inhibit further AHR/ARNT formation (Coretti et al., 2024; Grishanova & Perepechaeva, 2022). The NRF2-mediated oxidative stress response is a central cellular defense mechanism that regulates the response to oxidative and toxic stress. NRF2 serves as the master regulator of antioxidant and phase II detoxification enzymes. Under basal conditions, NRF2 is sequestered in the cytoplasm by KEAP1, which acts as a substrate adaptor for the Cullin 3 (Cul3)-based E3 ubiquitin ligase complex. This interaction facilitates the polyubiquitination and subsequent proteasomal degradation of NRF2. Upon exposure to oxidative stress, specific redox-sensitive cysteine residues on KEAP1 are modified, inducing a conformational change that disrupts its ability to promote NRF2 ubiquitination. As a result, stabilized NRF2 accumulates in the cytoplasm, translocates into the nucleus, and forms heterodimers with small Maf (sMaf) proteins. This complex then binds to antioxidant response elements (AREs) in the promoter regions of target genes, driving the expression of cytoprotective genes involved in the detoxification of reactive oxygen species and other oxidants, including phase II detoxification enzymes, such as glutathione peroxidase (GPx), glutathione S-transferases (GSTs), and UDP-glucuronosyltransferases (UGTs) and antioxidant enzymes such as heme oxygenase-1 (HOMX1),

and NAD(P)H:quinone oxidoreductase 1 (NQO1) (Ngo & Duennwald, 2022). In our study, only the 50 ppb and 500 ppb TaClo treatments activated the AHR signaling pathway and the NRF2-mediated oxidative stress response, with the 500 ppb TaClo group exhibiting a higher activation z-score. Notably, gene expression changes associated with these two canonical pathways were observed exclusively in larvae treated with 500 ppb TaClo. Given the known mechanisms of AHR and NRF2 signaling, we propose that the higher concentration of TaClo (50 and 500 ppb) activates these pathways through both **direct** and **indirect** mechanisms **(Figure 5-15)**. **(1) Direct mechanism.** For AHR signaling pathway, we suggest TaClo may act as a ligand for AHR, with a higher concentration of TaClo enhancing the frequency of AHR nuclear translocation and promoting the downstream transcription. In the previous research study, Hubbard et al. demonstrated 3-methyl indole could activate human AHR in a dose-dependent manner and exhibit a modest activation of mouse AHR (Hubbard et al., 2015). Additionally, environmental chemicals can modulate AHR signaling not only by acting as ligands interacting with AHR, but also by downregulating its repressor, AHRR. For example, benzo[a]pyrene (BaP) has been shown to enhance AHR signaling both by acting as an agonist and by suppressing AHRR expression (Niestroy et al., 2011). Similar to our findings, the 500 ppb TaClo-treated larval group showed not only a predicted activation of AHR, AHR/ARNT complex, and AHR/ARNT/aryl hydrocarbon complex, but also a predicted inhibition of AHRR and the AHRR:ARNT complex. Thus far, these findings suggest that activation of the AHR signaling pathway may require higher concentrations of TaClo (50 and 500 ppb), with 500 ppb potentially and directly acting both as a ligand for AHR and as a modulator of AHRR expression to further enhance AHR signaling. For the NRF2-mediated oxidative stress response pathway in our study, we also propose that the higher concentrations of TaClo exert a more direct and potent influence on pathway activation. For example, Zhuang et al. demonstrated that 1,4-diaminonaphthalene activated NRF2-mediated transcription in a dose-dependent manner using a cell-based ARE-luciferase reporter assay (Zhuang et al., 2017). Similarly, Li et al. found 5,6-dihydrocyclopenta-1,2-dithiole-3-thione (CPDT) and sulforaphane (SF) induced dose-dependent elevation of NRF2 (Li et al., 2012). Similar to our current findings, our study showed that among all concentrations of TaClo exposure in embryonic zebrafish, the highest dose (500 ppb) was associated with a predicted activation of NFE2L2 (NRF2). In addition, we observed a predicted inhibition of *KEAP1* and activation of actin in the 500 ppb TaClo-exposed 120 hpf zebrafish. Under homeostatic

conditions, KEAP1 forms part of an E3 ubiquitin ligase, which tightly regulates the activity of the transcription factor NRF2 by targeting it for ubiquitination and proteasome-dependent degradation (Baird & Yamamoto, 2020). Additionally, this regulatory function is facilitated by KEAP1's double glycine repeat domain, which anchors it to the actin cytoskeleton, providing a structural scaffold essential for repressing NRF2 activity in the cytoplasm (Guerrero-Escalera et al., 2022). Taken together, similar to AHR signaling pathway, these findings suggest that activation of the NRF2-mediated oxidative stress response may also require higher concentrations of TaClo (50 and 500 ppb). In addition, we suggest that 500 ppb TaClo may directly disrupt and inhibit KEAP1 function in addition to the actin cytoskeleton anchoring through conformational changes and trigger the release of NRF2, allowing its nuclear translocation and subsequent activation of the NRF2-mediated antioxidant pathway**. (2) Indirect mechanism.** HSPs have been shown to participate in both the AHR signaling pathway and the NRF2-mediated oxidative stress response. In the AHR signaling pathway, structural studies have revealed that HSP90 binds to AHR, forming a multiprotein complex that stabilizes AHR in its inactive cytoplasmic state (Diao et al., 2025). In the NRF2-mediated oxidative stress response pathway**,** HSP90 has been demonstrated to play a regulatory role in NRF2 activation under stress conditions**.** Under heat shock stress, HSP90 interacts with both NRF2 and its negative regulator KEAP1, modulating their stability and influencing the release and promotes NRF2 nuclear translocation and the activation of the downstream gene expression (H. Zhang et al., 2022). Moreover, a previous study showed that while upregulated HSPs can modulate NRF2 pathway activation, inhibition of HSP90 specifically enhanced NRF2 activation in a diabetic model, where HSP90 suppression led to an increased NRF2-mediated antioxidant response in the vasculature (Lazaro et al., 2017). In our study, many HSPs were found to be downregulated across all TaClo concentrations in the 0–120 hpf zebrafish-treated groups. We propose that TaClo-induced dysregulation of HSPs may indirectly modulate both the AHR signaling pathway and the NRF2-mediated oxidative stress response through disrupted interactions between HSPs and their associated regulatory proteins. In addition to responding to heat shock stress, the crosstalk between the AHR signaling pathway and NRF2-mediated oxidative stress response has been well-studied. For example, upon activation by environmental ligands, AHR can upregulate NRF2 expression by binding to xenobiotic response elements (XREs) in the NRF2 promoter, thereby enhancing the transcription of NRF2 and its downstream antioxidant genes. On the other

hand, NRF2 can influence AHR expression by binding to antioxidant response elements (AREs) in the AHR promoter, promoting the expression of AHR and facilitating the induction of phase I and phase II detoxification enzymes (Hwang et al., 2022; Shin et al., 2007). Collectively, these overall findings indicate that the TaClo-induced activation of the AHR signaling pathway and the NRF2-mediated oxidative stress response is a complex, multifactorial process, potentially involving both direct interactions and indirect regulatory mechanisms.

Lastly, we observed that only the 500 ppb TaClo-treated larval zebrafish exhibited significant upregulation of AHR- and NRF2-associated DEGs, including cyp1a, cyp1b1, nqo1, and hmox1, relative to other treatment groups. These findings suggest that exposure to 500 ppb TaClo induces a more robust cellular defense and antioxidant response in larval zebrafish. This enhanced response may account for the absence of diencephalic dopaminergic neuronal downregulation and apoptotic bodies, as well as the elevated glutathione peroxidase activity previously observed in this treatment group in Chapter 3. However, gene expression related to glutathione peroxidase was not significantly altered in the 500 ppb TaClo-treated 120 hpf zebrafish, as observed in both our previous study in Chapter 3, which utilized quantitative polymerase chain reaction (qPCR), and the current study employing RNA-seq analysis. While gene expression offers valuable insights into cellular responses to oxidative stress and the regulation of antioxidant systems, it does not always correlate directly with enzymatic activity in cells or tissues. This is because gene expression reflects the potential for enzyme production but does not directly measure enzyme activity or the overall antioxidant capacity of the system. Antioxidant activity is the result of multiple regulatory layers, including enzyme activation, post-translational modifications, substrate availability, and the broader cellular context, rather than gene transcription alone (Dudziak et al., 2019). This concept is supported by a study in fish exposed to benzyl butyl phthalate (BBP) and di(2-ethylhexyl) phthalate (DEHP). The authors found that antioxidant enzyme activity could be either stimulated or suppressed depending on the concentration and duration of exposure. However, changes in enzyme activity did not always align with mRNA expression levels. For example, BBP increased superoxide dismutase (SOD) activity at low concentrations, yet the pattern of SOD mRNA expression did not parallel the observed changes in enzymatic activity (Cong et al., 2020). Therefore, although our results

indicate activation of the NRF2-mediated oxidative stress response, along with upregulation of associated cytoprotective genes, the enhanced glutathione peroxidase activity observed in larval zebrafish exposed to 500 ppb TaClo occurred in the absence of corresponding changes in gene expression. This discrepancy may suggest that additional regulatory mechanisms beyond transcriptional control contribute to these findings.

Thus far, our transcriptomic analysis suggests that TaClo modulates the cellular stress response and may contribute to neurodegeneration and altered neurobehavior; however, these effects were not observed in 1.75 μM MPTP-treated zebrafish larvae. Therefore, we hypothesize that although TaClo and MPTP share structural similarities, they engage distinct mechanisms of action and may target different cell types, ultimately leading to neurobehavioral changes. Our study revealed that MPTP exposure targeted at multiple components of the glutamatergic synapse in the treated larval zebrafish. Specifically, MPTP significantly upregulated the glutamate transporter (SLCA12) and was predicted to activate glutamine synthetase**,** metabotropic glutamate receptors 3 and 5, and vesicular glutamate transporter. In addition, MPTP affected lipid metabolism and significantly altered canonical pathways related to neurotransmission, including glutamate receptor signaling**,** neurotransmitter release cycle**,** SUMOylation of SUMOylation proteins, and trans-Golgi network vesicle budding**.** Moreover, synaptic transmission and psychological disorders were reported to be affected by IPA. A delicate balance between glutamate release, receptor activation, and transporter-mediated clearance is essential for maintaining synaptic plasticity and neural function. Disruption of this balance can impair neuronal communication and plasticity, contributing to the development of various neurological disorders (Pajarillo et al., 2019). Glutamate is the primary excitatory neurotransmitter in the central nervous system and is synthesized predominantly in presynaptic neurons. The synthesized glutamate is loaded into synaptic vesicles by vesicular glutamate transporters for glutamate storage and transport in the presynaptic neurons before being released into the synaptic cleft. When an action potential arrives at the presynaptic terminal, calcium influx triggers vesicle fusion with the membrane, releasing glutamate into the synaptic cleft. Once glutamate is released into the synaptic cleft, glutamate binds to ionotropic or metabotropic receptors on the synaptic membrane (Du et al., 2020; Guimaraes et al., 2015). Excitatory

synaptic transmission relies on the precise release of glutamate activation of synaptic receptors. However, excess glutamate can overstimulate postsynaptic receptors, leading to excitotoxic neuronal death. To maintain glutamate homeostasis, astrocytic glutamate transporters rapidly clear synaptic glutamate by taking it up into adjacent astrocytes, where glutamine synthetase converts it to glutamine. The glutamine is then released, taken up by neighboring neurons, and converted back to glutamate by glutaminase, completing the glutamate–glutamine cycle in the brain (Jayakumar & Norenberg, 2016; Pajarillo et al., 2019; Soni et al., 2014). Therefore, glutamate levels and the enzymes, receptors, or transporters within the glutamatergic neuronal system can disrupt neuronal function, contributing to neurological disorders. For example, imbalances in glutamate levels or alterations in glutamate neurotransmission are implicated in anxiety and stress-related disorders (Riaza Bermudo-Soriano et al., 2012), dysregulation of the glutamate transporter has been implicated in excitotoxicity, neuronal death, and various acute and chronic neurological conditions, such as Alzheimer's disease (AD), Parkinson's disease (PD), amyotrophic lateral sclerosis (ALS), schizophrenia, anxiety, and epilepsy (Jia et al., 2020). Glutamate synthase dysfunction may relates to severe brain malformations, seizures, and other complications, such as early death, AD, schizophrenia, and epilepsy (Häberle et al., 2005; Robinson, 2000; Spodenkiewicz et al., 2016). Studies have linked VGLUT1 to learning and memory processes, and its dysfunction has been implicated in cognitive disorders. Recent studies have suggested VGLUT1 may contribute to the pathogenesis of AD, PD, and glioblastoma (Du et al., 2020). mGlu3 is particularly associated with cognitive function and its dysfunction has been linked to schizophrenia and other cognitive disorders (Dogra et al., 2022). mGluR5 has also been implicated in the pathophysiology of several neurological and psychiatric disorders, including anxiety, schizophrenia, and addiction (Guimaraes et al., 2015). Moreover, IPA analysis predicted that larvae exposed to 1.75 μM MPTP exhibited significant alterations in lipid and cholesterol concentrations. Previous studies demonstrated that cholesterol loss disrupted the trafficking and membrane distribution of glutamate transporters (Butchbach et al., 2004). Moreover, researchers have found EAAT2 is particularly enriched in lipid raft microdomains and is more sensitive to cholesterol depletion than other glutamate transporter subtypes (Allen et al., 2007). Lastly, the SUMOylation of proteins pathway was identified as one of the canonical pathways significantly predicted affected following exposure to 1.75 μM MPTP. SUMOylation is a post-translation modification where small ubiquitin-like modifier (SUMO) proteins

covalently attached to other proteins to regulate protein localization and function (Foran et al., 2014). Previous studies have shown that SUMOylation regulates the subcellular localization of the glutamate transporter (SLC1A2, EAAT2, GLT-1) (Pajarillo et al., 2019; Passlick et al., 2021). Specifically, SUMOylated EAAT2 is retained in intracellular compartments, whereas the non-SUMOylated form is localized to the plasma membrane (Foran et al., 2014; Peterson & Binder, 2019). Therefore, we suggest that exposure to 1.75 μM MPTP in larvae triggers alterations in gene expression, enzyme and receptor function, and post-translational modifications. These changes may contribute to the dysregulation of glutamatergic synaptic plasticity, leading to neuronal dysfunction and the development of neurological disease **(Figure 5-16)**. However, future studies should include neurotransmitter detection to assess glutamate levels in 1.75 μM MPTP-treated larvae, providing further insight into the potential disruption of glutamatergic signaling. Our transcriptomic analysis in zebrafish larvae revealed that MPTP exposure was strongly associated with psychological disorders, including mood disorders, major affective disorder, depressive disorder, anxiety disorders, and social anxiety disorder. Additionally, anxiety-related pathways were predicted to be significantly activated in the transcriptomic dataset from the adult zebrafish brain. Taken together, our findings align with the Developmental Origins of Health and Disease (DOHaD) concept, suggesting that embryonic exposure to 1.75 μM MPTP programs glutamatergic neurotransmission, which in turn can predispose individuals to heightened anxiety in adulthood.

Stress is a fundamental biological process that promotes adaptation to physical or psychological challenges, helping vertebrates maintain physiological and behavioral balance and protect against damage. However, excessive stress during vulnerable developmental windows can impose a high allostatic load, which may drive or accelerate maladaptive processes and disease (Lupien et al., 2009; Zou et al., 2020). In our study, we found that TaClo exposure suppressed heat shock proteins and inhibited cellular stress responses in zebrafish larvae. We propose that TaClo, at concentrations of 5 ppb, 50 ppb, and 500 ppb, exerts excessive stress on larval zebrafish, leading to a maladaptive response that impairs protective mechanisms. This disruption may increase vulnerability to protein misfolding, neuronal apoptosis, and organismal death, ultimately compromising neuroprotection and increasing the risk of neurological disorders. In line with the Developmental Origins of Health and Disease (DOHaD) concept, we

hypothesize that embryonic exposure to TaClo (5, 50, 500 ppb) or 1.75 µM MPTP "programs" long-lasting alterations in cellular stress response pathways and DEGs in zebrafish that persist into adulthood. However, transcriptomic analysis of the 6 mpf zebrafish brain following early life exposure to TaClo revealed a reversal of the stress response profile observed at the 120 hpf zebrafish. For example, HSPB1 and NFKBIA, which were downregulated in 120 hpf zebrafish, were upregulated in the 6 mpf adult brain. Similarly, predicted activation of apoptosis and organismal death during the 120 hpf zebrafish larvae was reversed to predicted inhibition in 6 mpf zebrafish brain. Furthermore, canonical pathways associated with cellular stress responses that were inhibited in 120 hpf zebrafish larvae were no longer detected in 6 mpf zebrafish brain; instead, pathways related to cellular stress responses, such as serotonin receptor signaling, G protein-coupled receptor signaling, and calcium signaling were predicted to be activated in the 6 mpf zebrafish brain. These findings suggest that adult zebrafish possess the capacity to reprogram their cellular stress response by activating compensatory adaptive mechanisms to restore homeostasis and mitigate the adverse effects induced by early-life exposure. Furthermore, the presence of this compensatory response, along with our previous findings in the 6 mpf zebrafish brain that we observed the increased mean fluorescence intensity of MitoSOX in the 500 ppb TaClo-treated group and elevated glutathione peroxidase enzymatic activity in 5 ppb and 500 ppb TaClo-exposed groups in Chapter 4, may indicate a continuous, albeit lower-level, oxidative stress in adulthood following embryonic TaClo exposure **(Figure 5-17)**.

TaClo and MPTP are chemically and structurally similar compounds, both reported as neurotoxicants targeting dopaminergic neurons and inducing hypolocomotion, sharing common mechanisms implicated in PD development. Consistent with previous studies and our findings in Chapter 3, both compounds caused locomotor deficits, reduced diencephalic dopaminergic neuronal expression, and increased apoptotic bodies in the diencephalon of treated larval zebrafish. However, transcriptomic analysis revealed that TaClo and 1.75 µM MPTP may act via distinct mechanisms and affect different cellular targets. In our study, we found that MPTP exposure was associated with dysregulated glutamatergic synaptic transmission and linked to anxiety-related disorders. Additionally, in the Chapter 3 we observed a significant decrease in 5-Hydroxyindoleacetic acid (5-HIAA), a metabolite of serotonin commonly used to assess serotonin production, in 1.75 µM MPTP-exposed larvae. These findings suggest several

possibilities: (1) 1.75 μM MPTP may target multiple neuronal populations, including dopaminergic, glutamatergic, and serotonergic neurons; (2) locomotor deficits may not solely result from dopaminergic neuron loss but also reflect anxiety-like phenotypes involving serotonin depletion and disrupted glutamate signaling; and (3) anxiety itself may independently influence locomotor behavior, separate from dopaminergic dysfunction. Similarly, although the specific cellular targets of TaClo have not yet been fully identified, transcriptomic analysis predicted significant activation of cell death in muscle cells and notable impacts on the muscular system, including cell death of smooth muscle cells, apoptosis of muscle cells, atrophy of skeletal muscle, and abnormal morphology of muscle. These observations imply that TaClo-induced locomotor deficits in 120 hpf zebrafish larvae may not be solely attributable to dopaminergic neuronal loss but could also arise from muscle-related dysfunction, contributing to neurobehavioral abnormalities. Furthermore, our transcriptomic analysis revealed that neither the 120 hpf larvae nor the 6 mpf zebrafish brains showed significant enrichment of the PD signaling canonical pathway, and no PD-related differentially expressed genes (DEGs) were identified in either the TaClo- or MPTP-treated groups. However, these outcomes may vary depending on factors such as exposure dosage, developmental stage at the time of exposure, exposure duration, anatomical region analyzed, and the analytic methods and endpoints. Therefore, further investigation is warranted to elucidate the underlying mechanisms.

## 5. Conclusion

In conclusion, our study demonstrates that TaClo and MPTP utilize different mechanisms to induce neurotoxic effects. In addition, our findings suggest that TaClo and MPTP are not only neurotoxicants but also contribute to the development of broader systemic diseases with long-term impacts.

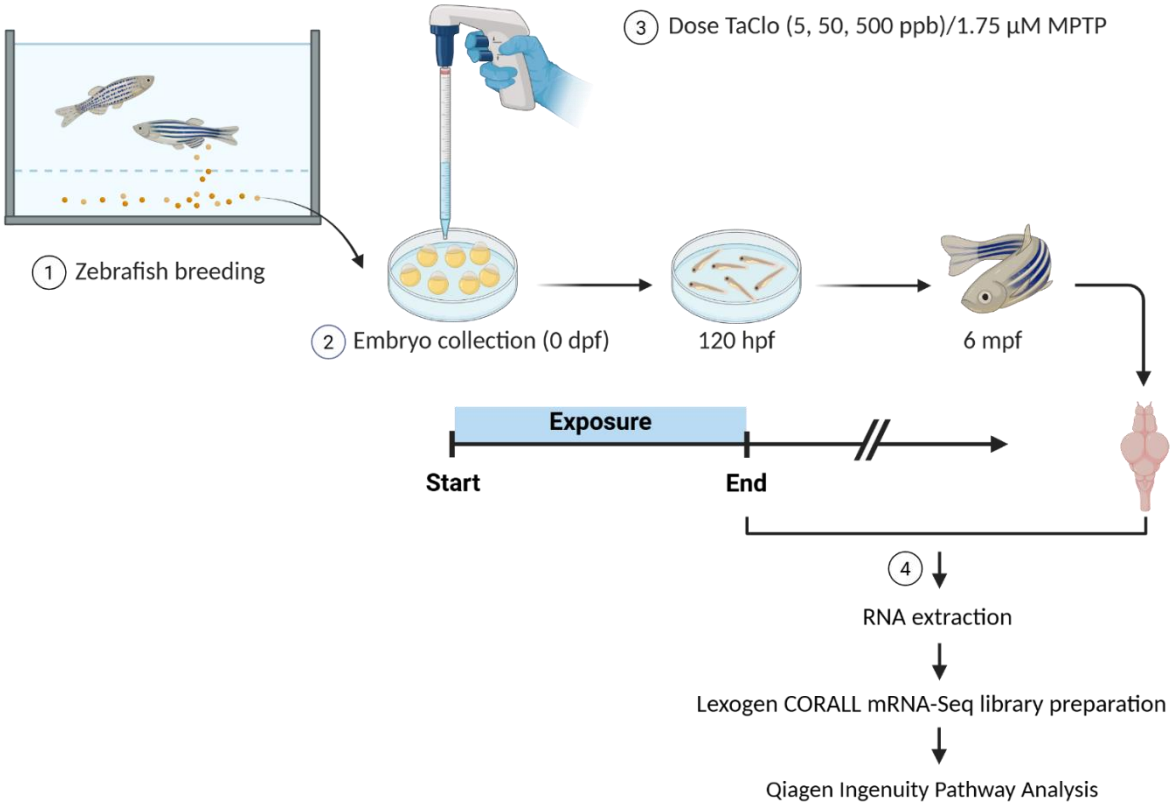


**Figure 5-1. Schematic overview of the experimental regime**

① Adult wild-type AB strain zebrafish (*Danio rerio*) were bred to obtain embryos for chemical exposure. ② Fertilized embryos at 0 days post-fertilization (dpf) were collected and ③ exposed to 1-trichloromethyl-1,2,3,4-tetrahydro-beta-carboline (TaClo) (0, 5, 50, 500 ppb), vehicle (dimethyl sulfoxide, 0.001% DMSO), or 1.75 µM 1-methyl-4-phenyl-1,2,3,6-tetrahydropyridine (MPTP) until 120 hours post-fertilization (hpf). 120 hpf treated zebrafish were rinsed and raised with chemical-free aquaria water and maintained until 6 months post-fertilization (mpf). ④ 120 hpf zebrafish and 6 mpf zebrafish were euthanized. The pool of 120 hpf zebrafish larvae (up to 50 larvae per treatment per group) and the brains removed from 6 mpf zebrafish were collected for RNA extraction, Lexogen CORALL mRNA-Seq library preparation, and QIAGEN Ingenuity Pathway Analysis.

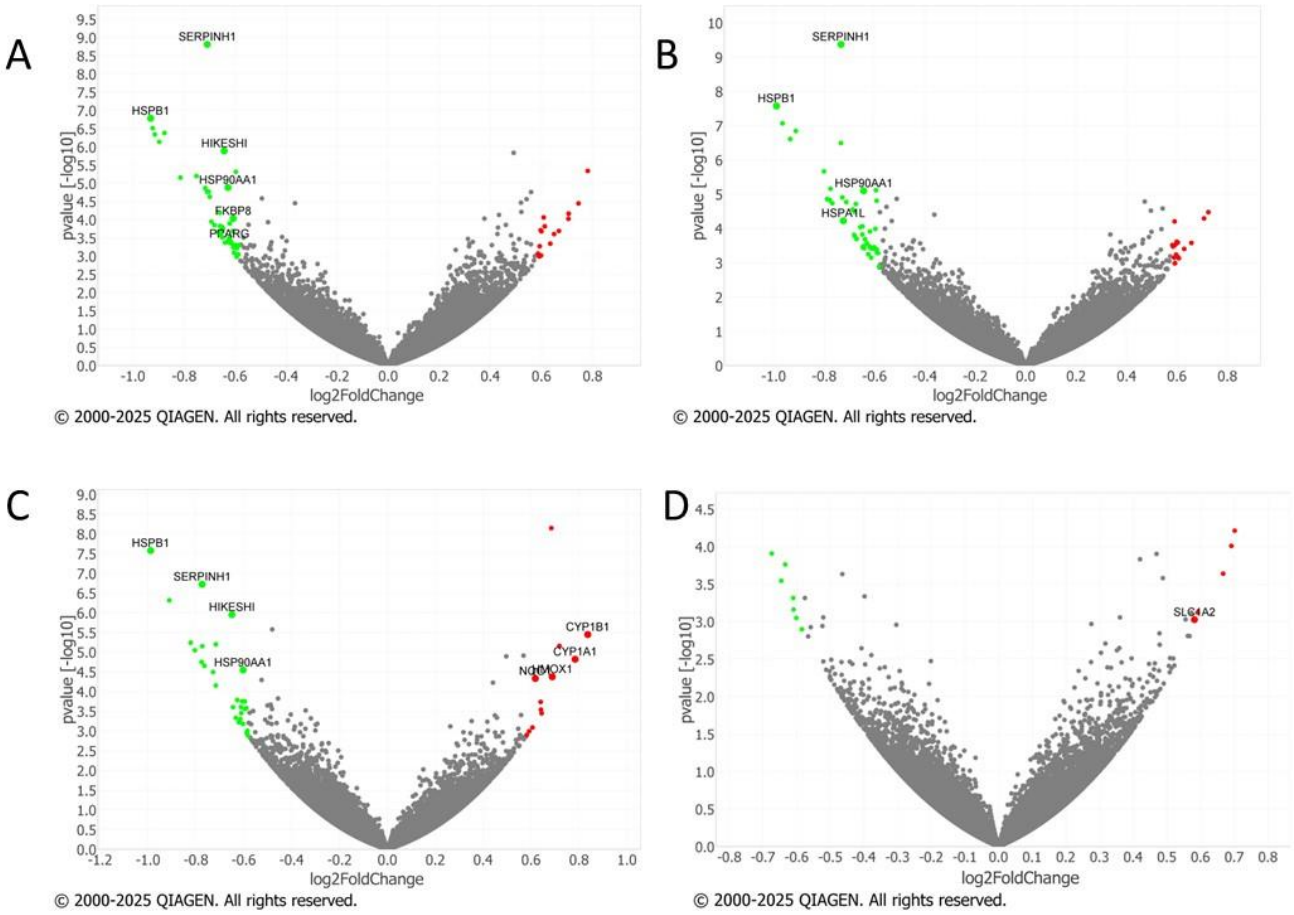


**Figure 5-2. Volcano plots generated by QIAGEN Ingenuity Pathway Analysis for each treatment group in 120 hours post-fertilization zebrafish**

5 ppb TaClo (A), 50 ppb TaClo (B), 500 ppb TaClo (C), and 1.75 µM MPTP (D). Green dots represent downregulated DEGs, red dots represent upregulated DEGs, and grey dots represent non-significant.

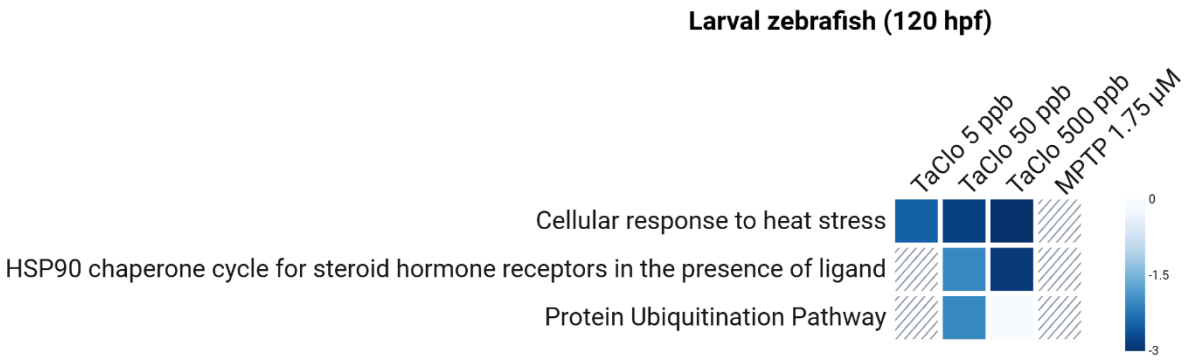


**Figure 5-3. Canonical pathways in 120 hours post-fertilization zebrafish larvae**
QIAGEN Ingenuity Pathway Analysis predicted significant inhibition of several stress response-related pathways, including the cellular response to heat stress, HSP90 chaperone cycle for steroid hormone receptors in the presence of ligand, and the protein ubiquitination pathway in TaClo (5, 50, and 500 ppb) and 1.75 µM MPTP-treated groups. The heatmap was generated by BioRender. The value on the scale bar represents z-score.

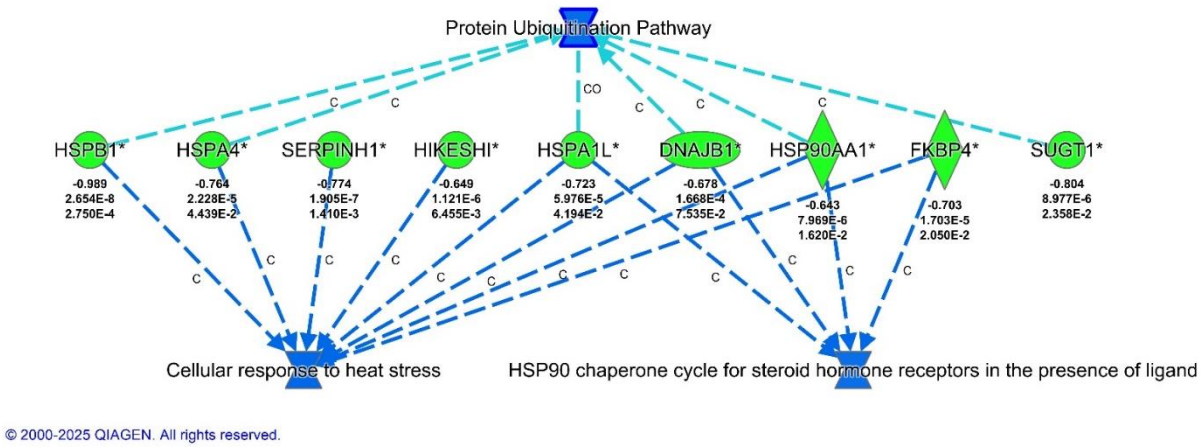


**Figure 5-4. Canonical pathways and the associated molecules in the TaClo-treated 120 hours post-fertilization zebrafish**

QIAGEN Ingenuity Pathway Analysis predicted that the inhibited cellular response to heat stress, HSP90 chaperone cycle for steroid hormone receptors in the presence of ligand, and protein ubiquitination canonical pathway were primarily regulated by a common set of downregulated heat shock genes. Green: decreased measurements, blue: predicted inhibition, blue dotted line: indirect interaction and lead to inhibition.

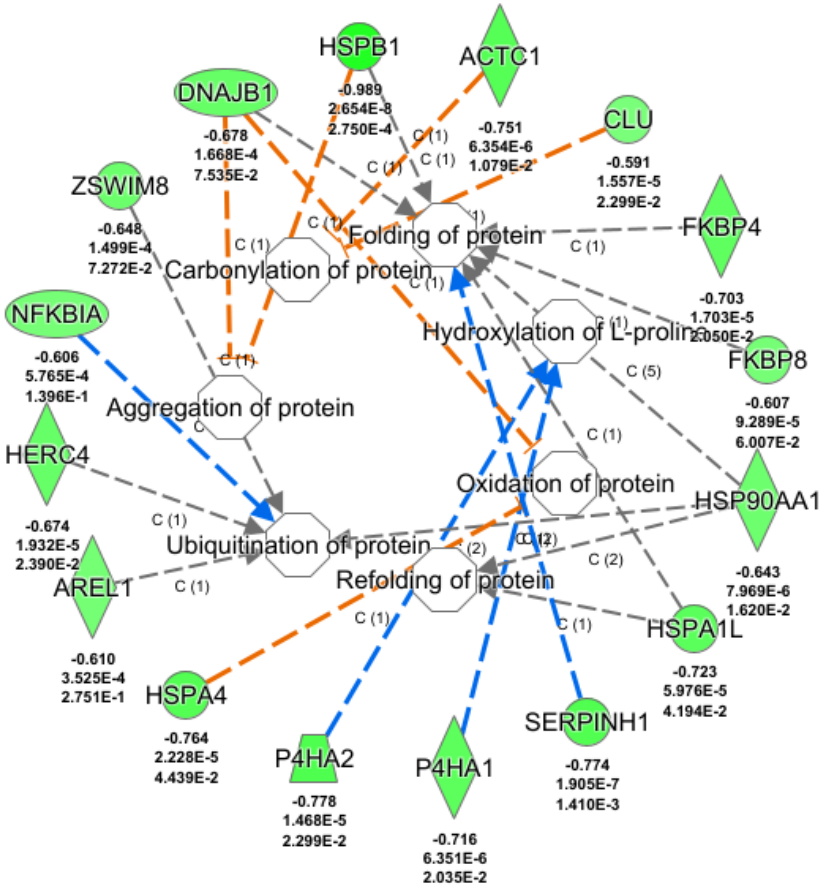


**Figure 5-5. Protein folding and post-translational modifications and the associated molecules in the TaClo-treated 120 hours post-fertilization zebrafish**

QIAGEN Ingenuity Pathway Analysis predicted downregulated molecules were significantly associated with protein folding and post-translational modifications. Green: decreased measurements, blue dotted line with arrow: indirect interaction and lead to inhibition, orange dotted line: indirect interaction and lead to activation, and grey line: unpredicted effects.

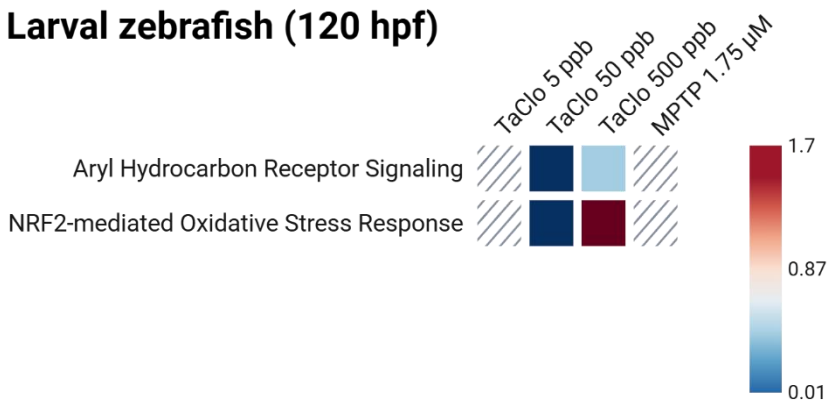


**Figure 5-6. Canonical pathways in 120 hours post-fertilization zebrafish larvae**
QIAGEN Ingenuity Pathway Analysis predicted the canonical pathways, Aryl Hydrocarbon receptor (AHR) signaling pathway and NRF-2 mediated oxidative stress response, significantly affected the 120 hpf zebrafish larvae treated with 50 ppb and 500 ppb TaClo. The heatmap was generated by BioRender. The value on the scale bar represents z-score.

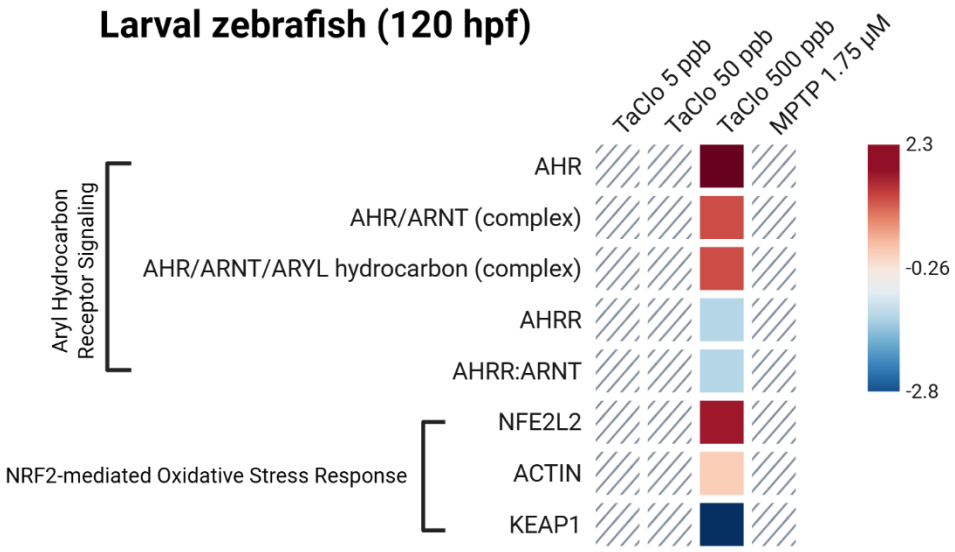


**Figure 5-7. Upstream regulators of Aryl Hydrocarbon receptor (AHR) signaling pathway and NRF-2 mediated oxidative stress response in the 120 hours post-fertilization zebrafish larvae**

QIAGEN Ingenuity Pathway Analysis predicted activation or inhibition of upstream regulators in Aryl Hydrocarbon receptor (AHR) signaling pathway and NRF-2 mediated oxidative stress response in 500 ppb TaClo treated group. The heatmap was generated by BioRender. The value on the scale bar represents z-score.

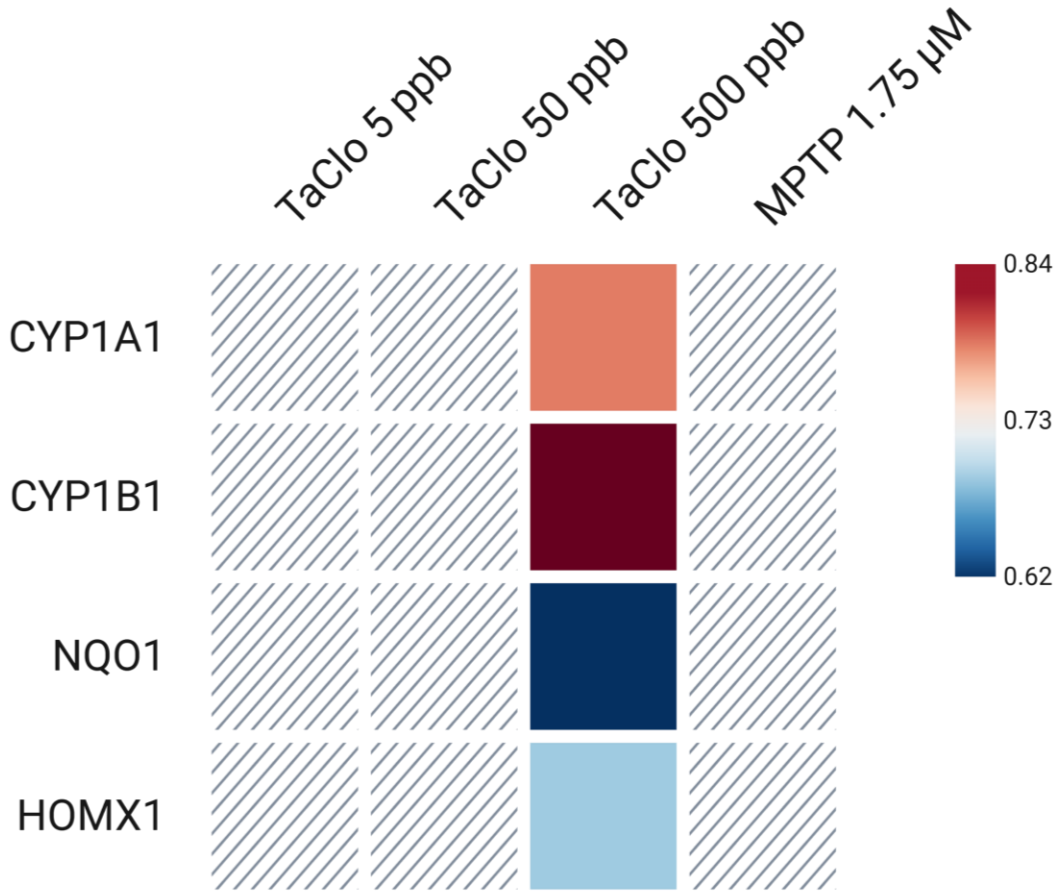


**Figure 5-8. Differential expression genes (DEG) in the 120 hours post-fertilization zebrafish larvae treated with TaClo**

Upregulation of downstream target genes associated with oxidative stress protection, such as CYP1A1, CYP1B1, NQO1, and HMOX1, was observed exclusively in the 500 ppb TaClo-treated group. The heatmap was generated by BioRender. The scale bar represents log2 fold change.

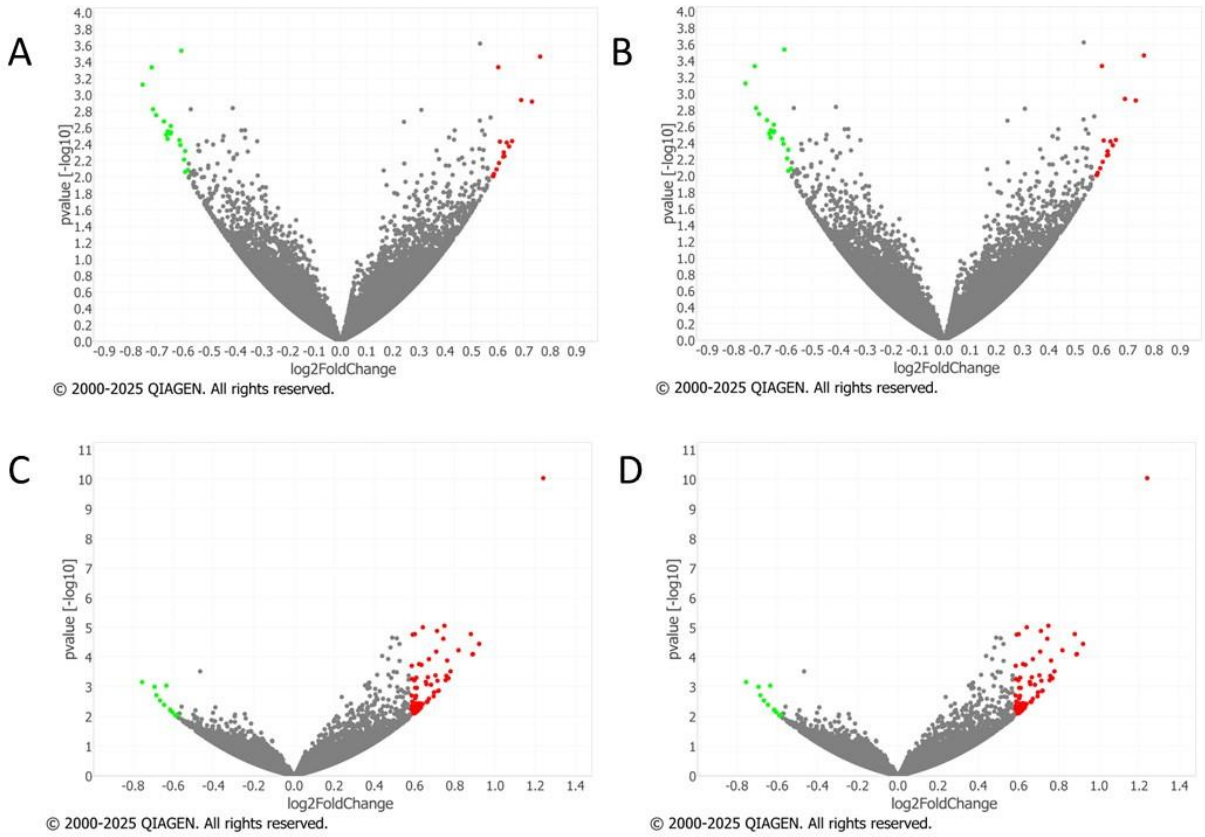


**Figure 5-9. Volcano plots generated by QIAGEN Ingenuity Pathway Analysis for each treatment group in the 6 months post-fertilization zebrafish brains**

5 ppb TaClo (A), 50 ppb TaClo (B), 500 ppb TaClo (C), and 1.75 µM MPTP (D). Green dots represent downregulated DEGs, red dots represent upregulated DEGs, and grey dots represent non-significant.

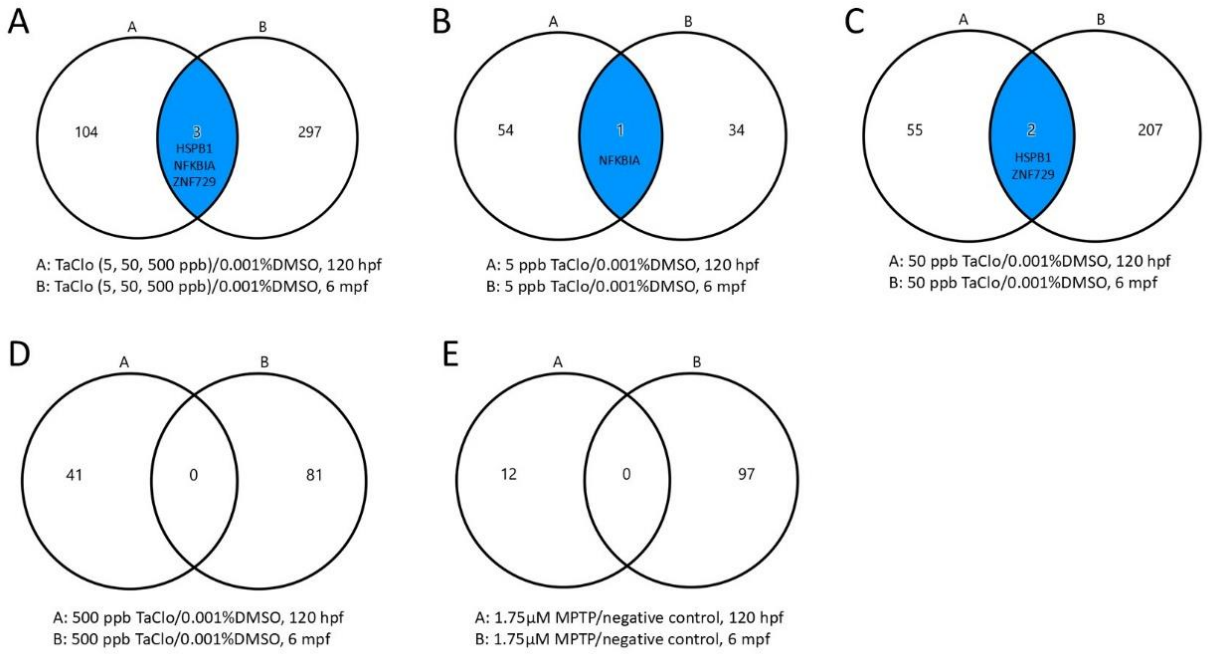


**Figure 5-10. Venn diagram showing the number of differentially expressed genes per comparison across 120 hours post-fertilization larvae and 6 months post-fertilization zebrafish brains**

Venn diagrams were generated by QIAGEN Ingenuity Pathway Analysis software and each diagram represents TaClo (5, 50, 500 ppb) (A), 5 ppb TaClo (B), 50 ppb TaClo (C), 500 ppb TaClo (D), and 1.75 μM MPTP (E).

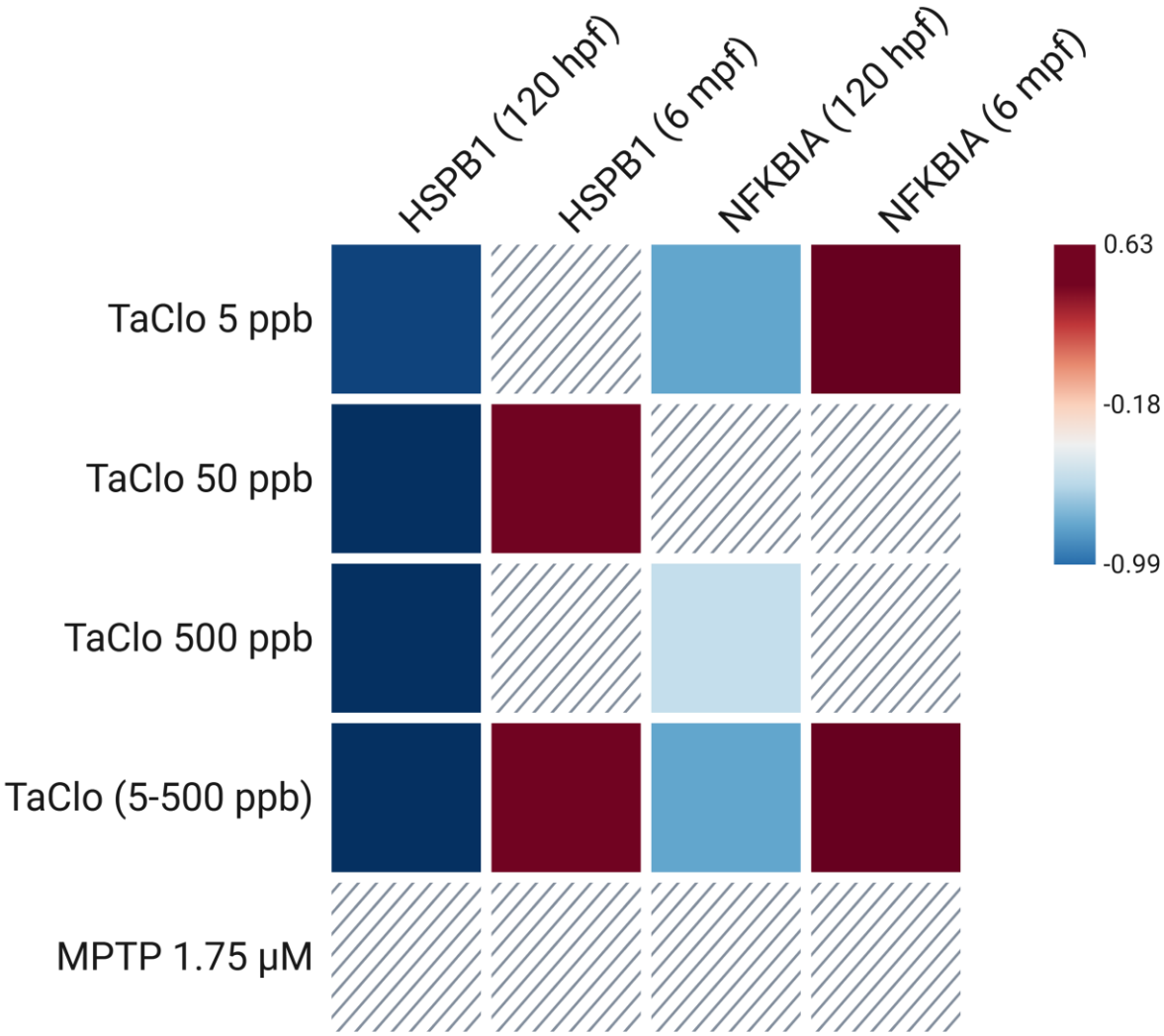


**Figure 5-11. Differential expression genes (DEGs) of HSPB1 and NFKBIA in 120 hours post-fertilization zebrafish larvae and 6 months post-fertilization zebrafish brains treated with early life TaClo and 1.75 µM MPTP**

The heatmap was generated by BioRender. The value on the scale bar represents $\log_2$ fold change.

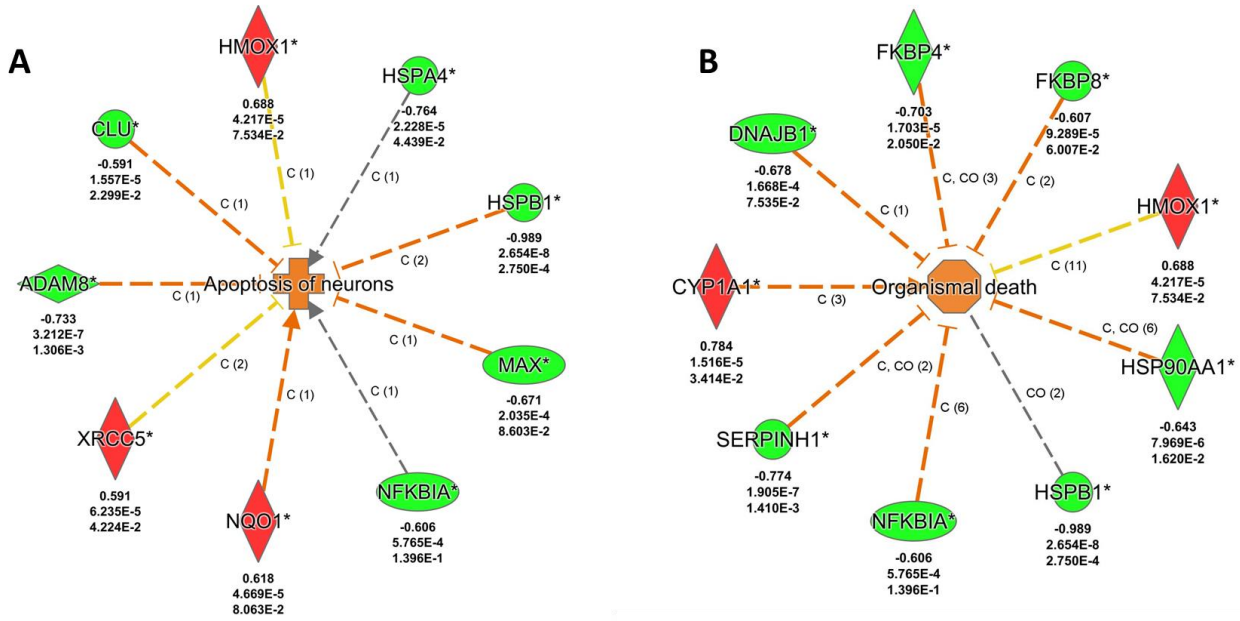


**Figure 5-12. Apoptosis of neurons and organismal death and the associated molecules in the TaClo-treated 120 hours post-fertilization zebrafish**

QIAGEN Ingenuity Pathway Analysis predicted downregulated molecules (HSPB1 and NFKBIA) were associated with the activation of the apoptosis of neurons (A) and organismal death (B). Green: decreased measurements, blue dotted line with arrow: indirect interaction and lead to inhibition, orange dotted line: indirect interaction and lead to activation, and grey line: unpredicted effects.

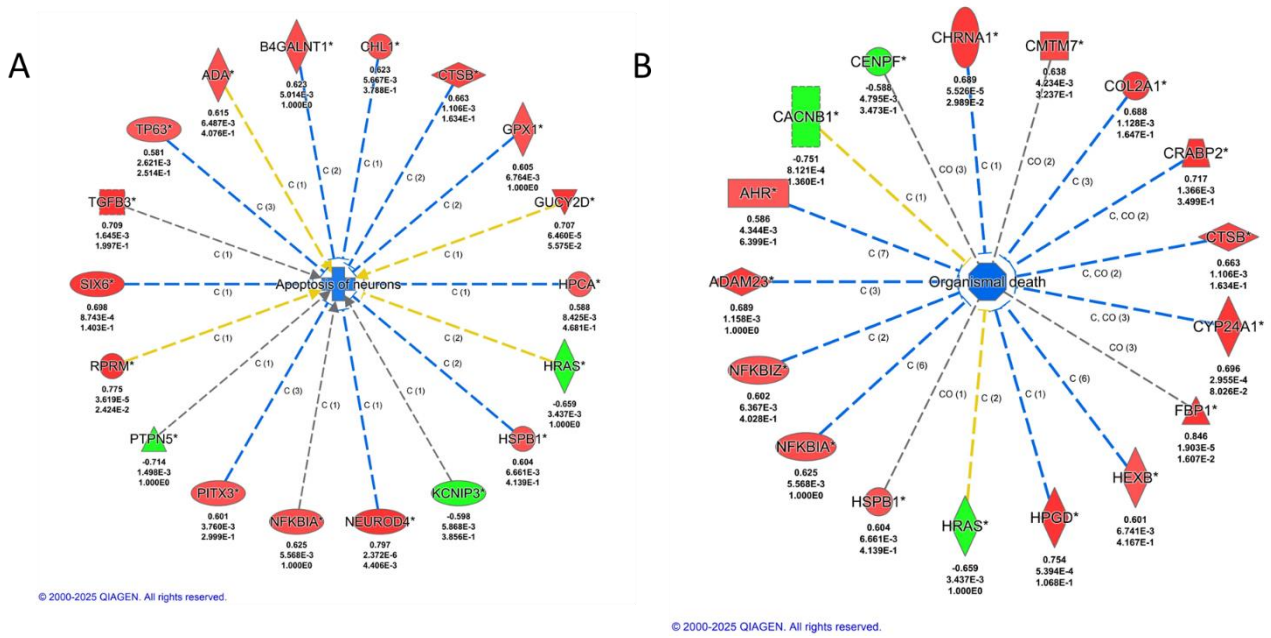


**Figure 5-13. Apoptosis of neurons and organismal death and the associated molecules in the TaClo-treated 120 hours post-fertilization zebrafish in 6 months post-fertilization zebrafish brain**

QIAGEN Ingenuity Pathway Analysis predicted upregulated molecules (HSPB1 and NFKBIA) were associated with the inhibition of apoptosis of neurons (A) and organismal death (B). Green: decreased measurements, blue dotted line with arrow: indirect interaction and lead to inhibition, orange dotted line: indirect interaction and lead to activation, and grey line: unpredicted effects. Green: decreased measurements, red: increased measurement, blue dotted line with arrow: indirect interaction and lead to inhibition, orange dotted line: indirect interaction and lead to activation, grey line: unpredicted effects, and yellow dotted line: findings inconsistent with state of downstream molecules.

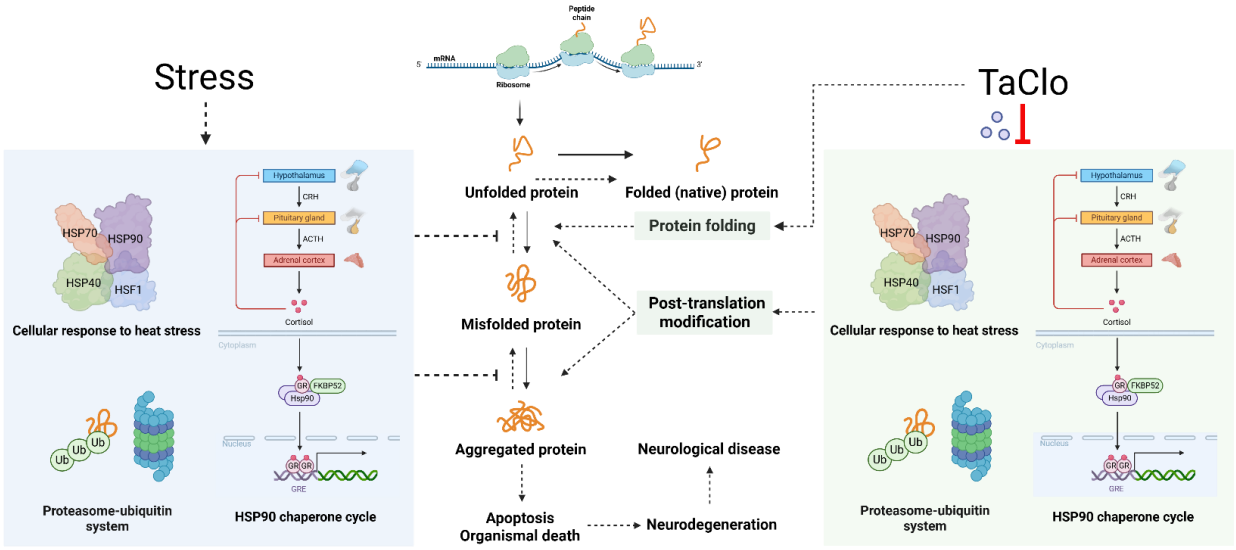


**Figure 5-14. Schematic representation of the cellular responses to stress and the impact of TaClo on protein folding and formation of neurodegeneration and neurologic disease**

TaClo inhibits cellular responses to stress, which may directly impact protein folding or indirectly leads to misfolded or aggregated proteins through post-translation modification. The misfolded and aggregated proteins may promote apoptosis and organismal death and further lead to neurodegeneration and the development of neurologic disease.

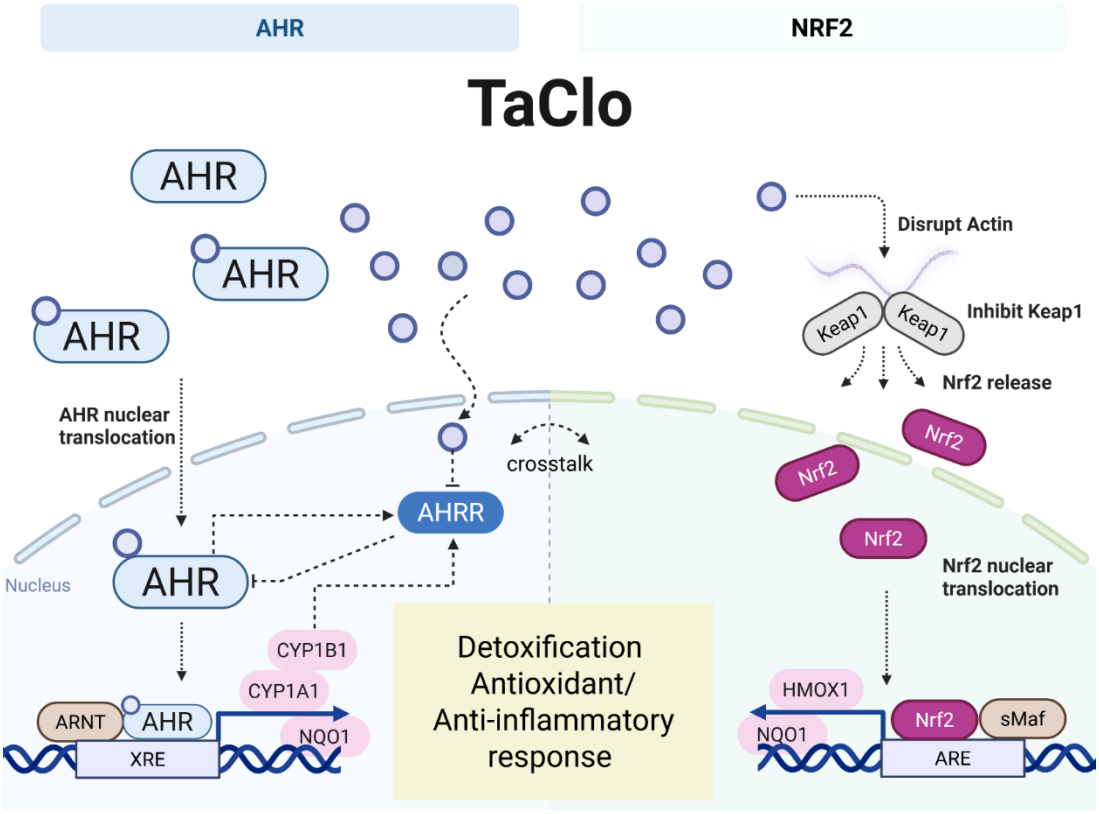


**Figure 5-15. Aryl hydrocarbon receptor and NR2-mediated oxidative stress response canonical pathways in 120 hours post-fertilization zebrafish treated with 500 ppb TaClo**
500 ppb TaClo triggered aryl hydrocarbon receptor and NR2-mediated oxidative stress response pathways and upregulated the transcription of phase I of xenobiotic metabolism enzymes (CYP1A1, CYP1B1), detoxifying enzyme (NQO1), and antioxidant and anti-inflammatory protein (HMOX1) in larval zebrafish.

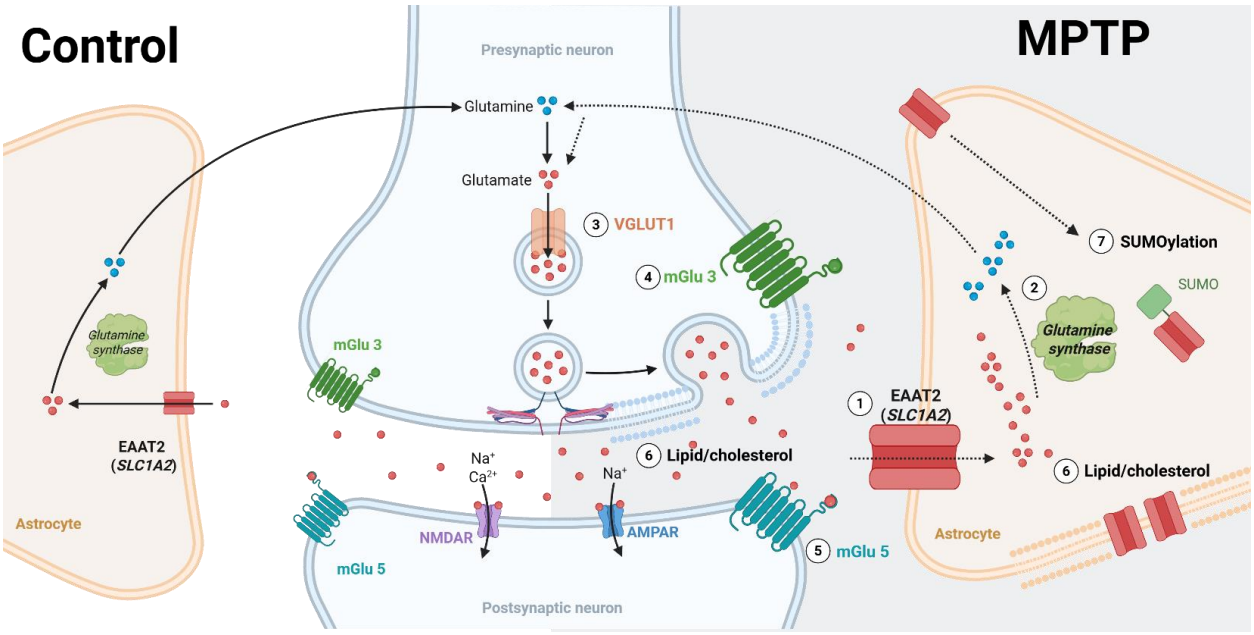


**Figure 5-16. 1.75 µM MPTP mediates the glutaminergic synaptic neuronal system**
1.75 µM MPTP significantly upregulates the glutamate transporter (*slc1a2*) and is predicted to activate glutamine synthetase, metabotropic glutamate receptors 3 and 5, and vesicular glutamate transporter. In addition, 1.75 µM MPTP affects lipid metabolism and significantly alters SUMOylation of SUMOylation proteins.

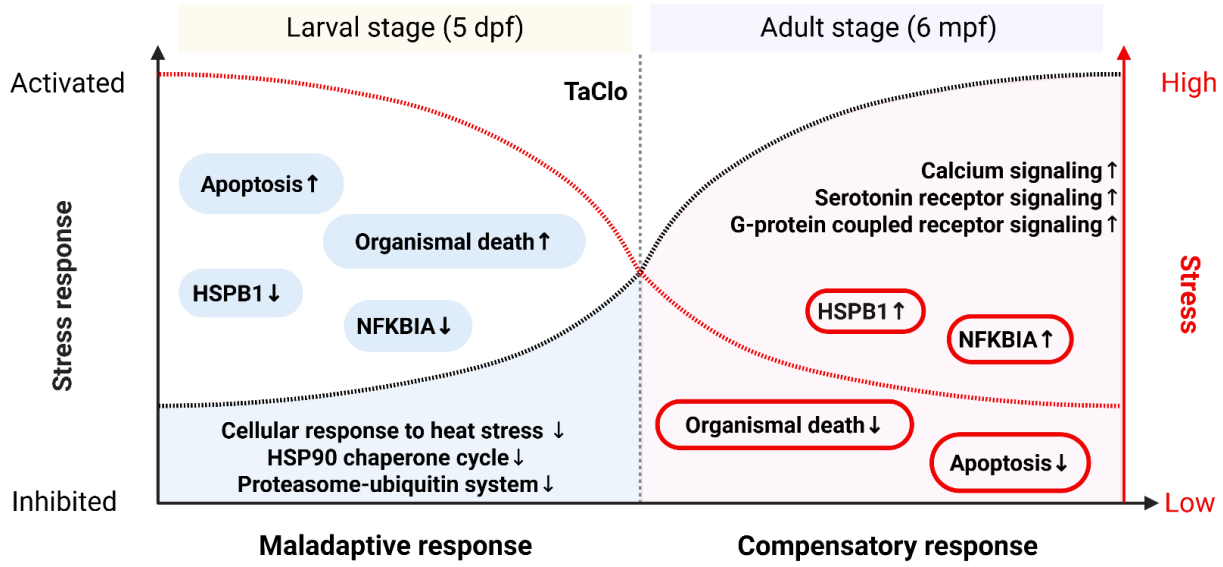


**Figure 5-17. Diagram of stress response to TaClo across larval and adult stage and the associated canonical pathways**

In TaClo-treated larvae, an inhibited stress response with increased apoptosis and organismal death, along with decreased HSPB1 (heat shock protein beta-1) and NFKBIA (NFKB Inhibitor Alpha) expression are presented. In contrast, adult brains with early life exposure to TaClo and MPTP exhibits activation of stress-responsive canonical pathways, including serotonin receptor signaling, G-protein coupled receptor signaling, and calcium signaling with decreased apoptosis and organismal death, along with upregulated HSPB1 and NFKBIA expression.

**Table 5-1. Differentially expressed genes (DEGs) in 120 hours post-fertilization zebrafish larvae treated with 5 ppb TaClo**

| ID | Symbol | Expr Log Ratio | Expr p-value | Expr False Discovery Rate (q-value) |
|---|---|---|---|---|
| ENSDART00000138548 | ABL2 | 0.649694287 | 0.000247801 | 0.098402579 |
| ENSDART00000080664 | ACTC1 | -0.750974445 | 6.35387E-06 | 0.010793467 |
| ENSDART00000140859 | ARK2N | -0.603786412 | 0.000806974 | 0.170748021 |
| ENSDART00000083317 | ARSK | -0.659011068 | 0.000148761 | 0.077096112 |
| ENSDART00000148365 | ATP2A1 | 0.668489544 | 0.000203055 | 0.09083239 |
| ENSDART00000163965 | BRDT | -0.64766817 | 0.000174713 | 0.083471938 |
| ENSDART00000062024 | CA4 | -0.698735512 | 2.34533E-05 | 0.025611821 |
| ENSDART00000169752 | CCDC40 | -0.648193275 | 0.000189008 | 0.0882011 |
| ENSDART00000137645 | CEP104 | -0.680457805 | 0.000141777 | 0.076054907 |
| ENSDART00000041249 | CHORDC1 | -0.92259233 | 3.07817E-07 | 0.002797876 |
| ENSDART00000056065 | CNPY2 | -0.595772359 | 0.000494445 | 0.12876126 |
| ENSDART00000187907 | CSAD | -0.661052042 | 0.000243567 | 0.098402579 |
| ENSDART00000111328 | CUTC | -0.716741968 | 1.35224E-05 | 0.019689282 |
| ENSDART00000102148 | D1Pas1 | 0.608834371 | 8.63449E-05 | 0.058670423 |
| ENSDART00000166146 | DNAJB1 | -0.665156493 | 0.000220701 | 0.095047575 |
| ENSDART00000130781 | EIF4A2 | -0.622493103 | 0.000313239 | 0.110091076 |
| ENSDART00000132227 | EIF4H | 0.745173374 | 3.56253E-05 | 0.034041099 |
| ENSDART00000173015 | ELMO2 | 0.613097855 | 0.000152049 | 0.07748647 |
| ENSDART00000024576 | FKBP4 | -0.703017156 | 1.70277E-05 | 0.020496726 |
| ENSDART00000002029 | FKBP8 | -0.607143995 | 9.28855E-05 | 0.060067679 |
| ENSDART00000076974 | GFPT2 | 0.60005118 | 0.000207943 | 0.09083239 |
| ENSDART00000043743 | Haus8l2 | -0.896478672 | 7.31037E-07 | 0.003193273 |
| ENSDART00000169685 | HIKESHI | -0.642399149 | 1.29539E-06 | 0.004472405 |
| ENSDART00000173648 | HMGB3 | 0.781480763 | 4.58287E-06 | 0.009167194 |
| ENSDART00000023550 | HSP90AA1 | -0.627534635 | 1.30478E-05 | 0.019689282 |
| ENSDART00000060162 | HSPB1 | -0.930550013 | 1.65141E-07 | 0.002524765 |
| ENSDART00000029528 | MOSPD2 | -0.639012297 | 0.000420623 | 0.127340622 |
| ENSDART00000156353 | MSS51 | -0.9141181 | 4.57513E-07 | 0.002797876 |
| ENSDART00000164351 | MTBP | 0.634794766 | 0.000452849 | 0.12876126 |
| ENSDART00000192783 | NEXN | -0.81379493 | 6.98943E-06 | 0.011248204 |
| ENSDART00000146625 | NFKBIA | -0.606161691 | 0.000576464 | 0.139556187 |
| ENSDART00000024137 | P4HA2 | -0.656128514 | 0.000259348 | 0.100380647 |
| ENSDART00000009223 | PDCD4 | -0.709327486 | 1.71867E-05 | 0.020496726 |
| ENSDART00000111552 | PHLDB2 | 0.586552511 | 0.000851041 | 0.177022323 |
| ENSDART00000059369 | PHYKPL | -0.609050206 | 0.000205171 | 0.09083239 |
| ENSDART00000102474 | PLEKHS1 | 0.705867425 | 9.42947E-05 | 0.060067679 |
| ENSDART00000173450 | PPARG | -0.622106492 | 0.000390484 | 0.12316628 |
| ENSDART00000008603 | PREPL | -0.620520676 | 0.00012756 | 0.073592658 |
| ENSDART00000135838 | PTP4A2 | -0.609081461 | 0.000477048 | 0.12876126 |
| ENSDART00000177475 | RDH5 | 0.592131318 | 0.001014642 | 0.188028513 |
| ENSDART00000185324 | RPGRIP1L | -0.584076808 | 0.000496414 | 0.12876126 |
| ENSDART00000140371 | RSRP1 | -0.650735374 | 0.000157932 | 0.079165607 |
| ENSDART00000035096 | SERPINH1 | -0.708700618 | 1.54779E-09 | 4.73266E-05 |
| ENSDART00000134283 | SORBS3 | -0.593147952 | 0.000525992 | 0.13390631 |
| ENSDART00000046349 | SPTY2D1 | -0.8761647 | 4.17683E-07 | 0.002797876 |
| ENSDART00000180117 | STMN3 | -0.593683853 | 0.001044228 | 0.190883571 |
| ENSDART00000138714 | Sult5a1 | 0.597046922 | 0.000193265 | 0.0882011 |
| ENSDART00000122972 | TCF7L2 | -0.649658418 | 0.000305122 | 0.109351857 |
| ENSDART00000112294 | TTC22 | 0.706651962 | 6.8203E-05 | 0.050864436 |
| ENSDART00000037692 | TTPA | 0.593225564 | 0.000533197 | 0.13390631 |
| ENSDART00000105064 | TXNDC16 | -0.659575037 | 6.46489E-05 | 0.049419235 |
| ENSDART00000151259 | U2AF2 | 0.598299799 | 0.000953096 | 0.184448152 |
| ENSDART00000183053 | XPO1 | -0.59682821 | 4.85079E-06 | 0.009167194 |
| ENSDART00000109228 | ZBTB24 | -0.692433808 | 0.000113388 | 0.067981404 |
| ENSDART00000180482 | ZNF729 | -0.656076171 | 0.000251572 | 0.098619415 |

**Table 5-2. Differentially expressed genes (DEGs) in 120 hours post-fertilization zebrafish larvae treated with 50 ppb TaClo**

| ID | Symbol | Expr Log Ratio | Expr p-value | Expr False Discovery Rate (q-value) |
|---|---|---|---|---|
| ENSDART00000169600 | ABHD4 | 0.581718707 | 0.000305983 | 0.097366364 |
| ENSDART00000138548 | ABL2 | 0.62872003 | 0.000395022 | 0.099141755 |
| ENSDART00000080664 | ACTC1 | -0.727118823 | 1.23945E-05 | 0.022986177 |
| ENSDART00000066471 | ADAM8 | -0.73318205 | 3.21177E-07 | 0.001305537 |
| ENSDART00000169401 | B4GALNT3 | 0.602535901 | 0.000674643 | 0.133307559 |
| ENSDART00000183615 | BPGM | 0.593208002 | 0.000299466 | 0.097366364 |
| ENSDART00000163965 | BRDT | -0.618299613 | 0.0003407 | 0.099141755 |
| ENSDART00000062024 | CA4 | -0.71177751 | 1.69646E-05 | 0.022986177 |
| ENSDART00000098734 | CACYBP | -0.655993301 | 9.12651E-05 | 0.056453429 |
| ENSDART00000163425 | CARNMT1 | -0.640163099 | 0.000377911 | 0.099141755 |
| ENSDART00000137645 | CEP104 | -0.767226706 | 1.84213E-05 | 0.023825416 |
| ENSDART00000125265 | CHERP | -0.637476323 | 0.000205591 | 0.086027775 |
| ENSDART00000041249 | CHORDC1 | -0.964937023 | 8.55079E-08 | 0.000675867 |
| ENSDART00000127173 | CLU | -0.591304161 | 1.55703E-05 | 0.022986177 |
| ENSDART00000020569 | CRELD1 | -0.685842036 | 2.78444E-05 | 0.028038483 |
| ENSDART00000166146 | DNAJB1 | -0.677949162 | 0.000166836 | 0.075351501 |
| ENSDART00000134178 | EIF4A2 | -0.601201796 | 0.000352443 | 0.099141755 |
| ENSDART00000184619 | EXOC1 | -0.589821953 | 0.000511092 | 0.11285751 |
| ENSDART00000024576 | FKBP4 | -0.679186412 | 3.26684E-05 | 0.028038483 |
| ENSDART00000180951 | GTPBP1 | 0.603204297 | 0.000257541 | 0.093377773 |
| ENSDART00000043743 | Haus8l2 | -0.934212392 | 2.45689E-07 | 0.001165137 |
| ENSDART00000083883 | HERC4 | -0.673866154 | 1.93191E-05 | 0.023900216 |
| ENSDART00000169685 | HIKESHI | -0.594155706 | 7.65209E-06 | 0.016196628 |
| ENSDART00000128242 | HMGB3 | 0.707448236 | 5.09856E-05 | 0.039209318 |
| ENSDART00000023550 | HSP90AA1 | -0.642887955 | 7.9691E-06 | 0.016196628 |
| ENSDART00000031650 | HSPA1L | -0.72348073 | 5.97567E-05 | 0.041938461 |
| ENSDART00000021037 | HSPA4 | -0.624615759 | 0.000563707 | 0.120599327 |
| ENSDART00000060162 | HSPB1 | -0.988739101 | 2.65868E-08 | 0.000378251 |
| ENSDART00000129858 | MAX | -0.670923691 | 0.000203541 | 0.086027775 |
| ENSDART00000156353 | MSS51 | -0.787439987 | 1.39719E-05 | 0.022986177 |
| ENSDART00000192783 | NEXN | -0.646233064 | 0.000359378 | 0.099141755 |
| ENSDART00000125616 | NFYA | -0.613156015 | 0.000713785 | 0.137229985 |
| ENSDART00000157861 | P3H2 | 0.588925157 | 0.000708587 | 0.137157459 |
| ENSDART00000024137 | P4HA2 | -0.777604819 | 1.46838E-05 | 0.022986177 |
| ENSDART00000009223 | PDCD4 | -0.647332461 | 8.74625E-05 | 0.055303484 |
| ENSDART00000165507 | PUS7 | 0.58458752 | 0.000337206 | 0.099141755 |
| ENSDART00000146368 | RBM4B | -0.616287288 | 0.000368424 | 0.099141755 |
| ENSDART00000165036 | RBM5 | -0.617735358 | 0.000121867 | 0.064214978 |
| ENSDART00000177475 | RDH5 | 0.657167706 | 0.00026481 | 0.093377773 |
| ENSDART00000185324 | RPGRIP1L | -0.799978563 | 2.15316E-06 | 0.006126595 |
| ENSDART00000140371 | RSRP1 | -0.774367045 | 6.9395E-06 | 0.016196628 |
| ENSDART00000156446 | RTF2 | 0.607171022 | 0.000737278 | 0.139856807 |
| ENSDART00000139615 | SEPTIN6 | 0.724628284 | 3.33916E-05 | 0.028038483 |
| ENSDART00000035096 | SERPINH1 | -0.732766816 | 4.24732E-10 | 1.20853E-05 |
| ENSDART00000056734 | SETD7 | -0.591113671 | 0.000409452 | 0.099141755 |
| ENSDART00000169730 | SIMC1 | -0.611682003 | 0.000382091 | 0.099141755 |
| ENSDART00000086490 | SMYD4 | 0.596605886 | 0.000578946 | 0.121801663 |
| ENSDART00000046349 | SPTY2D1 | -0.911836031 | 1.42967E-07 | 0.000813594 |
| ENSDART00000158187 | SUZ12 | 0.595667621 | 0.00064778 | 0.129747933 |
| ENSDART00000122972 | TCF7L2 | -0.680488822 | 0.000153346 | 0.072721966 |
| ENSDART00000171795 | U2AF2 | 0.591025001 | 0.001041364 | 0.161917823 |
| ENSDART00000165695 | UBTF | 0.599098203 | 0.000244422 | 0.09151034 |
| ENSDART00000167922 | XRCC5 | 0.590597737 | 6.2351E-05 | 0.042241299 |
| ENSDART00000064140 | YLPM1 | -0.629900738 | 0.000273738 | 0.093377773 |
| ENSDART00000171183 | ZMYND8 | -0.596234808 | 0.000102944 | 0.058330547 |
| ENSDART00000180482 | ZNF729 | -0.644109895 | 0.000328595 | 0.099141755 |
| ENSDART00000100965 | ZSWIM8 | -0.648344458 | 0.000149912 | 0.072721966 |

**Table 5-3. Differentially expressed genes (DEGs) in 120 hours post-fertilization zebrafish larvae treated with 500 ppb TaClo**

| ID | Symbol | Expr Log Ratio | Expr p-value | Expr False Discovery Rate (q-value) |
|---|---|---|---|---|
| ENSDART00000089543 | ABI3BP | 0.718 | 0.00000697 | 0.0204 |
| ENSDART00000080664 | ACTC1 | -0.627 | 0.000164 | 0.212 |
| ENSDART00000124051 | AP2M1 | 0.606 | 0.000817 | 0.411 |
| ENSDART00000170306 | AREL1 | -0.61 | 0.000352 | 0.275 |
| ENSDART00000148365 | ATP2A1 | 0.592 | 0.00101 | 0.456 |
| ENSDART00000149555 | CA4 | -0.776 | 0.0000178 | 0.037 |
| ENSDART00000041249 | CHORDC1 | -0.717 | 0.0000703 | 0.107 |
| ENSDART00000191303 | CMC2 | -0.606 | 0.000177 | 0.212 |
| ENSDART00000056065 | CNPY2 | -0.773 | 0.00000707 | 0.0204 |
| ENSDART00000140606 | CSDE1 | -0.596 | 0.000178 | 0.212 |
| ENSDART00000161538 | CYP1A1 | 0.784 | 0.0000152 | 0.0341 |
| ENSDART00000126013 | CYP1B1 | 0.837 | 0.00000358 | 0.0154 |
| ENSDART00000160713 | DHTKD1 | 0.641 | 0.000288 | 0.258 |
| ENSDART00000181373 | DROSHA | -0.612 | 0.000247 | 0.243 |
| ENSDART00000132227 | EIF4H | 0.644 | 0.000356 | 0.275 |
| ENSDART00000152789 | ETAA1 | -0.603 | 0.000659 | 0.366 |
| ENSDART00000182624 | FAH | 0.685 | 7.17E-09 | 0.000124 |
| ENSDART00000149350 | FKBP4 | -0.633 | 0.000467 | 0.314 |
| ENSDART00000043743 | Haus8l2 | -0.911 | 0.000000484 | 0.00313 |
| ENSDART00000169685 | HIKESHI | -0.649 | 0.00000112 | 0.00646 |
| ENSDART00000173648 | HMGB3 | 0.64 | 0.000183 | 0.212 |
| ENSDART00000179982 | HMOX1 | 0.688 | 0.0000422 | 0.0753 |
| ENSDART00000023550 | HSP90AA1 | -0.603 | 0.0000284 | 0.0545 |
| ENSDART00000148630 | HSPA4 | -0.764 | 0.0000223 | 0.0444 |
| ENSDART00000060162 | HSPB1 | -0.989 | 2.65E-08 | 0.000275 |
| ENSDART00000169626 | KCNC1 | -0.584 | 0.00099 | 0.453 |
| ENSDART00000129858 | MAX | -0.586 | 0.00118 | 0.48 |
| ENSDART00000156353 | MSS51 | -0.822 | 0.00000579 | 0.02 |
| ENSDART00000090332 | NEURL2 | -0.614 | 0.0005 | 0.325 |
| ENSDART00000192783 | NEXN | -0.581 | 0.00134 | 0.48 |
| ENSDART00000184547 | NQO1 | 0.618 | 0.0000467 | 0.0806 |
| ENSDART00000127952 | P4HA1 | -0.716 | 0.00000635 | 0.0204 |
| ENSDART00000160845 | P4HA2 | -0.728 | 0.000032 | 0.0592 |
| ENSDART00000135280 | PAIP2B | -0.62 | 0.000602 | 0.366 |
| ENSDART00000136331 | RBBP7 | -0.589 | 0.000263 | 0.252 |
| ENSDART00000133632 | RBM4B | -0.645 | 0.000249 | 0.243 |
| ENSDART00000158681 | SCARB1 | 0.582 | 0.00126 | 0.48 |
| ENSDART00000152365 | SERPINH1 | -0.774 | 0.000000191 | 0.00141 |
| ENSDART00000170737 | SMYD1 | -0.595 | 0.000276 | 0.255 |
| ENSDART00000162589 | SUGT1 | -0.804 | 0.00000898 | 0.0236 |
| ENSDART00000109228 | ZBTB24 | -0.587 | 0.00107 | 0.461 |

**Table 5-4. Differentially expressed genes (DEGs) in 120 hours post-fertilization zebrafish larvae treated with TaClo (5, 50, and 500 ppb)**

| ID | Symbol | Expr Log Ratio | Expr False Discovery Rate (q-value) |
|---|---|---|---|
| ENSDART00000169600 | ABHD4 | 0.581718707 | 0.097366364 |
| ENSDART00000089543 | ABI3BP | 0.71837559 | 0.020353748 |
| ENSDART00000138548 | ABL2 | 0.649694287 | 0.098402579 |
| ENSDART00000080664 | ACTC1 | -0.750974445 | 0.010793467 |
| ENSDART00000066471 | ADAM8 | -0.73318205 | 0.001305537 |
| ENSDART00000124051 | AP2M1 | 0.606253922 | 0.41089536 |
| ENSDART00000170306 | AREL1 | -0.609973524 | 0.275081421 |
| ENSDART00000140859 | ARK2N | -0.603786412 | 0.170748021 |
| ENSDART00000083317 | ARSK | -0.659011068 | 0.077096112 |
| ENSDART00000148365 | ATP2A1 | 0.668489544 | 0.09083239 |
| ENSDART00000169401 | B4GALNT3 | 0.602535901 | 0.133307559 |
| ENSDART00000183615 | BPGM | 0.593208002 | 0.097366364 |
| ENSDART00000163965 | BRDT | -0.64766817 | 0.083471938 |
| ENSDART00000149555 | CA4 | -0.775940521 | 0.036974638 |
| ENSDART00000098734 | CACYBP | -0.655993301 | 0.056453429 |
| ENSDART00000163425 | CARNMT1 | -0.640163099 | 0.099141755 |
| ENSDART00000169752 | CCDC40 | -0.648193275 | 0.0882011 |
| ENSDART00000137645 | CEP104 | -0.767226706 | 0.023825416 |
| ENSDART00000125265 | CHERP | -0.637476323 | 0.086027775 |
| ENSDART00000041249 | CHORDC1 | -0.964937023 | 0.000675867 |
| ENSDART00000127173 | CLU | -0.591304161 | 0.022986177 |
| ENSDART00000191303 | CMC2 | -0.606223305 | 0.211908501 |
| ENSDART00000056065 | CNPY2 | -0.773046966 | 0.020353748 |
| ENSDART00000020569 | CRELD1 | -0.685842036 | 0.028038483 |
| ENSDART00000187907 | CSAD | -0.661052042 | 0.098402579 |
| ENSDART00000140606 | CSDE1 | -0.595715409 | 0.211908501 |
| ENSDART00000111328 | CUTC | -0.716741968 | 0.019689282 |
| ENSDART00000161538 | CYP1A1 | 0.783983195 | 0.034144244 |
| ENSDART00000126013 | CYP1B1 | 0.836785511 | 0.015442549 |
| ENSDART00000102148 | D1Pas1 | 0.608834371 | 0.058670423 |
| ENSDART00000160713 | DHTKD1 | 0.641164557 | 0.257572591 |
| ENSDART00000166146 | DNAJB1 | -0.677949162 | 0.075351501 |
| ENSDART00000181373 | DROSHA | -0.611593945 | 0.243271367 |
| ENSDART00000130781 | EIF4A2 | -0.622493103 | 0.110091076 |
| ENSDART00000132227 | EIF4H | 0.745173374 | 0.034041099 |
| ENSDART00000173015 | ELMO2 | 0.613097855 | 0.07748647 |
| ENSDART00000152789 | ETAA1 | -0.60292976 | 0.366406009 |
| ENSDART00000184619 | EXOC1 | -0.589821953 | 0.11285751 |
| ENSDART00000182624 | FAH | 0.684591185 | 0.000123766 |
| ENSDART00000024576 | FKBP4 | -0.703017156 | 0.020496726 |
| ENSDART00000002029 | FKBP8 | -0.607143995 | 0.060067679 |
| ENSDART00000076974 | GFPT2 | 0.60005118 | 0.09083239 |
| ENSDART00000180951 | GTPBP1 | 0.603204297 | 0.093377773 |
| ENSDART00000043743 | Haus8l2 | -0.934212392 | 0.001165137 |
| ENSDART00000083883 | HERC4 | -0.673866154 | 0.023900216 |
| ENSDART00000169685 | HIKESHI | -0.649335548 | 0.006455059 |
| ENSDART00000173648 | HMGB3 | 0.781480763 | 0.009167194 |
| ENSDART00000179982 | HMOX1 | 0.688423585 | 0.075340949 |
| ENSDART00000023550 | HSP90AA1 | -0.642887955 | 0.016196628 |

| ID | Symbol | Expr Log Ratio | Expr False Discovery Rate (q-value) |
|---|---|---|---|
| ENSDART00000031650 | HSPA1L | -0.72348073 | 0.041938461 |
| ENSDART00000148630 | HSPA4 | -0.763856715 | 0.044388253 |
| ENSDART00000060162 | HSPB1 | -0.988753565 | 0.000275039 |
| ENSDART00000169626 | KCNC1 | -0.584341864 | 0.452978342 |
| ENSDART00000129858 | MAX | -0.670923691 | 0.086027775 |
| ENSDART00000029528 | MOSPD2 | -0.639012297 | 0.127340622 |
| ENSDART00000156353 | MSS51 | -0.9141181 | 0.002797876 |
| ENSDART00000164351 | MTBP | 0.634794766 | 0.12876126 |
| ENSDART00000090332 | NEURL2 | -0.613773077 | 0.324652915 |
| ENSDART00000192783 | NEXN | -0.81379493 | 0.011248204 |
| ENSDART00000146625 | NFKBIA | -0.606161691 | 0.139556187 |
| ENSDART00000125616 | NFYA | -0.613156015 | 0.137229985 |
| ENSDART00000184547 | NQO1 | 0.617926762 | 0.080629753 |
| ENSDART00000157861 | P3H2 | 0.588925157 | 0.137157459 |
| ENSDART00000127952 | P4HA1 | -0.716399821 | 0.020353748 |
| ENSDART00000024137 | P4HA2 | -0.777604819 | 0.022986177 |
| ENSDART00000135280 | PAIP2B | -0.62037437 | 0.366406009 |
| ENSDART00000009223 | PDCD4 | -0.709327486 | 0.020496726 |
| ENSDART00000111552 | PHLDB2 | 0.586552511 | 0.177022323 |
| ENSDART00000059369 | PHYKPL | -0.609050206 | 0.09083239 |
| ENSDART00000102474 | PLEKHS1 | 0.705867425 | 0.060067679 |
| ENSDART00000173450 | PPARG | -0.622106492 | 0.12316628 |
| ENSDART00000008603 | PREPL | -0.620520676 | 0.073592658 |
| ENSDART00000135838 | PTP4A2 | -0.609081461 | 0.12876126 |
| ENSDART00000165507 | PUS7 | 0.58458752 | 0.099141755 |
| ENSDART00000136331 | RBBP7 | -0.588673047 | 0.252466406 |
| ENSDART00000133632 | RBM4B | -0.644748722 | 0.243271367 |
| ENSDART00000165036 | RBM5 | -0.617735358 | 0.064214978 |
| ENSDART00000177475 | RDH5 | 0.657167706 | 0.093377773 |
| ENSDART00000185324 | RPGRIP1L | -0.799978563 | 0.006126595 |
| ENSDART00000140371 | RSRP1 | -0.774367045 | 0.016196628 |
| ENSDART00000156446 | RTF2 | 0.607171022 | 0.139856807 |
| ENSDART00000158681 | SCARB1 | 0.582074795 | 0.479582667 |
| ENSDART00000139615 | SEPTIN6 | 0.724628284 | 0.028038483 |
| ENSDART00000152365 | SERPINH1 | -0.773684751 | 0.001410011 |
| ENSDART00000056734 | SETD7 | -0.591113671 | 0.099141755 |
| ENSDART00000169730 | SIMC1 | -0.611682003 | 0.099141755 |
| ENSDART00000170737 | SMYD1 | -0.594631735 | 0.254706265 |
| ENSDART00000086490 | SMYD4 | 0.596605886 | 0.121801663 |
| ENSDART00000134283 | SORBS3 | -0.593147952 | 0.13390631 |
| ENSDART00000046349 | SPTY2D1 | -0.911836031 | 0.000813594 |
| ENSDART00000180117 | STMN3 | -0.593683853 | 0.190883571 |
| ENSDART00000162589 | SUGT1 | -0.804023855 | 0.023575235 |
| ENSDART00000138714 | Sult5a1 | 0.597046922 | 0.0882011 |
| ENSDART00000158187 | SUZ12 | 0.595667621 | 0.129747933 |
| ENSDART00000122972 | TCF7L2 | -0.680488822 | 0.072721966 |
| ENSDART00000112294 | TTC22 | 0.706651962 | 0.050864436 |
| ENSDART00000037692 | TTPA | 0.593225564 | 0.13390631 |
| ENSDART00000105064 | TXNDC16 | -0.659575037 | 0.049419235 |
| ENSDART00000151259 | U2AF2 | 0.598299799 | 0.184448152 |
| ENSDART00000165695 | UBTF | 0.599098203 | 0.09151034 |
| ENSDART00000183053 | XPO1 | -0.59682821 | 0.009167194 |
| ENSDART00000167922 | XRCC5 | 0.590597737 | 0.042241299 |
| ENSDART00000064140 | YLPM1 | -0.629900738 | 0.093377773 |
| ENSDART00000109228 | ZBTB24 | -0.692433808 | 0.067981404 |
| ENSDART00000171183 | ZMYND8 | -0.596234808 | 0.058330547 |
| ENSDART00000180482 | ZNF729 | -0.656076171 | 0.098619415 |
| ENSDART00000100965 | ZSWIM8 | -0.648344458 | 0.072721966 |

**Table 5-5. Differentially expressed genes (DEGs) in 120 hours post-fertilization zebrafish larvae treated with 1.75 µM MPTP**

| ID | Symbol | Expr Log Ratio | Expr p-value | Expr False Discovery Rate (q-value) |
|---|---|---|---|---|
| ENSDART00000144954 | AP1S2 | -0.645256813 | 0.00028525 | 0.784379564 |
| ENSDART00000185346 | CES1 | -0.610017244 | 0.000483328 | 0.999935454 |
| ENSDART00000136658 | CLTA | 0.691925505 | 9.79308E-05 | 0.622911137 |
| ENSDART00000149067 | FES | -0.633787543 | 0.000173042 | 0.679758971 |
| ENSDART00000134913 | FGA | 0.667522206 | 0.00022952 | 0.710014894 |
| ENSDART00000169483 | HYCC1 | 0.59186966 | 0.000757743 | 0.999935454 |
| ENSDART00000168099 | MCMBP | -0.600668128 | 0.000892704 | 0.999935454 |
| ENSDART00000144734 | NUP35 | -0.67350658 | 0.000123734 | 0.622911137 |
| ENSDART00000135280 | PAIP2B | -0.583914651 | 0.001263713 | 0.999935454 |
| ENSDART00000109340 | Prps1l3 | -0.60874996 | 0.000689989 | 0.999935454 |
| ENSDART00000193643 | SLC1A2 | 0.582148664 | 0.000941096 | 0.999935454 |
| ENSDART00000181806 | SLC27A2 | 0.701812848 | 6.13446E-05 | 0.562284843 |

**Table 5-6. Numbers of differentially expressed genes (DEGs) identified using a threshold of fold change > 1.5 and p-value < 0.05 in 120 hours post-fertilization (hpf) zebrafish following 0-120 hpf TaClo or 1.75 µM MPTP treatments.**

| 120 hpf zebrafish | All IDs | Mapped IDs | Unmapped IDs | Filtered | Upregulation | Downregulation |
|---|---|---|---|---|---|---|
| TaClo 5 ppb | 59466 | 32410 | 27056 | 55 | 15 | 40 |
| TaClo 50 ppb | 59466 | 32410 | 27056 | 57 | 16 | 41 |
| TaClo 500 ppb | 59466 | 32410 | 27056 | 41 | 12 | 29 |
| TaClo (5, 50, 500 ppb) | 178397 | 97230 | 81167 | 107 | 36 | 71 |
| 1.75 µM MPTP | 59466 | 32410 | 27056 | 12 | 5 | 7 |

**Table 5-7. Top five canonical pathways and the associated molecules in each TaClo concentration group (5, 50, and 500 ppb) and 1.75 µM MPTP in 120 hours post-fertilization zebrafish larvae**

| 5 ppb TaClo | | | |
|---|---|---|---|
| **Name** | **z-score** | **p-value** | **Molecules** |
| Cellular response to heat stress | -2.449489743 | 4.96E-08 | DNAJB1,FKBP4,HIKESHI,HSP90AA1,HSPB1,SERPINH1 |
| HSP90 chaperone cycle for steroid hormone receptors in the presence of ligand | | 1.99E-04 | DNAJB1,FKBP4,HSP90AA1 |
| Extra-nuclear estrogen signaling | 3.3 | 4.49E-04 | HSP90AA1,HSPB1,XPO1 |
| IL-17A Signaling in Fibroblasts | | 5.42E-04 | NFKBIA |
| PEDF Signaling | | 6.25E-04 | NFKBIA,PPARG,TCF7L2 |
| | | | |
| 50 ppb TaClo | | | |
| **Name** | **z-score** | **p-value** | **Molecules** |
| Cellular response to heat stress | -2.828427125 | 3.82E-11 | DNAJB1,FKBP4,HIKESHI,HSP90AA1,HSPA1L,HSPA4,HSPB1,SERPINH1 |
| HSP90 chaperone cycle for steroid hormone receptors in the presence of ligand | -2 | 6.27E-06 | DNAJB1,FKBP4,HSP90AA1,HSPA1L |
| Aldosterone Signaling in Epithelial Cells | | 2.96E-05 | DNAJB1,HSP90AA1,HSPA1L,HSPA4,HSPB1 |
| Protein Ubiquitination Pathway | -2 | 2.95E-04 | DNAJB1,HSP90AA1,HSPA1L,HSPA4,HSPB1 |
| Collagen biosynthesis and modifying enzymes | | 3.79E-04 | P3H2,P4HA2,SERPINH1 |

| 500 ppb TaClo | | | |
|---|---|---|---|
| **Name** | **z-score** | **p-value** | **Molecules** |
| Cellular response to heat stress | -3 | 8.63E-09 | BAG2,DNAJB1,EP300,FKBP4,HDAC6,HIKESHI,HSF1, HSP90AA1,HSPA1L,HSPA4,HSPA4L,HSPA5,HSPA9, HSPB1,NUP107,NUP133,NUP205,NUP35,PTGES3,SERPINH1,ST13 |
| NRF2-mediated Oxidative Stress Response | 1.732050808 | 2.94E-06 | ABCC1,ACTC1,ACTG1,AKR1A1,CYP1A1,CYP2J2,DNAJA1,DNAJB1, DNAJB12,DNAJC4,DNAJC5G,EP300,EPHX1,GSTM3,GSTO1,GSTP1, GSTZ1,HMOX1,HRAS,HSP90AA1,HSP90B1,MAP2K7,NQO1,PIK3C2A, PIK3C3,PIK3R1,PRDX1,RAP1B,SCARB1,SOD2,SQSTM1,STIP1,TXN |
| Aryl Hydrocarbon Receptor Signaling | 0.577350269 | 7.70E-06 | ALDH3A2,CCNA1,CDKN1B,CTSD,CYP1A1,CYP1B1,EP300,ESR1, GSTM3,GSTO1,GSTP1,GSTZ1,HSP90AA1,HSP90B1,HSPB1,IL1B, NQO1,NR2F1,PTGES3,RB1,RXRB,SRC |
| Xenobiotic Metabolism AHR Signaling Pathway | 1.666666667 | 2.13E-05 | ALDH3A2,CYP1A1,CYP1B1,EP300,GSTM3,GSTO1,GSTP1,GSTZ1, HSP90AA1,HSP90B1,IL1B,NQO1,PTGES3,SENP1,UGT1A1 |
| HSP90 chaperone cycle for steroid hormone receptors in the presence of ligand | -2.886751346 | 3.16E-05 | DCTN1,DNAJA1,DNAJB1,DYNC1I2,FKBP4,HSP90AA1,HSPA1L,NR3C2, PTGES3,STIP1,TUBA1A,TUBB4A |
| | | | |
| TaClo (5, 50, 500 ppb) | | | |
| **Name** | **z-score** | **p-value** | **Molecules** |
| Cellular response to heat stress | -2.828427125 | 6.44E-09 | DNAJB1,FKBP4,HIKESHI,HSP90AA1,HSPA1L,HSPA4,HSPB1,SERPINH1 |
| HSP90 chaperone cycle for steroid hormone | -2 | 7.55E-05 | DNAJB1,FKBP4,HSP90AA1,HSPA1L |

| | | | |
|---|---|---|---|
| receptors in the presence of ligand | | | |
| NRF2-mediated Oxidative Stress Response | | 9.92E-05 | ACTC1,CYP1A1,DNAJB1,HMOX1,HSP90AA1,NQO1,SCARB1 |
| Collagen biosynthesis and modifying enzymes | -1 | 1.42E-04 | P3H2,P4HA1,P4HA2,SERPINH1 |
| IL-17A Signaling in Fibroblasts | -2 | 2.82E-04 | NFKBIA,P4HA1,P4HA2,SERPINH1 |
| | | | |
| 1.75 μM MPTP | | | |
| **Name** | **z-score** | **p-value** | **Molecules** |
| trans-Golgi Network Vesicle Budding | | 5.03E-04 | AP1S2,CLTA |
| Virus Entry via Endocytic Pathways | | 1.28E-03 | AP1S2,CLTA |
| MHC class II antigen presentation | | 1.45E-03 | AP1S2,CLTA |
| PRPP Biosynthesis I | | 1.79E-03 | Prps1l3 |
| Neurotransmitter uptake and metabolism In glial cells | | 1.79E-03 | SLC1A2 |

**Table 5-8. Z scores and p-values of canonical pathways in TaClo-treated 120 hours post-fertilization zebrafish larvae**

| z score | TaClo 5 ppb | TaClo 50 ppb | TaClo 500 ppb | MPTP 1.75 µM |
|---|---|---|---|---|
| Cellular response to heat stress | -2.45 | -2.83 | -3 | - |
| HSP90 chaperone cycle for steroid hormone receptors in the presence of ligand | - | -2 | -2.886751346 | - |
| Protein Ubiquitination Pathway | - | -2 | 0 | - |
| | | | | |
| **p-value** | **TaClo 5 ppb** | **TaClo 50 ppb** | **TaClo 500 ppb** | **MPTP 1.75 µM** |
| Cellular response to heat stress | 7.304177 | 10.4183866 | 8.063755018 | 1.352637029 |
| HSP90 chaperone cycle for steroid hormone receptors in the presence of ligand | 3.7003611 | 5.20278449 | 2.480861953 | - |
| Protein Ubiquitination Pathway | 1.74645 | 3.53044888 | 3.103304053 | - |

"-" Indicates no values generated from QIAGEN Ingenuity Pathway Analysis

**Table 5-9. Molecular and Cellular Functions with protein folding and post-translational modification in TaClo-treated 120 hours post-fertilization zebrafish**

| 5 ppb TaClo | | |
|---|---|---|
| **Name** | **p-value** | **#Molecules** |
| **Post-Translational Modification** | **5.93E-03 - 7.42E-08** | **7** |
| Folding of protein | 7.42E-08 | DNAJB1,FKBP4,FKBP8,HSP90AA1,HSPB1,SERPINH1 |
| Aggregation of protein | 2.45E-03 | DNAJB1,HSPB1 |
| Hydroxylation of L-proline | 5.93E-03 | P4HA2 |
| 50 ppb TaClo | | |
| **Name** | **p-value** | **#Molecules** |
| **Post-Translational Modification** | **2.37E-02 - 1.04E-07** | **13** |
| Diseases or Functions Annotation | p-value | Molecules |
| Folding of protein | 1.04E-7 | DNAJB1,FKBP4,HSP90AA1,HSPA1L,HSPB1,SERPINH1 |
| Carbonylation of protein | 6.45E-4 | ACTC1,CLU |
| Refolding of protein | 9.68E-4 | HSP90AA1,HSPA1L |
| Oxidation of protein | 1.69E-3 | DNAJB1,HSPA4 |

| | | |
|---|---|---|
| Aggregation of protein | 2.74E-3 | DNAJB1,HSPB1 |
| **Protein Folding** | **9.68E-04 - 1.04E-07** | **6** |
| Diseases or Functions Annotation | p-value | Molecules |
| Folding of protein | 1.04E-7 | DNAJB1,FKBP4,HSP90AA1,HSPA1L,HSPB1,SERPINH1 |
| 500 ppb TaClo | | |
| **Name** | **p-value** | **#Molecules** |
| **Protein Synthesis** | **2.07E-03 - 2.73E-06** | **17** |
| Diseases or Functions Annotation | p-value | Molecules |
| Quantity of enzyme | 2.73E-06 | CNPY2,CYP1A1,DHTKD1,FAH,HMOX1 |
| Metabolism of toxin peptide | 7.8E-05 | CYP1A1,CYP1B1 |
| Quantity of protein in blood | 1.29E-04 | CNPY2,CYP1A1,DHTKD1,FAH,HMGB3,HMOX1, SCARB1 |
| Initiation of translation of mRNA | 1.33E-04 | EIF4H,HSPB1,PAIP2B |
| Initiation of translation of protein | 1.65E-04 | EIF4H,HSPB1,PAIP2B |
| TaClo (5, 50, 500 ppb) | | |
| **Name** | **p-value** | **#Molecules** |
| **Post-Translational Modification** | **9.30E-03 - 2.37E-07** | **19** |
| Diseases or Functions Annotation | p-value | Molecules |
| Folding of protein | 2.37E-07 | DNAJB1,FKBP4,FKBP8,HSP90AA1,HSPA1L,HSPB1,SERPINH1 |

| | | |
|---|---|---|
| Hydroxylation of L-proline | 4.57E-05 | P4HA1,P4HA2 |
| Carbonylation of protein | 4.6E-05 | ACTC1,CLU,HMOX1 |
| Oxidation of protein | 1.99E-04 | DNAJB1,HMOX1,HSPA4 |
| Refolding of protein | 3.35E-03 | HSP90AA1,HSPA1L |
| **Protein Folding** | **3.35E-03 - 2.37E-07** | **7** |
| Diseases or Functions Annotation | p-value | Molecules |
| Folding of protein | 2.37E-07 | DNAJB1,FKBP4,FKBP8,HSP90AA1,HSPA1L,HSPB1,SERPINH1 |
| Refolding of protein | 3.35E-3 | HSP90AA1,HSPA1L |

**Table 5-10. Disease and functional annotations related to apoptosis and organismal death with the associated molecules in early life zebrafish TaClo and 1.75 µM MPTP exposure in 120 hours post-fertilization (hpf) zebrafish larvae and 6 months post-fertilization (6 mpf) zebrafish brains**

| 120 hpf | Diseases or Functions Annotation | p-value | Activation z-score | Molecules |
|---|---|---|---|---|
| 5 ppb TaClo | Apoptosis of neuroblastoma cell lines | 4.22E-4 | No z score generated | DNAJB1,FKBP8,NFKBIA,PPARG |
| | Organismal death | 3.72E-05 | 2.383 | ABL2,ACTC1,ATP2A1,CA4,CNPY2,CSAD,DNAJB1,FKBP4,FKBP8, GFPT2,HSP90AA1,HSPB1,NEXN,NFKBIA,P4HA2,PDCD4,PPARG, PTP4A2,RPGRIP1L,SERPINH1,TCF7L2,TTPA,U2AF2,XPO1 |
| 50 ppb TaClo | Apoptosis of neurons | 4.3E-3 | 1.71 | ADAM8,CLU,HSPA4,HSPB1,MAX,XRCC5 |
| | Organismal death | 1.02E-05 | 1.618 | ABHD4,ABL2,ACTC1,CA4,CRELD1,DNAJB1,FKBP4,HSP90AA1, HSPB1,MAX,NEXN,NFYA,P3H2,P4HA2,PDCD4,PUS7,RPGRIP1L,SEPTIN6, SERPINH1,SETD7,SUZ12,TCF7L2,U2AF2,UBTF,XRCC5,ZSWIM8 |
| 500 ppb TaClo | Apoptosis of neurons | 4.62E-3 | 1.067 | HMOX1,HSPA4,HSPB1,MAX,NQO1 |
| | Organismal death | 6.57E-06 | 1.077 | ACTC1,AP2M1,ATP2A1,CA4,CNPY2,CSDE1,CYP1A1,FAH,FKBP4, HMOX1,HSP90AA1,HSPB1,KCNC1,MAX,NEXN,NQO1,P4HA1,P4HA2, SCARB1,SERPINH1,SMYD1 |
| TaClo (5, 50, 500 | Apoptosis of | 2.47E-3 | 1.446 | ADAM8,CLU,HMOX1,HSPA4,HSPB1,MAX,NFKBIA,NQO1,XRCC5 |

| | | | | |
|---|---|---|---|---|
| ppb) | neurons | | | |
| | Organismal death | 4.45E-08 | 1.257 | ABHD4,ABL2,ACTC1,AP2M1,ATP2A1,CA4,CNPY2,CRELD1,CSAD, CSDE1,CYP1A1,DNAJB1,FAH,FKBP4,FKBP8,GFPT2,HMOX1,HSP90AA1, HSPB1,KCNC1,MAX,NEXN,NFKBIA,NFYA,NQO1,P3H2,P4HA1,P4HA2, PDCD4,PPARG,PTP4A2,PUS7,RPGRIP1L,SCARB1,SEPTIN6,SERPINH1, SETD7,SMYD1,SUZ12,TCF7L2,TTPA,U2AF2,UBTF,XPO1,XRCC5,ZSWIM8 |
| | | | | |
| **6 mpf** | **Diseases or Functions Annotation** | **p-value** | **Activation z-score** | **Molecules** |
| 1.75 μM MPTP | Apoptosis of neurons | 2.31E-6 | 0.533 | ANP32A,B4GALNT1,ELAVL4,GNAO1,KCNQ3,KLF7,MAPK1,MEF2C, NFKBIA,NR4A3,PRDX1,STAMBP,XRCC4 |
| | Organismal death | 1.77E-7 | 0.472 | SETD7,ANP32A,ERBB4,GNAO1,GUCY1B1,NR4A3,OGDH,EIF4B,PPARA, PKP2,SHANK3,NR3C2,ELAVL4,RAB6A,NFKBIA,TWSG1,SUMO3,EXTL3, OSBPL3,STAMBP,TPD52,PRDX1,XRCC4,MLYCD,STEAP4,B4GALNT1, CP,WNT7B,GABARAP,CETP,PTK2,CLIC3,RAMP2,NRXN1,MEF2C,HCN4, KLF7,ARID4B,MAPK1,DNAAF11,CENPE,APRT |

**Table 5-11. Differentially expressed genes (DEGs) in 6 months post-fertilization zebrafish brains treated with 5 ppb TaClo**

| ID | Symbol | Expr Log Ratio | Expr p-value | Expr False Discovery Rate (q-value) |
|---|---|---|---|---|
| ENSDART00000188350 | ADAM23 | 0.689337423 | 0.00115843 | 0.999996026 |
| ENSDART00000090069 | AXDND1 | 0.582806749 | 0.009703573 | 0.999996026 |
| ENSDART00000187351 | B4GALNT1 | 0.623118124 | 0.005013576 | 0.999996026 |
| ENSDART00000152157 | CCDC150 | 0.601812795 | 0.000461387 | 0.999996026 |
| ENSDART00000193189 | CCDC47 | -0.719461673 | 0.000463606 | 0.999996026 |
| ENSDART00000167299 | CPSF1 | -0.646143226 | 0.002857719 | 0.999996026 |
| ENSDART00000166915 | CRB1 | -0.610084307 | 0.004078117 | 0.999996026 |
| ENSDART00000131397 | ENOX1 | 0.761609321 | 0.000343118 | 0.999996026 |
| ENSDART00000031761 | FZD5 | -0.672866024 | 0.002104891 | 0.999996026 |
| ENSDART00000015277 | GPX1 | 0.604757701 | 0.006763725 | 0.999996026 |
| ENSDART00000123713 | GRIA1 | -0.606556591 | 0.000290772 | 0.999996026 |
| ENSDART00000162445 | HMGXB3 | 0.583018934 | 0.009775439 | 0.999996026 |
| ENSDART00000148113 | HRAS | -0.659064487 | 0.003437262 | 0.999996026 |
| ENSDART00000180093 | IGSF9 | 0.634413297 | 0.003815426 | 0.999996026 |
| ENSDART00000155327 | IP6K2 | -0.591744653 | 0.00869044 | 0.999996026 |
| ENSDART00000160443 | IVNS1ABP | 0.730556694 | 0.001211625 | 0.999996026 |
| ENSDART00000134619 | MPP2 | -0.658536389 | 0.002788071 | 0.999996026 |
| ENSDART00000183474 | MTARC1 | -0.581025933 | 0.008202582 | 0.999996026 |
| ENSDART00000184875 | MYCL | -0.754556067 | 0.000751879 | 0.999996026 |
| ENSDART00000146488 | MYOZ2 | -0.647746037 | 0.002951519 | 0.999996026 |
| ENSDART00000183461 | NDST1 | -0.646637966 | 0.002389809 | 0.999996026 |
| ENSDART00000192514 | NFKBIA | 0.625487372 | 0.005567521 | 0.999996026 |
| ENSDART00000101582 | PCGF6 | 0.654645376 | 0.003659919 | 0.999996026 |
| ENSDART00000193693 | PER3 | -0.592085366 | 0.004832539 | 0.999996026 |
| ENSDART00000176022 | POLR3GL | -0.613751955 | 0.003561622 | 0.999996026 |
| ENSDART00000165224 | PPP1R13B | -0.596115416 | 0.006142946 | 0.999996026 |
| ENSDART00000114774 | PTPN5 | -0.714308219 | 0.001497972 | 0.999996026 |
| ENSDART00000127124 | RAB12 | -0.664115856 | 0.003059591 | 0.999996026 |
| ENSDART00000123619 | RAC2 | 0.643225897 | 0.004248902 | 0.999996026 |
| ENSDART00000162204 | RECQL | 0.580986467 | 0.009788195 | 0.999996026 |
| ENSDART00000137988 | RPL7A | -0.702675228 | 0.001768767 | 0.999996026 |
| ENSDART00000123645 | SMYD2 | 0.621272683 | 0.005657616 | 0.999996026 |
| ENSDART00000160347 | STAG2 | 0.60837886 | 0.003715182 | 0.999996026 |
| ENSDART00000155648 | UBE2I | 0.585518537 | 0.009200914 | 0.999996026 |
| ENSDART00000004689 | VWA5A | 0.595439692 | 0.008080207 | 0.999996026 |

**Table 5-12. Differentially expressed genes (DEGs) in 6 months post-fertilization zebrafish brains treated with 50 ppb TaClo**

| ID | Symbol | Expr Log Ratio | Expr p-value | Expr False Discovery Rate (q-value) |
|---|---|---|---|---|
| ENSDART00000053126 | AANAT | 0.877634768 | 9.65946E-06 | 0.010421485 |
| ENSDART00000161691 | ABCC3 | 0.729776084 | 0.000474626 | 0.097979415 |
| ENSDART00000168910 | ABLIM3 | 0.665788145 | 0.002898265 | 0.261649822 |
| ENSDART00000135585 | ACADM | 0.717483971 | 0.001465681 | 0.18912641 |
| ENSDART00000058629 | ACTA1 | 0.862423597 | 4.39812E-07 | 0.001423524 |
| ENSDART00000133319 | ACTG1 | 0.610226266 | 0.001279421 | 0.176897452 |
| ENSDART00000019519 | ADA | 0.614619053 | 0.00648748 | 0.407638267 |
| ENSDART00000031049 | AKAP13 | 0.810655178 | 0.000290977 | 0.080152897 |
| ENSDART00000018261 | AKR1B1 | 0.731109618 | 0.000568454 | 0.108229258 |
| ENSDART00000138893 | AKTIP | 0.5900092 | 0.00890183 | 0.476355799 |
| ENSDART00000042200 | ALDOA | 0.632856796 | 0.003050246 | 0.26972343 |
| ENSDART00000042755 | AMPD1 | 0.597216629 | 0.005417521 | 0.369800543 |
| ENSDART00000190191 | ANK1 | 0.594871447 | 0.008420368 | 0.468103388 |
| ENSDART00000132390 | ANKRD33B | 0.650191711 | 2.56935E-05 | 0.019958695 |
| ENSDART00000151304 | ANP32E | 0.704445995 | 0.00176186 | 0.207365537 |
| ENSDART00000182856 | ANXA2 | 0.701859202 | 0.001843827 | 0.20946532 |
| ENSDART00000075513 | AQP9 | 0.751368288 | 2.53541E-07 | 0.000984755 |
| ENSDART00000177573 | ARHGAP17 | 0.589848691 | 0.008867748 | 0.475722827 |
| ENSDART00000154077 | ARHGAP29 | 0.813305618 | 0.000155636 | 0.052573887 |
| ENSDART00000138232 | ARL13A | 0.769142295 | 2.38208E-06 | 0.00440571 |
| ENSDART00000104353 | ATP2B4 | 0.722583307 | 4.44365E-05 | 0.026811277 |
| ENSDART00000128710 | BTBD2 | 0.590934175 | 0.007572083 | 0.443589281 |
| ENSDART00000079709 | C6 | 0.708214936 | 0.000808527 | 0.135944587 |
| ENSDART00000138073 | CA13 | 0.708170946 | 0.001394026 | 0.184163107 |
| ENSDART00000043801 | CABP5 | 0.704419319 | 0.001437868 | 0.186778598 |
| ENSDART00000041564 | CACNA1F | 0.845171157 | 5.43597E-05 | 0.029886971 |
| ENSDART00000130611 | CACNB1 | -0.750748571 | 0.000812145 | 0.135955984 |
| ENSDART00000152964 | CALCOCO2 | 0.605083365 | 0.004262744 | 0.324637223 |
| ENSDART00000017902 | CAMK1G | 0.729106833 | 0.000112966 | 0.044319262 |
| ENSDART00000172488 | CAPN3 | 0.626168683 | 0.001546754 | 0.194420447 |
| ENSDART00000073726 | CAV2 | 0.767745862 | 0.00045531 | 0.09561061 |
| ENSDART00000063028 | CCN2 | 0.666058485 | 0.003166935 | 0.276510564 |
| ENSDART00000169412 | CCNE2 | 0.627264118 | 0.005395095 | 0.36891811 |
| ENSDART00000110005 | CDHR1 | 0.597259723 | 0.000399862 | 0.090822537 |
| ENSDART00000135517 | CENPF | -0.588423216 | 0.004795087 | 0.347344569 |
| ENSDART00000111028 | CHL1 | 0.622645203 | 0.005666796 | 0.378826747 |
| ENSDART00000020261 | CHRNA1 | 0.688570246 | 5.52607E-05 | 0.029886971 |
| ENSDART00000029492 | CMTM7 | 0.637880706 | 0.004234119 | 0.323726748 |
| ENSDART00000000948 | COCH | 0.587788426 | 0.006811333 | 0.416651549 |
| ENSDART00000137065 | COL15A1 | 0.676678158 | 0.002455031 | 0.241401001 |
| ENSDART00000100234 | COL2A1 | 0.687924586 | 0.001127933 | 0.164695191 |
| ENSDART00000073827 | COL4A5 | 0.684376058 | 0.001390402 | 0.184163107 |
| ENSDART00000174023 | COL4A6 | 0.688993494 | 0.001960528 | 0.214934449 |
| ENSDART00000137617 | CTSB | 0.662963023 | 0.001106417 | 0.163396265 |
| ENSDART00000140111 | CTSH | -0.680038603 | 0.001582694 | 0.196709047 |
| ENSDART00000143652 | Cutal | 0.60633212 | 0.005358963 | 0.368393118 |
| ENSDART00000160991 | CYP24A1 | 0.6957825 | 0.000295485 | 0.080256182 |
| ENSDART00000153070 | CYRIA | 0.58771923 | 0.009239397 | 0.485837039 |
| ENSDART00000124331 | DBNDD1 | 0.76452499 | 0.000139999 | 0.04964304 |

| ID | Symbol | Expr Log Ratio | Expr p-value | Expr False Discovery Rate (q-value) |
|---|---|---|---|---|
| ENSDART00000166172 | DDAH2 | 0.634515091 | 0.002174147 | 0.225785793 |
| ENSDART00000134461 | DDX19A | 0.58400407 | 0.005285635 | 0.367910508 |
| ENSDART00000173149 | DGKA | 0.648540816 | 0.00042763 | 0.095199713 |
| ENSDART00000156051 | DHX32 | 0.793055226 | 0.00036632 | 0.085710134 |
| ENSDART00000169687 | DLG1 | -0.610873428 | 0.000458293 | 0.095699527 |
| ENSDART00000173268 | DNAJC11 | -0.586237694 | 0.003206489 | 0.277915876 |
| ENSDART00000128681 | DYRK3 | 0.591559974 | 0.006349176 | 0.402287081 |
| ENSDART00000185215 | DYRK4 | 0.588495343 | 0.008833073 | 0.475722827 |
| ENSDART00000158674 | ELK1 | -0.630862537 | 0.00433666 | 0.325165746 |
| ENSDART00000065495 | EMP2 | 0.586502237 | 0.0084424 | 0.468103388 |
| ENSDART00000145905 | ENO3 | 0.686660965 | 0.002312681 | 0.232104698 |
| ENSDART00000129068 | ENTPD3 | 0.705929733 | 0.001750686 | 0.206805192 |
| ENSDART00000062898 | EPHX1 | 0.584815114 | 0.000311609 | 0.080834933 |
| ENSDART00000169805 | EPS8 | 0.660253301 | 0.003458856 | 0.286910153 |
| ENSDART00000115335 | ERICH1 | 0.611999821 | 1.17388E-06 | 0.003039571 |
| ENSDART00000147391 | FAM133B | 0.586543196 | 0.006162379 | 0.394497205 |
| ENSDART00000127216 | FAM161A | 0.617901363 | 0.001891447 | 0.210497953 |
| ENSDART00000153595 | FARP2 | 0.621878336 | 0.005888574 | 0.386338191 |
| ENSDART00000179907 | FAT4 | 0.608031563 | 0.003670678 | 0.296362706 |
| ENSDART00000003926 | FBP1 | 0.845992649 | 1.9027E-05 | 0.0160654 |
| ENSDART00000143957 | FLAD1 | -0.69609638 | 0.001489947 | 0.19098859 |
| ENSDART00000146237 | FST | 0.866541315 | 4.92431E-05 | 0.027718896 |
| ENSDART00000031761 | FZD5 | -0.587341844 | 0.007262177 | 0.429866885 |
| ENSDART00000164953 | GABRR1 | 0.66212946 | 0.002784526 | 0.257502391 |
| ENSDART00000104234 | GJD2 | 0.7736275 | 0.000482839 | 0.098185618 |
| ENSDART00000145258 | GLS | 0.610357953 | 0.006827116 | 0.416651549 |
| ENSDART00000130104 | GNB1 | 0.591649191 | 0.008111189 | 0.46039724 |
| ENSDART00000012673 | GNB3 | 0.748970769 | 1.33435E-05 | 0.012640491 |
| ENSDART00000133642 | GPD1L | -0.581517446 | 0.004356771 | 0.326044258 |
| ENSDART00000131652 | GPR146 | 0.635128435 | 0.003318303 | 0.282637892 |
| ENSDART00000151311 | GPR161 | -0.666943125 | 0.003083154 | 0.271541259 |
| ENSDART00000054408 | GSG1L | -0.791740037 | 4.4463E-05 | 0.026811277 |
| ENSDART00000162388 | GUCA1A | 0.628742925 | 9.18832E-06 | 0.010196405 |
| ENSDART00000106527 | GYG1 | 0.791867989 | 0.00019578 | 0.061260168 |
| ENSDART00000137361 | HECTD3 | 0.610825408 | 0.003840902 | 0.303270519 |
| ENSDART00000050271 | HEXB | 0.600506385 | 0.006740825 | 0.416651549 |
| ENSDART00000144705 | HMCN1 | 0.82812334 | 0.000155664 | 0.052573887 |
| ENSDART00000162445 | HMGXB3 | 0.610610752 | 0.00681434 | 0.416651549 |
| ENSDART00000165006 | HPCA | 0.587876432 | 0.008424898 | 0.468103388 |
| ENSDART00000018533 | HPGD | 0.753876925 | 0.00053939 | 0.106821595 |
| ENSDART00000109822 | HPS1 | 0.592008685 | 0.008687233 | 0.473893447 |
| ENSDART00000093155 | HPSE | 0.684185829 | 9.78521E-05 | 0.042091846 |
| ENSDART00000149816 | HSPB1 | 0.604110955 | 0.006660962 | 0.41393882 |
| ENSDART00000163026 | IGF2BP3 | -0.582564319 | 0.009717401 | 0.492725767 |
| ENSDART00000029308 | ITGB4 | 0.59255229 | 0.008448519 | 0.468103388 |
| ENSDART00000166540 | KCNIP3 | -0.597993817 | 0.005867606 | 0.385613904 |
| ENSDART00000174474 | KCNQ1 | 0.584149383 | 0.00086342 | 0.140324441 |
| ENSDART00000187407 | KDM4A | 0.756534585 | 0.000278129 | 0.077958865 |
| ENSDART00000045126 | LAMA5 | 0.660265212 | 0.00199261 | 0.215352162 |
| ENSDART00000147326 | LAMB2 | 0.600113893 | 0.007876897 | 0.453914982 |

| ID | Symbol | Expr Log Ratio | Expr p-value | Expr False Discovery Rate (q-value) |
|---|---|---|---|---|
| ENSDART00000140133 | LDHB | 0.644488328 | 0.00267284 | 0.255069083 |
| ENSDART00000138221 | LMOD2 | 0.986662268 | 7.60078E-06 | 0.009057315 |
| ENSDART00000161708 | LNP1 | 0.909542912 | 2.89695E-05 | 0.020457758 |
| ENSDART00000170695 | LRIT1 | 0.584382724 | 0.000615488 | 0.113485437 |
| ENSDART00000077823 | LRIT3 | 0.602718658 | 0.004608934 | 0.337120508 |
| ENSDART00000164392 | LRRC20 | 0.773247923 | 1.26529E-06 | 0.003071481 |
| ENSDART00000133848 | LRRFIP2 | -0.63178338 | 0.002889856 | 0.26163639 |
| ENSDART00000148973 | LTA4H | -0.604044803 | 0.00729357 | 0.429866885 |
| ENSDART00000174157 | LTBP4 | 0.594023974 | 0.003426651 | 0.286910153 |
| ENSDART00000173274 | MAP7D3 | 0.648722242 | 0.003616042 | 0.295056838 |
| ENSDART00000188103 | MAST2 | -0.582418366 | 0.006558629 | 0.410204743 |
| ENSDART00000161597 | MISP | 0.649288662 | 0.002231769 | 0.227344197 |
| ENSDART00000152788 | MKI67 | -0.741408314 | 0.000428938 | 0.095199713 |
| ENSDART00000136808 | MMRN2 | 0.698528671 | 0.000553482 | 0.106821595 |
| ENSDART00000134619 | MPP2 | -0.863518378 | 9.19053E-05 | 0.041506987 |
| ENSDART00000151558 | MPP4 | 0.580688959 | 0.005863435 | 0.385613904 |
| ENSDART00000167164 | MPV17L | 0.687550771 | 6.45872E-05 | 0.032806076 |
| ENSDART00000097427 | MSI1 | 0.594287055 | 0.008503689 | 0.470362268 |
| ENSDART00000173090 | MTUS1 | 0.592549161 | 0.008680566 | 0.473893447 |
| ENSDART00000131983 | MYH4 | 0.783470118 | 7.92865E-06 | 0.009057315 |
| ENSDART00000099532 | MYH7 | 0.780834345 | 0.000150822 | 0.052302846 |
| ENSDART00000105232 | MYH9 | 0.667210019 | 0.000428755 | 0.095199713 |
| ENSDART00000152777 | MYO1C | 0.64410104 | 0.002259574 | 0.227952907 |
| ENSDART00000067762 | MYO1D | 0.719006993 | 0.000746994 | 0.128947804 |
| ENSDART00000026000 | MYOF | 0.60971452 | 0.006810518 | 0.416651549 |
| ENSDART00000135296 | NCOA5 | 0.672215164 | 0.002088277 | 0.22160845 |
| ENSDART00000049420 | NDRG1 | 0.915365162 | 3.59335E-09 | 0.000139566 |
| ENSDART00000145072 | NEUROD4 | 0.797475563 | 2.37189E-06 | 0.00440571 |
| ENSDART00000172454 | NFKBIZ | 0.60229501 | 0.00636704 | 0.402761964 |
| ENSDART00000000069 | NHERF1 | 0.622426492 | 0.005680056 | 0.378894354 |
| ENSDART00000149039 | ODC1 | 0.829213011 | 0.000238808 | 0.069234894 |
| ENSDART00000138171 | OS9 | 0.608691044 | 0.006928165 | 0.418491317 |
| ENSDART00000168822 | PABPC4 | 0.879209345 | 4.69404E-05 | 0.026811277 |
| ENSDART00000165201 | PACSIN3 | 0.585935841 | 0.009001133 | 0.479566536 |
| ENSDART00000190447 | PARP6 | 0.702442829 | 0.001313408 | 0.180257181 |
| ENSDART00000018420 | PDHA1 | 0.650699942 | 0.000178512 | 0.057300882 |
| ENSDART00000080269 | PGAM2 | 0.675284512 | 0.001858398 | 0.20946532 |
| ENSDART00000102538 | PITX3 | 0.601190996 | 0.003759799 | 0.299857495 |
| ENSDART00000131460 | PLCH2 | 0.596865411 | 0.002842837 | 0.259141408 |
| ENSDART00000127769 | PLEKHG7 | 0.67565988 | 0.000575371 | 0.108482477 |
| ENSDART00000191547 | PLIN1 | 0.598607769 | 0.002113212 | 0.223035732 |
| ENSDART00000159459 | PMEL | 0.642327555 | 0.000836932 | 0.138916351 |
| ENSDART00000032996 | PPDPF | 0.718187727 | 2.29802E-05 | 0.01840456 |
| ENSDART00000089031 | PPFIBP2 | 0.657252392 | 0.000982608 | 0.14966467 |
| ENSDART00000152119 | PPP1R13B | -0.671477566 | 0.002827617 | 0.259141408 |
| ENSDART00000113197 | PROK1 | 0.659329702 | 0.000958692 | 0.147176241 |
| ENSDART00000185021 | PRX | 0.99678084 | 3.47439E-08 | 0.000282558 |
| ENSDART00000158726 | PSME4 | 0.693761241 | 0.002052017 | 0.218956992 |
| ENSDART00000138371 | PUF60 | 0.630689822 | 0.005124488 | 0.361225271 |

| ID | Symbol | Expr Log Ratio | Expr p-value | Expr False Discovery Rate (q-value) |
|---|---|---|---|---|
| ENSDART00000063714 | RAPGEF6 | -0.606003556 | 0.006918105 | 0.418491317 |
| ENSDART00000038465 | RASSF1 | 0.836538289 | 0.00011905 | 0.045781373 |
| ENSDART00000006619 | RBPMS2 | 0.716015118 | 0.001519582 | 0.192584388 |
| ENSDART00000049864 | RD3 | 0.654378741 | 0.001562525 | 0.195139799 |
| ENSDART00000017599 | REM1 | 0.808317314 | 0.000338416 | 0.08385073 |
| ENSDART00000127981 | RGS9 | 0.72115336 | 0.000381597 | 0.088221707 |
| ENSDART00000193777 | RNF38 | -0.591440978 | 0.008355578 | 0.466279683 |
| ENSDART00000038505 | RPRM | 0.775132518 | 3.61918E-05 | 0.024236036 |
| ENSDART00000135375 | RS1 | 0.64714634 | 3.69945E-05 | 0.024353664 |
| ENSDART00000128985 | RYK | 0.618135908 | 0.005905357 | 0.38678592 |
| ENSDART00000148961 | S100A10 | 0.592659042 | 0.007608189 | 0.444363997 |
| ENSDART00000189239 | SALL1 | 0.599592177 | 0.00788965 | 0.453976329 |
| ENSDART00000146463 | SAMD11 | 0.601216816 | 0.006293158 | 0.400043001 |
| ENSDART00000112457 | SAMSN1 | 0.620722015 | 0.000357543 | 0.085511403 |
| ENSDART00000150743 | SBF1 | -0.628845269 | 0.005338423 | 0.368393118 |
| ENSDART00000128198 | SCN5A | 0.590030745 | 0.000316347 | 0.080834933 |
| ENSDART00000144810 | SEC14L2 | 0.717576038 | 0.000722207 | 0.126353632 |
| ENSDART00000006971 | SEPTIN4 | 0.699376558 | 0.00152223 | 0.192584388 |
| ENSDART00000098815 | SERINC4 | 0.66510335 | 0.00038493 | 0.088465475 |
| ENSDART00000160608 | SH3D21 | 0.648498031 | 0.000197156 | 0.061260168 |
| ENSDART00000181342 | SHROOM2 | 0.638563335 | 0.000775982 | 0.132189269 |
| ENSDART00000125039 | SIX6 | 0.697853068 | 0.000874318 | 0.140324441 |
| ENSDART00000047896 | SLC15A1 | 0.659326764 | 0.003240137 | 0.279039718 |
| ENSDART00000164570 | SLC25A3 | 0.599659984 | 1.23924E-05 | 0.012341597 |
| ENSDART00000166618 | SLC43A3 | 0.67988759 | 0.000553315 | 0.106821595 |
| ENSDART00000148430 | SLC6A2 | 0.665314299 | 0.002068318 | 0.220091694 |
| ENSDART00000164799 | SLC6A6 | 0.631317228 | 0.003474672 | 0.286910153 |
| ENSDART00000081338 | SLC9A5 | 0.736943868 | 0.000329007 | 0.082978239 |
| ENSDART00000187280 | SMAD5 | 0.632191048 | 0.005092186 | 0.360913294 |
| ENSDART00000150975 | SMAD7 | 0.686485722 | 0.001146484 | 0.165945459 |
| ENSDART00000144570 | SMTN | 0.842768217 | 3.36607E-05 | 0.023346116 |
| ENSDART00000148039 | SNX19 | 0.584582331 | 6.21459E-05 | 0.032618221 |
| ENSDART00000143667 | SORT1 | -0.879315138 | 9.44824E-05 | 0.042091846 |
| ENSDART00000157340 | SPTBN5 | 0.620701341 | 0.000168702 | 0.05506193 |
| ENSDART00000165131 | SRL | 0.715151844 | 0.001335988 | 0.181432769 |
| ENSDART00000169942 | STX3 | 0.74126033 | 0.000185014 | 0.058901084 |
| ENSDART00000006061 | TCEA3 | 0.637834219 | 0.00473794 | 0.344609718 |
| ENSDART00000140338 | TCF12 | 0.806707645 | 2.05953E-06 | 0.004210107 |
| ENSDART00000028301 | TDO2 | 0.582296808 | 0.007946895 | 0.454926169 |
| ENSDART00000019766 | TGFB3 | 0.709059216 | 0.001645196 | 0.19968561 |
| ENSDART00000135321 | TIAL1 | 0.746252583 | 0.000895071 | 0.141645175 |
| ENSDART00000092343 | TJP2 | 0.665521808 | 0.002033294 | 0.218157879 |
| ENSDART00000188189 | TM6SF2 | 0.618557599 | 0.00535122 | 0.368393118 |
| ENSDART00000168228 | TMEM184A | 0.624664355 | 0.002720376 | 0.256866495 |
| ENSDART00000149439 | TNNI2 | 0.687054226 | 0.001333949 | 0.181432769 |
| ENSDART00000106152 | TOP2A | -0.597480465 | 0.006875267 | 0.417895698 |
| ENSDART00000065137 | TP63 | 0.58067519 | 0.002621486 | 0.251403764 |
| ENSDART00000062402 | TPD52L1 | 0.633989003 | 0.003168054 | 0.276510564 |
| ENSDART00000162158 | TRAPPC2 | -0.641438638 | 0.003366489 | 0.283953766 |
| ENSDART00000036513 | TRIB3 | 0.67029407 | 0.002759501 | 0.256866495 |
| ENSDART00000047055 | TRIM55 | 0.628770856 | 0.002934484 | 0.263222555 |
| ENSDART00000078594 | TYRP1 | 0.804842494 | 5.35702E-06 | 0.008322663 |
| ENSDART00000132854 | U2SURP | -0.582348013 | 0.009668829 | 0.492725767 |
| ENSDART00000102748 | UBR2 | 0.676330579 | 0.001789505 | 0.20930751 |
| ENSDART00000014176 | VENTX | -0.795967215 | 6.63568E-05 | 0.033042298 |
| ENSDART00000003745 | VIM | 0.614029206 | 0.004822567 | 0.348157093 |
| ENSDART00000154570 | VSIG10L | 0.662521666 | 0.000258044 | 0.073156538 |
| ENSDART00000114690 | VWF | 0.603711545 | 0.002845946 | 0.259141408 |
| ENSDART00000055225 | WNT9B | 0.795804546 | 7.70762E-06 | 0.009057315 |
| ENSDART00000045813 | ZIC4 | -0.605452584 | 0.005309026 | 0.368393118 |
| ENSDART00000164948 | ZNF729 | -0.587513785 | 0.005960124 | 0.388408087 |

## Table 5-13. Differentially expressed genes (DEGs) in 6 months post-fertilization zebrafish brains treated with 500 ppb TaClo

| ID | Symbol | Expr Log Ratio | Expr p-value | Expr False Discovery Rate (q-value) |
|---|---|---|---|---|
| ENSDART00000092809 | ABCG1 | 0.631744118 | 0.004823485 | 0.669246227 |
| ENSDART00000005682 | ACTN3 | 0.719724188 | 0.001336261 | 0.346002546 |
| ENSDART00000188350 | ADAM23 | 0.606620264 | 0.004288875 | 0.638237124 |
| ENSDART00000155915 | AHCYL2 | -0.64541348 | 0.004003527 | 0.617051483 |
| ENSDART00000028787 | AHR | 0.586093578 | 0.004343802 | 0.639861319 |
| ENSDART00000042755 | AMPD1 | 0.77841816 | 0.00029823 | 0.148718547 |
| ENSDART00000135248 | ANXA13 | 0.588242193 | 0.003131203 | 0.540515263 |
| ENSDART00000034802 | Apol3l1 | 0.620698888 | 0.00433796 | 0.639861319 |
| ENSDART00000066382 | AQP8 | 0.694379661 | 0.00207057 | 0.439458628 |
| ENSDART00000097822 | ATP1B2 | 0.761582436 | 0.000128755 | 0.088633781 |
| ENSDART00000144067 | CABP5 | 0.640788105 | 9.75433E-06 | 0.022285785 |
| ENSDART00000017902 | CAMK1G | 0.585107928 | 0.001945757 | 0.433438367 |
| ENSDART00000159951 | CASQ1 | 0.658624961 | 0.000809561 | 0.259862513 |
| ENSDART00000026679 | CDHR1 | 0.622158215 | 0.000170066 | 0.104846837 |
| ENSDART00000174562 | CDHR2 | 0.60561376 | 0.003581857 | 0.579663887 |
| ENSDART00000132527 | CEP78 | -0.580350991 | 0.00894714 | 0.866600791 |
| ENSDART00000157998 | CNGB3 | 0.600680137 | 1.66176E-05 | 0.031547752 |
| ENSDART00000050018 | CNKSR1 | 0.633967557 | 0.00018031 | 0.109425832 |
| ENSDART00000039597 | CRABP2 | 0.716636948 | 0.001366081 | 0.349863988 |
| ENSDART00000161253 | CRB1 | 0.627043591 | 0.004992717 | 0.673643322 |
| ENSDART00000100328 | CSNK1G3 | 0.615967269 | 0.00520178 | 0.680259728 |
| ENSDART00000163795 | DLG3 | -0.604536085 | 0.007029191 | 0.775607336 |
| ENSDART00000051974 | DRD4 | 0.655610756 | 0.000676656 | 0.2325782 |
| ENSDART00000104307 | EML1 | 0.593759988 | 0.00486807 | 0.669246227 |
| ENSDART00000127216 | FAM161A | 0.703540782 | 0.000408004 | 0.174869238 |
| ENSDART00000171829 | FRMPD3 | 0.670946038 | 0.002506909 | 0.481368421 |
| ENSDART00000111717 | FSCN2 | 0.711118723 | 1.2942E-05 | 0.027925966 |
| ENSDART00000173110 | GLRB | -0.692535083 | 0.00099135 | 0.291697126 |
| ENSDART00000108639 | GMIP | 0.920454343 | 3.54486E-05 | 0.039697067 |
| ENSDART00000097770 | GUCY2D | 0.707435563 | 6.45963E-05 | 0.055753783 |
| ENSDART00000126590 | H2BC21 | 0.598801132 | 0.000595691 | 0.212262653 |
| ENSDART00000152144 | HEMGN | -0.615062052 | 0.005816391 | 0.709556053 |
| ENSDART00000012318 | HTRA1 | 0.817888759 | 5.79962E-05 | 0.054940807 |
| ENSDART00000131411 | IMPA1 | 0.594255136 | 0.006842018 | 0.76462974 |
| ENSDART00000017619 | IMPDH1 | 0.584436958 | 0.005772668 | 0.709556053 |
| ENSDART00000103267 | INKA1 | 0.754394566 | 0.00059092 | 0.212262653 |
| ENSDART00000187956 | INPP5K | 0.665792111 | 0.000471733 | 0.191790169 |
| ENSDART00000147903 | LRIT1 | 0.747881816 | 8.66277E-06 | 0.021028881 |
| ENSDART00000077823 | LRIT3 | 0.620404436 | 0.0035504 | 0.578255163 |
| ENSDART00000162827 | MPDZ | 0.879365817 | 1.65244E-05 | 0.031547752 |
| ENSDART00000181711 | MPP7 | 0.590824735 | 0.00508181 | 0.673643322 |
| ENSDART00000156295 | MYH4 | 0.713350713 | 0.000617499 | 0.214139676 |
| ENSDART00000049066 | NET1 | 0.609750105 | 0.005018881 | 0.673643322 |
| ENSDART00000150899 | NIN | 1.239268297 | 9.12067E-11 | 3.54247E-06 |
| ENSDART00000162026 | NINL | 0.595041742 | 0.007874772 | 0.815871343 |
| ENSDART00000066407 | NPTX2 | 0.768321204 | 0.000507257 | 0.198608135 |
| ENSDART00000176170 | NR2F6 | 0.887399694 | 7.9811E-05 | 0.063728157 |
| ENSDART00000154658 | OAZ2 | 0.603345018 | 0.002415361 | 0.475236573 |
| ENSDART00000020667 | OSBPL7 | 0.590488978 | 1.7246E-05 | 0.031547752 |
| ENSDART00000166490 | PAX6 | 0.594959512 | 0.006404232 | 0.733747367 |
| ENSDART00000144448 | PCBP3 | 0.632243283 | 0.00364363 | 0.586074354 |
| ENSDART00000189157 | PDE6A | 0.585860363 | 0.000194725 | 0.114592775 |
| ENSDART00000160779 | PDZD7 | 0.615571583 | 0.006384533 | 0.733654587 |
| ENSDART00000127769 | PLEKHG7 | 0.60689331 | 0.001988149 | 0.433438367 |
| ENSDART00000114266 | PLEKHO1 | 0.660050832 | 0.003197534 | 0.549523078 |
| ENSDART00000032996 | PPDPF | 0.586950235 | 0.000539926 | 0.207630969 |
| ENSDART00000142287 | PPP1R18 | 0.742751641 | 2.37402E-05 | 0.032806804 |
| ENSDART00000013360 | PPP1R3C | 0.681508715 | 0.000844085 | 0.262274154 |
| ENSDART00000128859 | PRLR | 0.615797908 | 0.006376134 | 0.733654587 |
| ENSDART00000122474 | PTK2 | -0.665588927 | 0.00285415 | 0.50851002 |
| ENSDART00000190678 | PTP4A1 | -0.589777114 | 0.009000645 | 0.867456725 |
| ENSDART00000133049 | QRFPR | -0.634212005 | 0.000908371 | 0.275633889 |
| ENSDART00000127612 | RGS5 | 0.663147891 | 0.003228084 | 0.552329377 |
| ENSDART00000193777 | RNF38 | -0.615259634 | 0.006046512 | 0.717708598 |
| ENSDART00000153743 | RP1L1 | 0.696340595 | 0.00152861 | 0.375767171 |
| ENSDART00000189239 | SALL1 | 0.602676661 | 0.007554323 | 0.803862728 |
| ENSDART00000189843 | SAMD11 | 0.622729978 | 0.004893861 | 0.669246227 |
| ENSDART00000112457 | SAMSN1 | 0.671000061 | 0.000115327 | 0.081442178 |
| ENSDART00000135729 | SLC24A1 | 0.603090013 | 0.001072411 | 0.304341646 |
| ENSDART00000033325 | SLC25A24 | 0.889858846 | 7.78527E-05 | 0.063728157 |
| ENSDART00000030665 | SLC25A4 | 0.590026193 | 0.004706689 | 0.662347089 |
| ENSDART00000109459 | SMG9 | -0.683630489 | 0.001911201 | 0.431296227 |
| ENSDART00000155238 | TAF4 | 0.609559343 | 0.006850956 | 0.76462974 |
| ENSDART00000135321 | TIAL1 | 0.622899425 | 0.005563973 | 0.701788658 |
| ENSDART00000144047 | TNNC2 | 0.610574828 | 0.001081941 | 0.304511491 |
| ENSDART00000149439 | TNNI2 | 0.614618576 | 0.004108752 | 0.6209492 |
| ENSDART00000062402 | TPD52L1 | 0.757717869 | 0.000423884 | 0.178952765 |
| ENSDART00000030448 | VSX2 | 0.639445149 | 0.003777113 | 0.596353865 |
| ENSDART00000004689 | VWA5A | 0.629252964 | 0.005137378 | 0.675624366 |
| ENSDART00000142407 | WDR37 | 0.615660939 | 0.004462325 | 0.644987238 |
| ENSDART00000131396 | ZNF729 | -0.754536919 | 0.000684488 | 0.233206421 |

**Table 5-14. Differentially expressed genes (DEGs) in 6 months post-fertilization zebrafish brains treated with TaClo (5, 50, 500 ppb)**

| ID | Symbol | Expr Log Ratio | Expr p-value | Expr False Discovery Rate (q-value) |
|---|---|---|---|---|
| ENSDART00000053126 | AANAT | 0.877634768 | 9.65946E-06 | 0.010421485 |
| ENSDART00000161691 | ABCC3 | 0.729776084 | 0.000474626 | 0.097979415 |
| ENSDART00000092809 | ABCG1 | 0.631744118 | 0.004823485 | 0.669246227 |
| ENSDART00000168910 | ABLIM3 | 0.665788145 | 0.002898265 | 0.261649822 |
| ENSDART00000135585 | ACADM | 0.717483971 | 0.001465681 | 0.18912641 |
| ENSDART00000058629 | ACTA1 | 0.862423597 | 4.39812E-07 | 0.001423524 |
| ENSDART00000133319 | ACTG1 | 0.610226266 | 0.001279421 | 0.176897452 |
| ENSDART00000005682 | ACTN3 | 0.719724188 | 0.001336261 | 0.346002546 |
| ENSDART00000019519 | ADA | 0.614619053 | 0.00648748 | 0.407638267 |
| ENSDART00000188350 | ADAM23 | 0.689337423 | 0.00115843 | 0.999996026 |
| ENSDART00000155915 | AHCYL2 | -0.64541348 | 0.004003527 | 0.617051483 |
| ENSDART00000028787 | AHR | 0.586093578 | 0.004343802 | 0.639861319 |
| ENSDART00000031049 | AKAP13 | 0.810655178 | 0.000290977 | 0.080152897 |
| ENSDART00000018261 | AKR1B1 | 0.731109618 | 0.000568454 | 0.108229258 |
| ENSDART00000138893 | AKTIP | 0.5900092 | 0.00890183 | 0.476355799 |
| ENSDART00000042200 | ALDOA | 0.632856796 | 0.003050246 | 0.26972343 |
| ENSDART00000042755 | AMPD1 | 0.77841816 | 0.00029823 | 0.148718547 |
| ENSDART00000190191 | ANK1 | 0.594871447 | 0.008420368 | 0.468103388 |
| ENSDART00000132390 | ANKRD33B | 0.650191711 | 2.56935E-05 | 0.019958695 |
| ENSDART00000151304 | ANP32E | 0.704445995 | 0.00176186 | 0.207365537 |
| ENSDART00000135248 | ANXA13 | 0.588242193 | 0.003131203 | 0.540515263 |
| ENSDART00000182856 | ANXA2 | 0.701859202 | 0.001843827 | 0.20946532 |
| ENSDART00000034802 | Apol3l1 | 0.620698888 | 0.00433796 | 0.639861319 |
| ENSDART00000066382 | AQP8 | 0.694379661 | 0.00207057 | 0.439458628 |
| ENSDART00000075513 | AQP9 | 0.751368288 | 2.53541E-07 | 0.000984755 |
| ENSDART00000177573 | ARHGAP17 | 0.589848691 | 0.008867748 | 0.475722827 |
| ENSDART00000154077 | ARHGAP29 | 0.813305618 | 0.000155636 | 0.052573887 |
| ENSDART00000138232 | ARL13A | 0.769142295 | 2.38208E-06 | 0.00440571 |
| ENSDART00000097822 | ATP1B2 | 0.761582436 | 0.000128755 | 0.088633781 |
| ENSDART00000104353 | ATP2B4 | 0.722583307 | 4.44365E-05 | 0.026811277 |
| ENSDART00000090069 | AXDND1 | 0.582806749 | 0.009703573 | 0.999996026 |
| ENSDART00000187351 | B4GALNT1 | 0.623118124 | 0.005013576 | 0.999996026 |
| ENSDART00000128710 | BTBD2 | 0.590934175 | 0.007572083 | 0.443589281 |
| ENSDART00000079709 | C6 | 0.708214936 | 0.000808527 | 0.135944587 |
| ENSDART00000138073 | CA13 | 0.708170946 | 0.001394026 | 0.184163107 |
| ENSDART00000043801 | CABP5 | 0.704419319 | 0.001437868 | 0.186778598 |
| ENSDART00000041564 | CACNA1F | 0.845171157 | 5.43597E-05 | 0.029886971 |
| ENSDART00000130611 | CACNB1 | -0.750748571 | 0.000812145 | 0.135955984 |
| ENSDART00000152964 | CALCOCO2 | 0.605083365 | 0.004262744 | 0.324637223 |
| ENSDART00000017902 | CAMK1G | 0.729106833 | 0.000112966 | 0.044319262 |
| ENSDART00000172488 | CAPN3 | 0.626168683 | 0.001546754 | 0.194420447 |
| ENSDART00000159951 | CASQ1 | 0.658624961 | 0.000809561 | 0.259862513 |
| ENSDART00000073726 | CAV2 | 0.767745862 | 0.00045531 | 0.09561061 |
| ENSDART00000152157 | CCDC150 | 0.601812795 | 0.000461387 | 0.999996026 |
| ENSDART00000193189 | CCDC47 | -0.719461673 | 0.000463606 | 0.999996026 |
| ENSDART00000063028 | CCN2 | 0.666058485 | 0.003166935 | 0.276510564 |
| ENSDART00000169412 | CCNE2 | 0.627264118 | 0.005395095 | 0.36891811 |
| ENSDART00000026679 | CDHR1 | 0.622158215 | 0.000170066 | 0.104846837 |
| ENSDART00000174562 | CDHR2 | 0.60561376 | 0.003581857 | 0.579663887 |

| ID | Symbol | Expr Log Ratio | Expr p-value | Expr False Discovery Rate (q-value) |
|---|---|---|---|---|
| ENSDART00000135517 | CENPF | -0.588423216 | 0.004795087 | 0.347344569 |
| ENSDART00000132527 | CEP78 | -0.580350991 | 0.00894714 | 0.866600791 |
| ENSDART00000111028 | CHL1 | 0.622645203 | 0.005666796 | 0.378826747 |
| ENSDART00000020261 | CHRNA1 | 0.688570246 | 5.52607E-05 | 0.029886971 |
| ENSDART00000029492 | CMTM7 | 0.637880706 | 0.004234119 | 0.323726748 |
| ENSDART00000157998 | CNGB3 | 0.600680137 | 1.66176E-05 | 0.031547752 |
| ENSDART00000050018 | CNKSR1 | 0.633967557 | 0.00018031 | 0.109425832 |
| ENSDART00000000948 | COCH | 0.587788426 | 0.006811333 | 0.416651549 |
| ENSDART00000137065 | COL15A1 | 0.676678158 | 0.002455031 | 0.241401001 |
| ENSDART00000100234 | COL2A1 | 0.687924586 | 0.001127933 | 0.164695191 |
| ENSDART00000073827 | COL4A5 | 0.684376058 | 0.001390402 | 0.184163107 |
| ENSDART00000174023 | COL4A6 | 0.688993494 | 0.001960528 | 0.214934449 |
| ENSDART00000167299 | CPSF1 | -0.646143226 | 0.002857719 | 0.999996026 |
| ENSDART00000039597 | CRABP2 | 0.716636948 | 0.001366081 | 0.349863988 |
| ENSDART00000161253 | CRB1 | 0.627043591 | 0.004992717 | 0.673643322 |
| ENSDART00000100328 | CSNK1G3 | 0.615967269 | 0.00520178 | 0.680259728 |
| ENSDART00000137617 | CTSB | 0.662963023 | 0.001106417 | 0.163396265 |
| ENSDART00000140111 | CTSH | -0.680038603 | 0.001582694 | 0.196709047 |
| ENSDART00000143652 | Cutal | 0.60633212 | 0.005358963 | 0.368393118 |
| ENSDART00000160991 | CYP24A1 | 0.6957825 | 0.000295485 | 0.080256182 |
| ENSDART00000153070 | CYRIA | 0.58771923 | 0.009239397 | 0.485837039 |
| ENSDART00000124331 | DBNDD1 | 0.76452499 | 0.000139999 | 0.04964304 |
| ENSDART00000166172 | DDAH2 | 0.634515091 | 0.002174147 | 0.225785793 |
| ENSDART00000134461 | DDX19A | 0.58400407 | 0.005285635 | 0.367910508 |
| ENSDART00000173149 | DGKA | 0.648540816 | 0.00042763 | 0.095199713 |
| ENSDART00000156051 | DHX32 | 0.793055226 | 0.00036632 | 0.085710134 |
| ENSDART00000169687 | DLG1 | -0.610873428 | 0.000458293 | 0.095699527 |
| ENSDART00000163795 | DLG3 | -0.604536085 | 0.007029191 | 0.775607336 |
| ENSDART00000173268 | DNAJC11 | -0.586237694 | 0.003206489 | 0.277915876 |
| ENSDART00000051974 | DRD4 | 0.655610756 | 0.000676656 | 0.2325782 |
| ENSDART00000128681 | DYRK3 | 0.591559974 | 0.006349176 | 0.402287081 |
| ENSDART00000185215 | DYRK4 | 0.588495343 | 0.008833073 | 0.475722827 |
| ENSDART00000158674 | ELK1 | -0.630862537 | 0.00433666 | 0.325165746 |
| ENSDART00000104307 | EML1 | 0.593759988 | 0.00486807 | 0.669246227 |
| ENSDART00000065495 | EMP2 | 0.586502237 | 0.0084424 | 0.468103388 |
| ENSDART00000145905 | ENO3 | 0.686660965 | 0.002312681 | 0.232104698 |
| ENSDART00000131397 | ENOX1 | 0.761609321 | 0.000343118 | 0.999996026 |
| ENSDART00000129068 | ENTPD3 | 0.705929733 | 0.001750686 | 0.206805192 |
| ENSDART00000062898 | EPHX1 | 0.584815114 | 0.000311609 | 0.080834933 |
| ENSDART00000169805 | EPS8 | 0.660253301 | 0.003458856 | 0.286910153 |
| ENSDART00000115335 | ERICH1 | 0.611999821 | 1.17388E-06 | 0.003039571 |
| ENSDART00000147391 | FAM133B | 0.586543196 | 0.006162379 | 0.394497205 |
| ENSDART00000127216 | FAM161A | 0.703540782 | 0.000408004 | 0.174869238 |
| ENSDART00000153595 | FARP2 | 0.621878336 | 0.005888574 | 0.386338191 |
| ENSDART00000179907 | FAT4 | 0.608031563 | 0.003670678 | 0.296362706 |
| ENSDART00000003926 | FBP1 | 0.845992649 | 1.9027E-05 | 0.0160654 |
| ENSDART00000143957 | FLAD1 | -0.69609638 | 0.001489947 | 0.19098859 |
| ENSDART00000171829 | FRMPD3 | 0.670946038 | 0.002506909 | 0.481368421 |
| ENSDART00000111717 | FSCN2 | 0.711118723 | 1.2942E-05 | 0.027925966 |

| ID | Symbol | Expr Log Ratio | Expr p-value | Expr False Discovery Rate (q-value) |
|---|---|---|---|---|
| ENSDART00000146237 | FST | 0.866541315 | 4.92431E-05 | 0.027718896 |
| ENSDART00000031761 | FZD5 | -0.672866024 | 0.002104891 | 0.999996026 |
| ENSDART00000164953 | GABRR1 | 0.66212946 | 0.002784526 | 0.257502391 |
| ENSDART00000104234 | GJD2 | 0.7736275 | 0.000482839 | 0.098185618 |
| ENSDART00000173110 | GLRB | -0.692535083 | 0.00099135 | 0.291697126 |
| ENSDART00000145258 | GLS | 0.610357953 | 0.006827116 | 0.416651549 |
| ENSDART00000108639 | GMIP | 0.920454343 | 3.54486E-05 | 0.039697067 |
| ENSDART00000130104 | GNB1 | 0.591649191 | 0.008111189 | 0.46039724 |
| ENSDART00000012673 | GNB3 | 0.748970769 | 1.33435E-05 | 0.012640491 |
| ENSDART00000133642 | GPD1L | -0.581517446 | 0.004356771 | 0.326044258 |
| ENSDART00000131652 | GPR146 | 0.635128435 | 0.003318303 | 0.282637892 |
| ENSDART00000151311 | GPR161 | -0.666943125 | 0.003083154 | 0.271541259 |
| ENSDART00000015277 | GPX1 | 0.604757701 | 0.006763725 | 0.999996026 |
| ENSDART00000123713 | GRIA1 | -0.606556591 | 0.000290772 | 0.999996026 |
| ENSDART00000054408 | GSG1L | -0.791740037 | 4.4463E-05 | 0.026811277 |
| ENSDART00000162388 | GUCA1A | 0.628742925 | 9.18832E-06 | 0.010196405 |
| ENSDART00000097770 | GUCY2D | 0.707435563 | 6.45963E-05 | 0.055753783 |
| ENSDART00000106527 | GYG1 | 0.791867989 | 0.00019578 | 0.061260168 |
| ENSDART00000126590 | H2BC21 | 0.598801132 | 0.000595691 | 0.212262653 |
| ENSDART00000137361 | HECTD3 | 0.610825408 | 0.003840902 | 0.303270519 |
| ENSDART00000152144 | HEMGN | -0.615062052 | 0.005816391 | 0.709556053 |
| ENSDART00000050271 | HEXB | 0.600506385 | 0.006740825 | 0.416651549 |
| ENSDART00000144705 | HMCN1 | 0.82812334 | 0.000155664 | 0.052573887 |
| ENSDART00000162445 | HMGXB3 | 0.610610752 | 0.00681434 | 0.416651549 |
| ENSDART00000165006 | HPCA | 0.587876432 | 0.008424898 | 0.468103388 |
| ENSDART00000018533 | HPGD | 0.753876925 | 0.00053939 | 0.106821595 |
| ENSDART00000109822 | HPS1 | 0.592008685 | 0.008687233 | 0.473893447 |
| ENSDART00000093155 | HPSE | 0.684185829 | 9.78521E-05 | 0.042091846 |
| ENSDART00000148113 | HRAS | -0.659064487 | 0.003437262 | 0.999996026 |
| ENSDART00000149816 | HSPB1 | 0.604110955 | 0.006660962 | 0.41393882 |
| ENSDART00000012318 | HTRA1 | 0.817888759 | 5.79962E-05 | 0.054940807 |
| ENSDART00000163026 | IGF2BP3 | -0.582564319 | 0.009717401 | 0.492725767 |
| ENSDART00000180093 | IGSF9 | 0.634413297 | 0.003815426 | 0.999996026 |
| ENSDART00000131411 | IMPA1 | 0.594255136 | 0.006842018 | 0.76462974 |
| ENSDART00000017619 | IMPDH1 | 0.584436958 | 0.005772668 | 0.709556053 |
| ENSDART00000103267 | INKA1 | 0.754394566 | 0.00059092 | 0.212262653 |
| ENSDART00000187956 | INPP5K | 0.665792111 | 0.000471733 | 0.191790169 |
| ENSDART00000155327 | IP6K2 | -0.591744653 | 0.00869044 | 0.999996026 |
| ENSDART00000029308 | ITGB4 | 0.59255229 | 0.008448519 | 0.468103388 |
| ENSDART00000160443 | IVNS1ABP | 0.730556694 | 0.001211625 | 0.999996026 |
| ENSDART00000166540 | KCNIP3 | -0.597993817 | 0.005867606 | 0.385613904 |
| ENSDART00000174474 | KCNQ1 | 0.584149383 | 0.00086342 | 0.140324441 |
| ENSDART00000187407 | KDM4A | 0.756534585 | 0.000278129 | 0.077958865 |
| ENSDART00000045126 | LAMA5 | 0.660265212 | 0.00199261 | 0.215352162 |
| ENSDART00000147326 | LAMB2 | 0.600113893 | 0.007876897 | 0.453914982 |
| ENSDART00000140133 | LDHB | 0.644488328 | 0.00267284 | 0.255069083 |
| ENSDART00000138221 | LMOD2 | 0.986662268 | 7.60078E-06 | 0.009057315 |
| ENSDART00000161708 | LNP1 | 0.909542912 | 2.89695E-05 | 0.020457758 |
| ENSDART00000147903 | LRIT1 | 0.747881816 | 8.66277E-06 | 0.021028881 |

| ID | Symbol | Expr Log Ratio | Expr p-value | Expr False Discovery Rate (q-value) |
|---|---|---|---|---|
| ENSDART00000018420 | PDHA1 | 0.650699942 | 0.000178512 | 0.057300882 |
| ENSDART00000160779 | PDZD7 | 0.615571583 | 0.006384533 | 0.733654587 |
| ENSDART00000193693 | PER3 | -0.592085366 | 0.004832539 | 0.999996026 |
| ENSDART00000080269 | PGAM2 | 0.675284512 | 0.001858398 | 0.20946532 |
| ENSDART00000102538 | PITX3 | 0.601190996 | 0.003759799 | 0.299857495 |
| ENSDART00000131460 | PLCH2 | 0.596865411 | 0.002842837 | 0.259141408 |
| ENSDART00000127769 | PLEKHG7 | 0.67565988 | 0.000575371 | 0.108482477 |
| ENSDART00000114266 | PLEKHO1 | 0.660050832 | 0.003197534 | 0.549523078 |
| ENSDART00000191547 | PLIN1 | 0.598607769 | 0.002113212 | 0.223035732 |
| ENSDART00000159459 | PMEL | 0.642327555 | 0.000836932 | 0.138916351 |
| ENSDART00000176022 | POLR3GL | -0.613751955 | 0.003561622 | 0.999996026 |
| ENSDART00000032996 | PPDPF | 0.718187727 | 2.29802E-05 | 0.01840456 |
| ENSDART00000089031 | PPFIBP2 | 0.657252392 | 0.000982608 | 0.14966467 |
| ENSDART00000152119 | PPP1R13B | -0.671477566 | 0.002827617 | 0.259141408 |
| ENSDART00000142287 | PPP1R18 | 0.742751641 | 2.37402E-05 | 0.032806804 |
| ENSDART00000013360 | PPP1R3C | 0.681508715 | 0.000844085 | 0.262274154 |
| ENSDART00000128859 | PRLR | 0.615797908 | 0.006376134 | 0.733654587 |
| ENSDART00000113197 | PROK1 | 0.659329702 | 0.000958692 | 0.147176241 |
| ENSDART00000185021 | PRX | 0.99678084 | 3.47439E-08 | 0.000282558 |
| ENSDART00000158726 | PSME4 | 0.693761241 | 0.002052017 | 0.218956992 |
| ENSDART00000122474 | PTK2 | -0.665588927 | 0.00285415 | 0.50851002 |
| ENSDART00000190678 | PTP4A1 | -0.589777114 | 0.009000645 | 0.867456725 |
| ENSDART00000114774 | PTPN5 | -0.714308219 | 0.001497972 | 0.999996026 |
| ENSDART00000138371 | PUF60 | 0.630689822 | 0.005124488 | 0.361225271 |
| ENSDART00000133049 | QRFPR | -0.634212005 | 0.000908371 | 0.275633889 |
| ENSDART00000127124 | RAB12 | -0.664115856 | 0.003059591 | 0.999996026 |
| ENSDART00000123619 | RAC2 | 0.643225897 | 0.004248902 | 0.999996026 |
| ENSDART00000063714 | RAPGEF6 | -0.606003556 | 0.006918105 | 0.418491317 |
| ENSDART00000038465 | RASSF1 | 0.836538289 | 0.00011905 | 0.045781373 |
| ENSDART00000006619 | RBPMS2 | 0.716015118 | 0.001519582 | 0.192584388 |
| ENSDART00000049864 | RD3 | 0.654378741 | 0.001562525 | 0.195139799 |
| ENSDART00000162204 | RECQL | 0.580986467 | 0.009788195 | 0.999996026 |
| ENSDART00000017599 | REM1 | 0.808317314 | 0.000338416 | 0.08385073 |
| ENSDART00000127612 | RGS5 | 0.663147891 | 0.003228084 | 0.552329377 |
| ENSDART00000127981 | RGS9 | 0.72115336 | 0.000381597 | 0.088221707 |
| ENSDART00000193777 | RNF38 | -0.615259634 | 0.006046512 | 0.717708598 |
| ENSDART00000153743 | RP1L1 | 0.696340595 | 0.00152861 | 0.375767171 |
| ENSDART00000137988 | RPL7A | -0.702675228 | 0.001768767 | 0.999996026 |
| ENSDART00000038505 | RPRM | 0.775132518 | 3.61918E-05 | 0.024236036 |
| ENSDART00000135375 | RS1 | 0.64714634 | 3.69945E-05 | 0.024353664 |
| ENSDART00000128985 | RYK | 0.618135908 | 0.005905357 | 0.38678592 |
| ENSDART00000148961 | S100A10 | 0.592659042 | 0.007608189 | 0.444363997 |
| ENSDART00000189239 | SALL1 | 0.602676661 | 0.007554323 | 0.803862728 |
| ENSDART00000189843 | SAMD11 | 0.622729978 | 0.004893861 | 0.669246227 |
| ENSDART00000112457 | SAMSN1 | 0.671000061 | 0.000115327 | 0.081442178 |
| ENSDART00000150743 | SBF1 | -0.628845269 | 0.005338423 | 0.368393118 |
| ENSDART00000128198 | SCN5A | 0.590030745 | 0.000316347 | 0.080834933 |
| ENSDART00000144810 | SEC14L2 | 0.717576038 | 0.000722207 | 0.126353632 |
| ENSDART00000006971 | SEPTIN4 | 0.699376558 | 0.00152223 | 0.192584388 |

| ID | Symbol | Expr Log Ratio | Expr p-value | Expr False Discovery Rate (q-value) |
|---|---|---|---|---|
| ENSDART00000077823 | LRIT3 | 0.620404436 | 0.0035504 | 0.578255163 |
| ENSDART00000164392 | LRRC20 | 0.773247923 | 1.26529E-06 | 0.003071481 |
| ENSDART00000133848 | LRRFIP2 | -0.63178338 | 0.002889856 | 0.26163639 |
| ENSDART00000148973 | LTA4H | -0.604044803 | 0.00729357 | 0.429866885 |
| ENSDART00000174157 | LTBP4 | 0.594023974 | 0.003426651 | 0.286910153 |
| ENSDART00000173274 | MAP7D3 | 0.648722242 | 0.003616042 | 0.295056838 |
| ENSDART00000188103 | MAST2 | -0.582418366 | 0.006558629 | 0.410204743 |
| ENSDART00000161597 | MISP | 0.649288662 | 0.002231769 | 0.227344197 |
| ENSDART00000152788 | MKI67 | -0.741408314 | 0.000428938 | 0.095199713 |
| ENSDART00000136808 | MMRN2 | 0.698528671 | 0.000553482 | 0.106821595 |
| ENSDART00000162827 | MPDZ | 0.879365817 | 1.65244E-05 | 0.031547752 |
| ENSDART00000134619 | MPP2 | -0.863518378 | 9.19053E-05 | 0.041506987 |
| ENSDART00000151558 | MPP4 | 0.580688959 | 0.005863435 | 0.385613904 |
| ENSDART00000181711 | MPP7 | 0.590824735 | 0.00508181 | 0.673643322 |
| ENSDART00000167164 | MPV17L | 0.687550771 | 6.45872E-05 | 0.032806076 |
| ENSDART00000097427 | MSI1 | 0.594287055 | 0.008503689 | 0.470362268 |
| ENSDART00000183474 | MTARC1 | -0.581025933 | 0.008202582 | 0.999996026 |
| ENSDART00000173090 | MTUS1 | 0.592549161 | 0.008680566 | 0.473893447 |
| ENSDART00000184875 | MYCL | -0.754556067 | 0.000751879 | 0.999996026 |
| ENSDART00000131983 | MYH4 | 0.783470118 | 7.92865E-06 | 0.009057315 |
| ENSDART00000099532 | MYH7 | 0.780834345 | 0.000150822 | 0.052302846 |
| ENSDART00000105232 | MYH9 | 0.667210019 | 0.000428755 | 0.095199713 |
| ENSDART00000152777 | MYO1C | 0.64410104 | 0.002259574 | 0.227952907 |
| ENSDART00000067762 | MYO1D | 0.719006993 | 0.000746994 | 0.128947804 |
| ENSDART00000026000 | MYOF | 0.60971452 | 0.006810518 | 0.416651549 |
| ENSDART00000146488 | MYOZ2 | -0.647746037 | 0.002951519 | 0.999996026 |
| ENSDART00000135296 | NCOA5 | 0.672215164 | 0.002088277 | 0.22160845 |
| ENSDART00000049420 | NDRG1 | 0.915365162 | 3.59335E-09 | 0.000139566 |
| ENSDART00000183461 | NDST1 | -0.646637966 | 0.002389809 | 0.999996026 |
| ENSDART00000049066 | NET1 | 0.609750105 | 0.005018881 | 0.673643322 |
| ENSDART00000145072 | NEUROD4 | 0.797475563 | 2.37189E-06 | 0.00440571 |
| ENSDART00000192514 | NFKBIA | 0.625487372 | 0.005567521 | 0.999996026 |
| ENSDART00000172454 | NFKBIZ | 0.60229501 | 0.00636704 | 0.402761964 |
| ENSDART00000000069 | NHERF1 | 0.622426492 | 0.005680056 | 0.378894354 |
| ENSDART00000150899 | NIN | 1.239268297 | 9.12067E-11 | 3.54247E-06 |
| ENSDART00000162026 | NINL | 0.595041742 | 0.007874772 | 0.815871343 |
| ENSDART00000066407 | NPTX2 | 0.768321204 | 0.000507257 | 0.198608135 |
| ENSDART00000176170 | NR2F6 | 0.887399694 | 7.9811E-05 | 0.063728157 |
| ENSDART00000154658 | OAZ2 | 0.603345018 | 0.002415361 | 0.475236573 |
| ENSDART00000149039 | ODC1 | 0.829213011 | 0.000238808 | 0.069234894 |
| ENSDART00000138171 | OS9 | 0.608691044 | 0.006928165 | 0.418491317 |
| ENSDART00000020667 | OSBPL7 | 0.590488978 | 1.7246E-05 | 0.031547752 |
| ENSDART00000168822 | PABPC4 | 0.879209345 | 4.69404E-05 | 0.026811277 |
| ENSDART00000165201 | PACSIN3 | 0.585935841 | 0.009001133 | 0.479566536 |
| ENSDART00000190447 | PARP6 | 0.702442829 | 0.001313408 | 0.180257181 |
| ENSDART00000166490 | PAX6 | 0.594959512 | 0.006404232 | 0.733747367 |
| ENSDART00000144448 | PCBP3 | 0.632243283 | 0.00364363 | 0.586074354 |
| ENSDART00000101582 | PCGF6 | 0.654645376 | 0.003659919 | 0.999996026 |
| ENSDART00000189157 | PDE6A | 0.585860363 | 0.000194725 | 0.114592775 |

| ID | Symbol | Expr Log Ratio | Expr p-value | Expr False Discovery Rate (q-value) |
|---|---|---|---|---|
| ENSDART00000098815 | SERINC4 | 0.66510335 | 0.00038493 | 0.088465475 |
| ENSDART00000160608 | SH3D21 | 0.648498031 | 0.000197156 | 0.061260168 |
| ENSDART00000181342 | SHROOM2 | 0.638563335 | 0.000775982 | 0.132189269 |
| ENSDART00000125039 | SIX6 | 0.697853068 | 0.000874318 | 0.140324441 |
| ENSDART00000047896 | SLC15A1 | 0.659326764 | 0.003240137 | 0.279039718 |
| ENSDART00000135729 | SLC24A1 | 0.603090013 | 0.001072411 | 0.304341646 |
| ENSDART00000033325 | SLC25A24 | 0.889858846 | 7.78527E-05 | 0.063728157 |
| ENSDART00000164570 | SLC25A3 | 0.599659984 | 1.23924E-05 | 0.012341597 |
| ENSDART00000030665 | SLC25A4 | 0.590026193 | 0.004706689 | 0.662347089 |
| ENSDART00000166618 | SLC43A3 | 0.67988759 | 0.000553315 | 0.106821595 |
| ENSDART00000148430 | SLC6A2 | 0.665314299 | 0.002068318 | 0.220091694 |
| ENSDART00000164799 | SLC6A6 | 0.631317228 | 0.003474672 | 0.286910153 |
| ENSDART00000081338 | SLC9A5 | 0.736943868 | 0.000329007 | 0.082978239 |
| ENSDART00000187280 | SMAD5 | 0.632191048 | 0.005092186 | 0.360913294 |
| ENSDART00000150975 | SMAD7 | 0.686485722 | 0.001146484 | 0.165945459 |
| ENSDART00000109459 | SMG9 | -0.683630489 | 0.001911201 | 0.431296227 |
| ENSDART00000144570 | SMTN | 0.842768217 | 3.36607E-05 | 0.023346116 |
| ENSDART00000123645 | SMYD2 | 0.621272683 | 0.005657616 | 0.999996026 |
| ENSDART00000148039 | SNX19 | 0.584582331 | 6.21459E-05 | 0.032618221 |
| ENSDART00000143667 | SORT1 | -0.879315138 | 9.44824E-05 | 0.042091846 |
| ENSDART00000157340 | SPTBN5 | 0.620701341 | 0.000168702 | 0.05506193 |
| ENSDART00000165131 | SRL | 0.715151844 | 0.001335988 | 0.181432769 |
| ENSDART00000160347 | STAG2 | 0.60837886 | 0.003715182 | 0.999996026 |
| ENSDART00000169942 | STX3 | 0.74126033 | 0.000185014 | 0.058901084 |
| ENSDART00000155238 | TAF4 | 0.609559343 | 0.006850956 | 0.76462974 |
| ENSDART00000006061 | TCEA3 | 0.637834219 | 0.00473794 | 0.344609718 |
| ENSDART00000140338 | TCF12 | 0.806707645 | 2.05953E-06 | 0.004210107 |
| ENSDART00000028301 | TDO2 | 0.582296808 | 0.007946895 | 0.454926169 |
| ENSDART00000019766 | TGFB3 | 0.709059216 | 0.001645196 | 0.19968561 |
| ENSDART00000135321 | TIAL1 | 0.746252583 | 0.000895071 | 0.141645175 |
| ENSDART00000092343 | TJP2 | 0.665521808 | 0.002033294 | 0.218157879 |
| ENSDART00000188189 | TM6SF2 | 0.618557599 | 0.00535122 | 0.368393118 |
| ENSDART00000168228 | TMEM184A | 0.624664355 | 0.002720376 | 0.256866495 |
| ENSDART00000144047 | TNNC2 | 0.610574828 | 0.001081941 | 0.304511491 |
| ENSDART00000149439 | TNNI2 | 0.687054226 | 0.001333949 | 0.181432769 |
| ENSDART00000106152 | TOP2A | -0.597480465 | 0.006875267 | 0.417895698 |
| ENSDART00000065137 | TP63 | 0.58067519 | 0.002621486 | 0.251403764 |
| ENSDART00000062402 | TPD52L1 | 0.757717869 | 0.000423884 | 0.178952765 |
| ENSDART00000162158 | TRAPPC2 | -0.641438638 | 0.003366489 | 0.283953766 |
| ENSDART00000036513 | TRIB3 | 0.67029407 | 0.002759501 | 0.256866495 |
| ENSDART00000047055 | TRIM55 | 0.628770856 | 0.002934484 | 0.263222555 |
| ENSDART00000078594 | TYRP1 | 0.804842494 | 5.35702E-06 | 0.008322663 |
| ENSDART00000132854 | U2SURP | -0.582348013 | 0.009668829 | 0.492725767 |
| ENSDART00000155648 | UBE2I | 0.585518537 | 0.009200914 | 0.999996026 |
| ENSDART00000102748 | UBR2 | 0.676330579 | 0.001789505 | 0.20930751 |
| ENSDART00000014176 | VENTX | -0.795967215 | 6.63568E-05 | 0.033042298 |
| ENSDART00000003745 | VIM | 0.614029206 | 0.004822567 | 0.348157093 |
| ENSDART00000154570 | VSIG10L | 0.662521666 | 0.000258044 | 0.073156538 |
| ENSDART00000030448 | VSX2 | 0.639445149 | 0.003777113 | 0.596353865 |
| ENSDART00000004689 | VWA5A | 0.629252964 | 0.005137378 | 0.675624366 |
| ENSDART00000114690 | VWF | 0.603711545 | 0.002845946 | 0.259141408 |
| ENSDART00000142407 | WDR37 | 0.615660939 | 0.004462325 | 0.644987238 |
| ENSDART00000055225 | WNT9B | 0.795804546 | 7.70762E-06 | 0.009057315 |
| ENSDART00000045813 | ZIC4 | -0.605452584 | 0.005309026 | 0.368393118 |
| ENSDART00000131396 | ZNF729 | -0.754536919 | 0.000684488 | 0.233206421 |

**Table 5-15. Differentially expressed genes (DEGs) in 6 months post-fertilization zebrafish brains treated with 1.75 µM MPTP**

| ID | Symbol | Expr Log Ratio | Expr p-value | Expr False Discovery Rate (q-value) |
|---|---|---|---|---|
| ENSDART00000077548 | ABLIM2 | 0.699191947 | 0.001929936 | 0.998791371 |
| ENSDART00000188722 | ANKFN1 | 0.610560616 | 0.005282381 | 0.998791371 |
| ENSDART00000146420 | ANP32A | -0.584586628 | 0.008342696 | 0.998791371 |
| ENSDART00000168721 | APRT | -0.89045405 | 1.59277E-06 | 0.087226373 |
| ENSDART00000128415 | ARID4B | 0.604421898 | 0.007210429 | 0.998791371 |
| ENSDART00000016616 | ARL5C | -0.658234348 | 0.001360764 | 0.998791371 |
| ENSDART00000149919 | ATF7IP | -0.583060786 | 0.009132563 | 0.998791371 |
| ENSDART00000082510 | B3GALT6 | 0.713121159 | 0.001552499 | 0.998791371 |
| ENSDART00000104222 | B3GNTL1 | 0.716352167 | 0.001340772 | 0.998791371 |
| ENSDART00000187351 | B4GALNT1 | 0.639504476 | 0.004077289 | 0.998791371 |
| ENSDART00000145615 | CACNA1I | 0.618182491 | 0.004199107 | 0.998791371 |
| ENSDART00000027465 | CACNA2D4 | 0.666103709 | 0.00024114 | 0.998791371 |
| ENSDART00000155728 | CARF | 0.594470307 | 0.007505004 | 0.998791371 |
| ENSDART00000111806 | CENPE | 0.773844217 | 0.000603598 | 0.998791371 |
| ENSDART00000046891 | CETP | -0.588095488 | 0.008613932 | 0.998791371 |
| ENSDART00000041249 | CHORDC1 | 0.617562333 | 0.006085235 | 0.998791371 |
| ENSDART00000180323 | CLIC3 | -0.649139872 | 0.002755834 | 0.998791371 |
| ENSDART00000131596 | COQ10B | -0.611484394 | 0.002117275 | 0.998791371 |
| ENSDART00000010537 | CP | -0.596635211 | 0.002010971 | 0.998791371 |
| ENSDART00000098565 | CRACR2A | -0.580255513 | 0.006107889 | 0.998791371 |
| ENSDART00000153935 | CYP8B1 | -0.593286092 | 0.006883293 | 0.998791371 |
| ENSDART00000045111 | DCLK2 | 0.690721093 | 0.001236401 | 0.998791371 |
| ENSDART00000188370 | DENND4A | 0.61197812 | 0.00600934 | 0.998791371 |
| ENSDART00000132346 | DNAAF11 | 0.61941281 | 0.003360155 | 0.998791371 |
| ENSDART00000127365 | EIF4B | -0.702781037 | 0.001791942 | 0.998791371 |
| ENSDART00000132227 | EIF4H | -0.653231687 | 0.003812146 | 0.998791371 |
| ENSDART00000141173 | ELAVL4 | 0.593676799 | 0.006212753 | 0.998791371 |
| ENSDART00000182953 | ERBB4 | 0.604729327 | 0.005410177 | 0.998791371 |
| ENSDART00000148892 | EXTL3 | 0.592146803 | 0.006971421 | 0.998791371 |
| ENSDART00000133946 | FBXO6 | -0.68218772 | 0.001264922 | 0.998791371 |
| ENSDART00000058466 | FGFBP2 | -0.655949077 | 0.001356147 | 0.998791371 |
| ENSDART00000136463 | FOSB | -0.687449966 | 0.001870523 | 0.998791371 |
| ENSDART00000124379 | GABARAP | 0.672364648 | 0.002189181 | 0.998791371 |
| ENSDART00000187306 | GALR1 | -0.633295314 | 0.005024614 | 0.998791371 |
| ENSDART00000150106 | GNAO1 | -0.785932584 | 0.000496609 | 0.998791371 |
| ENSDART00000132082 | GUCY1B1 | 0.629315783 | 0.004858028 | 0.998791371 |
| ENSDART00000136140 | HCN4 | 0.612690735 | 0.004533785 | 0.998791371 |
| ENSDART00000171699 | HHATL | 0.606903908 | 0.006872462 | 0.998791371 |
| ENSDART00000160397 | IQCB1 | 0.680319469 | 0.001583554 | 0.998791371 |
| ENSDART00000179004 | IRX3 | -0.59743233 | 0.006599519 | 0.998791371 |
| ENSDART00000084303 | KCNQ3 | 0.624335878 | 0.004640429 | 0.998791371 |
| ENSDART00000035925 | KCTD2 | 0.631838057 | 0.00336729 | 0.998791371 |
| ENSDART00000064343 | KLF7 | -0.830024074 | 0.000198095 | 0.998791371 |
| ENSDART00000030103 | KRT15 | -0.586911419 | 0.002054902 | 0.998791371 |
| ENSDART00000150093 | LAPTM4A | -0.621731376 | 0.002275857 | 0.998791371 |
| ENSDART00000134860 | LCORL | 0.597764851 | 0.003192148 | 0.998791371 |
| ENSDART00000097685 | LINGO3 | 0.597111368 | 0.007738986 | 0.998791371 |
| ENSDART00000152987 | LOC400499 | -0.667926048 | 0.001076861 | 0.998791371 |
| ENSDART00000182850 | LRCH3 | 0.603110913 | 0.007522241 | 0.998791371 |

| ID | Symbol | Expr Log Ratio | Expr p-value | Expr False Discovery Rate (q-value) |
|---|---|---|---|---|
| ENSDART00000149440 | MAPK1 | 0.69524183 | 0.002063208 | 0.998791371 |
| ENSDART00000181883 | MAST2 | 0.665806735 | 0.002942479 | 0.998791371 |
| ENSDART00000132971 | MDM1 | 0.640838101 | 0.003986622 | 0.998791371 |
| ENSDART00000135911 | MEF2C | 0.604089853 | 0.00719345 | 0.998791371 |
| ENSDART00000166643 | MLYCD | 0.587229051 | 0.008771223 | 0.998791371 |
| ENSDART00000192514 | NFKBIA | -0.61956015 | 0.006038337 | 0.998791371 |
| ENSDART00000174111 | NHSL2 | 0.652025026 | 0.003282303 | 0.998791371 |
| ENSDART00000172111 | NR3C2 | 0.652916793 | 0.002558621 | 0.998791371 |
| ENSDART00000078250 | NR4A3 | -0.630895159 | 0.004569374 | 0.998791371 |
| ENSDART00000183180 | NRXN1 | 0.623173465 | 0.003873495 | 0.998791371 |
| ENSDART00000046064 | OGDH | 0.666435113 | 0.003152663 | 0.998791371 |
| ENSDART00000191285 | OSBPL3 | -0.643034926 | 0.000825174 | 0.998791371 |
| ENSDART00000048893 | PCBP3 | 0.58060907 | 0.009325236 | 0.998791371 |
| ENSDART00000134519 | PDE8B | 0.600278791 | 0.000760637 | 0.998791371 |
| ENSDART00000035899 | PKP2 | -0.642006278 | 0.003298227 | 0.998791371 |
| ENSDART00000173987 | PLEKHA7 | -0.635330417 | 0.004614731 | 0.998791371 |
| ENSDART00000004222 | PLXNC1 | -0.70359539 | 0.000493481 | 0.998791371 |
| ENSDART00000152064 | PPARA | 0.625351327 | 0.004066429 | 0.998791371 |
| ENSDART00000164269 | PRDX1 | -0.591095998 | 0.003323272 | 0.998791371 |
| ENSDART00000135665 | PRPF38B | -0.759500827 | 0.000485501 | 0.998791371 |
| ENSDART00000184164 | PRTFDC1 | -0.584947573 | 0.004468167 | 0.998791371 |
| ENSDART00000137745 | PTK2 | -0.585190299 | 0.007839666 | 0.998791371 |
| ENSDART00000190678 | PTP4A1 | -0.591388919 | 0.008823184 | 0.998791371 |
| ENSDART00000167735 | RAB6A | -0.610986696 | 0.006668421 | 0.998791371 |
| ENSDART00000055237 | RAMP2 | -0.753855797 | 0.000488392 | 0.998791371 |
| ENSDART00000016607 | RGS16 | -0.729881638 | 0.000654737 | 0.998791371 |
| ENSDART00000145377 | RPL38 | -0.605449104 | 0.00256579 | 0.998791371 |
| ENSDART00000141134 | RSRP1 | 0.640843462 | 0.002575946 | 0.998791371 |
| ENSDART00000135844 | RUSC1 | 0.590629684 | 0.008141641 | 0.998791371 |
| ENSDART00000137668 | RUSF1 | -0.667421698 | 0.002935637 | 0.998791371 |
| ENSDART00000189045 | SACS | 0.672075062 | 0.002830985 | 0.998791371 |
| ENSDART00000082664 | SBF2 | -0.606824527 | 4.22143E-05 | 0.770607927 |
| ENSDART00000143158 | SETD7 | 0.650491307 | 0.002759471 | 0.998791371 |
| ENSDART00000092456 | SHANK3 | 0.61949552 | 0.003766233 | 0.998791371 |
| ENSDART00000165052 | SPAG7 | 0.645344402 | 0.003949159 | 0.998791371 |
| ENSDART00000073631 | STAMBP | -0.636630186 | 0.00018398 | 0.998791371 |
| ENSDART00000145198 | STEAP4 | -0.648462906 | 0.00325086 | 0.998791371 |
| ENSDART00000144524 | SUMO3 | -0.638680621 | 0.004376334 | 0.998791371 |
| ENSDART00000093003 | SYT7 | 0.671834231 | 0.002847169 | 0.998791371 |
| ENSDART00000189975 | TCAIM | 0.596362049 | 0.007083981 | 0.998791371 |
| ENSDART00000162297 | TPD52 | 0.770697664 | 0.000570979 | 0.998791371 |
| ENSDART00000114470 | TTBK1 | 0.696039481 | 0.000885625 | 0.998791371 |
| ENSDART00000167269 | TWSG1 | -0.614341125 | 0.006115607 | 0.998791371 |
| ENSDART00000191178 | TXLNG | 0.612759485 | 0.006589456 | 0.998791371 |
| ENSDART00000104915 | WNT7B | -0.620610144 | 0.005513849 | 0.998791371 |
| ENSDART00000186932 | XRCC4 | -0.591986354 | 0.005724233 | 0.998791371 |
| ENSDART00000128889 | ZBTB40 | -0.591166639 | 0.00823848 | 0.998791371 |
| ENSDART00000113546 | ZNF729 | 0.616855433 | 0.002485865 | 0.998791371 |

**Table 5-16. Numbers of differentially expressed genes (DEGs) identified using a threshold of fold change > 1.5 and p-value < 0.05 in 6 months post-fertilization (mpf) zebrafish following 0-120 hpf TaClo or 1.75 µM MPTP treatments**

| 6 mpf zebrafish brain | All IDs | Mapped IDs | Unmapped IDs | Filtered | Upregulation | Downregulation |
|---|---|---|---|---|---|---|
| TaClo 5 ppb | 59466 | 32410 | 27056 | 35 | 17 | 18 |
| TaClo 50 ppb | 59466 | 32410 | 27056 | 209 | 180 | 29 |
| TaClo 500 ppb | 59466 | 32410 | 27056 | 81 | 71 | 11 |
| TaClo (5, 50, 500 ppb) | 178399 | 97230 | 81169 | 300 | 248 | 52 |
| 1.75 µM MPTP | 59466 | 32410 | 27056 | 97 | 51 | 46 |

**Table 5-17. Differential expression genes (DEGs) of hspb1 and nfkbia in 120 hours post-fertilization (hpf) zebrafish larvae and 6 months post-fertilization (mpf) zebrafish brain**

| | TaClo 5 ppb ($log_2$ fold change) | TaClo 50 ppb ($log_2$ fold change) | TaClo 500 ppb ($log_2$ fold change) | TaClo (5, 50, 500 ppb) ($log_2$ fold change) | MPTP 1.75 µM ($log_2$ fold change) |
|---|---|---|---|---|---|
| hspb1 (120 hpf) | -0.93 | -0.99 | -0.99 | -0.99 | - |
| hspb1 (6 mpf) | - | 0.60 | - | 0.60 | - |
| nfkbia (120 hpf) | -0.61 | - | -0.37 | -0.61 | - |
| nfkbia (6 mpf) | 0.63 | - | - | 0.63 | - |
| | | | | | |
| | TaClo 5 ppb (p-value) | TaClo 50 ppb (p-value) | TaClo 500 ppb (p-value) | TaClo (5, 50, 500 ppb) (p-value) | MPTP 1.75 µM (p-value) |
| hspb1 (120 hpf) | 1.65E-07 | 2.66E-08 | 2.65E-08 | 2.65E-08 | - |
| hspb1 (6 mpf) | - | 6.66E-03 | - | 6.66E-03 | - |
| nfkbia (120 hpf) | 5.76E-04 | - | 3.52E-02 | 5.76E-04 | - |
| nfkbia (6 mpf) | 5.57E-03 | - | - | 5.57E-03 | - |

"-" denotes not DEGs

**Table 5-18. Z score of apoptosis, apoptosis of neuron, and organismal death in 120 hpf zebrafish larvae and 6 mpf zebrafish brain in TaClo or 1.75 µM MPTP treated groups**

| z score | TaClo (120 hpf) | TaClo (6 mpf) | 1.75 µM MPTP (120 hpf) | 1.75 µM MPTP (6 mpf) |
|---|---|---|---|---|
| Apoptosis | 2.273 | -1.296 | Not generated | Not generated |
| Apoptosis of neurons | 1.446 | -1.566 | Not generated | 0.533 |
| Organismal death | 1.257 | -5.887 | Not generated | 0.472 |

**Table 5-19. QIAGEN Ingenuity Pathway Analysis predicted neurologic disease, nervous system development and function, and psychological disorders, and behavior in 120 hpf zebrafish larvae and 6 mpf zebrafish brain in TaClo or 1.75 µM MPTP-treated groups**

| | Larval zebrafish (120 hpf) | Adult zebrafish (6 mpf) |
|---|---|---|
| TaClo 5 ppb | Neurological Disease | Not generated |
| TaClo 50 ppb | Neurological Disease | Neurological Disease |
| TaClo 500 ppb | Not generated | Nervous System Development and Function |
| TaClo (5, 50, and 500 ppb) | Neurological disease | Neurological Disease<br>Nervous System Development and Function |
| MPTP 1.75 µM | Psychological Disorders<br>Nervous System Development and Function | Behavior<br>Nervous System Development and Function |

## Table 5-20. QIAGEN Ingenuity Pathway Analysis predicted neurologic disease in TaClo (5, 50, 500 ppb)-treated 120 hours post-fertilization zebrafish larvae

| Diseases or Functions Annotation | p-value | Predicted Activation State | Activation z-score | # Molecules |
|---|---|---|---|---|
| Central nervous system solid tumor | 3.81E-11 | | | 81 |
| Neurogenic lesion | 3.1E-10 | | -0.152 | 78 |
| Glioma | 5.58E-10 | | | 78 |
| Brain tumor | 1.05E-09 | | | 76 |
| Central nervous system cancer | 1.4E-09 | | | 77 |
| Brain glioma | 1.83E-09 | | | 75 |
| Glioma cancer | 2.24E-08 | | | 74 |
| Astrocytoma | 3.37E-08 | | | 66 |
| High grade astrocytoma | 0.000000077 | | | 65 |
| Grade 4 high grade glioma | 0.000000201 | | | 62 |
| Grade 4 astrocytoma | 0.000000211 | | | 62 |
| Brain astrocytoma | 0.000000237 | | | 62 |
| Grade 3-4 glioma cancer | 0.000000372 | | | 65 |
| Familial neurological disorder | 0.0000773 | | | 31 |
| Epilepsy or neurodevelopmental disorder | 0.000111 | | | 18 |
| Neurodevelopmental disorder | 0.000214 | | | 14 |
| Charcot-Marie-Tooth disease type 2A | 0.000227 | | | 2 |
| Familial encephalopathy | 0.000318 | | | 25 |
| Supratentorial neoplasm | 0.000372 | | | 4 |
| Diabetic cardiomyopathy | 0.000421 | | | 2 |
| Grade 2-3 glioma | 0.000423 | | | 22 |
| Cognitive impairment | 0.000536 | | | 17 |
| Autosomal dominant complex neurodevelopmental disorder | 0.000659 | | | 4 |
| Motor dysfunction or movement disorder | 0.000724 | | | 23 |
| Global developmental delay and speech delay | 0.00079 | | | 3 |
| Cerebral cortex glioma | 0.000895 | | | 3 |
| Oligodendroglioma | 0.000983 | | | 21 |
| Mental retardation | 0.000994 | | | 13 |
| Early-onset encephalopathy | 0.00118 | | | 14 |
| Neurological signs | 0.00131 | | | 15 |
| Early-onset ataxia | 0.00133 | | | 3 |
| Brain oligodendroglioma | 0.00156 | | | 20 |
| Disorder of basal ganglia | 0.00157 | | | 17 |
| Movement disorders | 0.00159 | | | 22 |
| Global developmental delay and seizures | 0.00177 | | | 2 |
| Friedreich ataxia | 0.00177 | | | 2 |
| Grade 3 glioma | 0.0019 | | | 20 |
| Myocardial infarction | 0.00198 | | | 9 |
| Familial neurodevelopmental disorder | 0.00214 | | | 10 |
| Hypotonia | 0.00228 | | | 4 |
| Dyskinesia | 0.00265 | | | 12 |
| Gliomatosis cerebri | 0.00374 | | | 26 |
| Autosomal recessive intellectual disability and developmental de | 0.00375 | | | 3 |
| Huntington Disease | 0.00392 | | | 11 |
| Damage of peripheral nerve | 0.00393 | | | 1 |
| Left ventricular noncompaction type 4 | 0.00393 | | | 1 |
| Progressive myoclonic epilepsy type 7 | 0.00393 | | | 1 |
| Benign glioma | 0.00393 | | | 1 |
| Autosomal recessive intellectual developmental disorder type 77 | 0.00393 | | | 1 |

| Diseases or Functions Annotation | p-value | Predicted Activation State | Activation z-score | # Molecules |
|---|---|---|---|---|
| Jeffries-Lakhani neurodevelopmental syndrome | 0.00393 | | | 1 |
| Childhood-onset neurodegeneration with brain atrophy | 0.00393 | | | 1 |
| UBTF E210K neuroregression syndrome | 0.00393 | | | 1 |
| Familial idiopathic dilated cardiomyopathy | 0.00393 | | | 1 |
| Dilated cardiomyopathy type 1CC | 0.00393 | | | 1 |
| Polydactyly-macrocephaly syndrome | 0.00393 | | | 1 |
| Joubert syndrome type 25 | 0.00393 | | | 1 |
| Autosomal recessive distal hereditary motor neuronopathy type I | 0.00393 | | | 1 |
| Developmental delay, dysmorphic facies, and brain anomalies | 0.00393 | | | 1 |
| Dilated cardiomyopathy 1R | 0.00393 | | | 1 |
| Vasospasm of basilar artery | 0.00393 | | | 1 |
| Ataxia with isolated vitamin E deficiency and retinitis pigmentosa | 0.00393 | | | 1 |
| Autosomal dominant Charcot-Marie-Tooth disease axonal type 2 | 0.00393 | | | 1 |
| Hypomyelinating leukodystrophy type 13 | 0.00393 | | | 1 |
| Charcot-Marie-Tooth disease axonal type 2Q | 0.00393 | | | 1 |
| Hypertrophy of heart apex | 0.00393 | | | 1 |
| Familial hypertrophic cardiomyopathy-11 | 0.00393 | | | 1 |
| Familial hypertrophic cardiomyopathy type 20 | 0.00393 | | | 1 |
| Meckel syndrome type 5 | 0.00393 | | | 1 |
| Autosomal recessive neurodevelopmental disorder with hypotoni | 0.00393 | | | 1 |
| Intellectual developmental disorder with abnormal behavior, micr | 0.00393 | | | 1 |
| Intellectual disability and impaired motor function | 0.00398 | | | 2 |
| Speech and language disorders | 0.00417 | | | 5 |
| Grade 3 malignant glioma | 0.00418 | | | 19 |
| Familial intellectual disability and developmental delay | 0.00421 | | | 4 |
| Cardiomyopathy | 0.00471 | | -0.219 | 18 |
| Spinal cord lesion | 0.00503 | | | 2 |
| Severe encephalopathy | 0.00523 | | | 3 |
| Brain cancer | 0.00559 | | | 27 |
| Loss of synapse | 0.00578 | | | 2 |
| Developmental delay of motor control | 0.00578 | | | 2 |
| Neuromuscular disease | 0.00585 | | | 19 |
| Syndromic encephalopathy | 0.00658 | | | 12 |
| Intellectual disability and hypotonia | 0.00659 | | | 2 |
| Autosomal dominant Charcot-Marie-Tooth disease type 2 | 0.00701 | | | 2 |
| Dilated cardiomyopathy 1A | 0.00745 | | | 2 |
| Injury of ventricular myocytes | 0.00784 | | | 1 |
| Invasion of neuroblastoma cells | 0.00784 | | | 1 |
| Joubert syndrome type 7 | 0.00784 | | | 1 |
| Damage of brain tissue | 0.00784 | | | 1 |
| Autosomal dominant distal hereditary motor neuronopathy type 3 | 0.00784 | | | 1 |
| Autosomal dominant intellectual developmental disorder with ser | 0.00784 | | | 1 |
| Autosomal dominant progressive myoclonic epilepsy | 0.00784 | | | 1 |
| Formation of cerebral aneurysm | 0.00784 | | | 1 |
| Rupture of cerebral aneurysm | 0.00784 | | | 1 |
| Congenital myasthenic syndrome type 22 | 0.00784 | | | 1 |
| Hypotonic syndrome | 0.00825 | | | 3 |
| Grade 3 astrocytoma | 0.00869 | | | 3 |
| Hereditary neuromuscular disease | 0.00891 | | | 12 |
| Speech disorder | 0.00893 | | | 4 |

| Diseases or Functions Annotation | p-value | Predicted Activation State | Activation z-score | # Molecules |
|---|---|---|---|---|
| Calcification of aortic valve | 0.00959 | | | 5 |
| Autosomal dominant hypertrophic cardiomyopathy | 0.00979 | | | 2 |
| Developmental delay and hypotonia | 0.00979 | | | 2 |
| Cerebral astrocytoma | 0.00979 | | | 2 |
| Left ventricular dysfunction | 0.00991 | | | 7 |
| Autosomal recessive mental retardation | 0.0103 | | | 5 |
| Joubert syndrome type 1 | 0.0108 | | | 2 |
| Abnormal morphology of synapse | 0.0111 | | | 3 |
| Autosomal recessive ataxia | 0.0116 | | | 3 |
| Abnormal morphology of myocardium | 0.0116 | | | 3 |
| Charcot-Marie-Tooth disease axonal type 2A2 | 0.0117 | | | 1 |
| COACH syndrome type 1 | 0.0117 | | | 1 |

**Table 5-21. QIAGEN Ingenuity Pathway Analysis predicted nervous system development and function in 1.75 µM MPTP-treated 120 hours post-fertilization zebrafish larvae**

| Diseases or Functions Annotation | p-value | Predicted Activation State | Activation z-score | Molecules | # Molecules |
|---|---|---|---|---|---|
| Transition of Schwann cells | 0.000449 | | | FGA | 1 |
| Tubulation of nervous tissue cell lines | 0.00179 | | | FES | 1 |
| Remyelination of sciatic nerve | 0.00224 | | | FGA | 1 |
| Replenishment of synaptic vesicles | 0.00269 | | | CLTA | 1 |
| Loss of hippocampal neurons | 0.00358 | | | SLC1A2 | 1 |
| Formation of cerebral neocortex | 0.00358 | | | SLC1A2 | 1 |
| Myelination | 0.00691 | | | FGA,HYCC1 | 2 |
| Migration of nervous tissue cell lines | 0.0116 | | | FES | 1 |
| Synaptic transmission of hippocampal neurons | 0.0129 | | | CLTA | 1 |
| Abnormal quantity of synaptic vesicles | 0.0143 | | | CLTA | 1 |
| Loss of neurons in hippocampus | 0.0174 | | | SLC1A2 | 1 |
| Recycling of synaptic vesicles | 0.0187 | | | CLTA | 1 |
| Cell viability of motor neurons | 0.0218 | | | SLC1A2 | 1 |
| Synaptic transmission | 0.0232 | | | CLTA,SLC1A2 | 2 |
| Loss of neurons in central nervous system | 0.0358 | | | SLC1A2 | 1 |
| Activation of astrocytes | 0.0375 | | | FGA | 1 |
| Endocytosis of synaptic vesicles | 0.0388 | | | CLTA | 1 |

**Table 5-22. QIAGEN Ingenuity Pathway Analysis predicted psychologic disorder in 1.75 µM MPTP-treated 120 hours post-fertilization zebrafish larvae**

| Diseases or Functions Annotation | p-value | Predicted Activation State | Activation z-score | Molecules | # Molecules |
|---|---|---|---|---|---|
| Mood disorders | 0.0000553 | | | CLTA,FGA,HYCC1,MCMBP,PAIP2B,SLC1A2 | 6 |
| Major affective disorder | 0.000452 | | | CLTA,HYCC1,MCMBP,PAIP2B,SLC1A2 | 5 |
| Severe psychological disorder | 0.000873 | | | CLTA,FES,HYCC1,MCMBP,PAIP2B,SLC1A2 | 6 |
| Hypomyelinating leukodystrophy type 5 | 0.000897 | | | HYCC1 | 1 |
| Damage of CA1 neuron | 0.00135 | | | SLC1A2 | 1 |
| Depressive disorder | 0.00248 | | | FGA,MCMBP,PAIP2B,SLC1A2 | 4 |
| Delay in amyotrophic lateral sclerosis | 0.00314 | | | SLC1A2 | 1 |
| Familial degenerative brain disorder | 0.00536 | | | HYCC1,SLC1A2 | 2 |
| Anxiety disorders | 0.0124 | | | FES,SLC1A2 | 2 |
| Major depression | 0.0151 | | | MCMBP,PAIP2B,SLC1A2 | 3 |
| Cerebral amyloid angiopathy | 0.0248 | | | SLC1A2 | 1 |
| Progressive supranuclear palsy | 0.0297 | | | SLC1A2 | 1 |
| Bipolar disorder | 0.0352 | | | CLTA,HYCC1 | 2 |
| Familial amyotrophic lateral sclerosis | 0.0358 | | | SLC1A2 | 1 |
| Social anxiety disorder | 0.0392 | | | SLC1A2 | 1 |
| Multiple system atrophy | 0.0414 | | | SLC1A2 | 1 |

## Table 5-23. QIAGEN Ingenuity Pathway Analysis predicted neurologic disease in TaClo (5, 50, 500 ppb)-treated 6 months post-fertilization zebrafish brain

| Diseases or Functions Annotation | p-value | Predicted Activation State | Activation z-score | # Molecules |
|---|---|---|---|---|
| Neurogenic lesion | 3.28E-26 | | 1.103 | 221 |
| Central nervous system solid tumor | 3.9E-26 | | | 225 |
| Nervous system neoplasm | 4.11E-26 | | 0.762 | 227 |
| Glioma | 4.7E-26 | | | 222 |
| Brain tumor | 1.24E-25 | | | 217 |
| Brain lesion | 2E-25 | | | 218 |
| Brain glioma | 2.2E-25 | | | 215 |
| Central nervous system cancer | 2.86E-24 | | | 218 |
| Glioma cancer | 1.09E-23 | | | 215 |
| Grade 3-4 glioma cancer | 4.13E-22 | | | 194 |
| Grade 4 high grade glioma | 2.94E-20 | | | 180 |
| Grade 4 astrocytoma | 3.39E-20 | | | 180 |
| Brain astrocytoma | 1.41E-19 | | | 179 |
| High grade astrocytoma | 6.63E-19 | | | 183 |
| Movement disorders | 1.45E-13 | | -1.833 | 77 |
| Neuromuscular disease | 7.69E-13 | | | 71 |
| Familial neurological disorder | 9.03E-13 | | | 92 |
| Sensory disorders | 1.38E-12 | Decreased | -2.162 | 40 |
| Disorder of basal ganglia | 5.82E-12 | | | 58 |
| Abnormal morphology of photoreceptors | 2.23E-10 | | | 13 |
| Abnormal morphology of photoreceptor outer segments | 3.87E-10 | | | 11 |
| Degeneration of photoreceptors | 6.91E-10 | Decreased | -2.151 | 13 |
| Abnormal morphology of sensory neurons | 7.83E-10 | | | 17 |
| Neurological signs | 8.13E-10 | | | 47 |
| Dyskinesia | 2.29E-09 | | | 39 |
| Abnormal morphology of neurons | 2.4E-09 | Decreased | -2.055 | 33 |
| Neurodegeneration of sensory neurons | 2.63E-09 | Decreased | -2.548 | 15 |
| Degeneration of nervous system | 2.71E-09 | Decreased | -2.559 | 25 |
| Brain cancer | 2.74E-09 | | | 87 |
| Neurodegeneration of nervous tissue | 3.99E-09 | Decreased | -2.522 | 23 |
| Abnormal morphology of nervous system | 5.09E-09 | Decreased | -2.154 | 42 |
| Gliomatosis cerebri | 8.04E-09 | | | 81 |
| Familial central nervous system disease | 9.61E-09 | | | 71 |
| Sensory loss | 1.05E-08 | Decreased | -2.582 | 28 |
| Degeneration of neurons | 1.28E-08 | Decreased | -2.472 | 22 |
| Progressive neurological disorder | 1.32E-08 | | | 76 |
| Hereditary neuromuscular disease | 1.69E-08 | | | 41 |
| Neurodegeneration | 1.84E-08 | Decreased | -2.549 | 25 |
| Hearing loss | 2.45E-08 | Decreased | -2.383 | 26 |
| Huntington Disease | 0.000000026 | | | 35 |
| Recessive congenital stationary night blindness | 7.26E-08 | | | 5 |
| Oligodendroglioma | 7.67E-08 | | | 59 |
| Familial encephalopathy | 0.00000014 | | | 66 |
| Parkinson's disease | 0.000000165 | | | 28 |
| Grade 2-3 glioma | 0.000000226 | | | 58 |
| Grade 3 glioma | 0.000000227 | | | 57 |
| Autosomal recessive neurological disorder | 0.0000004 | | | 41 |
| Progressive neuromuscular disease | 0.000000427 | | | 38 |
| Neuromuscular disease with neuropathy | 0.000000559 | | | 39 |
| Brain oligodendroglioma | 0.000000715 | | | 55 |
| Progressive neuropathy | 0.000000954 | | | 46 |
| Grade 3 malignant glioma | 0.00000102 | | | 55 |
| Progressive motor neuropathy | 0.00000179 | | | 45 |
| Congenital stationary night blindness type 1 | 0.00000182 | | | 4 |
| Macular dystrophy | 0.00000225 | | | 6 |
| Optic atrophy | 0.00000294 | | | 12 |
| Autosomal recessive stationary night blindness | 0.00000301 | | | 4 |
| Degeneration of eye photoreceptor cells | 0.00000316 | Decreased | -2.408 | 6 |
| Hereditary hearing loss | 0.00000327 | | | 15 |
| Stargardt disease | 0.00000374 | | | 5 |
| Spinocerebellar ataxia type 7 | 0.00000882 | | | 7 |
| Syndromic hearing loss | 0.00000953 | | | 9 |
| Degeneration of photoreceptors in retina | 0.00000976 | | -1.309 | 7 |
| Vestibular disorder | 0.0000109 | | | 9 |
| Nonsyndromic hearing impairment | 0.0000119 | | | 10 |
| Cerebrovascular dysfunction | 0.0000189 | | -0.314 | 29 |
| Maculopathy | 0.0000265 | | | 12 |
| Balance disorder | 0.0000321 | | | 11 |
| Cardiomyopathy | 0.0000347 | | -0.525 | 48 |
| Stroke | 0.0000404 | | | 21 |
| Fundus flavimaculatus | 0.0000409 | | | 4 |
| Familial nonsyndromic hearing impairment | 0.0000469 | | | 9 |
| Abnormal morphology of synapse | 0.0000516 | | | 8 |
| Damage of central nervous system | 0.0000556 | | 0 | 16 |
| Congenital neurological disorder | 0.000057 | | -0.577 | 37 |
| Coordination disorder | 0.0000607 | | -1.452 | 18 |
| Autosomal dominant spinocerebellar ataxia | 0.0000695 | | | 8 |
| Cannabis abuse | 0.0000736 | | | 3 |
| Myocardial dysfunction | 0.0000805 | | | 20 |

| Diseases or Functions Annotation | p-value | Predicted Activation State | Activation z-score | # Molecules |
|---|---|---|---|---|
| Progressive encephalopathy | 0.0000817 | | | 57 |
| Abnormal morphology of neurosensory retina | 0.0000922 | | | 8 |
| Autosomal dominant cardiomyopathy | 0.0000951 | | | 7 |
| Visual disturbance | 0.000108 | | | 7 |
| Brain damage | 0.000111 | | 0.351 | 15 |
| Ménière disease | 0.000112 | | | 6 |
| Degeneration of retinal rods | 0.000113 | | | 4 |
| Autosomal dominant intrinsic cardiomyopathy | 0.000121 | | | 6 |
| Charcot-Marie-Tooth disease type 4 | 0.000135 | | | 4 |
| Ataxia | 0.000136 | | -1.452 | 17 |
| Autosomal dominant encephalopathy | 0.00015 | | | 19 |
| Abnormal morphology of photoreceptor inner segments | 0.000288 | | | 4 |
| Postoperative delirium | 0.000335 | | | 6 |
| Vertigo | 0.000346 | | | 8 |
| Autosomal recessive nonsyndromic hydrocephalus type 2 | 0.000369 | | | 2 |
| Hydrocephalus | 0.000387 | | | 9 |
| Familial cardiomyopathy | 0.000441 | | | 10 |
| Left ventricular dysfunction | 0.000494 | | | 17 |
| Brain stroke | 0.000506 | | | 8 |
| Macular degeneration | 0.000614 | | | 9 |
| Addictive behavior | 0.00069 | | | 6 |
| Progressive high frequency hearing impairment | 0.000732 | | | 2 |
| Autosomal dominant familial nonsyndromic hearing impairment | 0.000747 | | | 4 |
| Autosomal dominant hypertrophic cardiomyopathy | 0.000827 | | | 4 |
| Autosomal dominant deafness | 0.000903 | | | 6 |
| Autosomal dominant nonsyndromic hearing impairment | 0.000912 | | | 5 |
| Infarction of cerebrum | 0.00093 | | | 7 |
| Sedation | 0.000976 | | | 5 |
| Hearing loss and retinitis pigmentosa | 0.00101 | | | 4 |
| Development of oligodendroglioma | 0.00121 | | | 2 |
| Calcification of aortic valve | 0.00122 | | | 11 |
| Dysmyelination | 0.00126 | | -1.741 | 22 |
| Restrictive cardiomyopathy | 0.00136 | | | 3 |
| Nerve degeneration | 0.00143 | | -1.342 | 5 |
| Cerebellar ataxia | 0.00144 | | | 10 |
| Cognitive impairment | 0.00147 | | | 34 |
| Intrinsic cardiomyopathy | 0.00149 | | | 18 |
| Hereditary neuropathy | 0.00157 | | | 16 |
| Autosomal dominant maculopathy | 0.00157 | | | 3 |
| CADASIL | 0.0018 | | | 2 |
| Brain heterotopia | 0.0018 | | | 2 |
| Sporadic age-related sensorineural hearing loss | 0.0018 | | | 3 |
| Demyelination | 0.00181 | | -1.741 | 20 |
| Migraines | 0.00181 | | | 13 |
| Abnormal morphology of brain | 0.00193 | | -1.633 | 17 |
| Autosomal recessive deafness | 0.00201 | | | 8 |
| Spinocerebellar disease | 0.00217 | | | 11 |

**Table 5-24. QIAGEN Ingenuity Pathway Analysis predicted nervous system development and function in TaClo (5, 50, 500 ppb)-treated 6 months post-fertilization zebrafish brain**

| Diseases or Functions Annotation | p-value | Predicted Activation State | Activation z-score | # Molecules |
|---|---|---|---|---|
| Electrophysiology of eye | 9.57E-12 | | | 15 |
| Sensory system development | 6.07E-08 | | 1.539 | 25 |
| Development of photoreceptors | 9.55E-08 | | | 9 |
| Development of neural cells | 0.000000297 | | 1.474 | 44 |
| Electrophysiology of retinal rods | 0.000000434 | | | 8 |
| Development of neurons | 0.00000162 | | 1.442 | 41 |
| Formation of eye | 0.00000526 | | | 18 |
| Righting reflex | 0.0000119 | | 0.896 | 7 |
| Morphology of eye | 0.000014 | | | 9 |
| Myelination | 0.0000203 | | -1.095 | 13 |
| Quantity of neurons | 0.0000215 | Increased | 2.546 | 23 |
| Morphogenesis of neurons | 0.000117 | | 1.488 | 30 |
| Development of central nervous system | 0.000159 | | 0.225 | 28 |
| Neuritogenesis | 0.000219 | | 1.488 | 29 |
| Formation of brain | 0.000269 | | | 23 |
| Quantity of sensory neurons | 0.000378 | | 1.219 | 8 |
| Development of neuroglia | 0.000517 | | -1 | 7 |
| Proliferation of neuronal cells | 0.000541 | | -0.239 | 21 |
| Neurotransmission | 0.000626 | | -1.979 | 18 |
| Formation of Muller glia | 0.000732 | | | 2 |
| Quantity of radial glial cells | 0.000987 | | | 3 |
| Electrophysiology of retinal cone cells | 0.00101 | | | 4 |
| Synaptic transmission | 0.00109 | | -1.71 | 15 |
| Quantity of photoreceptors | 0.00119 | Increased | 2.2 | 5 |
| Development of amacrine cells | 0.00121 | | | 2 |
| Migration of pyramidal neurons | 0.00121 | | | 2 |
| Size of eye | 0.00136 | | | 3 |
| Quantity of amacrine cells | 0.00157 | | | 3 |
| Morphology of cornea | 0.00157 | | | 4 |
| Formation of retinal cells | 0.00171 | | | 4 |
| Photoresponse of retina | 0.0018 | | | 3 |
| Formation of forebrain | 0.00203 | | | 11 |

**Table 5-25. QIAGEN Ingenuity Pathway Analysis predicted nervous system development and function in 1.75 µM MPTP-treated 6 months post-fertilization zebrafish brain**

| Diseases or Functions Annotation | p-value | Predicted Activation State | Activation z-score | # Molecules |
|---|---|---|---|---|
| Neurotransmission | 0.000000888 | | 1.026 | 13 |
| Guidance of axons | 0.0000107 | | | 7 |
| Synaptic transmission | 0.0000232 | | 1.026 | 10 |
| Growth of neurites | 0.0000412 | | 1.654 | 11 |
| NMDA-mediated synaptic current | 0.0000417 | | | 3 |
| Proliferation of neuronal cells | 0.0000485 | | 1.884 | 12 |
| Size of nervous tissue | 0.000133 | | | 5 |
| Development of neurons | 0.000277 | Increased | 2.68 | 16 |
| Development of central nervous system | 0.000312 | | -0.339 | 13 |
| Branching of neurons | 0.000318 | Increased | 2.767 | 9 |
| Recognition memory | 0.000387 | | | 4 |
| Morphology of neurons | 0.000425 | | | 7 |
| Differentiation of hippocampal neurons | 0.000563 | | | 2 |
| Morphogenesis of central nervous system | 0.000565 | | | 4 |
| Neuritogenesis | 0.000606 | Increased | 2.777 | 13 |
| Development of nerves | 0.000769 | | | 4 |
| Quantity of interneurons | 0.000777 | | | 3 |
| Paired-pulse inhibition | 0.000822 | | | 2 |
| Outgrowth of neurites | 0.000857 | | 1.809 | 8 |
| Coordination | 0.000909 | | 1.097 | 6 |
| Differentiation of neurons | 0.000946 | | 0.762 | 9 |
| Morphology of nervous system | 0.001 | | | 9 |
| Development of neuroglia | 0.00108 | | | 4 |
| Branching of neurites | 0.00128 | Increased | 2.6 | 8 |
| Size of neurons | 0.0014 | | | 4 |
| Formation of brain | 0.00167 | | | 10 |
| Density of neurons | 0.0017 | | 0.927 | 5 |
| Dendritic growth/branching | 0.00184 | Increased | 2.412 | 7 |
| Quantity of neurons | 0.00186 | | -1.083 | 9 |
| Density of dendritic spines | 0.00192 | | | 4 |
| Differentiation of granule cells | 0.0021 | | | 2 |
| Long-term potentiation of hippocampal neurons | 0.00281 | | | 2 |
| Quantity of motor neurons | 0.00323 | | | 3 |
| Projection of mossy fibers | 0.00359 | | | 1 |
| Arrest in differentiation of dentate granule cells | 0.00359 | | | 1 |
| Specification of primary neurons | 0.00359 | | | 1 |
| Delay in initiation of migration of pyramidal neurons | 0.00359 | | | 1 |
| Myelination | 0.00363 | | | 5 |
| Action potential of neurons | 0.00502 | | | 4 |
| Excitatory postsynaptic potential | 0.00512 | | | 4 |
| Sensation | 0.00582 | | 1.176 | 6 |
| Myelination of nerves | 0.00664 | | | 2 |
| Working memory | 0.00664 | | | 2 |
| Memory | 0.00679 | Increased | 2.195 | 6 |
| Development of Schwann cells | 0.00702 | | | 2 |
| Firing of mechanosensory neurons | 0.00717 | | | 1 |
| Morphology of oligodendrocytes | 0.00717 | | | 1 |
| Excitation of indirect pathway medium spiny projection neurons | 0.00717 | | | 1 |
| Conduction of optic nerve | 0.00717 | | | 1 |
| Morphology of cranial nerve ganglion | 0.00717 | | | 1 |
| Neuroprotection of pituitary cancer cell lines | 0.00717 | | | 1 |
| Quantity of v2 neuron | 0.00717 | | | 1 |
| Quantity of v1 neuron | 0.00717 | | | 1 |
| Cooling sensation | 0.00717 | | | 1 |
| Quantity of oxytocin neurons | 0.00717 | | | 1 |
| Prepulse inhibition | 0.00909 | | | 3 |
| Development of astrocytes | 0.00955 | | | 2 |
| Morphology of neurites | 0.00984 | | | 4 |
| Recycling of synaptic vesicles | 0.01 | | | 2 |
| Sprouting of sensory neurons | 0.0107 | | | 1 |
| Sensory function of olfactory receptor neurons in vomeronasal organ | 0.0107 | | | 1 |
| Quantity of neurosphere cells | 0.0107 | | | 1 |
| Innervation of epidermis | 0.0107 | | | 1 |
| Fragmentation of myelin sheath | 0.0107 | | | 1 |
| Length of nodes of Ranvier | 0.0107 | | | 1 |
| Volume of gray matter | 0.0107 | | | 1 |

**Table 5-26. QIAGEN Ingenuity Pathway Analysis predicted behavior in 1.75 µM MPTP-treated 6 months post-fertilization zebrafish brain**

| Diseases or Functions Annotation | p-value | Predicted Activation State | Activation z-score | # Molecules |
|---|---|---|---|---|
| Locomotion | 0.000000829 | | 0 | 12 |
| Emotional behavior | 0.00000129 | | -0.858 | 11 |
| Anxiety-like behavior | 0.0000628 | | 0 | 5 |
| Cognition | 0.000218 | | 1.625 | 11 |
| Nest building behavior | 0.00027 | | | 3 |
| Learning | 0.000384 | | 1.988 | 10 |
| Recognition memory | 0.000387 | | | 4 |
| Social behavior | 0.000475 | | 1.199 | 5 |
| Fear | 0.000545 | | | 4 |
| Conditioning | 0.000955 | | 0.218 | 6 |
| Nursing | 0.00392 | | | 2 |
| Grooming | 0.00474 | | | 3 |
| Aggressive behavior | 0.00595 | | | 3 |
| Working memory | 0.00664 | | | 2 |
| Memory | 0.00679 | Increased | 2.195 | 6 |
| Anxiety | 0.00714 | | 0.889 | 6 |
| Scratching of wound in skin | 0.00717 | | | 1 |
| Contextual conditioning | 0.00848 | | | 3 |
| Maternal nurturing | 0.0091 | | | 2 |
| Emotional response conditioning | 0.0107 | | | 1 |
| Perseverance behavior | 0.0107 | | | 1 |
| Circling behavior | 0.0109 | | | 2 |

**Table 5-27. QIAGEN Ingenuity Pathway Analysis predicted top five disease categories in TaClo (5, 50, 500 ppb)-treated 120 hours post-fertilization zebrafish larvae**

| Name | p-value | #Molecules |
|---|---|---|
| **Cancer** | 1.17E-02 - 3.42E-17 | 104 |
| **Organismal Injury and Abnormalities** | 1.17E-02 - 3.42E-17 | 104 |
| **Gastrointestinal Disease** | 1.17E-02 - 1.01E-13 | 101 |
| **Neurological Disease** | 1.17E-02 - 3.81E-11 | 90 |
| **Reproductive System Disease** | 1.17E-02 - 5.62E-11 | 92 |

**Table 5-28. QIAGEN Ingenuity Pathway Analysis predicted top five disease categories in 1.75 µM MPTP-treated 120 hours post-fertilization zebrafish larvae**

| Name | p-value | #Molecules |
|---|---|---|
| Organismal Injury and Abnormalities | 4.99E-02 - 5.53E-05 | 11 |
| Psychological Disorders | 4.14E-02 - 5.53E-05 | 7 |
| Gastrointestinal Disease | 3.71E-02 - 1.22E-04 | 3 |
| Hepatic System Disease | 9.38E-03 - 1.22E-04 | 2 |
| Connective Tissue Disorders | 3.97E-02 - 1.61E-04 | 4 |

**Table 5-29. QIAGEN Ingenuity Pathway Analysis predicted top five disease categories in TaClo (5, 50, 500 ppb)-treated 6 months post-fertilization zebrafish brain**

| Name | p-value | #Molecules |
|---|---|---|
| Cancer | 2.13E-03 - 1.35E-35 | 296 |
| Organismal Injury and Abnormalities | 2.17E-03 - 1.35E-35 | 298 |
| Gastrointestinal Disease | 2.13E-03 - 1.22E-29 | 285 |
| Neurological Disease | 2.17E-03 - 3.28E-26 | 260 |
| Endocrine System Disorders | 1.88E-03 - 7.83E-26 | 269 |

**Table 5-30. QIAGEN Ingenuity Pathway Analysis predicted top five disease categories in 1.75 µM MPTP-treated 6 months post-fertilization zebrafish larvae**

| Name | p-value | #Molecules |
|---|---|---|
| Cancer | 1.14E-02 - 6.72E-13 | 96 |
| Organismal Injury and Abnormalities | 1.14E-02 - 6.72E-13 | 96 |
| Gastrointestinal Disease | 1.14E-02 - 2.43E-11 | 90 |
| Hematological disease | 1.09E-02 - 3.37E-08 | 58 |
| Endocrine System Disorders | 1.07E-02 - 3.79E-08 | 90 |

**References**


Akundi, R. S., Hüll, M., Clement, H. W., & Fiebich, B. L. (2003). 1-trichloromethyl-1,2,3,4-tetrahydro-beta-carboline (TaClo) induces apoptosis in human neuroblastoma cell lines. *Ann N Y Acad Sci*, *1010*, 304-306. https://doi.org/10.1196/annals.1299.053

Allen, J. A., Halverson-Tamboli, R. A., & Rasenick, M. M. (2007). Lipid raft microdomains and neurotransmitter signalling. *Nat Rev Neurosci*, *8*(2), 128-140. https://doi.org/10.1038/nrn2059

Arrigo, A. P. (2017). Mammalian HspB1 (Hsp27) is a molecular sensor linked to the physiology and environment of the cell. *Cell Stress Chaperones*, *22*(4), 517-529. https://doi.org/10.1007/s12192-017-0765-1

Backe, S. J., Sager, R. A., Regan, B. R., Sit, J., Major, L. A., Bratslavsky, G., Woodford, M. R., Bourboulia, D., & Mollapour, M. (2022). A specialized Hsp90 co-chaperone network regulates steroid hormone receptor response to ligand. *Cell Rep*, *40*(2), 111039. https://doi.org/10.1016/j.celrep.2022.111039

Baird, L., & Yamamoto, M. (2020). The Molecular Mechanisms Regulating the KEAP1-NRF2 Pathway. *Mol Cell Biol*, *40*(13). https://doi.org/10.1128/mcb.00099-20

Bringmann, G., God, R., Fähr, S., Feineis, D., Fornadi, K., & Fornadi, F. (1999). Identification of the dopaminergic neurotoxin 1-trichloromethyl-1,2, 3,4-tetrahydro-beta-carboline in human blood after intake of the hypnotic chloral hydrate. *Anal Biochem*, *270*(1), 167-175. https://doi.org/10.1006/abio.1999.4088

Bringmann, G., God, R., Feineis, D., Janetzky, B., & Reichmann, H. (1995). TaClo as a neurotoxic lead: improved synthesis, stereochemical analysis, and inhibition of the mitochondrial respiratory chain. *J Neural Transm Suppl*, *46*, 245-254.

Bringmann, G., God, R., Feineis, D., Wesemann, W., Riederer, P., Rausch, W. D., Reichmann, H., & Sontag, K. H. (1995). The TaClo concept: 1-trichloromethyl-1,2,3,4-tetrahydro-beta-carboline (TaClo), a new toxin for dopaminergic neurons. *J Neural Transm Suppl*, *46*, 235-244.

Butchbach, M. E., Tian, G., Guo, H., & Lin, C. L. (2004). Association of excitatory amino acid transporters, especially EAAT2, with cholesterol-rich lipid raft microdomains: importance for excitatory amino acid transporter localization and function. *J Biol Chem*, *279*(33), 34388-34396. https://doi.org/10.1074/jbc.M403938200

Cong, B., Liu, C., Wang, L., & Chai, Y. (2020). The Impact on Antioxidant Enzyme Activity and Related Gene Expression Following Adult Zebrafish (Danio rerio) Exposure to Dimethyl Phthalate. *Animals (Basel)*, *10*(4). https://doi.org/10.3390/ani10040717

Coretti, L., Buommino, E., & Lembo, F. (2024). The aryl hydrocarbon receptor pathway: a linking bridge between the gut microbiome and neurodegenerative diseases. *Front Cell Neurosci*, *18*, 1433747. https://doi.org/10.3389/fncel.2024.1433747

Dasgupta, S., Dunham, C. L., Truong, L., Simonich, M. T., Sullivan, C. M., & Tanguay, R. L. (2021). Phenotypically Anchored mRNA and miRNA Expression Profiling in Zebrafish Reveals Flame Retardant Chemical Toxicity Networks. *Front Cell Dev Biol*, *9*, 663032. https://doi.org/10.3389/fcell.2021.663032

Diao, X., Shang, Q., Guo, M., Huang, Y., Zhang, M., Chen, X., Liang, Y., Sun, X., Zhou, F., Zhuang, J., Liu, S. J., Vogel, C. F. A., Rastinejad, F., & Wu, D. (2025). Structural basis for the ligand-dependent activation of heterodimeric AHR-ARNT complex. *Nat Commun*, *16*(1), 1282. https://doi.org/10.1038/s41467-025-56574-7

Dogra, S., Putnam, J., & Conn, P. J. (2022). Metabotropic glutamate receptor 3 as a potential therapeutic target for psychiatric and neurological disorders. *Pharmacol Biochem Behav*, *221*, 173493. https://doi.org/10.1016/j.pbb.2022.173493

Du, X., Li, J., Li, M., Yang, X., Qi, Z., Xu, B., Liu, W., Xu, Z., & Deng, Y. (2020). Research progress on the role of type I vesicular glutamate transporter (VGLUT1) in nervous system diseases. *Cell Biosci*, *10*, 26. https://doi.org/10.1186/s13578-020-00393-4

Dudziak, K., Zapalska, M., Börner, A., Szczerba, H., Kowalczyk, K., & Nowak, M. (2019). Analysis of wheat gene expression related to the oxidative stress response and signal transduction under short-term osmotic stress. *Sci Rep*, *9*(1), 2743. https://doi.org/10.1038/s41598-019-39154-w

Fang, X., Corrales, J., Thornton, C., Clerk, T., Scheffler, B. E., & Willett, K. L. (2015). Transcriptomic Changes in Zebrafish Embryos and Larvae Following Benzo[a]pyrene Exposure. *Toxicol Sci*, *146*(2), 395-411. https://doi.org/10.1093/toxsci/kfv105

Foran, E., Rosenblum, L., Bogush, A., Pasinelli, P., & Trotti, D. (2014). Sumoylation of the astroglial glutamate transporter EAAT2 governs its intracellular compartmentalization. *Glia*, *62*(8), 1241-1253. https://doi.org/10.1002/glia.22677

Freyaldenhoven, T. E., & Ali, S. F. (1997). Role of heat shock proteins in MPTP-induced neurotoxicity. *Ann N Y Acad Sci*, *825*, 167-178. https://doi.org/10.1111/j.1749-6632.1997.tb48427.x

Grishanova, A. Y., & Perepechaeva, M. L. (2022). Aryl Hydrocarbon Receptor in Oxidative Stress as a Double Agent and Its Biological and Therapeutic Significance. *Int J Mol Sci*, *23*(12). https://doi.org/10.3390/ijms23126719

Grote, C., Clement, H. W., Wesemann, W., Bringmann, G., Feineis, D., Riederer, P., & Sontag, K. H. (1995). Biochemical lesions of the nigrostriatal system by TaClo (1-trichloromethyl-1,2,3,4-tetrahydro-beta-carboline) and derivatives. *J Neural Transm Suppl*, *46*, 275-281.

Guerrero-Escalera, D., Alarcón-Sánchez, B. R., Arellanes-Robledo, J., Cruz-Rangel, A., Del Pozo-Yauner, L., Chagoya de Sánchez, V., Resendis-Antonio, O., Villa-Treviño, S., Torres-Mena, J. E., & Pérez-Carreón, J. I. (2022). Comparative subcellular localization of NRF2 and KEAP1 during the hepatocellular carcinoma development in vivo. *Biochim Biophys Acta Mol Cell Res*, *1869*(5), 119222. https://doi.org/10.1016/j.bbamcr.2022.119222

Guimaraes, I. M., Carvalho, T. G., Ferguson, S. S., Pereira, G. S., & Ribeiro, F. M. (2015). The metabotropic glutamate receptor 5 role on motor behavior involves specific neural substrates. *Mol Brain*, *8*, 24. https://doi.org/10.1186/s13041-015-0113-2

Häberle, J., Görg, B., Rutsch, F., Schmidt, E., Toutain, A., Benoist, J. F., Gelot, A., Suc, A. L., Höhne, W., Schliess, F., Häussinger, D., & Koch, H. G. (2005). Congenital glutamine deficiency with glutamine synthetase mutations. *N Engl J Med*, *353*(18), 1926-1933. https://doi.org/10.1056/NEJMoa050456

Horzmann, K. A., Lin, L. F., Taslakjian, B., Yuan, C., & Freeman, J. L. (2022). Anxiety-related behavior and associated brain transcriptome and epigenome alterations in adult female zebrafish exposed to atrazine during embryogenesis. *Chemosphere*, *308*(Pt 3), 136431. https://doi.org/10.1016/j.chemosphere.2022.136431

Hoter, A., El-Sabban, M. E., & Naim, H. Y. (2018). The HSP90 Family: Structure, Regulation, Function, and Implications in Health and Disease. *Int J Mol Sci*, *19*(9). https://doi.org/10.3390/ijms19092560

Hubbard, T. D., Murray, I. A., Bisson, W. H., Lahoti, T. S., Gowda, K., Amin, S. G., Patterson, A. D., & Perdew, G. H. (2015). Adaptation of the human aryl hydrocarbon receptor to sense microbiota-derived indoles. *Sci Rep*, *5*, 12689. https://doi.org/10.1038/srep12689

Hwang, J., Newton, E. M., Hsiao, J., & Shi, V. Y. (2022). Aryl hydrocarbon receptor/nuclear factor E2-related factor 2 (AHR/NRF2) signalling: A novel therapeutic target for atopic dermatitis. *Exp Dermatol*, *31*(4), 485-497. https://doi.org/10.1111/exd.14541

Ito, S., & Nagata, K. (2017). Biology of Hsp47 (Serpin H1), a collagen-specific molecular chaperone. *Semin Cell Dev Biol*, *62*, 142-151. https://doi.org/10.1016/j.semcdb.2016.11.005

Jayakumar, A. R., & Norenberg, M. D. (2016). Glutamine Synthetase: Role in Neurological Disorders. *Adv Neurobiol*, *13*, 327-350. https://doi.org/10.1007/978-3-319-45096-4_13

Jia, Y. F., Wininger, K., Ho, A. M., Peyton, L., Baker, M., & Choi, D. S. (2020). Astrocytic Glutamate Transporter 1 (GLT1) Deficiency Reduces Anxiety- and Depression-Like Behaviors in Mice. *Front Behav Neurosci*, *14*, 57. https://doi.org/10.3389/fnbeh.2020.00057

Keane, P. C., Hanson, P. S., Patterson, L., Blain, P. G., Hepplewhite, P., Khundakar, A. A., Judge, S. J., Kahle, P. J., LeBeau, F. E. N., & Morris, C. M. (2019). Trichloroethylene and its metabolite TaClo lead to degeneration of substantia nigra dopaminergic neurones: Effects in wild type and human A30P mutant α-synuclein mice. *Neurosci Lett*, *711*, 134437. https://doi.org/10.1016/j.neulet.2019.134437

Kose, S., Furuta, M., & Imamoto, N. (2012). Hikeshi, a nuclear import carrier for Hsp70s, protects cells from heat shock-induced nuclear damage. *Cell*, *149*(3), 578-589. https://doi.org/10.1016/j.cell.2012.02.058

Kowalczyk, M., Kucia, K., Owczarek, A., Suchanek-Raif, R., Merk, W., Paul-Samojedny, M., & Kowalski, J. (2018). Association Studies of HSPA1A and HSPA1L Gene Polymorphisms With Schizophrenia. *Arch Med Res*, *49*(5), 342-349. https://doi.org/10.1016/j.arcmed.2018.10.002

Lazaro, I., Oguiza, A., Recio, C., Lopez-Sanz, L., Bernal, S., Egido, J., & Gomez-Guerrero, C. (2017). Interplay between HSP90 and Nrf2 pathways in diabetes-associated atherosclerosis. *Clin Investig Arterioscler*, *29*(2), 51-59. https://doi.org/10.1016/j.arteri.2016.10.003

Lee, J., Horzmann, K. A., & Freeman, J. L. (2018). An embryonic 100µg/L lead exposure results in sex-specific expression changes in genes associated with the neurological system in female or cancer in male adult zebrafish brains. *Neurotoxicol Teratol*, *65*, 60-69. https://doi.org/10.1016/j.ntt.2017.10.006

Li, Y., Paonessa, J. D., & Zhang, Y. (2012). Mechanism of chemical activation of Nrf2. *PLoS One*, *7*(4), e35122. https://doi.org/10.1371/journal.pone.0035122

Liu, M., Shin, E. J., Dang, D. K., Jin, C. H., Lee, P. H., Jeong, J. H., Park, S. J., Kim, Y. S., Xing, B., Xin, T., Bing, G., & Kim, H. C. (2018). Trichloroethylene and Parkinson's Disease: Risk Assessment. *Mol Neurobiol*, *55*(7), 6201-6214. https://doi.org/10.1007/s12035-017-0830-x

Lupien, S. J., McEwen, B. S., Gunnar, M. R., & Heim, C. (2009). Effects of stress throughout the lifespan on the brain, behaviour and cognition. *Nat Rev Neurosci*, *10*(6), 434-445. https://doi.org/10.1038/nrn2639

McClure, R. S., Rericha, Y., Waters, K. M., & Tanguay, R. L. (2023). 3' RNA-seq is superior to standard RNA-seq in cases of sparse data but inferior at identifying toxicity pathways in a model organism. *Front Bioinform*, *3*, 1234218. https://doi.org/10.3389/fbinf.2023.1234218

Monistrol, J., Beton, J. G., Johnston, E. C., Dang, T. L., Bukau, B., & Saibil, H. R. (2025). Stepwise recruitment of chaperone Hsc70 by DNAJB1 produces ordered arrays primed for bursts of amyloid fibril disassembly. *Commun Biol*, *8*(1), 522. https://doi.org/10.1038/s42003-025-07906-2

Ngo, V., & Duennwald, M. L. (2022). Nrf2 and Oxidative Stress: A General Overview of Mechanisms and Implications in Human Disease. *Antioxidants (Basel)*, *11*(12). https://doi.org/10.3390/antiox11122345

Niestroy, J., Barbara, A., Herbst, K., Rode, S., van Liempt, M., & Roos, P. H. (2011). Single and concerted effects of benzo[a]pyrene and flavonoids on the AhR and Nrf2-pathway in the human colon carcinoma cell line Caco-2. *Toxicol In Vitro*, *25*(3), 671-683. https://doi.org/10.1016/j.tiv.2011.01.008

Ou, J., Ou, Z., McCarver, D. G., Hines, R. N., Oldham, K. T., Ackerman, A. W., & Pritchard, K. A., Jr. (2003). Trichloroethylene decreases heat shock protein 90 interactions with

endothelial nitric oxide synthase: implications for endothelial cell proliferation. *Toxicol Sci*, *73*(1), 90-97. https://doi.org/10.1093/toxsci/kfg062

Pajarillo, E., Rizor, A., Lee, J., Aschner, M., & Lee, E. (2019). The role of astrocytic glutamate transporters GLT-1 and GLAST in neurological disorders: Potential targets for neurotherapeutics. *Neuropharmacology*, *161*, 107559. https://doi.org/10.1016/j.neuropharm.2019.03.002

Pare, J. M., LaPointe, P., & Hobman, T. C. (2013). Hsp90 cochaperones p23 and FKBP4 physically interact with hAgo2 and activate RNA interference-mediated silencing in mammalian cells. *Mol Biol Cell*, *24*(15), 2303-2310. https://doi.org/10.1091/mbc.E12-12-0892

Passlick, S., Rose, C. R., Petzold, G. C., & Henneberger, C. (2021). Disruption of Glutamate Transport and Homeostasis by Acute Metabolic Stress. *Front Cell Neurosci*, *15*, 637784. https://doi.org/10.3389/fncel.2021.637784

Peterson, A. R., & Binder, D. K. (2019). Post-translational Regulation of GLT-1 in Neurological Diseases and Its Potential as an Effective Therapeutic Target. *Front Mol Neurosci*, *12*, 164. https://doi.org/10.3389/fnmol.2019.00164

Rausch, W. D., Abdel-mohsen, M., Koutsilieri, E., Chan, W. W., & Bringmann, G. (1995). Studies of the potentially endogenous toxin TaClo (1-trichloromethyl-1,2,3,4-tetrahydro-beta-carboline) in neuronal and glial cell cultures. *J Neural Transm Suppl*, *46*, 255-263.

Riaza Bermudo-Soriano, C., Perez-Rodriguez, M. M., Vaquero-Lorenzo, C., & Baca-Garcia, E. (2012). New perspectives in glutamate and anxiety. *Pharmacol Biochem Behav*, *100*(4), 752-774. https://doi.org/10.1016/j.pbb.2011.04.010

Robinson, S. R. (2000). Neuronal expression of glutamine synthetase in Alzheimer's disease indicates a profound impairment of metabolic interactions with astrocytes. *Neurochem Int*, *36*(4-5), 471-482. https://doi.org/10.1016/s0197-0186(99)00150-3

Shin, S., Wakabayashi, N., Misra, V., Biswal, S., Lee, G. H., Agoston, E. S., Yamamoto, M., & Kensler, T. W. (2007). NRF2 modulates aryl hydrocarbon receptor signaling: influence on adipogenesis. *Mol Cell Biol*, *27*(20), 7188-7197. https://doi.org/10.1128/mcb.00915-07

Soni, N., Reddy, B. V., & Kumar, P. (2014). GLT-1 transporter: an effective pharmacological target for various neurological disorders. *Pharmacol Biochem Behav*, *127*, 70-81. https://doi.org/10.1016/j.pbb.2014.10.001

Spodenkiewicz, M., Diez-Fernandez, C., Rüfenacht, V., Gemperle-Britschgi, C., & Häberle, J. (2016). Minireview on Glutamine Synthetase Deficiency, an Ultra-Rare Inborn Error of Amino Acid Biosynthesis. *Biology (Basel)*, *5*(4). https://doi.org/10.3390/biology5040040

Wasel, O., Thompson, K. M., & Freeman, J. L. (2022). Assessment of unique behavioral, morphological, and molecular alterations in the comparative developmental toxicity profiles of PFOA, PFHxA, and PFBA using the zebrafish model system. *Environ Int*, *170*, 107642. https://doi.org/10.1016/j.envint.2022.107642

Yan, J. J., Zhang, Y. B., & Ding, Y. (2012). Binding mechanism between Hsp90 and Sgt1 explored by homology modeling and molecular dynamics simulations in rice. *J Mol Model*, *18*(10), 4665-4673. https://doi.org/10.1007/s00894-012-1464-6

Yang, Y., Pang, B., Liu, Z., Li, J., Zhang, Z., Zhang, R., Hou, X., Guo, H., Chi, L., Pang, Q., & Xin, T. (2019). 1-Trichloromethyl-1,2,3,4-tetrahydro-beta-carboline (TaClo) Induces the Apoptosis of Dopaminergic Neurons via Oxidative Stress and Neuroinflammation. *Oxid Med Cell Longev*, *2019*, 1292891. https://doi.org/10.1155/2019/1292891

Zhang, H., Gong, W., Wu, S., & Perrett, S. (2022). Hsp70 in Redox Homeostasis. *Cells*, *11*(5). https://doi.org/10.3390/cells11050829

Zhuang, C., Wu, Z., Xing, C., & Miao, Z. (2017). Small molecules inhibiting Keap1-Nrf2 protein-protein interactions: a novel approach to activate Nrf2 function. *Medchemcomm*, *8*(2), 286-294. https://doi.org/10.1039/c6md00500d

Zou, W. J., Song, Y. L., Wu, M. Y., Chen, X. T., You, Q. L., Yang, Q., Luo, Z. Y., Huang, L., Kong, Y., Feng, J., Fang, D. X., Li, X. W., Yang, J. M., Mei, L., & Gao, T. M. (2020). A discrete serotonergic circuit regulates vulnerability to social stress. *Nat Commun*, *11*(1), 4218. https://doi.org/10.1038/s41467-020-18010-w

Zuehlke, A. D., Beebe, K., Neckers, L., & Prince, T. (2015). Regulation and function of the human HSP90AA1 gene. *Gene*, *570*(1), 8-16. https://doi.org/10.1016/j.gene.2015.06.018

# Chapter 6
# Conclusion

This dissertation investigates the neurotoxic effects of TaClo (5, 50, 500 ppb) and 1.75 μM MPTP in zebrafish models.

In **Chapter 2**, we concluded that embryonic zebrafish serve as a powerful platform for evaluating neurotoxicity induced by environmentally relevant concentrations of pollutants. When integrated with diverse assessment approaches, the zebrafish model offers valuable insights into the complex interactions between environmental exposures and neurodegenerative disorders, which further advances our understanding of the underlying mechanisms of environmental toxicants.

**In Chapter 3,** we established an MPTP-induced Parkinson's disease-like larval zebrafish model. We then validated zebrafish models for studying TaClo-induced neurotoxicity by demonstrating that TaClo elicited MPTP-like effects following early-life exposure. We observed larval zebrafish exposed to 5 ppb TaClo exhibited significant neurotoxic effects, including diencephalic dopaminergic neuronal loss, increased apoptosis in the diencephalon, and locomotor deficits. We also found TaClo altered antioxidative enzymatic activity and modulated astrocytic and microglial responses. These findings provide important insights into the neurotoxic mechanisms of TaClo and suggest a potential link between TaClo exposure and PD and the potential environmental risks associated with TCE exposure.

**In Chapter 4**, we demonstrated that early-life exposure to TaClo and MPTP induced long-term neurotoxic effects, characterized by irreversible and progressive diencephalic neurodegeneration, altered antioxidative activity, and neurobehavioral deficits. These findings reinforce the potential environmental health risks posed by TCE and highlight its possible contribution to the development of neurodegenerative diseases from early life through adulthood.

**In Chapter 5**, our transcriptomic analysis revealed that TaClo and MPTP elicited neurotoxic effects through distinct mechanisms. We observed that TaClo primarily dysregulated cellular stress responses, whereas MPTP predominantly targeted glutamatergic neurotransmission in larval zebrafish. Additionally, TaClo-exposed zebrafish exhibited a maladaptive stress response during early development, which was later reversed by a compensatory adaptation in adulthood. Furthermore, both compounds were found to influence broader systemic diseases in addition to neurological disorders.

Taken together, our studies demonstrate that TaClo is a neurotoxicant capable of inducing both short-term and long-term neurotoxicity in zebrafish models, with effects and mechanisms closely aligned to those observed in the MPTP-induced PD-like zebrafish model. Although TaClo and MPTP share structural similarities, our transcriptomic analysis revealed that they utilize distinct mechanisms to exert their neurotoxic effects. Moreover, both TaClo and MPTP act not only as neurotoxicants but also as potential triggers of broader systemic diseases.

While transcriptomic profiling provided valuable mechanistic insights, future research should integrate proteomic, metabolomic, and epigenetic analyses to achieve a more comprehensive understanding of the neurotoxic pathways involved. Additionally, building on the principles of the DoHaD, studies should examine later life stages and investigate the multi-generational effects of TaClo exposure to assess its long-term impact. Furthermore, research should explore potential interventions aimed at mitigating oxidative stress and modulating astrocytic and microglial responses associated with TaClo-induced neurotoxicity. Finally, assessing the systemic effects of these toxicants on non-neural organ systems will further elucidate their broader health implications and support the identification of potential therapeutic or preventive strategies.

Overall, this dissertation provides novel insights into metabolite-driven neurotoxicity and contributes to our growing understanding of the environmental origins of neurodegenerative diseases. By highlighting the neurotoxic potential of TaClo, a metabolic byproduct of TCE, this

work emphasizes the importance of identifying and regulating harmful environmental exposures. These findings lay the groundwork for future research and inform strategies aimed at safeguarding public health against pollutant-induced neurological risks.